Sex differences in the lateral ventricle choroid plexus

Inauguraldissertation
zur
Erlangung der Würde eines Doktors der Philosophie
vorgelegt der
Philosophisch-Naturwissenschaftlichen Fakultät
der Universität Basel

von

Luca von Allmen

2023

Genehmigt von der Philosophisch-Naturwissenschaftlichen Fakultät
auf Antrag von:

Erstbetreuerin:	Prof. Dr. Fiona Doetsch
Zweitbetreuer:	Prof. Dr. Peter Scheiffele
Externe Expertin:	Prof. Dr. Britta Engelhardt

Basel, den 20.06.2023

The Dean of Faculty
Prof. Dr. Marcel Mayor

Table of Contents

ABBREVIATIONS **7**

ABSTRACT **8**

ACKNOWLEDGEMENTS **9**

1 INTRODUCTION TO THE CHOROID PLEXUS **10**

1.1 History of the choroid plexus/ CSF system 10

1.2 Development of the choroid plexus 12

1.3 The adult choroid plexus structure 13

1. 4 Cell types of the ChP 14

1.5 Functions of the ChP 17

1.5.1 CSF production *18*

1.5.2 Barrier properties *20*

1.5.3 Regulation of neural stem cells/ neurogenesis *21*

1.5.4 Immune surveillance *23*

1.5.5 Circadian clock *24*

1.5.6 Detoxification and chemical surveillance *25*

2 SEX DIFFERENCES **26**

2.1 Sexual dimorphism 27

2.1.1 Sexual dimorphism in the brain *27*

2.2 Sex hormones 28

2.2.1 The estrous cycle *29*

2.3 Sex differences in the LVChP 30

2.3.1 The LVChP is a sex hormone target *31*

3 MACROPHAGES **32**

3.1 Introduction 32

3.2 Macrophage function in immunity and homeostasis 32

3.2.1 The polarisation spectrum *33*

3.3 Macrophages in the CNS 34

3.3.1 Microglia *34*

3.3.2 Border-associated macrophages *35*

3.4 Choroid plexus macrophage populations 35

3.4.1 Stromal ChP macrophages *36*

3.4.2 Epiplexus macrophages *36*

3.5 Sex differences in the microglia CNS 37

3.6 The LVChP: a central hub for CNS homeostasis 38

4 AIM OF THIS THESIS **39**

5 RESULTS: SEX DIFFERENCES IN THE LVCHP 40

5.1 COMPARISON OF MALE AND FEMALE LVCHP STRUCTURE 40

5.2 TRANSCRIPTOME ANALYSIS OF MALE AND FEMALE LVCHP 42

5.2.1 GSEA analysis of the whole LVChP transcriptome 43

5.2.2 Differentially expressed genes between male and female LVChP 45

5.2.3 Validation of DEGs between male and female LVChP 47

5.2.4 Female DEGs are associated with macrophages 51

5.3 SEX DIFFERENCES IN LVCHP MACROPHAGES 52

5.3.1 Sex differences in LVChP stromal macrophages 54

5.3.2 LVChP epiplexus macrophage sex differences 57

5.3.3 Transcriptome analysis of male and female LVChP macrophage-associated genes 61

5. 4 THE LVCHP AS A SOURCE OF SIGNALLING FACTORS 63

5.4.1 Baseline clone activation in qNSCs and aNSCs 63

5.4.2 Activation of aNSCs cultured with LVChP-derived factors 64

5.4.3 Sex differences in LVChP ligands 66

5.4.4 Antibody array of male and female LVChP secreted proteins 66

5.5 THE LVCHP AND THE ESTROUS CYCLE 68

5.5.1 LVChP transcriptome changes during the estrous cycle 69

5.5.2 Changes in LVChP secretome due to fluctuating sex hormones 70

5.5.3 Macrophages and the estrous cycle 71

6 DEVELOPING TOOLS TO STUDY THE LVCHP 73

6.1 PROTOCOL FOR IMMUNOSTAININGS OF LVCHP WHOLE MOUNT EXPLANTS 73

6.2 OPTIMISING CONDITIONS FOR PREPARATION OF LVCHP CM 75

6.3 ESTABLISHING A CELL DISSOCIATION PROTOCOL FOR ADULT LVCHP SINGLE CELL ANALYSIS 77

6.3.1 Flow Cytometry for LVChP cell types 81

7 DISCUSSION 82

7.1 CONCLUSIONS 82

7.2 OUTLOOK 93

7.3 CLOSING REMARKS 96

8 MATERIAL AND METHODS 98

8.1 ANIMAL USE 98

8.2 TISSUE PREPARATION FOR IMMUNOHISTOCHEMISTRY AND FLUORESCENT RNA *IN SITU* HYBRIDIZATION 98

8.3 IMMUNOHISTOCHEMISTRY 99

8.4 FLUORESCENT *IN SITU* HYBRIDIZATION (FISH) 100

8.5 FLUORESCENT ACTIVATED CELL SORTING (FACS) 101

8.6 MOLECULAR ANALYSES 103

8.6.1 Bulk RNA sequencing of male and female LVChP 103

8.6.2 Proteomic analyses 109

8.7 IMAGE ACQUISITION AND QUANTIFICATION 111
8.7.1 Image quantifications *111*
8.8 *IN VITRO* EXPERIMENTS 113
8.8.1 Medium composition *113*
8.8.2 In vitro NSC cultures *113*
8.9 STATISTICAL ANALYSIS 114
9 APPENDIX 115
10 REFERENCES 139

List of Figures

Figure 1: The location of the LVChP, 3VChP and 4VChP 13
Figure 2: Schema depicting the major cell types found in the LVChP 14
Figure 3: Functions of the lateral ventricle choroid plexus (LVChP). 18
Figure 4: The ventricular system of the mouse brain. 19
Figure 5: The V-SVZ stem cell niche showing a schema of the composition and organisation of the V-SVZ lateral wall. 21
Figure 6: Sex differences 26
Figure 7: Hormone levels during the estrous cycle 29
Figure 8: M1 and M2 macrophage polarisation. 33
Figure 9: The LVChP integrates different signals resulting in transcriptome and secretome changes 38
Figure 10: Comparison of LVChP structure between the sexes 40
Figure 11: Alternating patterns of arteries and veins throughout the LVChP. 41
Figure 12: RNA sequencing workflow of whole adult male and female LVChP 42
Figure 13: GSEA analysis of male and female LVChP transcriptome. 44
Figure 14: Analysis of DEGs between male and female LVChP. 46
Figure 15: DEGs in male and female LVChP 47
Figure 16: Validation of DEGs in female (magenta) and male (blue) LVChP 50
Figure 17: ENRICHR cell type analysis of DEGs 51
Figure 18: Border-associated macrophages (BAMs) in the LVChP 53
Figure 19: Sex differences in LVChP stromal macrophages. 55
Figure 20: Expression of MRC1 in stromal macrophages 56
Figure 21: Expression of P2RY12 in epiplexus macrophages 58
Figure 22: Expression of TMEM119 in epiplexus macrophages 60
Figure 23: Upregulated macrophage-associated genes in male and female LVChP. 62
Figure 24: *In vitro* functional experiments of LVChP regulation of V-SVZ NSCs 65
Figure 25: LVChP ligands and secreted factors between sex. 67

Figure 26: Hormone levels during the estrous cycle. 68
Figure 27: Analysis of DEGs between estrous and diestrous phase. 69
Figure 28: Antibody array of estrous and diestrous LVChPsec 70
Figure 29: Differences in LVChP macrophages during the estrous cycle 71
Figure 30: Whole mount LVChP explants 73
Figure 31: Testing different conditions in whole mount preparations 75
Figure 32: Preparation and proteomic analysis of LVChP CM. 76
Figure 33: Workflow for dissociation of the LVChP into single cells 77
Figure 34: Flow analysis of dissociated LVChP. 78
Figure 35: Dissociation of the LVChP into single cells 80
Figure 36: Flow cytometry for LVChP cell types. 81
Figure 37: Expression of ChP-ligand receptors in V-SVZ NSCs. 87
Figure 38: Differences in the LVChP ECM between the sexes 90
Figure 39: The four core genotype (FCG) mouse model. 95

List of Tables

Table 1: Parameters tested for dissociation of LVChP into single cells. 78
Table 2: Male and female LVChP DEGs. 116
Table 3: GSEA analysis of male and female LVChP transcriptome 118
Table 4: Ligands upregulated in male and female LVChP. 126
Table 5: Estrous and diestrous LVChP DEGs. 127
Table 6: Upregulated male and female macrophage-associated genes. 131
Table 7: Upregulated diestrous and estrous LVChP macrophage-associated genes 136

Abbreviations

A2m	alpha-2-macroglobulin
AD	Alzheimer's disease
aNSC	activated neural stem cell
BAM	border associated macrophage
Bst2	bone marrow stromal cell antigen 2
ChP	choroid plexus
CM	conditioned medium
CNS	central nervous system
CSF	cerebrospinal fluid
ECM	extracellular matrix
FACS	fluorescence activated cell sorting
IBA1	allograft inhibitory factor 1 = AIF1
IFN	interferon
IHC	immunohistochemistry
IL	interleukin
LVChP	lateral ventricle choroid plexus
LVChPsec	LVChP secretome = CM
MRC1	Mannose Receptor 1 = CD206
MS	Multiple sclerosis
NSC	neural stem cell
PD	Parkinson's disease
P2RY12	purinergic receptor P2Y12
qNSC	quiescent neural stem cell
qPCR	quantitative PCR
RNAseq	RNA sequencing
TMEM119	transmembrane protein 119
TTR	transthyretin
V-SVZ	ventricular-subventricular zone

Abstract

The cerebrospinal fluid (CSF) flows through the ventricles of the brain and plays an important role in the transport of nutrients and signalling molecules throughout the ventricular system. CSF composition is dynamic and changes with ageing, but also in different physiological states. The choroid plexus (ChP) produces CSF and by physically separating the CSF from the circulation, forms the blood-CSF barrier. As a central hub with multiple functions, the ChP is emerging as a key contributor to normal brain physiology and disease. Despite its important role in brain function, sex differences in the ChP remain poorly understood. Here we investigate sex differences in the lateral ventricle choroid plexus (LVChP) at the anatomical, cellular and molecular levels. Our comparison of the male and female LVChP transcriptome revealed marked sex differences in various aspects of LVChP functions. Furthermore, cell type analysis of differentially expressed genes in male and female LVChP revealed a prevalence of macrophage-associated genes in the female LVChP. Quantification of LVChP macrophages *in vivo* revealed enrichment of different subpopulations in males and females, with an overall higher number of macrophages in females. In addition, male and female LVChP-secreted factors had different effects on FACS-purified male and female adult neural stem cells *in vitro*. Taken together, these results show that male and female LVChP differ at cellular, transcriptomic and secretory levels, suggesting differences in their function and differential regulation of adult neural stem cells of the ventricular-subventricular zone (V-SVZ). Finally, the establishment of a dissociation method to obtain single viable LVChP cells opens the way for further ongoing analyses, including single cell RNAseq profiling of adult male and female LVChP, which will shed light on further cell type-specific sex differences in gene expression and function. These findings contribute to a better understanding of sex differences in the LVChP at the cellular and molecular level. Further research in this field will provide insights into the underlying processes and functional relevance of sex differences in the LVChP, which in turn may drive the development of sex-specific therapeutic strategies in clinical settings.

Acknowledgements

This thesis is the culmination of almost five years of challenges and triumphs, including the navigation a global pandemic and starting a family, including the arrival of not one, but two incredible sons. My time in the Doetsch lab would not have been possible without the help and support of colleagues, friends and family members. They have supported me endlessly and for that I am very grateful.

First of all, I would like to express my deepest appreciation to my supervisor, Fiona Doetsch. Your belief in me and the opportunities you have provided have shaped me into a better researcher and scientist. Your invaluable advice has made me grow not only in the field of scientific research but also as a person. I admire your ability to remember the smallest details and synthesise knowledge thoughtfully and that you remind me to see the bigger picture.

Next, I would like to thank Violeta Silva-Vargas, whose unwavering presence and camaraderie strengthened me during the “trials” of numerous experiments. Together we have navigated the rollercoaster of emotions and shared laughter and frustration. Viole, you truly bring a radiant glow to the lab. Your unwavering commitment has exceeded all my expectations and has had an indelible impact on my scientific journey.

The tapestry of my experience at the Biozentrum would be incomplete without the colourful threads woven by my exceptional colleagues and students whose presence filled the corridors of our shared endeavours. Ana, Celina, Corina, Dimitris, Eleni, Fabrizio, Hanae, Karol, Melvin, Thomas, Valérie and Zayna, each of you holds a special place in my heart. Your collective brilliance, boundless support, kindness and guidance have shaped not only my scientific growth but also my personal development during my time in the Doetsch lab. Thank you, thank you, thank you.

Finally, I would like to thank my family, who have supported me from the very beginning of my studies and without whom I would not be who I am. A special thanks goes to my beloved wife, Natascha, who so often waited patiently for the elusive "five more minutes" before I made my way home to her. Your unwavering encouragement, unwavering support and boundless love have strengthened my spirit and brightened my path. And Milo and Devin, your infectious smiles and joyful laughter have brightened every evening and filled even the most difficult days with light. I love you three with all my heart and am forever grateful for your presence and love.

1 Introduction to the choroid plexus

1.1 History of the choroid plexus/ CSF system

The central nervous system (CNS) is involved in the integration and processing of peripheral information to ensure the proper functioning of the entire body. It consists of the spinal cord and the brain, and given its important role, is highly protected. The vertebrae protect the spinal cord from physical harm, while the brain is protected by the skull. Additionally, the brain is cushioned by a liquid called the cerebrospinal fluid (CSF) [1]. The main producers of CSF are the choroid plexuses (ChPs), found in each of the brain ventricles. The ChPs form a barrier between the CSF and the blood and play an important role in brain homeostasis [2, 3].

Cerebrospinal fluid (CSF) has captivated the scientific community for several millennia, evoking both interest and confusion. The earliest known reference to brain fluid dates back to ancient Egypt (~1700 BC) [4]. It wasn't until over a millennium later, when the Greek physician Hippocrates introduced the term "hydrocephalus" to describe the enlargement of the brain ventricles, which he associated to an excess of "water" causing expansion of the ventricles [4]. However, after Hippocrates' report, and Galen's description of an "excretory fluid" in the brain, the CSF was not a subject of discussion for centuries [4]. The discovery of the presence of CSF in the ventricles is attributed to Domenico Felice Cotugno [5]. The advent of new autopsy techniques at this time allowed the retention of CSF in the ventricular spaces and facilitated observation of its existence. Nevertheless, it took until 1842 for Francois Magendie to provide the first empirical evidence of the circulation of CSF through experimental studies, thus introducing the term "cerebrospinal fluid", which is used today [5]. This term replaced the earlier generic term "water in the brain" and emphasised the important role that this clear and colourless liquid plays in the function and protection of the CNS.
Herophilus, a Greek physician who lived between 335-280 BC, is credited with discovering the ChP. Due to its resemblance to the choroid of a foetus, he called it "choroid meninx" [2]. Galen of Pergamum, who lived between 129-200 AD, was the first to acknowledge the role of the ChP in producing CSF in the brain [2, 4]. It was Galen's hypothesis that this tissue transformed the "vital spirits" of the blood into "animal spirits," which then passed through the brain ventricles [2]. Later, during the Renaissance period, Andreas Vesalius provided a detailed description of the ventricles, estimating that the CSF filling the ventricles and encircling the brain accounts for approximately one-sixth of the brain's volume [2, 6]. Remarkably, modern magnetic resonance imaging (MRI) techniques estimate the volume of CSF to be 18% of the brain's volume, which is very close to Vesalius' estimation [7]. William Mestrezat was the first to provide an accurate description of the chemical composition of CSF [8]. Harvey Cushing, also known as the "father of neurosurgery", established that CSF is secreted by the ChP [9, 10] thereby bringing the "*two-thousand-year saga of the CSF into the modern era*" (cited from [11]).

The choroid plexuses: a short overview

The ChPs are highly vascularised epithelial structures that are found floating in each of the brain ventricles. As such, there are two lateral ventricle choroid plexuses (LVChPs), one third ventricle choroid plexus (3VChP) and one fourth ventricle choroid plexus (4VChP). They are best known for producing most of the CSF via transport of water and ions across their epithelium and also forming a barrier between the blood and the CSF. The ChP actively secretes blood-derived and ChP-derived factors into the CSF to regulate CNS homeostasis. [12]. It contains a number of stromal cells, including endothelial cells, pericytes, fibroblasts, oligodendrocytes, neurons and immune cell populations such as macrophages, dendritic cells and T cells [13]. In addition, there is another unique population of macrophages that sit on top of the epithelial layer directly exposed to the CSF, called Kolmer or epiplexus cells [14]. Other described functions of the ChP include immune surveillance and regulation of neurogenesis and oligodendrogenesis in the adult ventricular-subventricular zone (V-SVZ) stem cell niche [15]. Finally, dysfunction of the ChP may contribute to the development of neurological diseases such as hydrocephalus, Alzheimer's disease (AD), and multiple sclerosis (MS). Therefore, it is important for both basic research and clinical treatment to gain a better understanding of the ChP and its functions [3, 16].

1.2 Development of the choroid plexus

The choroid plexus (ChP) arises from neuroepithelial cells lining the ventricles early in embryonic development [17]. The ChP develops shortly after neural tube closure and first appears in the mouse at embryonic day 11 (E11) [18]. The ChP is functionally and morphologically distinct from the ependyma, although it is continuous with it [6].

In mammals, the ChPs of the different ventricles develop in a specific sequence: the 4VChP develops first, followed by the LVChPs, and finally the 3VChP [18]. Four stages of ChP cell development have been identified in humans and sheep, which can be roughly correlated with those in mice [19, 20].

In mice, stage I occurs around E11-E12, stage II between E13-E15, stage III between E16-E18 and the final stage around postnatal day 0 (P0). During these stages, the ChP cells undergo morphological changes from pseudostratified to cuboidal, develop different glycogen content and show altered apical-basal polarity of the cell nuclei [19].

As a highly active secretory tissue, the ChP is so abundantly supplied with blood that it pulsates slightly with every heartbeat [21]. During maturation, ChP cells show an increase in the total volume of mitochondria and more extensive development of their apical brush border, thus adopting properties characteristic of highly active secretory epithelia [22]. Early CSF production causes the brain ventricles to expand while the system is still closed, contributing to the shaping of the brain [23]. Additionally, a number of growth factors and cell cycle modulators are produced during ChP development, including retinoic acid, members of the wingless-related integration site (WNT) and transforming growth factor β superfamily, insulin-like growth factor 2 (IGF2) and fibroblast growth factors (FGFs) [6, 24]. These substances are released from the ChP into the CSF and have both autocrine and paracrine effects and are involved in the development, growth and survival of neurons, but also in other processes including hindbrain morphogenesis in the developing nervous system [25-27]. Given that these processes are crucial for proper brain growth and function, it is not surprising that the ChP develops barrier functions very early, allowing for tightly regulated production of CSF at early stages of development.

1.3 The adult choroid plexus structure

The two LVChPs differ in structure from the choroid plexuses of the third and fourth ventricles. While the ChP of the third and fourth ventricles have a coiled and rolled appearance with finger-like projections (Figure 1C'', D') [28], the LVChP typically has a more sheet-like appearance (Figure 1B, C'). This thesis will focus on the structure and function of the LVChP in adult mice.

The LVChP has an approximate length of five to seven mm and extends from the caudal towards the rostral area of the lateral ventricles, thereby spanning almost the entire ventricular lumen. The LVChP shows distinct morphological differences between the rostro-caudal and dorso-ventral regions (Figure 1B). The rostral region occupies a larger surface area compared to the caudal region. The folding of the ChP is most prominent in the dorso-rostral and caudal region and is best observed in coronal sections of the brain. A non-folded/ straight stalk portion connects the folded dorsal part to the ventral region of the tissue (Figure 1C'). The ChP is connected to the brain parenchyma at its most caudal part. Additionally, filiform-like extensions of cells are distributed in the ventral part of the LVChP, anchoring the tissue to the ventricular cavity (Figure 1B).

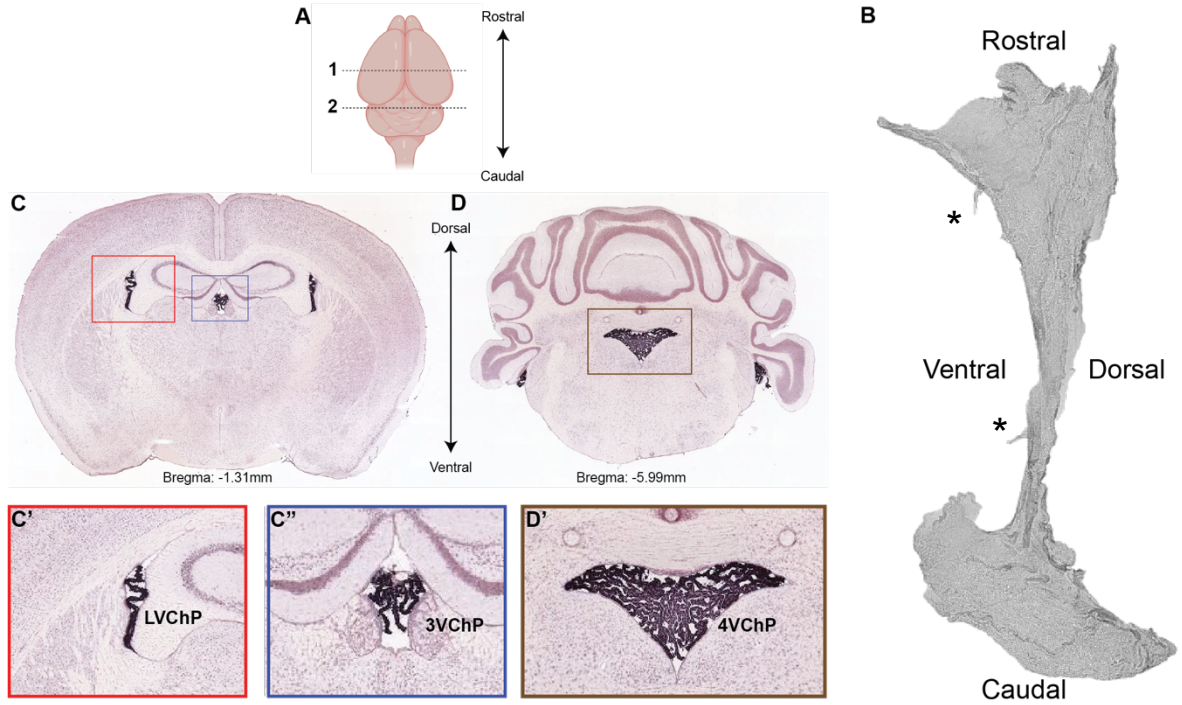

Figure 1: The location of the LVChP, 3VChP and 4VChP
A) Schema of a mouse brain showing the rostro-caudal axis and where the two sections in C and D are found along this axis. B) is a whole mount preparation of the LVChP showing its rostro-caudal and dorsal-ventral orientation. The * show filiform-like extensions on the ventral side of the LVChP. C) is a cross-section at Bregma -1.31mm showing the LVChP and 3VChP, with C') and C'') showing higher magnification. D) is a cross-section at Bregma -5.99 showing the 4VChP, with D') showing higher magnification. All images are coronal cross-sections taken from the Allen Brain Atlas (https://mouse.brain-map.org/experiment/show/72119590) of in situ hybridization experiments for Klotho, a gene highly expressed in the ChP epithelium. The brain schema in (A) was created with BioRender.com.

1. 4 Cell types of the ChP

The LVChP is a complex structure composed of various cell types, which support its multifunctional properties. In adults, it comprises a monolayer of cuboidal epithelial cells, enclosing a highly vascularised stroma composed of a network of fenestrated blood vessels, pericytes, fibroblasts, neurons and immune cells (Figure 2).

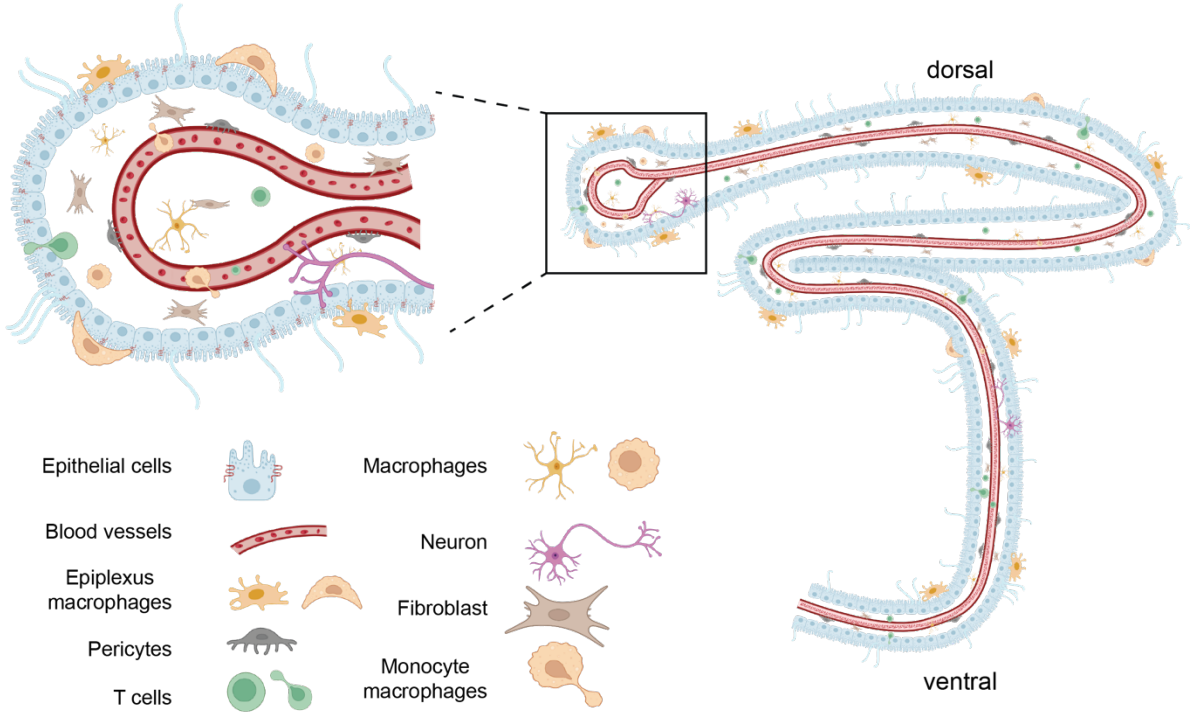

Figure 2: Schema depicting the major cell types found in the LVChP
Created with BioRender.com

1.4.1 ChP epithelial cells

Epithelial cells make up the majority of cells in the ChP. They have a polarised cuboidal morphology and form, via their tight junctions, the blood-CSF barrier.

On their apical side, ChP epithelial cells increase their surface contact with the CSF via a dense carpet of microvilli and finger-like projections called "fronds" that extend from the surface of the plexus into the ventricular cavity [29, 30]. In addition, primary cilia with a 9+0 microtubule arrangement are found on the apical surface of epithelial cells [22, 31-33]. These ciliary tufts presumably serve as mechano- and chemo-sensory organelles [31]. In contrast, virtually all ependymal cells lining the ventricular wall have a typical 9+2 arrangement of motile cilia. The microvilli and cilia located on the ChP result in a larger ratio of apical surface area to epithelial volume. This ratio is about 30 times greater than would be expected for a 10µm cuboidal cell without microvilli [22].

Epithelial cells function as an active interface characterised by a high proportion of mitochondria throughout the cytoplasm and numerous Golgi apparatuses involved in a high degree of transport [34, 35]. Epithelial cells of the choroid plexus are involved in actively regulating the transport of factors from the bloodstream, and also ChP-derived factors, into the CSF via its abundance of transporters and channels situated on the apical side. On the basolateral side of the epithelium, extensive infoldings/interdigitations increase the surface area between the epithelium and the interstitial fluid in the stroma of the ChP, which increases with maturation [22]. Transporters and ion channels are also concentrated on the basal side of the cell to facilitate vectorial transport and CSF production.

1.4.2 ChP stroma

The ChP stroma is separated from the epithelium by a basal lamina. Many cell types are found inside the ChP stroma, including pericytes, fibroblasts, immune cells and neurons (Figure 2) [13]. The ChP is highly vascularised and contains fenestrated capillaries that allow access of water, ions and other blood-borne factors and cells into the ChP stroma. Blood enters the ChP via the anterior and posterior choroidal arteries and exits via the choroidal vein [36]. Because of the extensive network of large capillaries throughout the choroidal stroma, the local blood flow in the ChP is ten times higher than the rest of the brain and five times higher than in the kidneys [37, 38].

The ChP also contains immune cells that play a role in several immunological activities, including the uptake and presentation of antigens and the release of cytokines. Macrophages and dendritic cells (DCs) can be found in the stroma of the ChP. They extend protrusions between the epithelial cells towards the CSF [39, 40], which allow them to scan the CSF for antigens to present to T cells located in the ChP stroma [41, 42]. In contrast to stromal macrophages, which are eventually partly replaced by bone marrow-derived cells, Kolmer, or epiplexus macrophages are located on the apical side of the epithelial layer facing the CSF and share ontogeny with microglia, without being replenished by bone-marrow derived monocytes [14, 39, 43, 44]. Macrophage populations will be discussed in more detail in section 3. The current understanding of the ChP lymphocyte population is unclear. While some studies have detected T cells in human ChP from control donors [45], other studies have not [39]. Further, B and plasma cells have not been detected in the ChP under healthy conditions [39]. A comprehensive description of the immune cell populations in the human ChP, including T cell subsets and their distribution in the different compartments of the CNS, as well as unknown cell types such as granulocytes and natural killer cells, remains an important aspect of ChP biology to be addressed.

1.4.3 The LVChP extracellular matrix

The LVChP contains a rich extracellular matrix (ECM), consisting of a network of proteins and molecules, collectively known as the matrisome, that provide structural support to its cells and the tissue as a whole. Despite being commonly associated with mechanical support, the ECM consists of biologically active molecules involved in an array of functions [46]. It consists of two categories: the core proteins and matrisome-associated proteins that interact with the former [47]. There are three main classes of core matrisome proteins: collagens, glycosaminoglycans and adhesive glycoproteins [46]. Collagens provide the main structural support [48], while glycosaminoglycans and adhesive glycoproteins (including laminin and fibronectin) are involved in cellular processes including differentiation, migration and survival. In addition, they are involved in cytokine production and leukocyte recruitment [49-51]. Our knowledge of the ECM in the LVChP is very limited and how it affects LVChP function and CSF composition is virtually unknown.

1.5 Functions of the ChP

The primary function of the ChP is CSF production, which plays a critical role in cushioning and protecting the brain from physical harm and maintaining CNS homeostasis. Secretion of CSF is facilitated by the epithelial monolayer that controls the rate of secretion and also the composition of CSF through *de novo* synthesis of ChP proteins and selective transcytosis of factors from the blood [52, 53]. However, all ChP cells can contribute to the CSF composition, and the effects of the secreted signalling moieties on different brain regions depends on the region that is analysed [25].

In addition to its secretory functions, the tight junctions between ChP epithelial cells form the Blood-CSF-Barrier (BCSFB), which protects the brain from toxic compounds present in the blood and dramatic fluctuations in plasma composition, thereby forming a neuroprotective barrier [54, 55]. Furthermore, the ChP plays a critical role in removing toxins and waste products of brain metabolism and regulates the flow and distribution of numerous factors that can impact brain function. Its location in the brain ventricles allows for continuous immunological surveillance by immune cells found in the LVChP, making the ChP an essential gateway for immune cells' passage into the CSF [56, 57].

The expression of numerous receptors on epithelial cells enables the ChP to respond rapidly and dynamically to a variety of signals. As such, the ChP functions as an “antenna” in the brain, receiving signals from the body and responding by altering its transcriptome, translatome, and secretome, thus being fundamental for the control of metabolic and neuroendocrine processes in different regions of the CNS. It synthesises several signalling factors necessary for CNS function, including regulatory factors of adult neural stem cell niches [3, 15, 58]. Finally, emerging evidence suggests that the LVChP plays a role in regulating circadian rhythm [59]. Overall, the ChP cells play a crucial role in brain development, nutrition, protection, homeostasis, and repair. Deterioration of ChP function due to ageing, disease, or injury can have a substantial impact on brain physiology (Figure 3) [17].

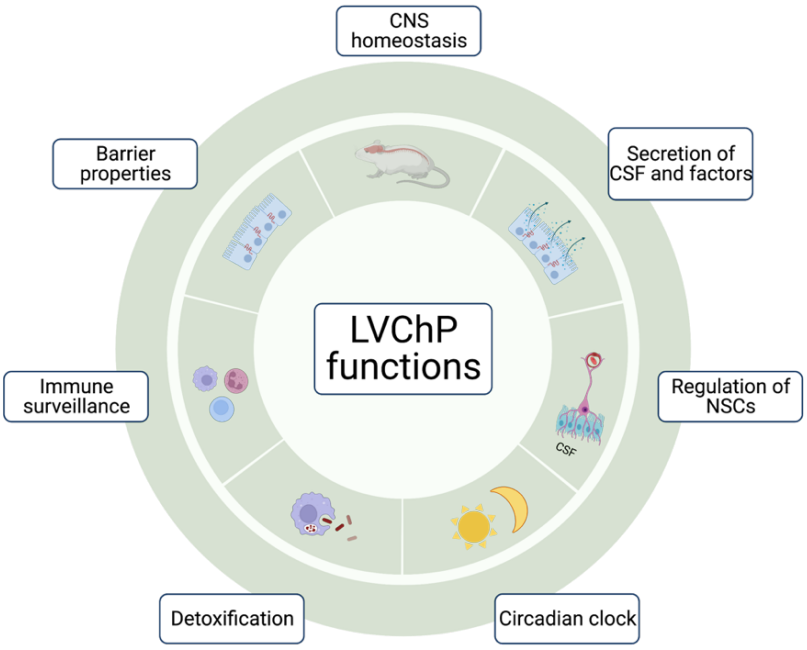

Figure 3: Functions of the lateral ventricle choroid plexus (LVChP).
Created with BioRender.com

1.5.1 CSF production

In the brain, the interstitial fluid (ISF) and the CSF are the two most frequently encountered extracellular fluid environments. It has been suggested that 10-30% of CSF arises from the outflow of ISF, produced, among others, by glia and neurons, through the ependyma into the brain ventricles [6].

The CSF is not solely a filtrate of blood, but is produced via an active and tightly regulated process by the ChP [60]. The ChP is responsible for producing the bulk amount of the CSF (~70-80%) [53, 61, 62]. Secretion of CSF from the ChP is facilitated by an osmotic gradient, with the ChP promoting the transport of osmotically active ions prior to the influx of water from the plasma into the CSF [60]. This process is regulated by the interaction of a number of membrane transporters and water channels, including AQP1, which is located in the apical membrane of ChP epithelial cells [60]. The first step in the process of CSF secretion is the passive filtration of plasma through the fenestrated capillary network and into the connective tissue of the ChP. The second step is the active transport of ions through the epithelial cells of the ChP into the ventricle. This is supported by transport proteins located in the apical and basolateral membranes of the epithelial cells [63]. However, a recent study has shown that secretion of CSF can also occur independently of an osmotic gradient, through the active regulation of membrane transporters such as NKCC1 [64].

1.5.1.1 CSF dynamics and the ventricular system

The CSF flows through the ventricular system, the spinal cord and the subarachnoid spaces [53]. The ventricular system comprises interconnected cavities that run throughout the brain and brainstem (Figure 4). The CSF provides buoyancy to the brain by filling the cerebral ventricles and surrounding the pia mater, reducing the weight of the brain [65, 66]. The total volume of CSF in humans is about 150mL. However, only about 25mL is found in the ventricles, while the rest is found in the spinal cord and subarachnoid space.

CSF is produced at a rate of 0.2-0.4mL per minute per gram of tissue, resulting in a turnover of three to four times per day. In mice, the volume of CSF is much smaller (35µl) and its production rate is about 0.3µl per minute. As in humans, CSF turnover in mice occurs three to four times per day [53, 63, 67]. CSF turnover facilitates the efficient removal of waste products and toxins and also allows for the high turnover of factors present in the CSF. CSF content is dynamic and undergoes significant changes during development, age, pathological conditions and even in various physiological states [68]. CSF production and turnover decrease with age and in various neurodegenerative diseases, leading to accumulation of amyloid proteins, metabolites and toxins [69].

1.5.1.2 CSF circulation and drainage

In the brain CSF circulation goes from a rostral-to-caudal direction, beginning in the lateral ventricles (LV), then flowing through the interventricular foramina into the third ventricle (3V), crossing the cerebral aqueduct to enter the fourth ventricle (4V) (Figure 4). CSF then exits the brain and circulates around the spinal cord and in the subarachnoid space [70]. Drainage of CSF occurs at multiple sites, including the arachnoid, perineural sheaths, and dural lymphatics [60, 71-73]. The unidirectional and pulsatile flow of CSF is influenced by various factors such as the beating of cilia of ependymal cells, pulmonary respiration and even vasomotion [74, 75].

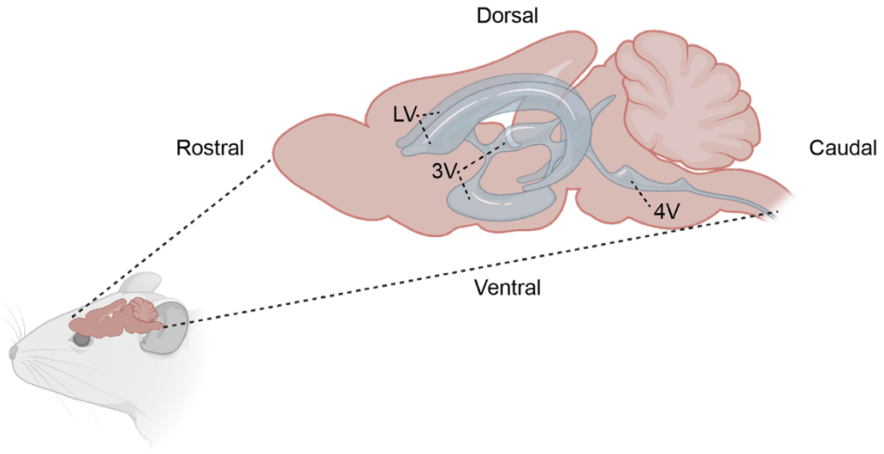

Figure 4: The ventricular system of the mouse brain.
This schema depicts a sagittal view of the mouse brain showing the ventricular system (grey). Abbreviations: LV = Lateral ventricles, 3V = Third ventricle, 4V = Fourth ventricle. Created with BioRender.com

1.5.1.3 The ChP secretome and factors in the CSF

The biochemical composition of CSF is tightly regulated as it plays a role in maintaining CNS homeostasis under normal physiological conditions [6]. The CSF is a complex mixture of components, not “just” an aqueous solution containing ions including sodium, chloride and phosphate, as was commonly believed [76]. This mixture contains lipids, microRNAs, extracellular vesicles, hormones, glucose and a variety of proteins (including growth factors, neuropeptides and cytokines) [77-80]. Both blood- and brain-derived molecules contribute to the highly variable composition of CSF. Albumin, immunoglobulins, vitamin C, prolactin, leptin and folate are examples of actively transported factors from the blood into the CSF [78, 81]. At the same time, the ChP has been shown to synthesize and secrete different classes of signalling molecules including transthyretin (TTR), insulin growth factor 2 (IGF2), brain-derived neurotrophic factor (BDNF) and prolactin into the CSF, which all play a role in important biological processes in the brain including development, growth and neuroprotection [15, 78, 82]. In this way, the ChP secretome and CSF composition can be rapidly adjusted to demand, helping to maintain brain homeostasis [35, 83].

1.5.2 Barrier properties

Brain barriers, which include the blood-brain-barrier, the blood-arachnoid-barrier, blood-spinal cord barrier, and the blood-cerebrospinal fluid-barrier (BCSFB), play a crucial role in regulating the concentrations of ions and nutrients in the CSF and ISF, ensuring optimal brain function [84-86]. The variability of barriers is contingent upon both species-specific factors and the distinct expression and functional properties of transporter proteins [86]. The BCSFB is formed by all the ChPs, which acts as a checkpoint to limit the transfer of substances from the blood to the CSF and protects the CNS from harmful substances.

The integrity of this barrier depends on maintaining a tight epithelial layer, primarily achieved through tight junctions (TJs), formed by claudins, occludins and junctional adhesion molecules coupled to adaptor proteins (zonula occludens proteins). Other junctional proteins supporting this barrier are adherens junctions and desmosomes [87, 88]. TJs limit passive transport of substrates from the blood to the CSF, thereby reducing paracellular diffusion, and protect the CNS despite being highly permeable to certain substances. This process is tightly regulated by transport mechanisms and metabolic enzymes to prevent the entry or exit of toxins, drugs, and other xenobiotics [85, 89-91].

Dysregulation of the transport mechanisms by the BCSFB has been associated with several CNS pathologies, such as AD, Parkinson’s disease (PD), epilepsy, inflammation, depression, ischemia, brain tumours, mental retardation and HIV [55, 87, 92]. Destruction of the BCSFB has severe consequences and strongly contributes to the pathophysiology of CNS inflammation [93]. These characteristics indicate that the BCSFB is an active interface as opposed to a passive barrier.

1.5.3 Regulation of neural stem cells/ neurogenesis

1.5.3.1 The ventricular-subventricular zone (V-SVZ)

Neurogenesis occurs in two distinct areas of the adult mouse brain, the ventricular-subventricular zone (V-SVZ) and the subgranular zone [94]. The V-SVZ is responsible for producing interneurons for the olfactory bulb and consists of three main regions: the more oligodendrogenic septal wall adjacent to the septum, the more proliferative and neurogenic lateral wall, and the roof beneath the corpus callosum [94, 95]. A monolayer of multiciliated ependymal cells propel the CSF through the ventricular system and create a diffuse barrier between the CSF and the V-SVZ neural stem cell (NSC) niche [96, 97]. Adult NSCs in the V-SVZ are a unique type of astrocyte that express glial fibrillary acidic protein (GFAP) [98]. They can be either quiescent or in an activated state and show an apical-basal polarity. Apically, NSCs project a primary cilium into the CSF at the centre of pinwheel-shaped structures of the ependymal cells, thereby bringing them into direct contact with the CSF. As a result, they can be regulated by factors in the CSF, making the LVChP an important niche component of the V-SVZ [15, 99-102]. On the basal side, the stem cells are in contact with the planar vasculature of the BBB, which is permeable to small molecules (Figure 5) [103].

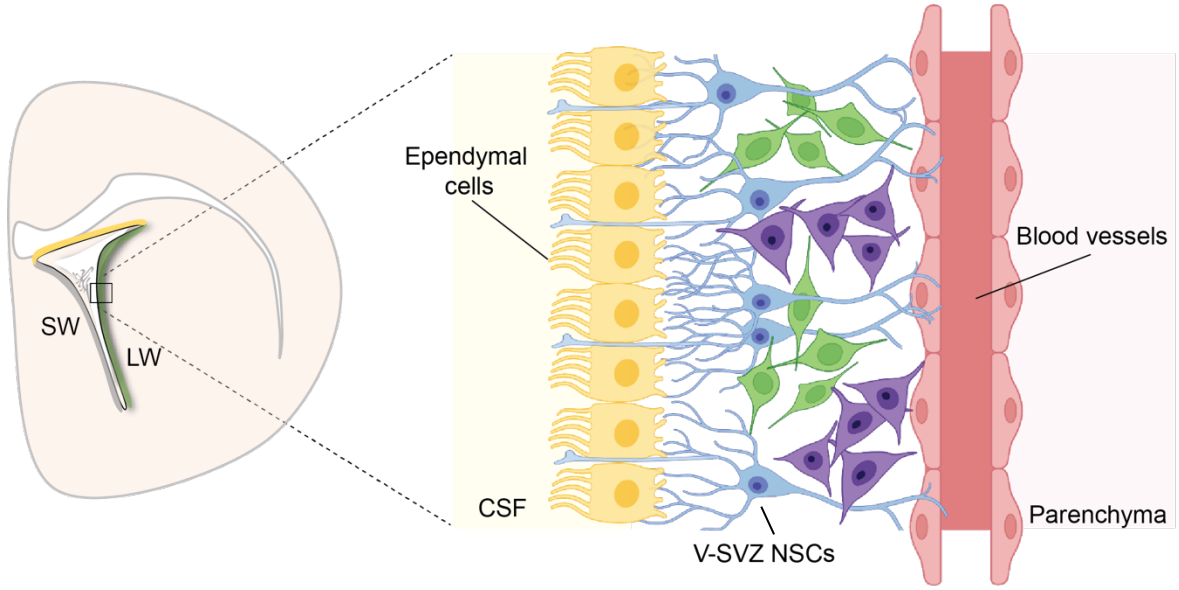

Figure 5: The V-SVZ stem cell niche showing a schema of the composition and organisation of the V-SVZ lateral wall.
Abbreviations SW: septal wall, LW: lateral wall, CSF: cerebrospinal fluid, NSCs: neural stem cells, V-SVZ: ventricular-subventricular zone. Created with BioRender.com

1.5.3.2. LVChP regulation of neural stem cells

Neural stem cell maintenance is a highly intricate process, modulated by a wide range of signalling moieties such as hormones, growth factors, and neurotransmitters [15, 104-106]. The CSF composition is essential for foetal development and regulation of NSC maintenance during adulthood, instructed to a large extent by extrinsic factors released from the LVChP [105]. The LVChP secretome, serving as a source of signalling molecules, plays a crucial role in the regulation of quiescence, activation, and proliferation of V-SVZ cells. Notably, the influence of the ChP secretome appears to be age-dependent with a decline in NSC activation *in vitro* and *in vivo* with age [15, 27].

LVChP secreted factors, including leukaemia inhibitory factor (LIF), wingless / frizzled pathway modulators, and growth factors such as insulin like growth factor 1 and 2 (IGF1, IGF2) and bone morphogenetic protein 5 (BMP5), promote NSC proliferation, survival, and recruitment [15, 17, 27]. In contrast, prostaglandin D2, interleukin 1 beta (IL1-β) and neurotrophin-3 (NT-3) inhibit NSC proliferation [15, 104, 107]. Additionally, vitamin A, converted to retinoic acid by the LVChP, promotes cell differentiation and causes cell cycle arrest [108, 109]. LVChP secreted microRNA-204 (mir-204) regulates several genes involved in cell cycle regulation, neuronal migration, and differentiation and controls the maintenance of quiescent NSCs [110]. Similarly, another LVChP-derived factor, OTX2, affects neuroblast migration and the number of new-born olfactory bulb neurons, and its activation alters ECM components and signalling molecules produced by astrocytes [111]. Finally, a recent study has shown that small extracellular vesicles secreted by the LVChP can also regulate adult neurogenesis and maintenance of olfaction [112]. .

In summary, several studies have shown that the LVChP is an integral part of the V-SVZ niche, and that its secreted factors play a crucial role in regulating NSCs and neurogenesis.

1.5.4 Immune surveillance

The brain was long considered an immune-privileged site, meaning that it was fundamentally excluded from immune surveillance. However, research over the past years has demonstrated that the brain is in fact immune-supervised to some degree. This is supported by several lines of evidence indicating the controlled migration of lymphocytes from the blood into the CSF via the ChP [113-116].

In healthy humans, the CSF contains about 3000 lymphocytes per mL, and the T-cell population in the CSF is greater than in the blood plasma, specifically with a higher concentration of CD4+ T cells that have surface markers associated with central memory cells [117]. This notion is consistent with the fact that fluorescently labelled lymphocytes can be detected in the ChP stroma and meninges in mice within two hours of intravenous injection [118]. These observations suggest that the ChP plays an active role in screening the CSF. Under normal conditions, the brain contains very few lymphocytes in the absence of an inflammatory stimulus [119]. After an inflammatory insult, however, lymphocytes can enter the CNS via at least three pathways, including blood to the parenchymal perivascular space, blood to the subarachnoid space (via CSF flow), and blood to the CSF via the ChP [119].

Given these results, it is possible that the ChP is a site of lymphocyte infiltration into the CSF since the LVChP plays a crucial role in the communication between the immune system and the nervous system [120-123]. Moreover, ICAM-1 is also crucial for the migration of immune cells from the ventricular CSF back into the ChP stroma in mice, a process associated with T cell reactivation and CSF surveillance [124-127]. This bidirectional movement of immune cells between the periphery and the CSF is regulated by the ChP epithelium, highlighting its involvement in the monitoring of immune cells and homeostasis [128].

The ChP responds differently to acute and recurrent peripheral inflammation. Recurrent peripheral inflammation triggers signalling mechanisms associated with leukocyte migration and the complement cascade [121], while acute peripheral inflammation triggers the innate immune response [129]. Interferons (IFNs) are master regulators of innate immunity and have been linked to many CNS diseases [123, 130]. Altered expression of IFN1 or IFN2 has been linked to cognitive decline in AD. Blocking IFN1 signalling partially restores cognitive function and neurogenesis and restores IFN2-dependent LVChP activity, which is lost with age [123, 130]. Finally, epithelial cells possess the ability to present antigens to T cells along with various adhesion molecules, which suggests that migration across the epithelium is primarily regulated by these cells [56, 131].

1.5.5 Circadian clock

In the body, circadian rhythms are controlled by internal biological clocks that follow an approximate 24-hour cycle [132]. In mammals, the hypothalamic suprachiasmatic nucleus (SCN) acts as the main circadian oscillator, coordinating physiological processes during the 24-hour day-night cycle [133]. The SCN integrates and synchronises other peripheral oscillators located in different tissues and organs, ensuring that physiological activities are appropriately timed in relation to the environment [133, 134]. Disruption of circadian rhythm regulation can lead to sleep disorders, psychological disorders, metabolic diseases and even an increased risk of neurodegenerative diseases [135-138].

The LVChP epithelium expresses various circadian clock genes [139], suggesting the presence of a circadian oscillator specifically in these cells [140, 141]. The LVChP interactions with the SCN and pineal gland are believed to ensure a stable 24-hour rhythmicity [141]. Remarkably, even after tissue removal, the LVChP maintains a circadian rhythm for six to seven days [142]. Furthermore, the expression of canonical clock genes precedes that of the SCN, which contributes to the regulation and timing of CSF production and clearance, showing that the LVChP may be regulating the SCN clock by an undescribed mechanism [59, 140].

These findings have uncovered a novel role for the LVChP in the control of circadian rhythms, which presents exciting avenues for future research into the underlying mechanisms of this complex physiological process. However, this area remains relatively understudied, and additional investigations are necessary to further elucidate the LVChP's role in the regulation of circadian rhythms.

1.5.6 Detoxification and chemical surveillance

The ChP plays a critical role in maintaining homeostasis in the brain by producing CSF, secreting proteins that regulate stem cell pools in the V-SVZ, responding to pathogens, and eliminating potentially harmful chemicals coming from the blood and the brain. Therefore it is undeniable that the ChP responds to the demands of the CNS based on the chemical composition of the blood and CSF. The ChP employs various enzymes and antioxidant systems to metabolise drugs and eliminate potentially harmful chemicals from the blood and the brain [143]. Many hazardous chemicals can be converted by cellular metabolic processes into water-soluble, less pharmacologically or toxicologically active metabolites. Multiple studies have demonstrated the presence of enzymes in the ChP involved in these processes, including phase I and II enzymes and antioxidant enzymes [144-147].

The expression of receptors involved in olfactory and taste signalling have been reported in the LVChP [147-149]. Olfactory receptors are also expressed in other organs and are involved in detection of non-volatile chemicals in body fluids [150, 151]. For this reason. it is likely that expression of olfactory and taste genes allows the LVChP to detect and “taste” the chemical composition of the CSF and the blood [149].

In addition, accumulation of amyloid β in the CSF, a protein considered to be one of the underlying causes of AD, causes impaired oxidative phosphorylation and leads to increased oxidative stress, morphological structural changes, toxicity, inflammation, and neurodegeneration. Thus, proper clearance of amyloid β is crucial for brain homeostasis. Specialised transport mechanisms and proteolysis by amyloid-degrading enzymes secreted by the ChP, including ABC transporters, promote amyloid β clearance [152-154].

In summary, the LVChP is a critical component of the CNS, responsible for a number of essential functions. These include CSF production, formation of the BCSFB, immune surveillance, circadian rhythmicity and chemical surveillance. The ChP serves as a dynamic hub that integrates signals from the CSF and circulation and responds accordingly by changing its transcriptome and secretome. Any abnormalities or disruptions in the LVChP’s function can have devastating consequences, leading to hydrocephalus or neurodegenerative diseases. Therefore, understanding the molecular mechanisms underlying ChP functions is vital for our ability to develop methods to actively ameliorate different aspects of CNS homeostasis in various pathological conditions. As such it may be important to study the ChP in different physiological states, but also to compare differences in the ChP biology based on sex.

2 Sex differences

The study of sex plays an important role in medicine and biology [155]. Several common diseases, such as AD, schizophrenia, autoimmune diseases and cardiovascular disease, have sex differences in prevalence, severity and progression, suggesting that sex is an important variable in understanding the causes of these diseases [156]. However, sex differences are not limited to diseases. Many aspects of normal physiology and development, including the brain and its behaviour, are also profoundly affected by sex differences [155, 157]. Furthermore, there are fundamental differences between the sexes that go down even to the molecular level of an individual cell [158].

Unfortunately, biomedical research uses more male than female animals, and many studies do not report the sex of the samples or cells used, making it difficult to determine whether sex affects the results observed [159, 160]. The bias towards male animal models is generally due to the widespread assumption that females are more variable due to hormonal fluctuations related to the estrous cycle [161-163]. As such, this raises the concern that previous scientific findings may only apply to males.

The study of sex biology is usually divided into two areas: Sexual dimorphism and differences as a result of sex hormones (Figure 6). Sexual dimorphism refers to anatomical and behavioural differences, while the study of sex hormones examines how differences between the sexes arise due to varying sex hormone levels. Understanding the individual and combined effect of these two areas allows us to determine the biological and physiological differences between the sexes, providing valuable information for various fields such as medicine, developmental biology and psychology.

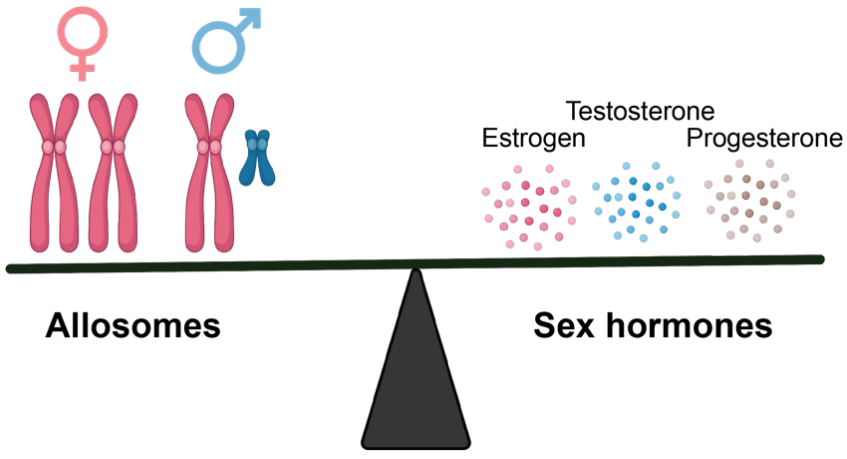

Figure 6: Sex differences
Sex differences can be due to sex chromosomes (allosomes, XX in females and XY in males) or as a result of sex hormones (estrogens, testosterone and progesterone). Created with BioRender.com

2.1 Sexual dimorphism

Sexual dimorphism is the phenomenon in which males and females of the same species show consistent differences in phenotype and genotype [164]. There are examples of sexual dimorphism in nature, including differences in feather colours between males and females in ducks and peacocks. In addition, men and women have different average size and shape and genital anatomy. However, sexual dimorphism also includes differences in cellular and bodily processes such as metabolism and response to drugs and disease [165-167]. These differences are the result of differential gene expression, which ultimately leads to phenotypic differences [168]. Main contributors of sexual dimorphism are the heteromorphic allosomes, also known as sex chromosomes (XX in females and XY in males) [169]. However, sexual dimorphism in gene expression occurs not only in reproductive organs, but also in somatic tissues such as the liver, heart, kidney and brain [170-172]. For example, a study comparing the transcriptomes of several organs from males and females showed that in the mouse liver, about 72% of genes show differential expression between the sexes [172, 173].

2.1.1 Sexual dimorphism in the brain

In the same study mentioned above, the researchers showed that in the brain, only about 13.6% of genes have a sexually dimorphic expression [172]. However, the brains of men and women have striking structural differences, including the size of different regions, grey and white matter content, and also hemispheric asymmetry [174-176]. In fact, in many mammals, the male brain is slightly heavier and larger than the female brain, and sex differences can be seen in different brain regions, even down to the level of individual cells [157, 158]. Finally, sexual dimorphisms in the mammalian brain are not limited to regions with sex-specific behaviours, and they can manifest at various levels of brain complexity, such as synaptic patterns and neuronal density [177, 178].

A recent study by Mizrak et al. compared male and female adult V-SVZ neural stem cell lineages using single cell analysis. This analysis revealed distinct differences between the sexes [95]. Astrocytes isolated from the male V-SVZ were enriched in molecular and metabolic processes associated with stem cell self-renewal, maintenance and proliferation, as well as in G protein-coupled receptor (GPCR) signalling associated with NSC quiescence, whereas astrocytes in the female V-SVZ were enriched in neurotransmitter activity and ion channel pathways [95].

2.2 Sex hormones

The other area studied in the biology of sex differences concerns sex hormones. Testosterone, estrogen and progesterone are the "classic" sex hormones [179]. They regulate numerous facets of development and physiology, including growth and metabolism [180].

Although the gonads are responsible for the majority of sex hormone production [181, 182], evidence for sex hormone production in other tissues, including the brain, has also been published [183-185].

The first estrogen (estrone) was identified in 1923. Originally, estrogen was thought to be a purely female hormone, but it has since been shown to play a crucial role in male reproductive functions as well [186, 187]. Among the estrogens, estradiol is the most abundant form in adults. While its main function is the development of female reproductive tissue, it also plays a role in neuroprotection and influences memory and cognition [188]. Its action is mediated by binding to nuclear and membrane estrogen receptors, which allows it to regulate gene expression [189, 190].

Testosterone is required for testicular development and is often considered the male sex hormone [191]. However, testosterone is also important for women. Before it binds to the androgen receptors, testosterone is usually converted into dihydrotestosterone [165, 192].

Progesterone acts synergistically with estrogen and is important for lordosis, reproduction, the estrous cycle, steroid hormone production, while in the CNS it is involved in physiological processes involved in of neuronal and glial regulation [193, 194]. Progesterone triggers gene expression either by binding directly to its receptor or via signal transduction by transcription factors [195].

In female mice, estrogen and progesterone levels are subject to a cyclical fluctuation called the estrous cycle [196].

2.2.1 The estrous cycle

The estrous cycle of a typical young adult female mouse lasts between four and five days and can be divided into four phases with varying hormone levels (Figure 7) [196, 197]. The first phase is proestrous, which lasts less than twenty-four hours and is associated with the onset of mating behaviour [198]. In the proestrous phase, levels of prolactin, luteinising hormone (LH) and follicle- stimulating hormone (FSH) increase, initiating the process of ovulation. These hormone levels remain elevated until the end of the second phase, estrous, which lasts 12-48 hours in mice. The third phase, metestrous, is short and lasts between 8 and 24 hours. If mating does not occur and progesterone levels are too low, the corpus luteum cannot luteinise or make further changes to initiate the pregnancy cascades [197]. The metestrous phase is followed by the diestrous phase, which can last up to 48-72 hours and is characterised by the lowest level of estrogen [197-200]. Metestrous and diestrous are characterised by low but gradually increasing levels of estradiol. During the proestrous phase, the increased estradiol levels cause the hypothalamus to release a bolus of gonadotropin-releasing hormone, which triggers proestrous via LH and the FSH surge. Ovulation occurs 12-14 hours later [201]. The gold standard and most accurate method of monitoring the estrous cycle is cytological analysis of vaginal lavage samples. Briefly, vaginal cells are collected, transferred to a slide, air dried, stained and observed [197]. Each phase of the cycle is characterised by different proportions of nucleated cells, keratinised cells and leukocytes in the vaginal lavage [200]. Taking the estrous cycle into account greatly improves the resolution of studies and facilitates the discovery of underlying female sex differences, which can lead to a reduction in the variability of female samples. Numerous scientific studies have demonstrated the influence of sex hormone fluctuations during the estrous cycle on the CNS [202-205]. Despite these findings, studies investigating the fluctuations in the LVChP associated with the estrous cycle are still missing.

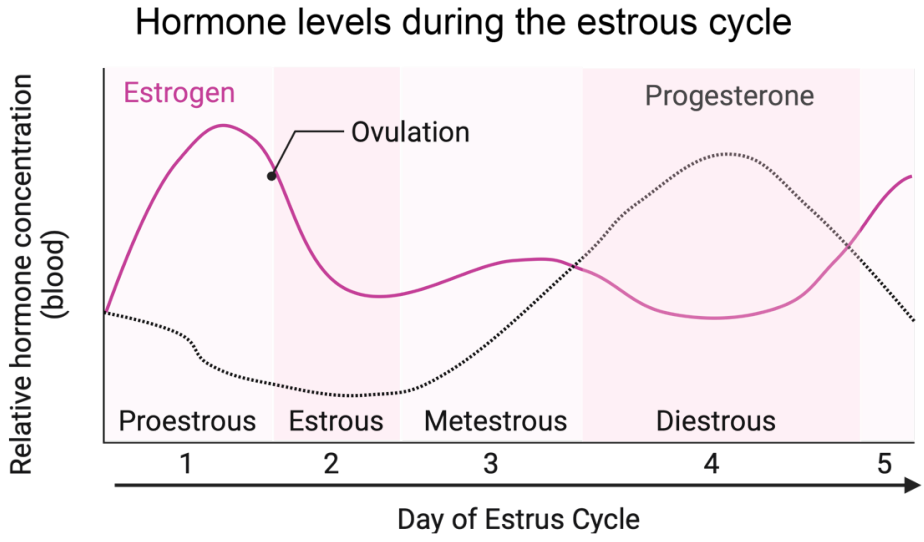

Figure 7: Hormone levels during the estrous cycle
During the four phases of the estrous cycle, the levels of estrogen and progesterone fluctuate. Created with BioRender.com

2.3 Sex differences in the LVChP

Only few studies have examined sex differences in the LVChP. In female rats, intracerebroventricular injection of thrombin, which is associated with the development of hydrocephalus, resulted in greater ventricular dilation, ventricular wall damage and neutrophil infiltration into the LVChP compared to male rats, most likely via the estrogen signalling pathway [206]. In male and female rats, examination of transcripts encoding transporters and channels revealed a high degree of similarity in expression profile, suggesting a comparable CSF secretory apparatus in both sexes [207]. Furthermore, no significant differences were found between male and female mice in the expression of AQP1, 2 and 4 [208]. However interestingly, a recent study measuring CSF production in mice showed that female mice had a 30% higher CSF production rate than age-matched males [209].

Thyroid hormone bound and distributed by transthyretin (TTR) secreted by LVChP is an essential factor for neuro- and oligodendrogenesis in the V-SVZ, with sex-specific differences in NSC regulation. Knockout of TTR decreased neurogenesis and promoted oligodendrogenesis in the dorsal V-SVZ of male mice, but had no effect on the ratio of neurons to glia in females [210].

Quintela et al. compared the ChP transcriptome of male and female rats and also gonadectomised and ovariectomised rats using cDNA microarrays. These are perhaps the most comprehensive studies comparing the LVChP between the sexes [147, 211]. Pathways involved in CSF production, BCSFB formation, neurogenesis, immune surveillance, circadian rhythm and chemical surveillance showed differences in gene expression between sex, highlighting the importance of sex differences in the LVChP and their relevance to known ChP functions [212].

2.3.1 The LVChP is a sex hormone target

The LVChP is a target for sex hormones. It expresses progesterone receptors [213], α and β estrogen receptors [214] and androgen receptors [215], which can modulate the ChP transcriptome and secretome to influence CSF composition and thus control brain homeostasis [212]. The influence of progesterone on the LVChP is not well understood. Previous studies have shown that TTR, which is both produced and secreted by the LVChP, is increased in response to progesterone [216, 217]. Further, a membrane-bound progesterone receptor associated with osmoregulation in the adult LVChP suggests that progesterone may play a role in maintaining water and ion homeostasis [213, 218, 219]. The LVChP contains both nuclear and membrane-bound estrogen receptors with higher expression of estrogen receptor beta (ERβ) than alpha (ERα) [212]. Treatment with estradiol promotes the expression of ERβ [220]. Estrogen has been described to play a neuroprotective role against neurodegenerative diseases such as AD and PD, however its actions in the LVChP remain unclear. The effect of testosterone in the LVChP has received very little attention. The androgen receptor is expressed in both male and female LVChP [215], and gonadectomy in males results in upregulation of interferon 1 alpha (IFN1α), a cytokine with potent antiproliferative and immunomodulatory properties involved in the innate immune response, suggesting that androgens may actively downregulate its expression [212].
Ovariectomy and gonadectomy in rats alter the expression of chemokines, adhesion molecules and cytokine transcripts, which have different basal levels in males and females, with female ovariectomy having a stronger effect on genes involved in immune surveillance than male gonadectomy [147, 212]. This is consistent with reports showing that sex hormone receptors are expressed in immune cells, suggesting that they may be regulated by sex hormones [221]. However, the physiological implications of these interactions in the LVChP are not yet fully understood, highlighting the importance of studying these cells in more detail.

In summary, sex differences can be due to varying gene expression as a result of heteromorphic sex chromosomes or due to differences in sex hormone levels [172]. In females the levels of sex hormones fluctuate during the estrous cycle. There has only been very limited research investigating sex differences in the LVChP. While these reports do suggest differences between the sexes, a thorough investigation is still lacking.
Given the prevalence of several neurodegenerative diseases in both men and women, it is important to understand how sex differences in the cellular composition, transcriptome and secretome of the LVChP may influence contribute to this prevalence.

3 Macrophages

3.1 Introduction

The body's first line of defense consists of innate immune cells that constantly monitor their environment for signs of danger. Although the innate immune response is rapid, it lacks specificity [222]. The more specific immune response is mediated by adaptive immune cells, particularly lymphocytes such as T cells and B cells. When innate immune cells such as macrophages and dendritic cells present antigens to adaptive immune cells, a precise and specific immune response is triggered [223].

Myeloid cells give rise to the vast majority of innate immune cells [224]. These include monocytes and macrophages (whose name in Greek means “big eater”), mononuclear phagocytes that are crucial for the development and maintenance of the innate immune system by clearing pathogens, dead cells and other debris [225]. Macrophages, are often referred to as patrol cells, and found in a variety of tissues where they are constantly on the lookout for microbes [226]. Their functions, including phagocytosis, bacterial killing and wound healing, can vary depending on the signals they receive.

3.2 Macrophage function in immunity and homeostasis

Macrophages are important players in infections, but also in homeostasis. Under homeostatic conditions, they remove apoptotic cells from tissues and play a role at both ends of the red blood cell life cycle thereby preventing any toxic accumulation [227-229]. Further, microglia, which are the macrophages of the CNS, play an important role in synapse pruning and remodelling, while subepithelial macrophages in the gut respond to cellular damage by promoting epithelial proliferation and survival [228, 230].

During early phases of infection, inflammatory macrophages perform phagocytosis, present antigens to T cells and elicit a pro-inflammatory response by secreting chemokines, cytokines and reactive oxygen [231, 232]. Then, in the final stages of inflammation, macrophages can switch their functions and become anti-inflammatory [231, 232]. After infection, they remove dead or dying cells from the site of infection [233, 234]. In addition, macrophages secrete growth factors and substrates that promote fibroblast differentiation and extracellular matrix formation, two crucial steps in wound healing and regeneration [235].

Macrophages are regulated by both exogenous and endogenous signals. Exogenous signals originate from microbial signatures such as lipopolysaccharide (LPS) and flagellin [236-238], while endogenous signals originate from cytokines such as IFNɣ, interleukin 4 (IL-4) or host defence peptides [239, 240]. These signals can trigger not only transcriptional but also epigenetic changes [241]. However, macrophages are not only determined by pathogen signals, but also by their surrounding extracellular environment, which promotes their diversity. This heterogeneity in macrophages is often referred to as macrophage polarisation [242].

3.2.1 The polarisation spectrum

Macrophages are very sensitive to their environment, allowing them to quickly react to changes. As a result, macrophages are very heterogeneous and have different polarised activation states, referred to as M1 and M2, which affect how they respond to the stimuli they receive [243]. Depending on their polarisation, significant changes occur in the gene expression of various factors, including lipid mediators and chemokines [244]. In addition, their activation can also lead to changes in metabolism that may result in further immunomodulatory effects [245, 246]. However, there is widespread disagreement and debate about this polarisation spectrum [247]. Originally, the consensus was that M1 macrophages are pro-inflammatory and M2 macrophages are anti-inflammatory and consist of multiple M2 variants, each with their own receptors, cytokines and chemokines (Figure 8) [239, 242, 248-250].

Different stimuli trigger different subsets of markers and functional responses in M1 and M2 macrophages. Nowadays, this M1 and M2 way of thinking is changing and the nature of macrophages is not limited to M1 and M2. Rather, it is thought that different stimuli acting on macrophages can lead to a spectrum of intermediate states [251]. This idea is supported by a study in which 299 macrophage transcriptomes were compared [252]. This study showed that macrophage activation and polarisation is based on a spectrum, rather than the previously postulated states. The researchers introduced nine additional polarisation states triggered by different microbial molecules, cytokines and environmental stimuli. While traditional M1/M2 polarisation based on gene expression and phenotype is represented in some of these polarisation states, some of them are not [252]. This highlights the plastic and heterogeneous nature of macrophages rather than the "black and white" M1 and M2 polarisation [253].

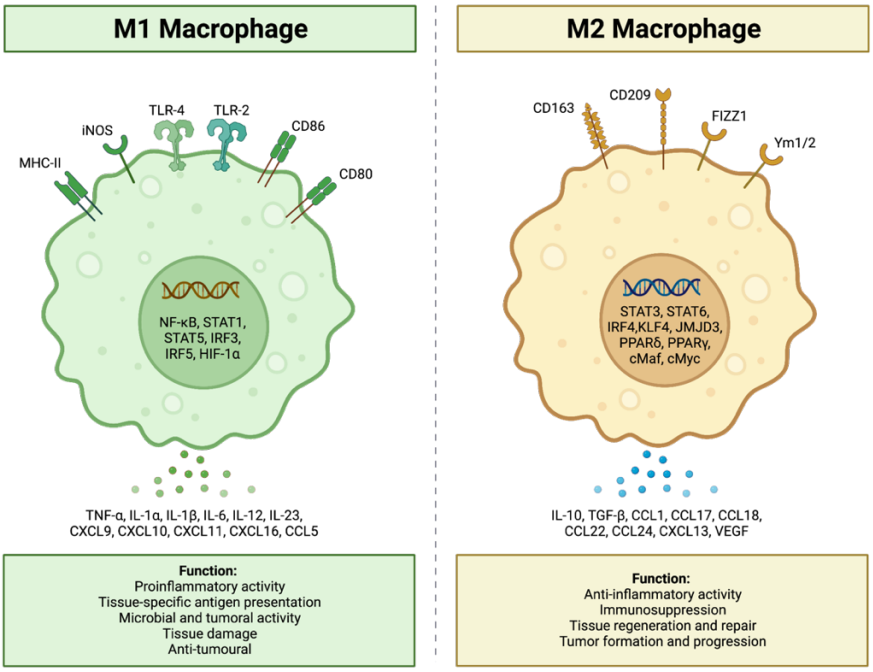

Figure 8: M1 and M2 macrophage polarisation.
M1 macrophages (left) have a more pro-inflammatory activity, while M2 macrophages are more anti-inflammatory. Created with BioRender.com

3.3 Macrophages in the CNS

Macrophages are found throughout the body, and many tissues contain their own specialised subpopulations of macrophages [254]. Resident CNS macrophages can be divided into two groups: those that reside in the parenchyma, called microglia [255], and those that are found at CNS interfaces, such as the perivascular space, the subdural meninges and the choroid plexus [256]. These cells are called CNS-associated macrophages or border-associated macrophages (BAMs) and play a unique role in coordinating immunological responses between the brain and the rest of the body [257, 258].

3.3.1 Microglia

Microglia are located in the parenchyma of the CNS and are specialised to function in this sensitive environment where a strong reaction could cause tissue damage. The functions of microglia vary greatly depending on their environment; nevertheless, their overall functions are essential for the formation, maintenance and restoration of CNS homeostasis [259, 260]. Microglia have a small cell body and adopt a ramified morphology with multiple branched processes in the absence of infection, dying cells or other danger signals [260]. This resting state primarily serves to monitor the environment for changes and react accordingly. To do this, they use their processes, which act like sensors and constantly extend and retract to sense changes in the environment almost immediately [261]. When homeostasis in the brain is disturbed, their cell body enlarges and takes on a more amoeboid appearance while the long processes are retracted [260]. This morphology allows them to more easily engulf foreign pathogens and cellular debris and present antigens to T cells [259]. In addition, microglia play an important role in neurogenesis and CNS development. During CNS development, microglia are involved in production of oxygen radicals to regulate respiratory bursts required for development [262]. Finally, microglia are able to control synaptogenesis, remove mature synapses from neurons (a process called synaptic stripping) and monitor and influence synaptic function [260, 263, 264].

Several microglia markers have been identified over the years, including the fractalkine receptor (CX3CR1), ionised calcium-binding adaptor molecule 1 (IBA1 = AIF1) and the G-protein-coupled adhesion receptor (F4/80). These markers are expressed by microglia and other macrophages as well [265]. However, there are specific genes that are expressed almost exclusively by microglia. These include the expression of the purinergic receptor P2Y12 (*P2ry12*), the transmembrane protein *Tmem119*, and spalt like transcription factors *Sall1* and *Sall3* [266, 267].

Given their important role in many aspects of the brain, identification of microglia-specific markers will allow researchers to consider more appropriate targets to fight CNS diseases.

3.3.2 Border-associated macrophages

In general, BAMs have been categorised according to their specific anatomical location, morphology and expression of certain molecular markers [43, 44]. Like microglia, BAMs can all be identified by the markers IBA1, CX3CR1 and F4/80 [43, 268]. New markers for BAMs, including CD206/ MRC1, LYVE1, CD38, MHC-II and CD163, have been identified as highly expressed in adult BAMs thanks to single-cell studies of CNS myeloid cells [43, 44, 269, 270]. Importantly, different BAM populations are found in various regions of the brain [255, 271]. Perivascular (PV) macrophages are found between the endothelia and glial basement membrane in the perivascular space. They rarely move, and like microglia, their projections extend and retract to sense the environment [43]. They maintain capillary and BBB stability by supporting and ensuring healthy endothelial cells [256, 272]. They can help cause, maintain or prevent disease [268]. Subdural meningeal (SDM) macrophages are found in the subarachnoid space, often in close proximity to ER-TR7-positive fibroblasts. They are the most migratory of the BAMs and therefore adopt a more amoeboid morphology [43, 256]. They exhibit a dualistic nature, acting as a double-edged sword by adopting an anti-inflammatory phenotype to aid with CNS pathologies, while also promoting the progression of certain diseases [273]. The third BAM population in the CNS consists of choroid plexus macrophages. In my thesis I have focussed on macrophages residing in the LVChP.

3.4 Choroid plexus macrophage populations

Macrophages in the ChP can be divided into stromal macrophages and Kolmer's epiplexus cells. Stromal macrophages are located between the vasculature and the basement membrane of the ChP [274], while epiplexus macrophages are located on the apical side of the epithelium. Fate-mapping experiments using CX3CR1CreER Rosa26-YFP mice showed that embryonically labelled PV and SDM macrophages persist into adulthood and do not undergo significant exchange with blood-derived monocytes. In contrast, $IBA1^{+}$ ChP macrophages showed a gradual loss of YFP labelling, suggesting a continuous but slow turnover of cells by bone marrow-derived monocytes with age. Interestingly, epiplexus cells remained YFP labelled, suggesting a different ontogeny between these cells and LVChP stromal macrophages [43]. In addition, parabiosis experiments showed that donor-derived blood cells contributed to the stromal ChP macrophage population, while having no effect on PV or SDM macrophage populations [43].

3.4.1 Stromal ChP macrophages

Transcriptionally, stromal macrophages can be divided into cells with low and high expression of MHC-II. Most ChP macrophages have low expression of MHC-II at birth, but the proportion of cells with high expression of MHC-II increases rapidly with age [13, 44]. This phenotypic transition is thought to be driven by interferon regulatory factor 8 (IRF8), as IRF8-deficient mice produce few MHC-II high BAMs in the ChP [44]. Although the functional diversity and heterogeneity of ChP immune cells needs further investigation it is tempting to postulate that the different macrophage populations found in the ChP may have different functions in the tissue [275]. For example, a subpopulation of embryonic ChP macrophages showed increased motility and mobility in response to elevated CSF-CCL2 levels [276]. Another study showed that injection of LPS into adult mice to mimic inflammation in the periphery caused stromal LVChP macrophages to spread and flatten in the periluminal region of blood vessels, while epiplexus cells did not undergo any morphological changes [277].

These results illustrate how different stimuli can trigger different responses in immune cells, leading to a pro- or anti-inflammatory response [276, 278, 279]. Finally, the fenestrated vasculature in the ChP allows a higher number of monocytes to enter the stroma and differentiate, which may explain the observed intercompartmental macrophage heterogeneity [275].

3.4.2 Epiplexus macrophages

Kolmer's epiplexus cells were first observed by Walter Kolmer as flattened granular cells on the surface of the ChP facing the ventricle of the frog (*Pelophylax kl. esculentus*). He theorised that these cells were migrating phagocytes, as they had apparently ingested pigment granules from nearby cells [14]. Using *in vivo* time-lapse imaging techniques, Kolmer's hypothesis that epiplexus cells migrate was confirmed. In addition, these cells were shown to be highly phagocytic, likely due to a large number of lysosomes [39, 277].

The differences in ontogeny and transcriptional status between stromal BAMs and epiplexus macrophages have received increasing attention in recent years. While the majority of ChP-associated macrophages in healthy mice express the central BAM signature (e.g., MRC1/CD206), epiplexus macrophages do not. Instead, they express microglial signature genes such as *Sall1*, *P2ry12* and *Slc205*. However, epiplexus cells are not microglia. In contrast to parenchymal microglia, epiplexus cells have lower expression of homeostatic microglial genes (*P2ry12*, *Tmem119*, *Hexb*) but higher expression of phagocytosis and lipid metabolism genes (*Lpl*, *Apoe*, *Clec7a*, *Cst7*). Interestingly, they share a comparable gene expression signature with the more "active" microglia that respond to disease and inflammation [44, 280]. While the typical mature epiplexus macrophage has a smooth, elongated cell body with three to five processes, its morphology can be highly heterogeneous including bipolar, spherical and stellate morphologies [281, 282].

However, the functional implications of these morphological variations and the extent to which epiplexus macrophages contribute to favourable or unfavourable disease progression remain unclear. Finally, it should be noted that macrophage heterogeneity is also likely to be influenced by genetic make-up, sex and age.

3.5 Sex differences in the microglia CNS

In the CNS, sex differences in microglia have been studied in great detail, whereas BAM sex differences have not yet been studied. Studies looking at differences between male and female microglia have found that the number, morphology and immunological molecular load of these cells varies with age, brain region, hormones and environment [283-287].

Importantly, differences in microglial morphology and numbers are first observed at P4 when testosterone levels increase in males, resulting in more microglia with activated morphology. This pattern then shifts at P30, before the onset of circulating hormones in adults [288]. Sex differences in microglia are found throughout the brain, with numbers and morphology varying depending on the region studied [288]. Remarkably, however, in a flow cytometry study of all microglia in the brain, no age- or sex-specific changes in microglial numbers were found [289]. Microglia are known to be affected by sex hormones in both healthy and injured brains. Studies have shown that microglia express sex hormone receptors and that both estrogen and testosterone can influence microglia to produce more anti-inflammatory cytokines [284-287]. Interestingly, microglia isolated from male and female embryos, pups and during puberty do not show significant transcriptome differences, but sex-specific divergence in gene expression only occurs at maturity [247, 283]. These results suggest that sex differences in early adult microglia are maintained even in the absence of hormones. Another transcriptomic analysis showed that female microglia transplanted into male brains maintained their profile after depletion of microglia by a CSF1R inhibitor [290]. These results suggested that sex differences in microglial gene expression are maintained despite changes in the hormonal environment. This suggests that sex chromosomes also play a role in the differences in microglia between the sexes. [291, 292]. With increasing age, microglia may become more divergent between males and females. These differences may accelerate and contribute to age-related disorders, including neurodegenerative diseases. Given the sex differences found in microglia, it can be hypothesised that LVChP BAMs might also differ between the sexes. However, no study has yet been conducted to investigate this.

3.6 The LVChP: a central hub for CNS homeostasis

The role of the LVChP in maintaining CNS homeostasis encompasses many critical functions, including production of CSF, functioning as a barrier, secretion of LVChP-derived factors and factors from the periphery, regulation of NSCs, exertion of immunological functions, and facilitation of elimination of waste products and debris to eliminate toxins and other harmful substances. Its involvement in numerous neurological diseases indicates its indispensable role in the proper functioning of the entire CNS.

The intricate mechanisms by which the LVChP fulfils these multiple functions are still the subject of investigation. In particular, the LVChP expresses a variety of receptors for different signalling molecules [15, 293-295]. With this in mind, our laboratory's working model rests on the idea that the LVChP acts as a dynamic sensor that receives and responds to signals from the periphery and CSF by dynamically modulating its transcriptome and secretome in different physiological states and under homeostasis (Figure 9). These physiological states may include changes in fed and fasting states, physical activity, circadian rhythms and fluctuations in sex hormone levels.

Our research group is interested whether there are sex differences in the LVChP at the anatomical, cellular and molecular levels, as this has been comparatively little studied.

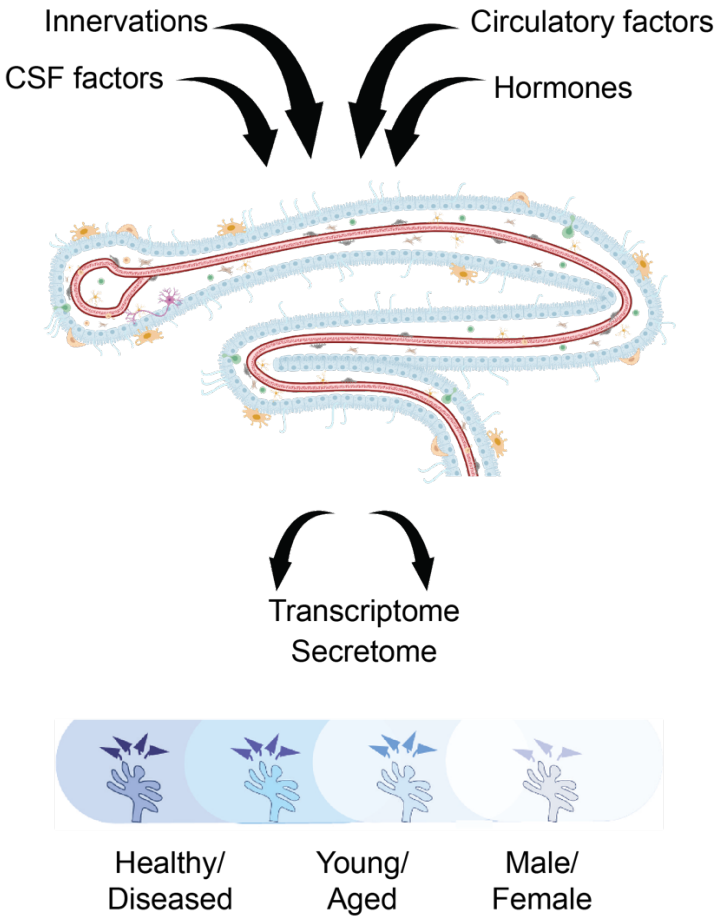

Figure 9: The LVChP integrates different signals resulting in transcriptome and secretome changes
Created with BioRender.com and bottom schema modified from [120].

4 Aim of this thesis

The LVChP is emerging as a key player in brain physiology in both health and disease. It has important roles in brain homeostasis, including CSF production, formation of the blood-CSF barrier formation, detoxification and immune surveillance. Moreover, transport of blood-derived factors and local synthesis and secretion of diverse signalling moieties into the CSF exert effects not only on stem cells in the adult V-SVZ, but also on distant brain regions. Further highlighting its central role in the brain, the LVChP has also been linked to neurodegenerative diseases [296], several of which exhibit sex-specific prevalence, suggesting a possible sex-related difference in LVChP function.

Despite its multi-faceted roles, studies of sex differences in the LVChP remain limited and the functional implications of these differences are largely unknown. Early cDNA microarray analyses performed in male and female rats suggested differences in some LVChP functions [211]. Recently, LVChP secretion was shown to be 30% higher in female compared to male mice [209]. In other organs, immune cells have been shown to exhibit important sex differences [292]. However, whether immune cell sex differences are also present in the LVChP is unknown. The expression of sex hormone receptors in the LVChP raises interesting questions about the influence of sex hormones on ChP function. In particular, the effects of fluctuating sex hormone levels during the estrous cycle in female mice on the LVChP remain to be explored.

To this end, this thesis will investigate sex differences in the LVChP in four distinct aims:

1. To perform a comparative analysis of the LVChP transcriptome between males and females

2. Compare the cellular composition and in particular the immune cells of the male and female LVChP

3. Examine the LVChP secretome and assess whether male and female LVChP exhibit differential regulation of V-SVZ NSCs

4. Investigate changes in the female LVChP in estrous and diestrous phases in the estrous cycle

5 Results: Sex differences in the LVChP

The LVChP plays an important role in maintaining CNS homeostasis and has been shown to be involved in neurodegenerative diseases. In addition, evidence shows that several neurodegenerative or CNS diseases have a sex prevalence, suggesting possible sex differences in LVChP function. To investigate this, my thesis focusses on structural, cellular and molecular comparison between the sexes to better understand how these differences may modulate LVChP function to maintain CNS homeostasis.

5.1 Comparison of male and female LVChP structure

As described in the introduction, the LVChP is a highly folded structure. To be able to better compare the overall structure between males and females, we used whole mount preparations, in which the entire LVChP is flattened and mounted. These whole mounts allowed us to compare the cell density between male and female LVChPs (Figure 10A, C, D). The cell density was analysed using the Cellpose segmentation software pipeline [297] to automatically count the total number of cells and calculate tissue volumes in the LVChP whole mounts (Figure 10D). No significant differences in cell density were found between the sexes (Figure 10A). Quantifications of the cell density in cross-sections confirmed these results (Figure 10B). Interestingly, not all LVChPs had the same cell density. Within each sex there was a high range of variability regardless of the LVChP originating from the left or right hemisphere. The denser LVChPs had a range of 1,000,000 to 1,500,000 cells per mm^3, while the less dense LVChP ranged from 450,000 to 600,000 cells per mm^3 (Figure 10A). However, the reason for this is unknown.

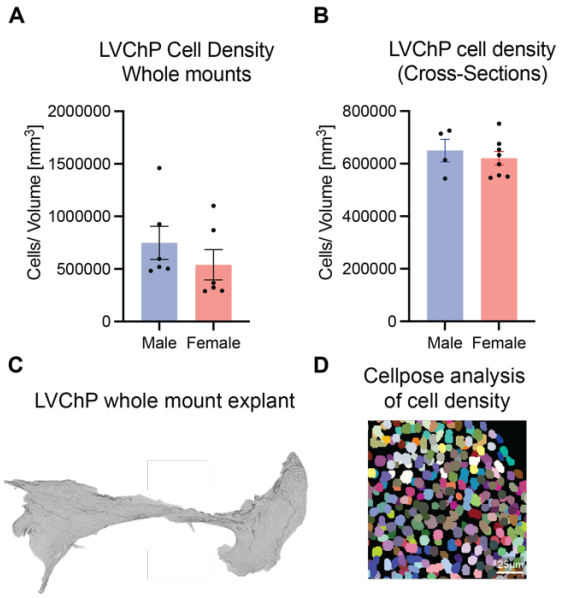

Figure 10: Comparison of LVChP structure between the sexes
A) Quantification of LVChP cell density in male and female whole mounts. B) Quantification of LVChP cell density between sex in cross-sections. C) A LVChP whole mount explant D) Nuclei segmented using Cellpose for automatic quantification of DAPI and tissue volume.

The ChP is the most highly vascularised tissue in the brain. Immunostaining in whole mount preparations for the vasculature showed a high density of $CD31^+$ blood vessels. An alternating pattern of arteries (thick $CD31^+$ $ACTA2^+$ vessels, cyan arrowheads) and veins (thick $CD31^+$ $ACTA2^-$ vessels, yellow arrowheads) was present in the LVChP in both sexes. Between these arteries and veins, a dense carpet of capillaries was present throughout the entire LVChP, forming the connections between them (Figure 11). Overall, no global structural differences in terms cell density and vascular distribution were observed between male and female LVCHP.

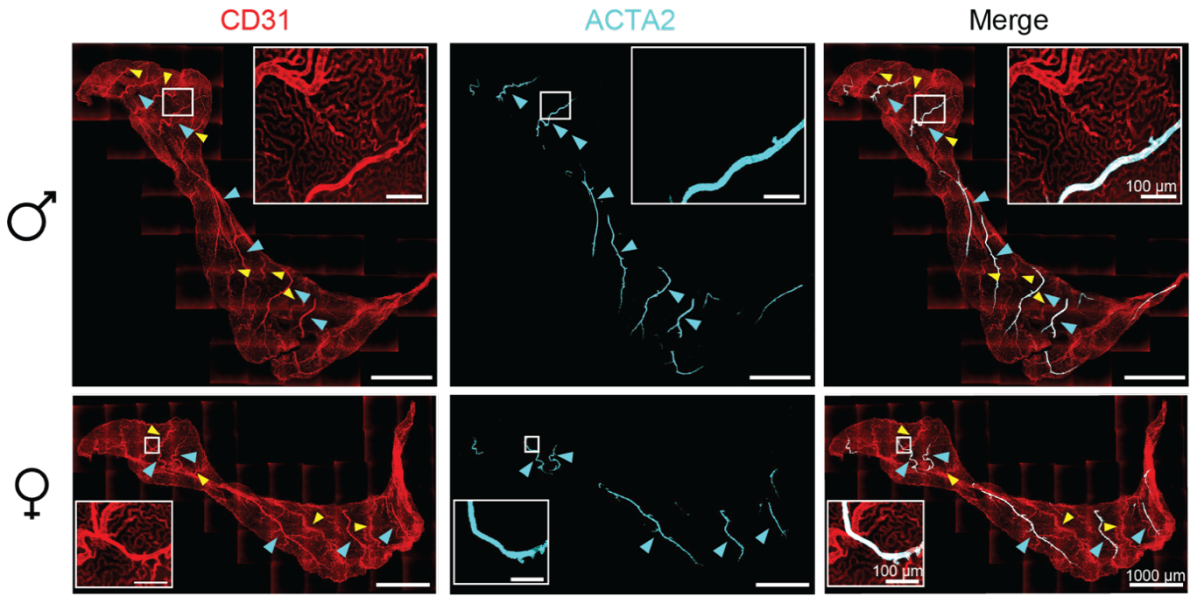

Figure 11: Alternating patterns of arteries and veins throughout the LVChP.
Representative images of whole mount preparations of male (top) and female (bottom) LVChP immunostained for CD31(red) and ACTA2 (mural cells lining arteries, cyan). Arteries are depicted by cyan arrowheads; veins are depicted by yellow arrowheads showing alternating expression. Inserts show a higher magnification view of the areas in boxes.

5.2 Transcriptome analysis of male and female LVChP

To investigate sex differences at the molecular level, we performed RNA sequencing of whole LVChP of males and females (Figure 12). As the female transcriptome may change with the estrous cycle, we compared females in estrous (characterised by higher estrogen and lower progesterone levels, Figure 7) and diestrous (characterised by lower estrogen and higher progesterone levels, Figure 7) phase.

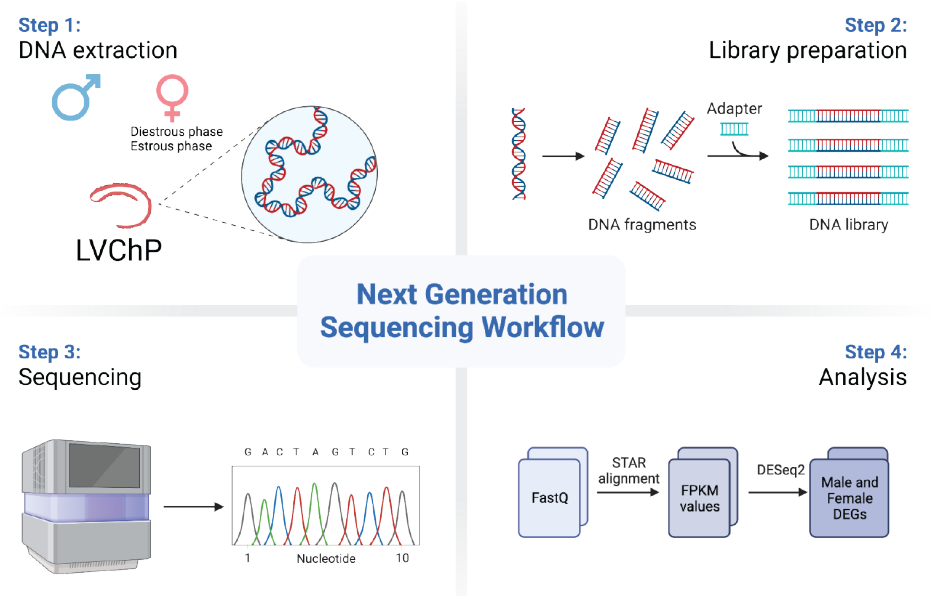

Figure 12: RNA sequencing workflow of whole adult male and female LVChP
Created with BioRender.com

In the following results, we first compared the male samples with all the female samples to assess the overall differences between the sexes, and later we examined the differences between estrous and diestrous phases in the females.

5.2.1 GSEA analysis of the whole LVChP transcriptome

We first performed Gene Set Enrichment Analysis (GSEA) of the entire LVChP transcriptome comparing males versus all female samples. GSEA is a computational method that determine gene sets which are enriched between two biological states. Genes involved in the major functions of the LVChP functions were present in both sexes. These include metabolic processes, immune regulation, cellular and membrane transport processes, processes involved in surveillance, such as the response to ROS, secretory processes and ciliogenesis. However, an overall higher number of biological processes were enriched in females (449 gene sets) compared to males (31 gene sets). Furthermore, shared biological processes between male and female LVChP had different subcategories. For example, zooming into metabolic processes revealed that female LVChP genes were enriched in lipid metabolism, response to oxidative stress and carbohydrate metabolism, whereas the gene set enriched in males was oxidative phosphorylation. In addition, gene sets corresponding to immune regulation, signalling and phototransduction were enriched in females, while gene sets corresponding to axoneme/ dynein complex, and post-translational modifications were enriched in males (Figure 13A).

Given that several diseases such as stroke, schizophrenia, PD and AD show prevalence between sex, we investigated gene sets associated with these diseases using our transcriptome data (Figure 13B). Stroke has a higher prevalence in females than males. Our GSEA analysis for stroke-related genes in the LVChP also showed higher enrichment in females than males. Schizophrenia, which is reported to be slightly more abundant in men, did not show an enrichment between sex in the LVChP. However, PD, which is reported to be two times higher in men [298], showed a specific enrichment in the male LVChP. Interestingly, contrary to the reports described in literature showing a higher prevalence of AD in females [299], the gene set for AD was enriched in male instead of the female LVChP (Figure 13B).

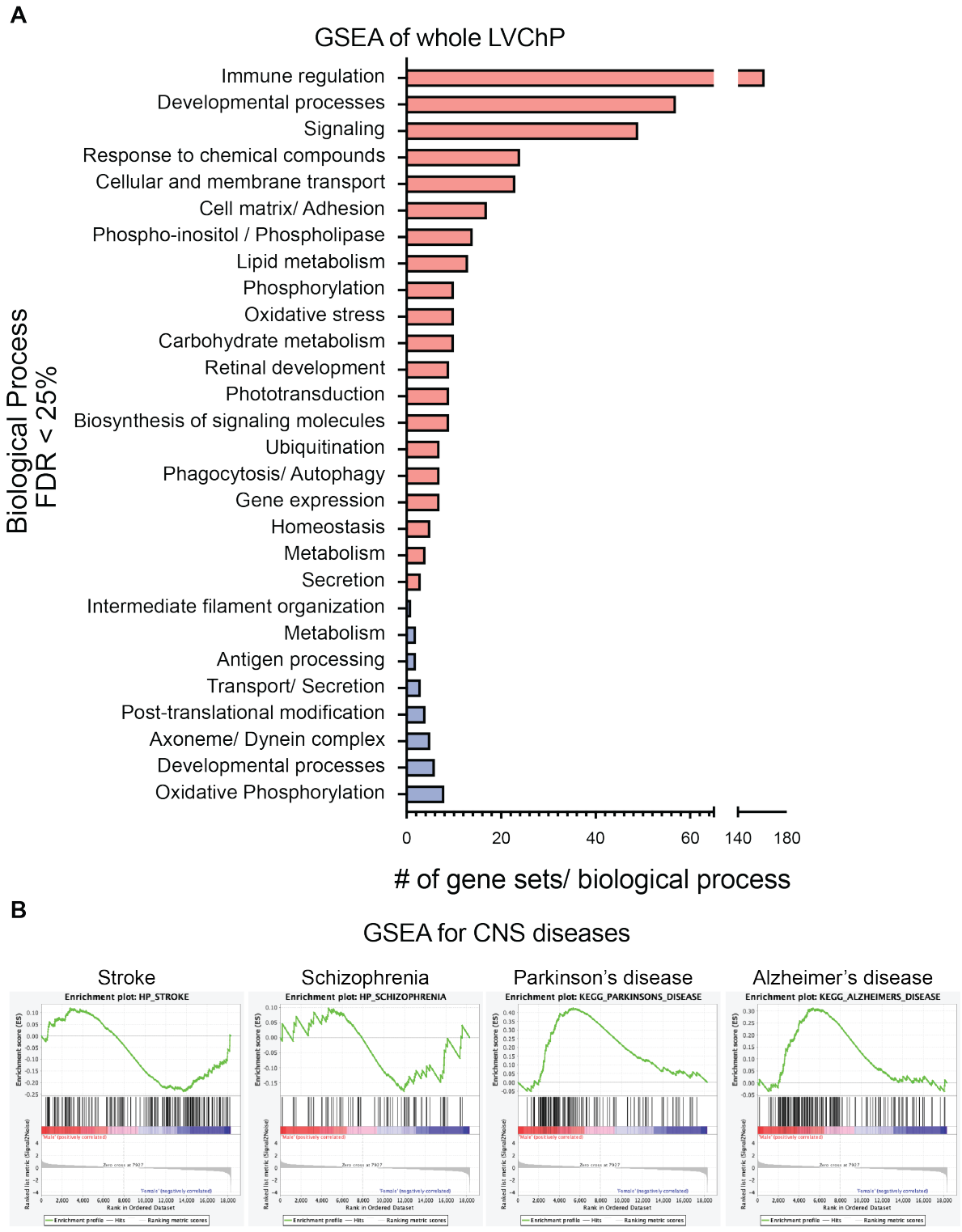

Figure 13: GSEA analysis of male and female LVChP transcriptome.
A) GSEA analysis of female (red) and male (blue) LVChP transcriptome. Biological processes with an FDR <25% were considered enriched. B) GSEA analysis for CNS disease gene sets, In each GSEA plot males are on the left, females are on the right

5.2.2 Differentially expressed genes between male and female LVChP

While the majority of genes in male and female LVChP showed similar expression, further analysis of the transcriptome data revealed 120 differentially expressed genes (DEGs, adjusted p-value < 0.05). Among these, 45 genes were upregulated in males, while 75 genes were upregulated in females (Figure 14A, see Appendix Table 2).

A closer examination of the DEGs in the female LVChP revealed their involvement in different functional gene ontology categories. These include crystallins/ chaperones (*Cryba1*, *Crygd*, *Crybb2*, *Cryba2*, *Cryaa*), matrisome-associated genes (*A2m*, *Fgf2*, *Cspg4*, *Npnt*, *Itih5*, *Fstl1*), immune peptides and receptors (*Cx3cr1*, *Csf1r*, *Mpeg1*), metabolic synthesis and degradation enzymes (*Agpat9*/ *Gpat3*, *Cpxm2*, *Pbdc1*) and genes linked to the X chromosome (*Xist*, *Eif2s3x*, *Pbdc1*, *Kdm5c*, *Kdm6a*). On the other hand, DEGs in male LVChP were associated with lipid metabolism and storage (*Apoe*, *Bscl2*, *Apmap*, *Pld3*), neuropeptide/adipokine signalling (*Gh*, *Pomc*, *C1qtnf12*), ion channel transport (*Nnat*, *Slc35d3*), RNA binding (*Ddx3y*), ciliary (*Spag1*, *Wdr66*, *Ttll6*) and Y- chromosome linked processes (*Uty*, *Ddx3y*, *Eif2s3y*, *Kdm5d*, *Hyal3*) (Figure 14B). While several biological processes including transcription, translation, protein folding/ trafficking and immune responses were shared between male and female LVChP, the genes contributing to these categories were different between the sexes (Figure 14B)

Finally, we performed STRING plot analysis, to assess whether DEGs are involved in known and predicted protein-protein interactions. K-means clustering revealed the following five clusters in females; photoreception/ visual perception (cyan; *Gnat1*, *Crx*, *Prph2*, *Nrl*, *Rrh*, *Rho*), methylation (yellow; *Pbdc1*, *Eif2s3x*, *Kdm6a*, *Plag1*, *Kdm5c*, *Ddx3x*, *Hnrnpu*, *Plagl2*), ECM-related genes (blue; *Gpc6*, *Cspg4*, *Fgf2*), retinal differentiation (green; *Crygc*, *Crygb*, *Cryaa*, *Crybb2*, *Crygs*, *Cryba4*, *Cryba2*, *Cryba1*, *Crygd*) and macrophage-associated genes (red; *Csf1r*, *Cx3cr1*, *Emr1*, *Mpeg1*, *Vav1*, *Arhgdib*, *Laptm5*, *Emr1*, *Irf5*, *Fam167a*) (Figure 14C). The same analysis performed on the male LVChP samples did not show a specific association between the DEGs. The only genes forming a small network were genes associated with the Y-chromosome (*Ddx3y*, *Kdm5d*, *Uty*, *Eif2s3y*) (Figure 14C).

These findings highlight the importance of considering sex differences in gene expression patterns in the LVChP and their potential impact on functional differences between males and females in this context.

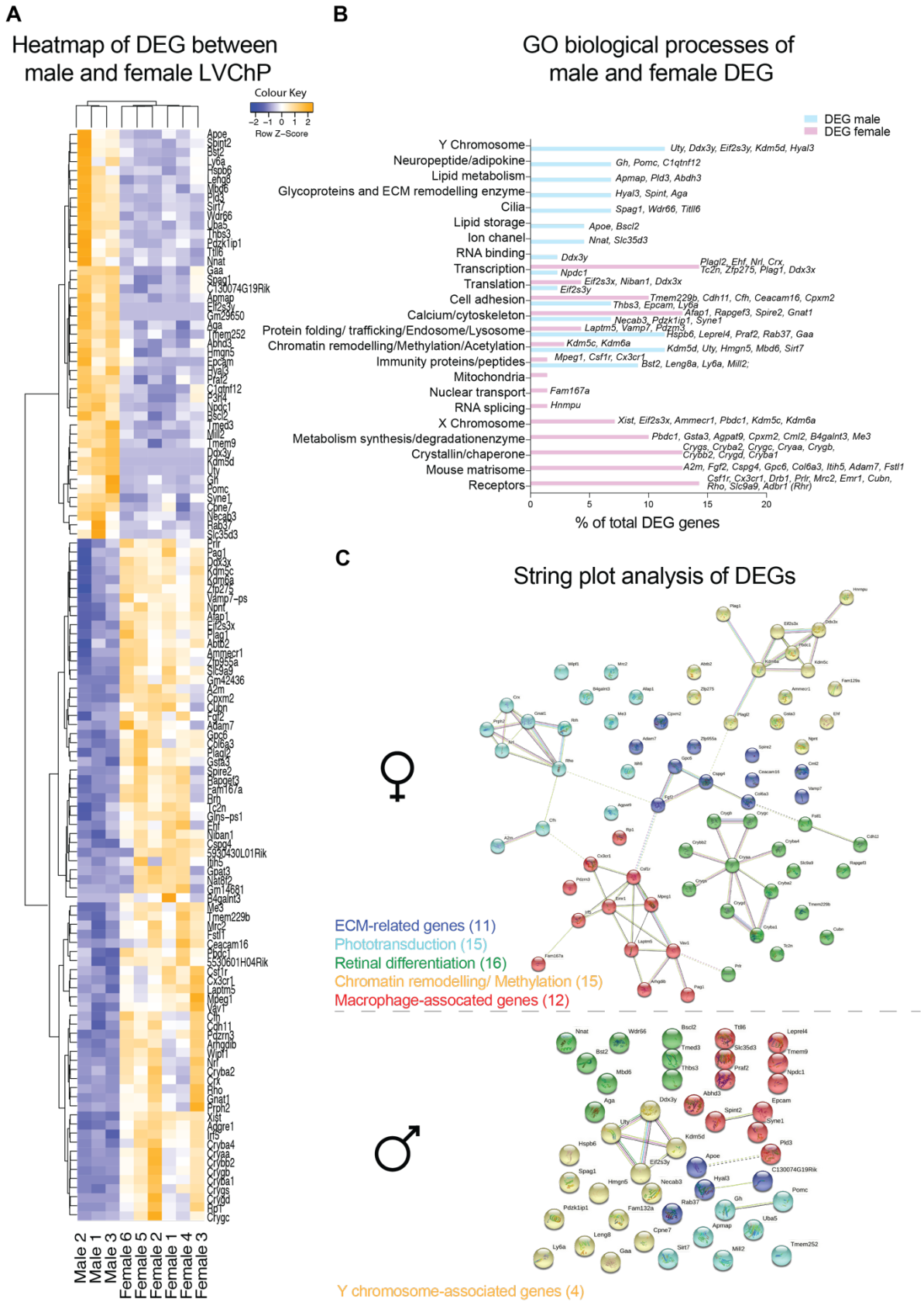

Figure 14: Analysis of DEGs between male and female LVChP.
A) Heatmap of 120 male and female DEGs. B) GO biological processes of male and female DEGs. C) String plot analysis of the female (top) and male (bottom) DEGs by k-means clustering into five functional categories based on their association with each other.

5.2.3 Validation of DEGs between male and female LVChP

To visualise the extent of significance of the DEGs, we created a volcano plot by plotting the negative logarithm of the adjusted p-values (base 10) on the y-axis and the log2 fold change (male/female) on the x-axis. The highest DEGs in males were associated with the Y chromosome (*Uty*, *Ddx3y*, *Kdm5d*, *Eif2s3y*). These results confirmed the identity of the male samples. In contrast, the gene *Xist*, known for its central role in X chromosome inactivation, showed high expression levels in the female samples, further confirming the identity of the female samples (Figure 15A).

We then validated a subset of the DEGs in males and females using quantitative polymerase chain reaction (qPCR) and fluorescent *in situ* hybridisation (FISH). We selected candidates to validate based on their expression levels and enrichment in different biological processes. The genes highlighted in blue were validated as male DEGs (*Bst2*, *Syne1*, *Bscl2*, *Hyal3*), while genes highlighted in red were further validated as female DEGs (*Cpxm2*, *A2m*, *Gpat3*, *Itih5*) (Figure 15A).

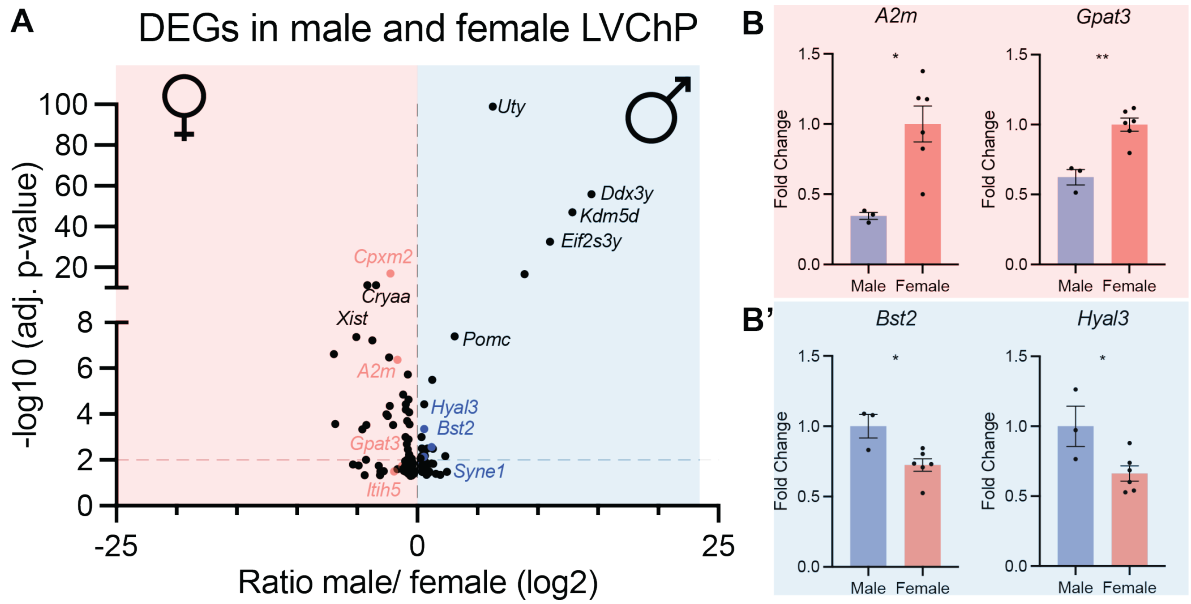

Figure 15: DEGs in male and female LVChP
A) Volcano plot showing DEGs in female (left) and male (right) LVChP B,B') qPCR analysis for *A2m* (p-value: 0.01), *Gpat3* (p-value: 0.001) (red) and *Bst2* (p-value: 0.014), *Hyal3* (p-value: 0.029) (blue).

5.2.3.1 Validated female LVChP DEGs

Alpha-2-macroglobulin (*A2m*) plays a role in various biological processes. It is a protease inhibitor that scavenges and inhibits proteinases such as trypsin, thrombin and collagenase through a unique trapping mechanism that triggers a conformational change upon protease binding [300]. *A2m* also has anti-inflammatory properties by inhibiting inflammatory cytokines [300. In addition, *A2m* is associated with AD due to its role in mediating clearance and degradation of amyloid β, making it an important player in the immune response [301]. Our LVChP transcriptome data showed significantly higher expression of *A2m* in females compared to males (log2 fold change (FC) Females/Males (F/M): 1.64, adjusted p-value: 4.27e-7).

Glycerol-3-phosphate acyltransferase 3 (*Gpat3*; log2FC F/M: 1.9, adjusted p-value 3.1e-2) is an enzyme that catalyses the conversion of glycerol-3-phosphate to lysophosphatidic acid. *Gpat3* has been shown to play a crucial role in protecting cells from lipotoxicity [302].

Carboxypeptidase X, M14 Family Member 2 (*Cpxm2*), another validated DEG in females (log2FC F/M: 2.24; adjusted p-value: 1.07e-17) is a secreted metallocarboxypeptidase predicted to be involved in peptide metabolic processes in the extracellular space [303]. It is therefore likely that *Cpxm2* plays a role in peptide processing in the LVChP.

The fourth DEG, which was validated as being differentially expressed in females (log2FC F/M: 1.26, adjusted p-value: 1.8e-2), is Inter-α-Trypsin Inhibitor Heavy Chain 5 (*Itih5*), which is involved in the regulation of the matrisome of the LVChP, including stabilisation of the ECM and prevention of tumour metastasis [304].

5.2.3.2 Validated male LVChP DEGs

A DEG validated in male LVChP is bone marrow stromal cell antigen 2 (*Bst2*; log2FC M/F: 1.2, adjusted p-value 2.7e-3). *Bst2* is an interferon-inducible host restriction factor that exerts antiviral effects by binding virions directly to infected cell membranes, thereby inhibiting viral release [305]. It has also been shown to inhibit the proteolytic activity of MMP14, leading to a reduced effect of MMP15, which in turn inhibits cell growth and migration [306]. In addition, *Bst2* is involved in the organisation of the subapical actin cytoskeleton in polarised epithelial cells [307].

Hyaluronidase 3 (*Hyal3*) is an endoglycosidase enzyme that specifically degrades hyaluronan, a major component of the extracellular matrix involved in cell proliferation, migration and differentiation [308]. *Hyal3* had a log2FC M/F of 0.6 with an adjusted p-value of 4.3e-4.

The protein encoded by spectrin repeat containing nuclear envelope protein 1 (*Syne1*; log2FC M/F: 0.4, adjusted p-value: 2.8e-2) plays a crucial role in binding organelles to the actin cytoskeleton, contributing to the organisation of the subcellular space. In addition, *Syne1* is involved in nuclear mobility and localisation by transmitting mechanical forces to the nuclear

envelope. *Syne1* is also required for the migration of the centrosome to the apical cell surface during early ciliogenesis [309].

The fourth validated DEG in males is seipin (*Bscl2*), with a log2 fold change of 0.4 compared to females and an adjusted p-value of 1.4e-2. *Bscl2* is known to play a critical role in regulating lipid droplet morphology, including lipid droplet formation and facilitating the transport of proteins and lipids from the endoplasmic reticulum to lipid droplets [310].

5.2.3.3 Spatial distribution of male and female DEGs

To validate the results of the DEGs from male and female LVChP, I first performed qPCR analysis for the differentially expressed genes *A2m*, *Gpat3*, *Bst2* and *Hyal3* in female and male LVChP samples respectively. The qPCR analysis confirmed the observed increase in the expression of *A2m* and *Gpat3* in females and the higher expression of *Bst2* and *Hyal3* in males (Figure 15B).

In addition to validating DEGs between male and female LVChP with qPCR, we examined the spatial distribution of gene expression in the LVChP using fluorescent *in situ* hybridisation (FISH), specifically using the RNAscope protocol. Our RNAscope analysis revealed robust expression of the *A2m* transcript in the epithelial and some stromal cells of the LVChP in both sexes, with higher expression in females than in males (Figure 16A, B). Similarly, the expression of *Cpxm2* was higher overall in females than in males and localised in the epithelial layer of the LVChP (Figure 16C, D). In contrast, the expression of *Itih5* in the LVChP was restricted to the stromal compartment and was higher in females (Figure 16E, F).

DEGs in males, including *Bst2*, *Syne1* and *Bscl2*, were validated using RNAscope analysis. *Bst2* expression was found to be higher in males than females, confirming the results of qPCR and transcriptome data (Figure 16G, H). Interestingly, cells located on the apical surface of the LVChP showed increased *Bst2* expression in both sexes (Figure 16H'), although further investigation is required to determine whether these cells are epiplexus cells or epithelial cells. RNAscope analysis revealed that the *Syne1* transcript was distributed in both the stroma and epithelium of the LVChP, with higher expression in males than females, consistent with our transcriptome data (Figure 16I, J). The expression of *Bscl2* was also higher in males than in females (Figure 16K, L).

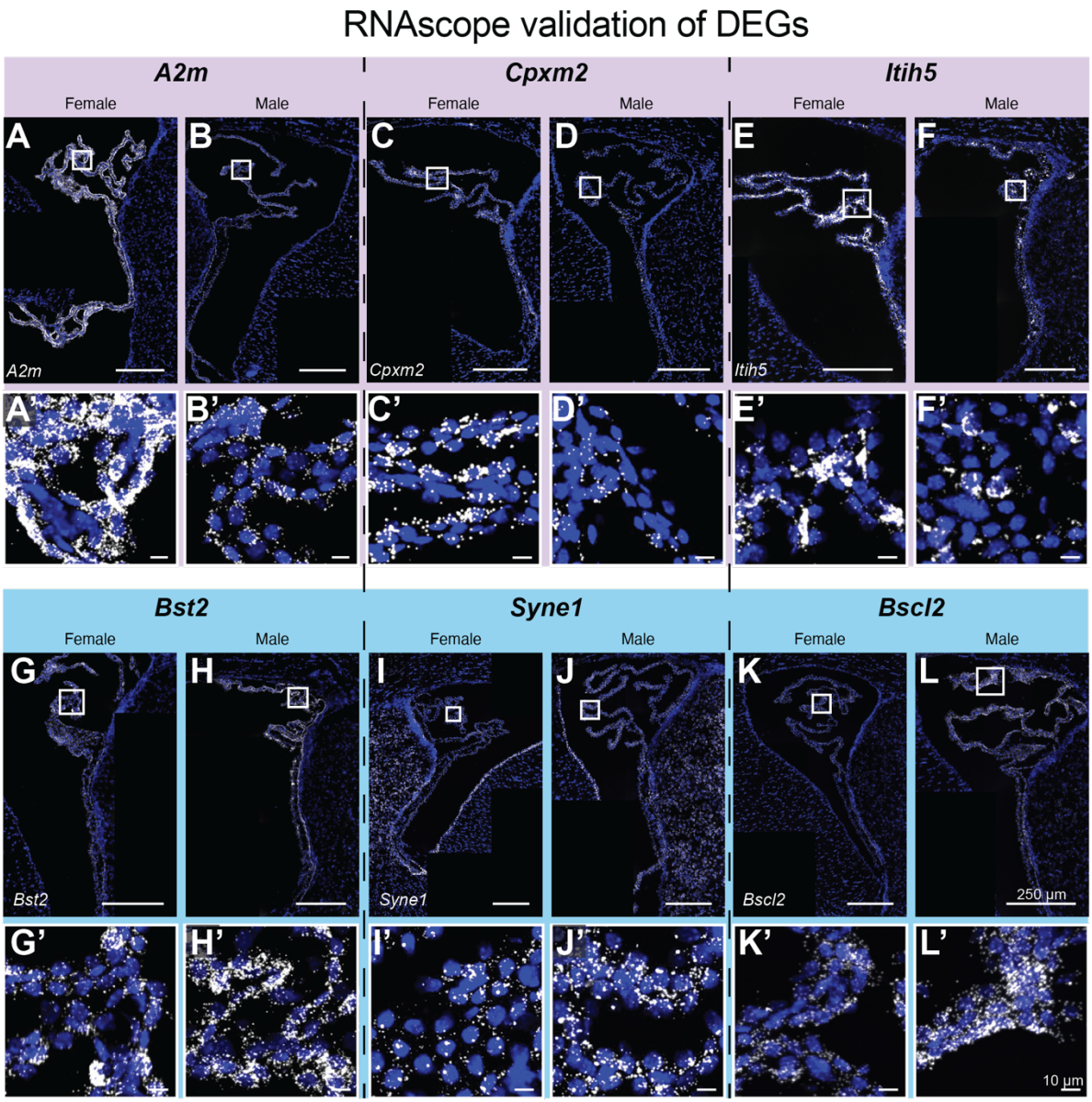

Figure 16: Validation of DEGs in female (magenta) and male (blue) LVChP
A-F) Representative images of RNAscope of female DEGs in females and males respectively. A-B) *A2m*. C-D) *Cpxm2*. E-F) *Itih5*. G-L) Representative images of RNAscope of male DEGs in females and males respectively. G-H) *Bst2*. I-J) *Syne1*. K-L) *Bscl2*. N= 3

5.2.4 Female DEGs are associated with macrophages

To infer whether particular cell identities were enriched in the DEGs we performed ENRICHR CellMarker Augmented 2021 cell type analysis. The analysis of the male DEGs showed no enrichment for any particular cell type, with diverse representation of progenitor cells, epithelial cells and cancer (stem) cells, among others (Figure 17A). In contrast, cell type analysis of the female LVChP DEGs revealed an enrichment in immune cells, particularly macrophages (Figure 17B), which piqued our interest in further investigating sex differences in this cell type in the LVChP.

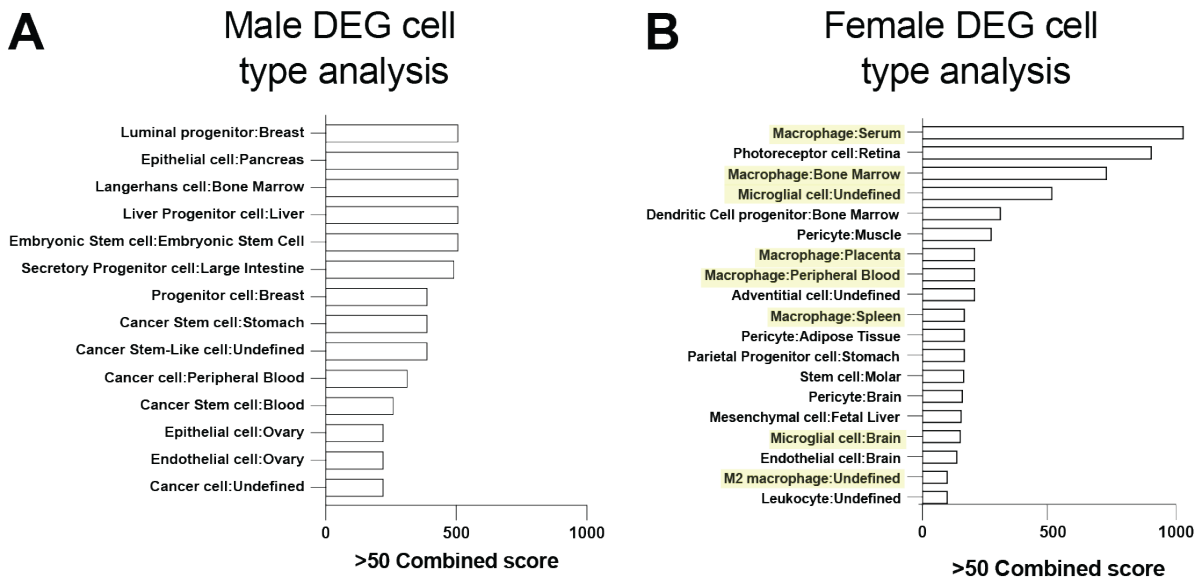

Figure 17: ENRICHR cell type analysis of DEGs.
A) Cell type analysis in males. B) Cell type analysis in females. Only cell types with a combined score >50 were considered as significant. Macrophages/ microglia are highlighted in yellow in (B).

In summary, the transcriptome of male and female LVChP shows marked differences in genes involved in several important LVChP processes, which may lead to differences in function between the sexes. Several CNS diseases are often more prevalent in one sex. The ChP may play a role in this prevalence, as some of the DEGs between the sexes are associated with some diseases and disorders including PD and stroke (Figure 13B). Finally, cell type ENRICHR analysis revealed macrophage genes enriched in female DEGs. Therefore, we investigated these cells in the LVChP in more detail as described in the next section.

5.3 Sex differences in LVChP macrophages

The CNS contains parenchymal microglia and border-associated macrophages (BAMs). Allograft inflammatory factor (AIF1), also known as ionised calcium-binding adapter molecule (IBA1) is a global macrophage marker, and labels both microglia and BAMs in immunohistochemistry. Immunostaining for IBA1 in cross-sections of the brain showed differences in intensity and morphology between parenchymal microglia and LVChP macrophages (Figure 18A). While parenchymal microglia have small soma and thin, branched processes with a weaker IBA1 immunostaining intensity (Figure 18A''), LVChP macrophages have a thicker process and fewer branches and were more intensely labelled than the parenchymal microglia (Figure 18A').

As described in the introduction, LVChP macrophages can be divided into two subpopulations based on their location; macrophages located in the LVChP stroma and epiplexus cells, which are located on the apical layer of the epithelium (Figure 18B).

IBA1 is not the only pan-macrophage marker. Fractalkine receptor (CX3CR1) and colony stimulating factor 1 receptor (CSF1R) also reliably label macrophages in the LVChP (Figure 18C). We validated the overlap of these markers in CX3CR1-GFP mice, showing that 100% of IBA1+ cells were CSFR1, while 95% of IBA1+ cells were $CX3CR1^{+}$ (with the same percentage applying for $CSFR1^{+}$ cells and CX3CR1 overlap) (Figure 18D). IBA1, CSF1R and CX3CR1 are expressed by both LVChP macrophage populations.

To compare the overall numbers of LVChP macrophages between males and females, we quantified the number of $IBA1^{+}$ cells in coronal cross-sections of both sexes (Figure 18E). Our analysis revealed a higher number (p-value = 0.025) of $IBA1^{+}$ cells in females compared to males (Figure 18F). Given the existence of subpopulations of LVChP macrophages, we were interested in comparing differences between stromal and epiplexus cells between sex.

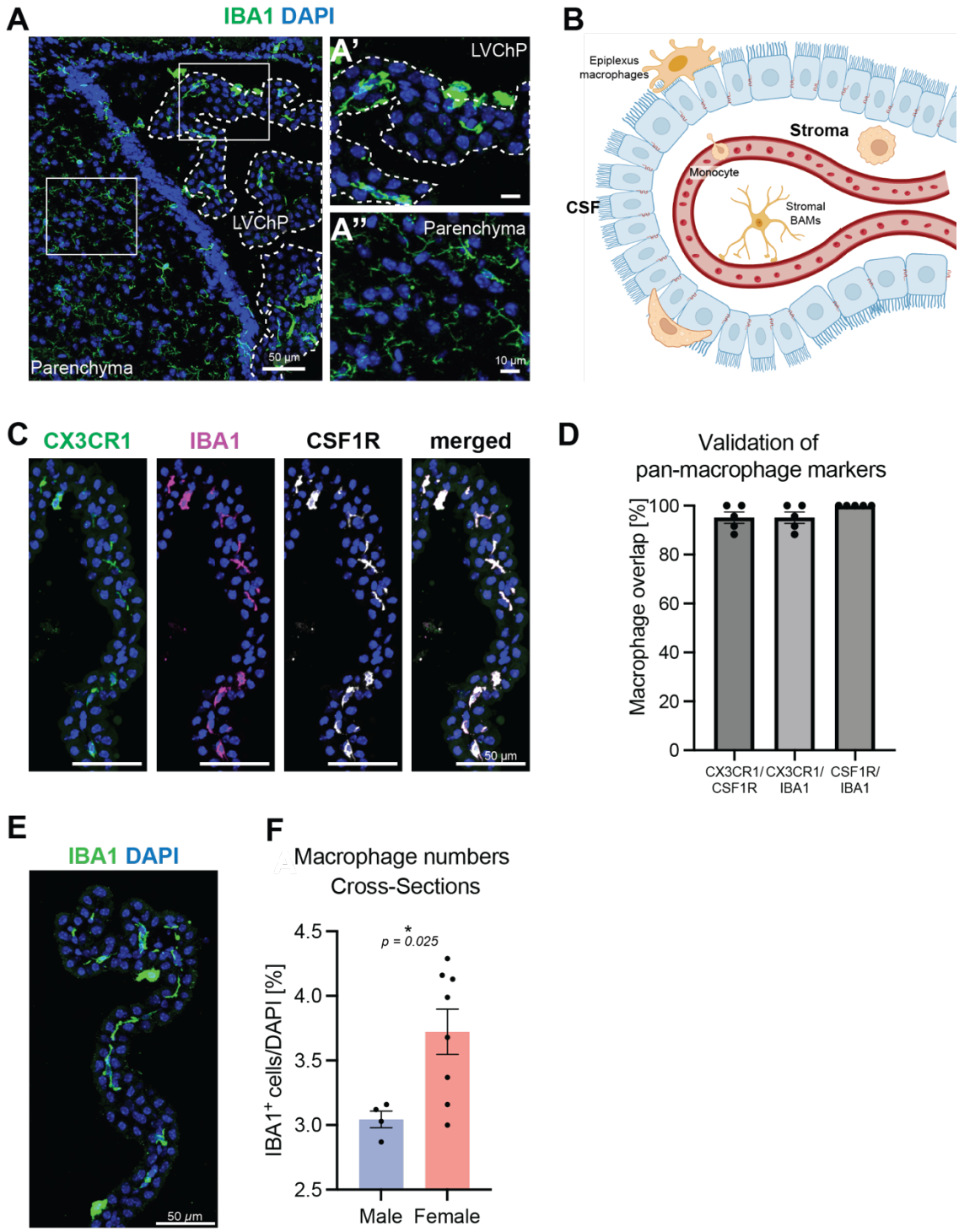

Figure 18: Border-associated macrophages (BAMs) in the LVChP.
A) Representative image of a cross-section immunostained for IBA1 (green) and DAPI (blue). The LVChP is indicated by a dashed line. B) Schema of the LVChP macrophage compartments (stromal and epiplexus). C) Representative image of a cross-section immunostained for GFP (green, labels CX3CR1$^+$ cells), IBA1 (magenta) and CSF1R (white). D) Overlap of pan-macrophage markers in the LVChP. E) Representative image of a cross-section immunostained for IBA1 (green) and DAPI (blue). F) Quantification of male and female IBA1$^+$ cells in cross-sections.

5.3.1 Sex differences in LVChP stromal macrophages

We first examined the macrophages residing in the LVChP stromal compartment using whole mount explants of males and females. Immunostaining for IBA1 showed a significantly higher density of IBA1+ cells in females compared to males (p-value 0.0059) (Figure 19A, B). Using whole mount preparations allowed us to investigate the spatial distribution of macrophages in the LVChP tissue. Previous studies have described a grid-like distribution of macrophages throughout the choroid plexus [13]. Quantification of macrophages in the rostral, mid and caudal region in LVChP whole mounts of both sexes revealed no regional differences along the rostro-caudal axis (Figure 19C, D). Furthermore, the whole mount preparations revealed different morphologies of $IBA1^+$ macrophages in the stromal compartment, including amoeboid cells with large round cells without projections, intermediate cells with a thick cell soma and truncated projections, and bipolar cells with a thin cell soma and multiple ramifications (Figure 19E). Stellate macrophages in the LVChP were not as branched as resting parenchymal microglia (Compare Figure 18A and 19A). Interestingly, no difference was observed in the density of amoeboid and bipolar cells between the sexes, but there were more intermediate and stellate macrophages in the stromal compartment of females (Figure 19E').

Macrophage morphology has been associated with functional differences, with amoeboid cells being more migratory and phagocytic, and stellate macrophages described as immunosurveillant, sensing their environment and releasing chemokines and cytokines. However, the functional implications of these morphological differences in the LVChP and between the sexes remain to be elucidated.

Another interesting observation was the proximity and association of several stellate macrophages in the stromal compartment to the vasculature, suggesting a possible role in receiving information from the circulation for transmission to the LVChP (Figure 19F, F'). The stellate macrophages in Figure 19E' were divided into two groups based on their association with blood vessels (Figure 19F'). Notably, female LVChP had a higher density of vessel-associated stellate macrophages than male LVChP (Figure 19F').

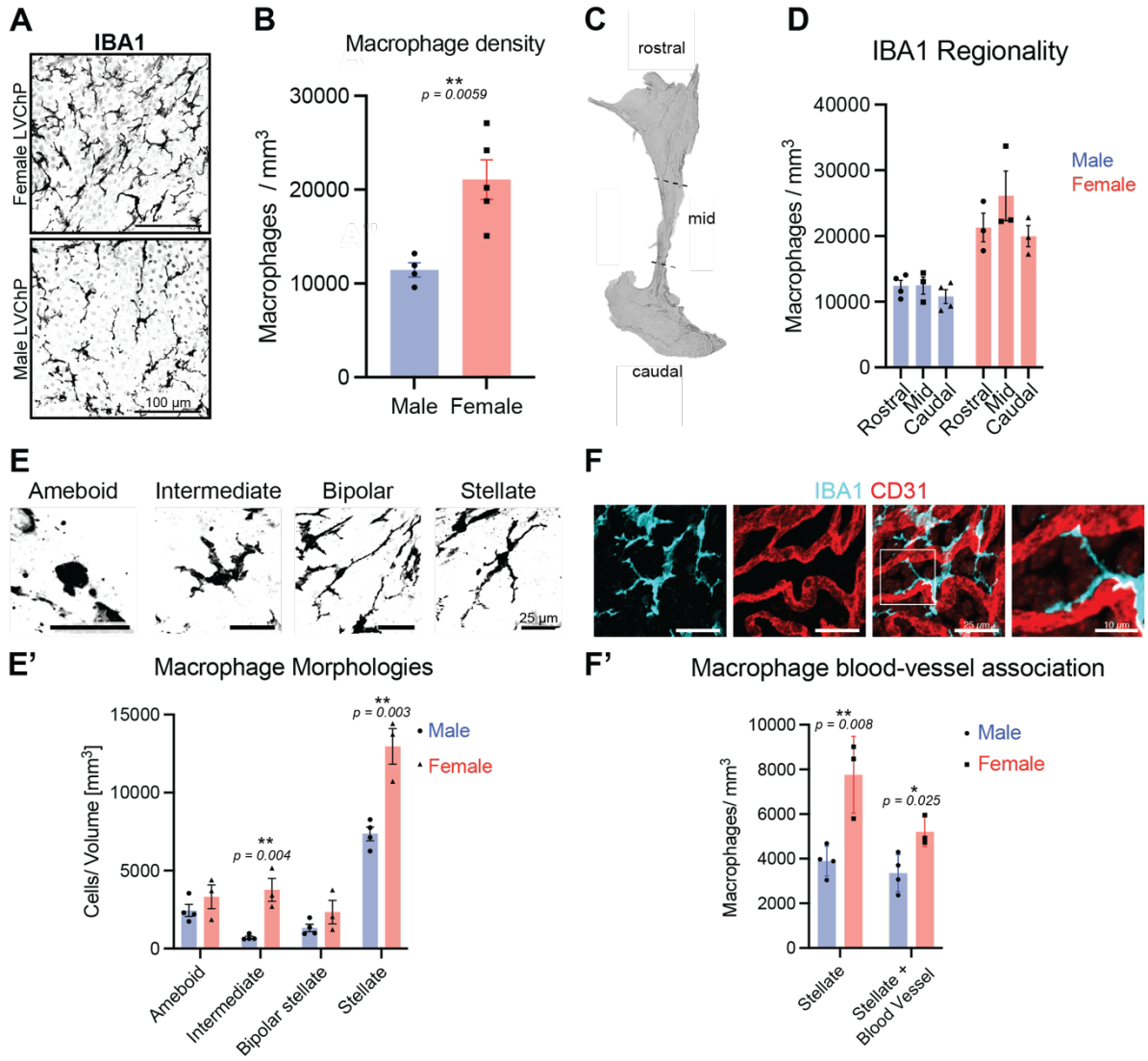

Figure 19: Sex differences in LVChP stromal macrophages.
A) Representative image of whole mount preparations immunostained for IBA1 (black) in female (top) and male (bottom) LVChP. B) Quantification of total IBA1+ stromal macrophages between males and females. C) Whole mount preparation showing the rostral, mid and caudal areas used in quantification in (D). D) Quantification of IBA1$^+$ stromal macrophages in rostral, mid and caudal regions. E, E') Representative images of whole mounts preparations immunostained for IBA1 (black) showing different macrophage morphologies and their quantification. F, F') Representative image of whole mount preparations immunostained for IBA1 (cyan) and CD31 (red) and quantification of macrophage blood-vessel association in male and female LVChP.

5.3.1.1 Stromal LVChP macrophages are MRC1$^+$

The transmembrane receptor mannose receptor C-type 1 (MRC1/ CD206) plays an important role in the endocytosis of glycoproteins and pathogenic microorganisms by macrophages [311]. AQP1, a water channel located on the apical side of the epithelium, allowed differentiation between stromal and epiplexus macrophages (Figure 20B). Immunostaining for MRC1 in coronal cross-sections of male and female LVChP confirmed its reliability as a stromal marker and no labelling of epiplexus cells was detected. Remarkably, 96% of all stromal IBA1$^+$ cells were positive for MRC1 (Figure 20B, C). Comparison of MRC1 expression between male and female LVChP revealed significant differences in the number of MRC1$^+$ IBA1$^+$ cells, with the number of MRC1$^+$ cells being higher in females than in males. Of note, MRC1$^-$ stromal cells showed no differences between the sexes (Figure 20D). Further quantification of MRC1-positive or -negative cells as a proportion of total IBA1$^+$ cells (MRC1/ IBA1) provided information on the distribution of stromal macrophage populations. MRC1$^-$ stromal macrophages accounted for approximately 3% of all IBA1$^+$ cells, while MRC1$^+$ cells accounted for approximately 70-75% of all IBA1$^+$ cells (Figure 20E).

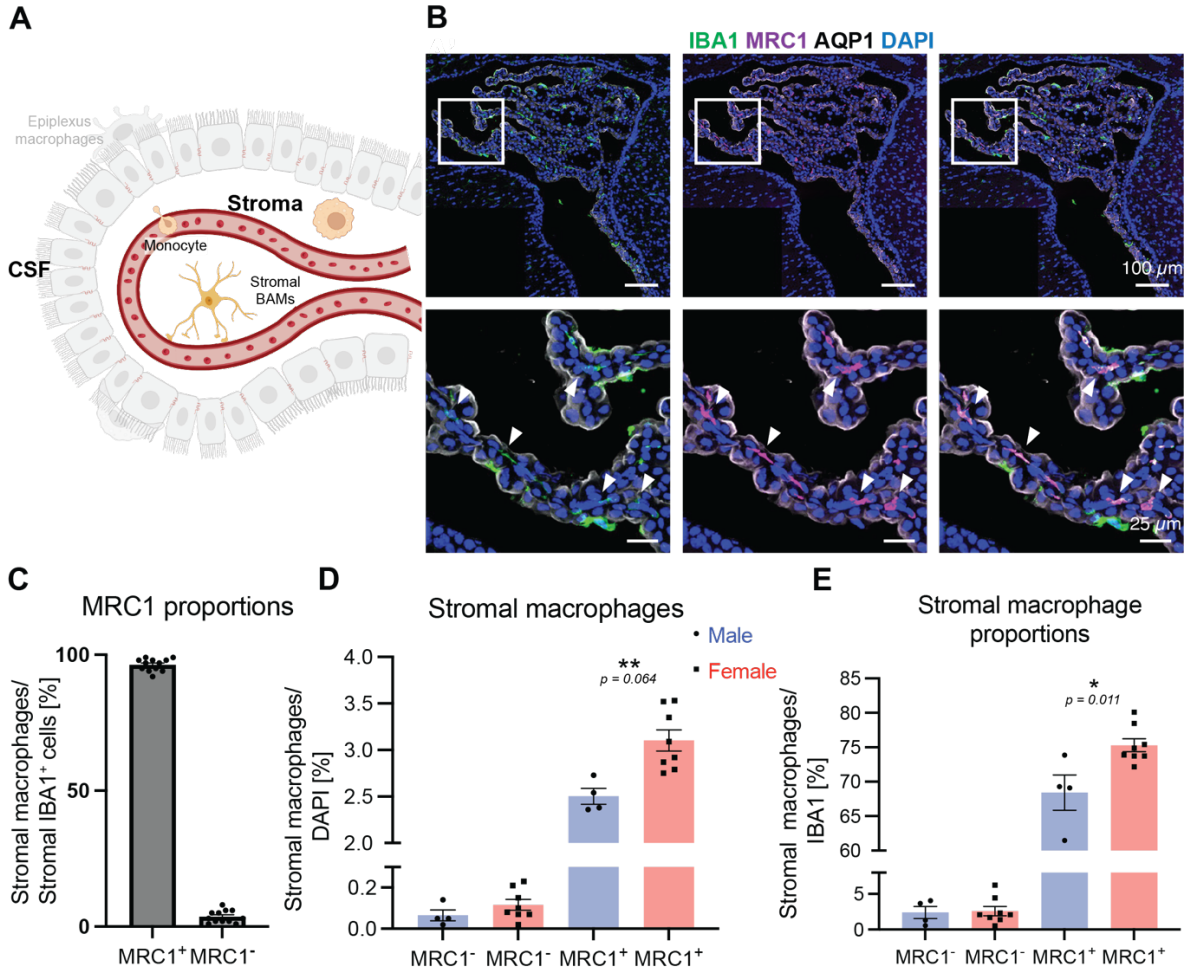

Figure 20: Expression of MRC1 in stromal macrophages
A) Schema showing the location of stromal macrophages. B) Representative image of a cross-section immunostained for IBA1 (green), MRC1 (magenta), AQP1 (white) and DAPI (blue) showing stromal macrophages (white arrowheads). C) Quantification of proportions of MRC1+ and MRC1- cells in the LVChP stroma. D) Quantification of MRC1+ and MRC1- cells in male and female LVChPs per total DAPI. E) Quantification of MRC1+ and MRC1- cells per total IBA1+ cells

5.3.2 LVChP epiplexus macrophage sex differences

Epiplexus cells can be identified by their location on the apical surface of epithelial cells, which is labelled with AQP1 (white arrowheads in Figure 21B). Interestingly, their quantification revealed a significantly higher number in the male compared to female LVChP (Figure 21C). Recent single-cell studies focusing on LVChP macrophages have shed light on specific genes that are upregulated in epiplexus cells, including *P2ry12*, *Tmem119*, *Sall1* and *Sall3* [44]. P2RY12 is known to play a role in the extension of microglial processes during injury and facilitates the clearance of infected cells and cell debris [312]. TMEM119, a transmembrane protein expressed on the surface of microglia, has been reported to increase its expression in response to tissue inflammation, although the further functional implications of this gene remain to be elucidated [313].

5.3.2.1 Males have higher numbers of P2RY12^{+} epiplexus cells

IHC staining targeting P2RY12 revealed that P2RY12-positive (P2RY12^{+}) IBA1^{+} cells make up the majority (84%) of all epiplexus cells, while the remaining 16% were P2RY12-negative (P2RY12^{-}) (Figure 21D, E). These quantifications suggest possible heterogeneity within the epiplexus cell population, despite the predominant presence of P2RY12^{+} cells. This analysis also revealed that the number of P2RY12^{+} IBA^{+} epiplexus cells was higher in males than females, while there was no significant difference in the number of P2RY12^{-} IBA1^{+} epiplexus cells between the sexes (Figure 21F). In addition, quantification of P2RY12^{+} or P2RY12^{-} cells as a proportion of total IBA1^{+} cells (P2RY12/ IBA1) provided insights into the proportions of these epiplexus macrophage populations. P2RY12^{-} macrophages accounted for about 5% of all IBA1^{+} cells, while P2RY12^{+} cells accounted for about 20% in females and 30% in males of all IBA1^{+} cells (Figure 21G).

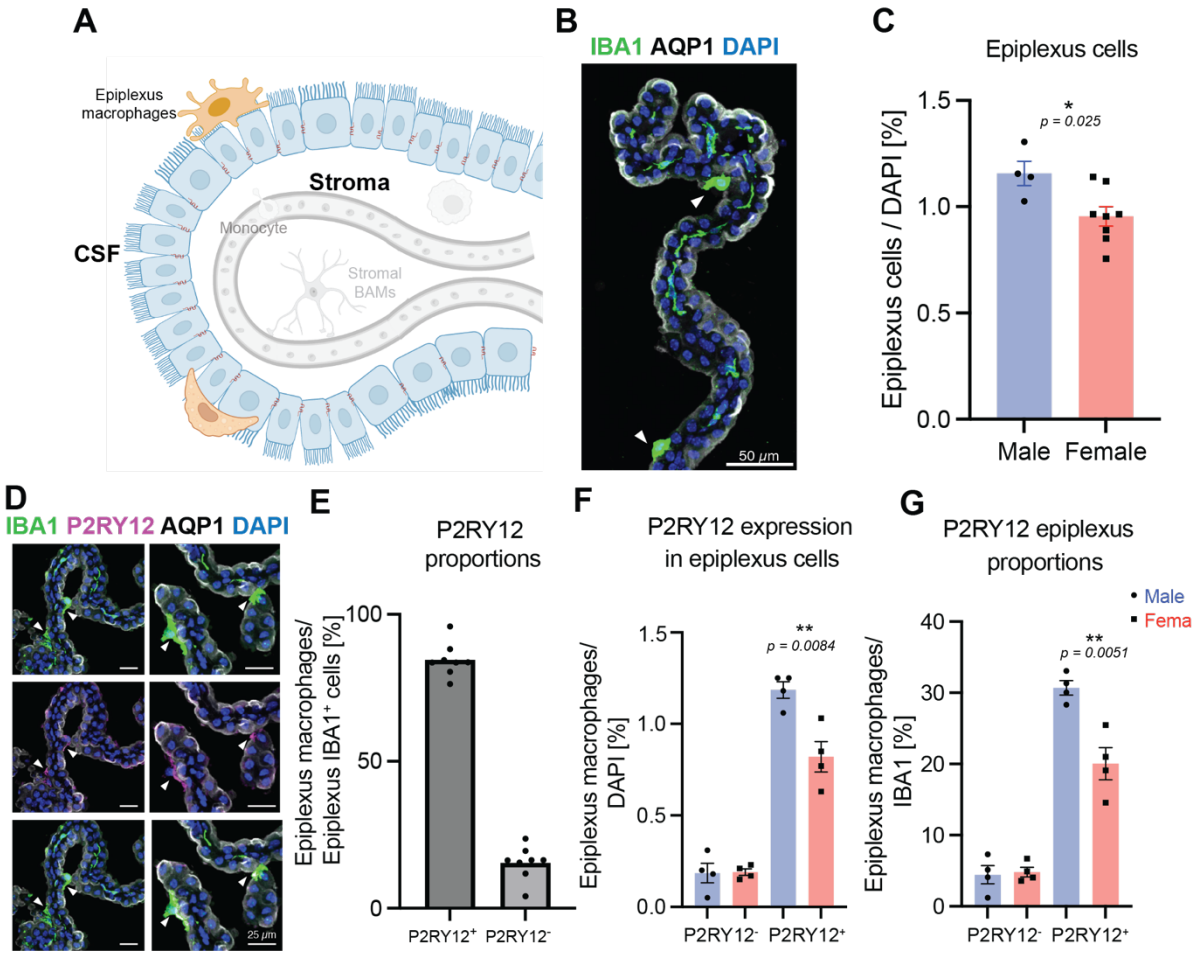

Figure 21: Expression of P2RY12 in epiplexus macrophages

A) Schema showing location of epiplexus macrophages. B) Representative image of a cross-section immunostained for IBA1 (green), AQP1 (white) and DAPI (blue) showing epiplexus macrophages (white arrowheads). C) Quantification of total IBA1$^+$ epiplexus macrophages in males and females. D) Representative image of a cross-section immunostained for IBA1 (green), P2RY12 (magenta), AQP1 (white) and DAPI (blue) showing P2RY12$^+$ epiplexus macrophages (white arrowheads) E) Quantification of proportions of P2RY12$^+$ and P2RY12$^-$ cells. F) Quantification of P2RY12$^+$ and P2RY12$^-$ cells in males and females per total DAPI. G) Quantification of P2RY12$^+$ and P2RY12$^-$ cells per total IBA1$^+$ cells.

5.3.2.2 Females show higher numbers of TMEM119$^+$ epiplexus cells

Tmem119, a gene associated with microglial and LVChP epiplexus cells, was also examined by immunostaining (Figure 22A). Interestingly, only a small percentage (13.5%) of epiplexus cells in the LVChP were TMEM119-positive (TMEM119$^+$), while the majority of IBA1$^+$ epiplexus cells were TMEM119-negative (TMEM119$^-$) (86.5%) (Figure 22B). Remarkably, a comparison between male and female LVChP revealed a significantly higher number of TMEM119$^+$ IBA1$^+$ cells in females, while TMEM119$^-$ IBA1$^+$ cells were more abundant in males (Figure 22C). This validated our transcriptome data of male and female LVChP, which showed a 1.7-fold higher expression in females compared to males. Quantitative analysis of TMEM119-expressing cells as a proportion of total macrophages showed that TMEM119$^+$ epiplexus cells accounted for only 2-4% of all macrophages, while TMEM119$^-$ epiplexus cells accounted for 20% (in females) to 30% (in males) of all macrophages in the LVChP (Figure 22D). These results highlight the presence of a distinct subpopulation of epiplexus cells in the LVChP, characterised by differential TMEM119 expression and apparent sex differences.

To explore the possible functions of TMEM$^+$ and TMEM$^-$ epiplexus macrophages, we performed an ENRICHR analysis using the published single-cell dataset of van Hove et al. to investigate genes associated with *Tmem119*-expressing cells [44]. The Brain Immune Atlas showed differential expression of *Tmem119* in epiplexus cells (Figure 22E) [44]. Further analysis of the epiplexus populations from the single cell dataset showed contrasting gene profiles between *Tmem119*-expressing and *Tmem119*-lacking epiplexus cells (Figure 22F). Genes expressed in *Tmem119-lacking* epiplexus cells included *Gzma*, *Gzmc* and *Nkg7*, while genes expressed in *Tmem119*-expressing epiplexus cells included *C1qa*, *Ctss*, *Csf1r*, *Lgmn*, *Hexb*, *Apoe*, *Trem2*, *Il1a* and *Sparc*. ENRICHR analysis of genes associated with *Tmem119*-lacking epiplexus cells revealed associations with granzyme release, apoptosis and phagocytosis (not shown), which is consistent with the existing literature for epiplexus cells, as *Tmem119*-lacking epiplexus cells constitute the majority of epiplexus cells. On the other hand, *Tmem119*-expressing cells were associated with genes involved in synapse pruning, chemotaxis, microglial cell activation and migration, and chemokine production, indicating distinct functional differences between *Tmem119*$^+$ and *Tmem119*$^-$ epiplexus cells (Figure 22G).

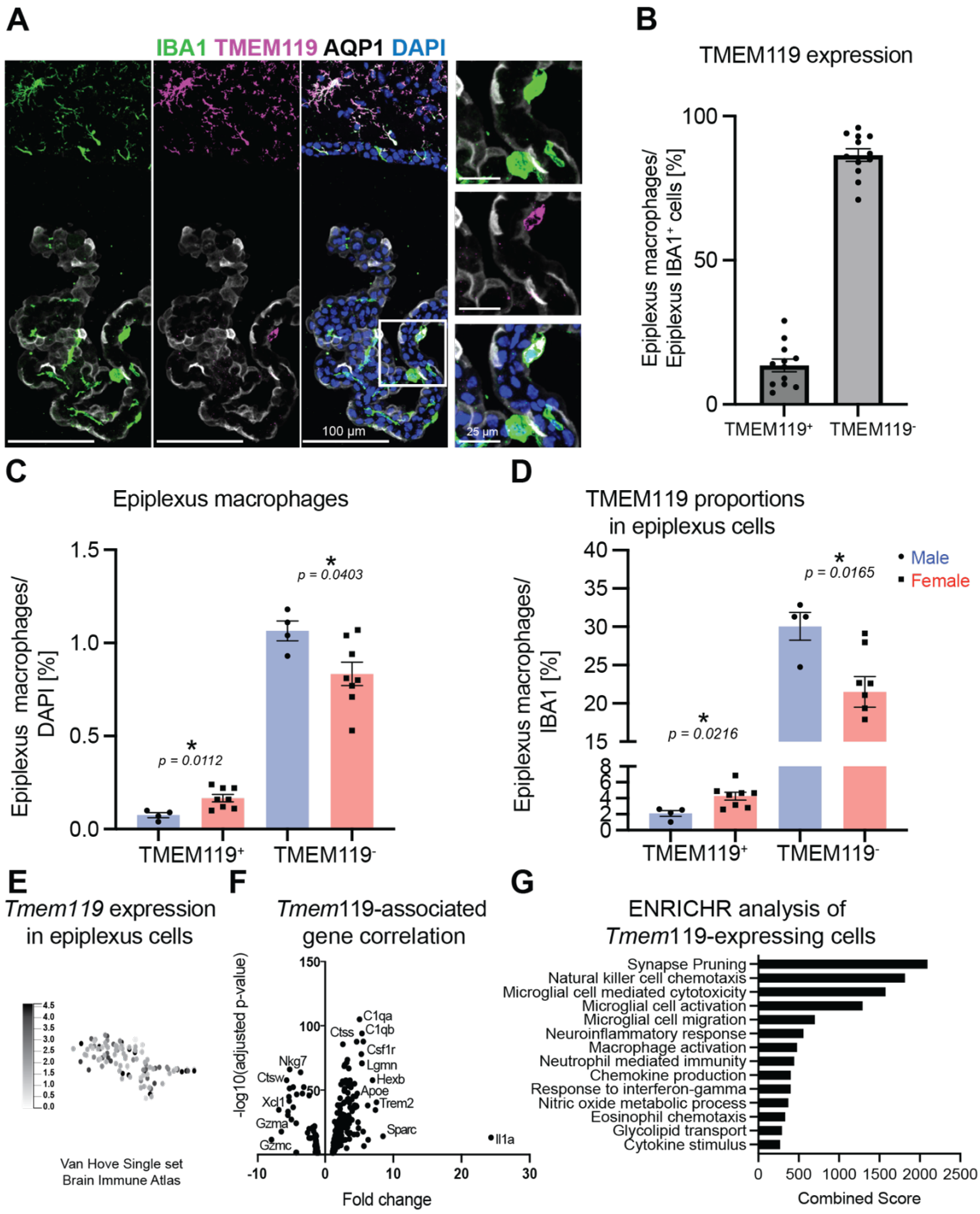

Figure 22: Expression of TMEM119 in epiplexus macrophages

A) Representative images of macrophages and TMEM-expressing cells. Cross-sections were immunostained for IBA1 (green), TMEM119 (magenta), AQP1 (white) and DAPI (blue). B) Quantification of proportions of TMEM119^{+} and TMEM119^{-} cells. C) Quantification of TMEM119^{+} and TMEM119^{-} cells in males and females per total ChP cells. D) Quantification of TMEM119^{+} and TMEM119^{-} cells per total IBA1^{+} cells. E) *Tmem119* expression in epiplexus macrophages using the Brain immune atlas [44]. Volcano plot showing genes associated with *Tmem119*-lacking (left) or *Tmem119*-expressing cells (right). G) ENRICHR analysis of *Tmem119*-expressing cells for GO biological processes.

5.3.3 Transcriptome analysis of male and female LVChP macrophage-associated genes

To investigate possible differences in macrophage functions between male and female LVChP we performed gene expression omnibus (GEO) analysis of macrophage-associated genes upregulated in either males or females. A list of 2215 macrophage genes (Harmonizome [314], see Methods) was compared against our transcriptome data. Only genes with a fold-change >1.5 and a p-value <0.05 were considered as upregulated. The plotted heat map shows that male and female LVChP are clustered by sex. In addition, genes associated with a more M1 phenotype (green boxes) and those associated with a more M2 phenotype (red boxes) were found in both sexes, suggesting that there is no clear tendency towards M1 or M2 polarisation in either males or females (Figure 23A).

Subsequent ENRICHR analysis of these genes unveiled that females exhibited a higher proportion of genes linked to inflammation and cytokine/ chemokine signalling (referred to as immune response), compared to males (Figure 23B). Furthermore, females showed increased expression of genes involved in macrophage regulation (*Tlr1*, *Itgam*, *Csf1r*, *Pld4*). On the contrary, males displayed macrophage-associated genes that were predominantly involved in metabolism (*Apoe*, *Uty*, *Kdm5d*) and lipid storage/ transport (*Apoe*), suggesting that gene expression profiles of macrophages may differ between sexes, potentially leading to functional differences (Figure 23B).

In summary, there are significant sex differences between LVChP macrophages. Overall, females have more macrophages, with differences between the stromal and epiplexus compartments quantified between the sexes. Interestingly, while there are more $MRC1^+$ stromal macrophages in females, males have a higher number of epiplexus macrophages. Remarkably, there is a subpopulation of $TMEM119^+$ epiplexus macrophages enriched in females, indicating the presence of heterogeneity among epiplexus macrophages. Finally, analysis of our transcriptomic data revealed differential gene expression profiles in macrophages between the sexes, with females having a higher proportion of genes related to inflammation and the immune response, while males had genes related to metabolism and lipid processing. These results highlight the diversity and functional differences between male and female LVChP macrophages.

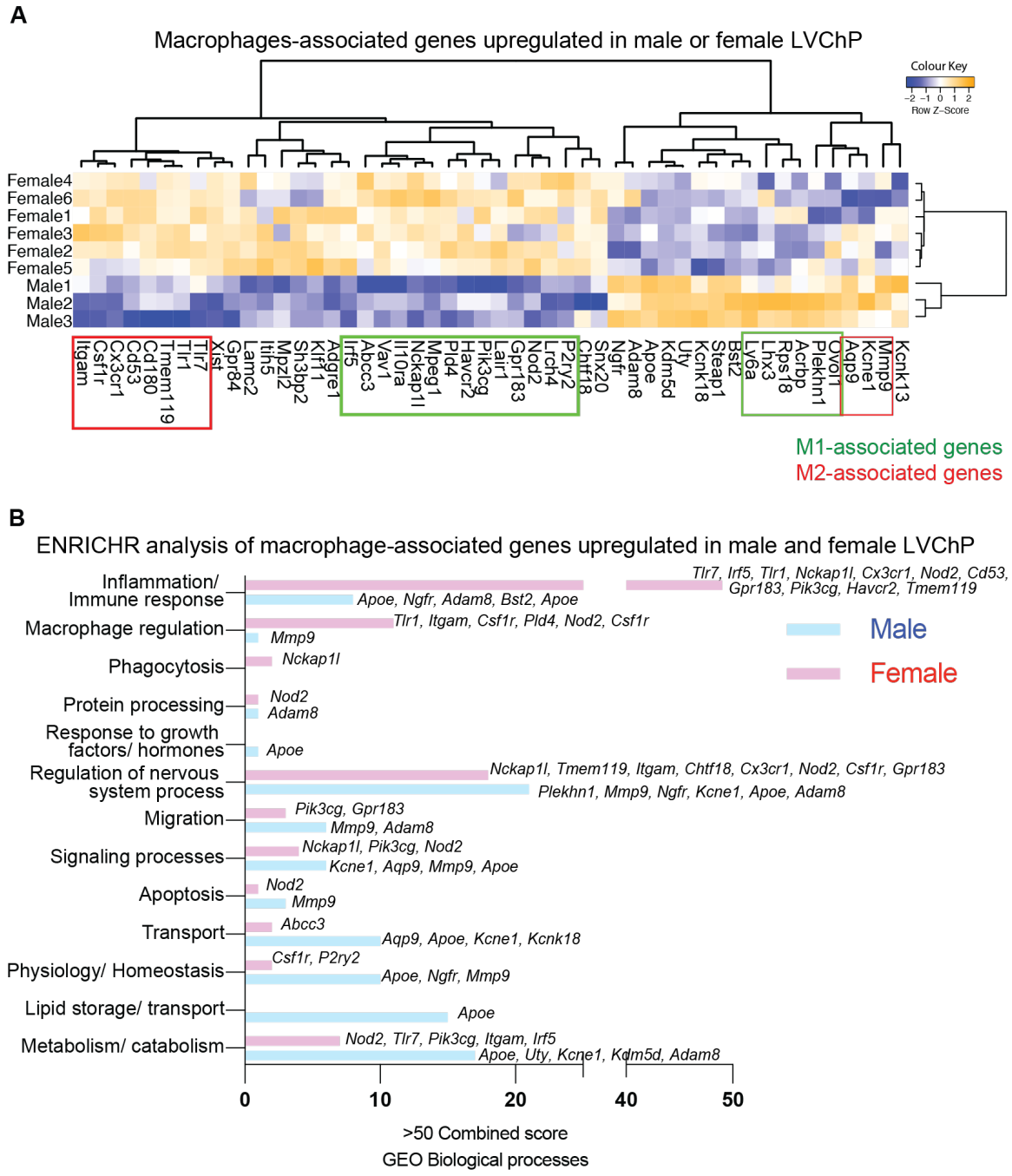

Figure 23: Upregulated macrophage-associated genes in male and female LVChP.
A) Hierarchical clustering showing the relative gene expression for upregulated macrophages in male or female LVChP. B) ENRICHR analysis of upregulated macrophage-associated genes for GO biological processes.

5. 4 The LVChP as a source of signalling factors

One of the described functions of the LVChP is its role in the active transport and secretion of blood-borne and LVChP-derived factors. In addition, recent evidence shows that the LVChP plays a regulatory role for neural stem cells (NSCs) located in the ventricular-subventricular zone (V-SVZ) and that factors secreted from the LVChP change with age, resulting in distinct effects on V-SVZ NSCs [15, 104]. However, despite increasing research in this area, studies on possible sex differences in the secretion of factors by the LVChP are limited. A recent study in our laboratory investigated sex differences in the V-SVZ and revealed differences in gene expression between male and female NSCs [95].

To find out whether secreted factors differ between male and female LVChP, we performed *in vitro* experiments in which we purified NSCs from adult male and female mice and then cultured them with male or female LVChP-derived factors. We also re-examined our transcriptome data to compare ligand expression between the sexes, which revealed notable differences. Finally, we performed proteomic analysis using antibody arrays of LVChP-derived factors encompassing a range of signalling peptides, hormones and ligands, which also revealed differences in the LVChP secretome between males and females.

5.4.1 Baseline clone activation in qNSCs and aNSCs

We aimed to determine whether male and female NSCs are differentially regulated by male or female LVChP-derived factors (LVChPsec). A first important step was to establish a minimal medium for conditioning with the LVChP in order to specifically investigate the effect of LVChP-derived factors. Therefore, we first compared the formation of doublets by NSCs cultured in standard neurosphere medium or in minimal medium (with lower concentrations of factors just sufficient to maintain cell viability). In both media, the concentration of mitogens (EGF & FGF) was the same. FACS-purified male quiescent (qNSCs) and activated neural stem cells (aNSCs) from the V-SVZ niche [107] showed a lower number of doublets when grown in minimal medium, but cell viability was maintained. Therefore, we continued to use minimal medium for the remaining experiments (Figure 24B).

Progesterone is normally used in NSC cultures. However, since LVChP expresses progesterone receptor, progesterone could affect the conditioning process. Therefore, we compared the effect of minimal medium with or without the addition of progesterone on the formation of aNSC doublets. aNSCs cultured with progesterone had a significantly higher number of doublets and showed higher cell viability (determined by viability markers, data not shown) compared to cells cultured in minimal medium without the addition of progesterone (Figure 24C). These results suggest that the addition of progesterone to cell culture medium is important. We therefore excluded progesterone during the conditioning process to rule out a possible influence of progesterone on LVChP secretion in our *in vitro* experiments. After

harvesting, we then added progesterone to the LVChPsec to ensure optimal viability of NSCs in culture during our experiments.

After establishing the appropriate experimental conditions, we examined the baseline formation of doublets by qNSCs and aNSCs from male and female cells with EGF and FGF in minimal medium. Our analysis revealed no significant difference in the number or percentage of doublets in qNSCs or aNSCs between male and female cells from either the septal or lateral wall (Figure 24A, D). However, we observed a significantly higher number of doublets in both males and females when we compared purified cells from the lateral wall to those from the septal wall, with aNSCs showing higher doublet formation compared to qNSCs in both sexes and in both the septal and lateral walls (Figure 24D). Due to the low number of NSCs in the septal wall, we focused on NSCs from the lateral wall.

5.4.2 Activation of aNSCs cultured with LVChP-derived factors

To assess the effect of male and female LVChP-derived factors on NSC activation, we examined clone formation by FACS-purified male and female NSCs cultured with minimal medium, minimal medium containing EGF/FGF (EGF control medium) or LVChP conditioned medium (CM = LVChPsec) under sex-matched or sex-swapped conditions (Figure 24E). Although qNSC formation was very low, we were interested whether LVChP-derived factors could increase clone formation and whether there were differences between the sexes. However, the number of doublets five days after seeding was very low and highly variable (Figure 24F). Therefore, we focused on aNSCs for the remaining experiments. The results of the *in vitro* cultures of aNSCs revealed three important findings: First, both male and female aNSCs showed increased doublet formation when cultured with male or female LVChP CM compared to control medium with or without the addition of mitogens. This suggests that the CM contains factors other than EGF and FGF alone. Second, female aNSCs showed greater sensitivity to LVChP factors than male aNSCs. Finally, female cells cultured with female CM formed more doublets than those cultured with male CM, suggesting differences in LVChP secretome between males and females (Figure 24G, H).

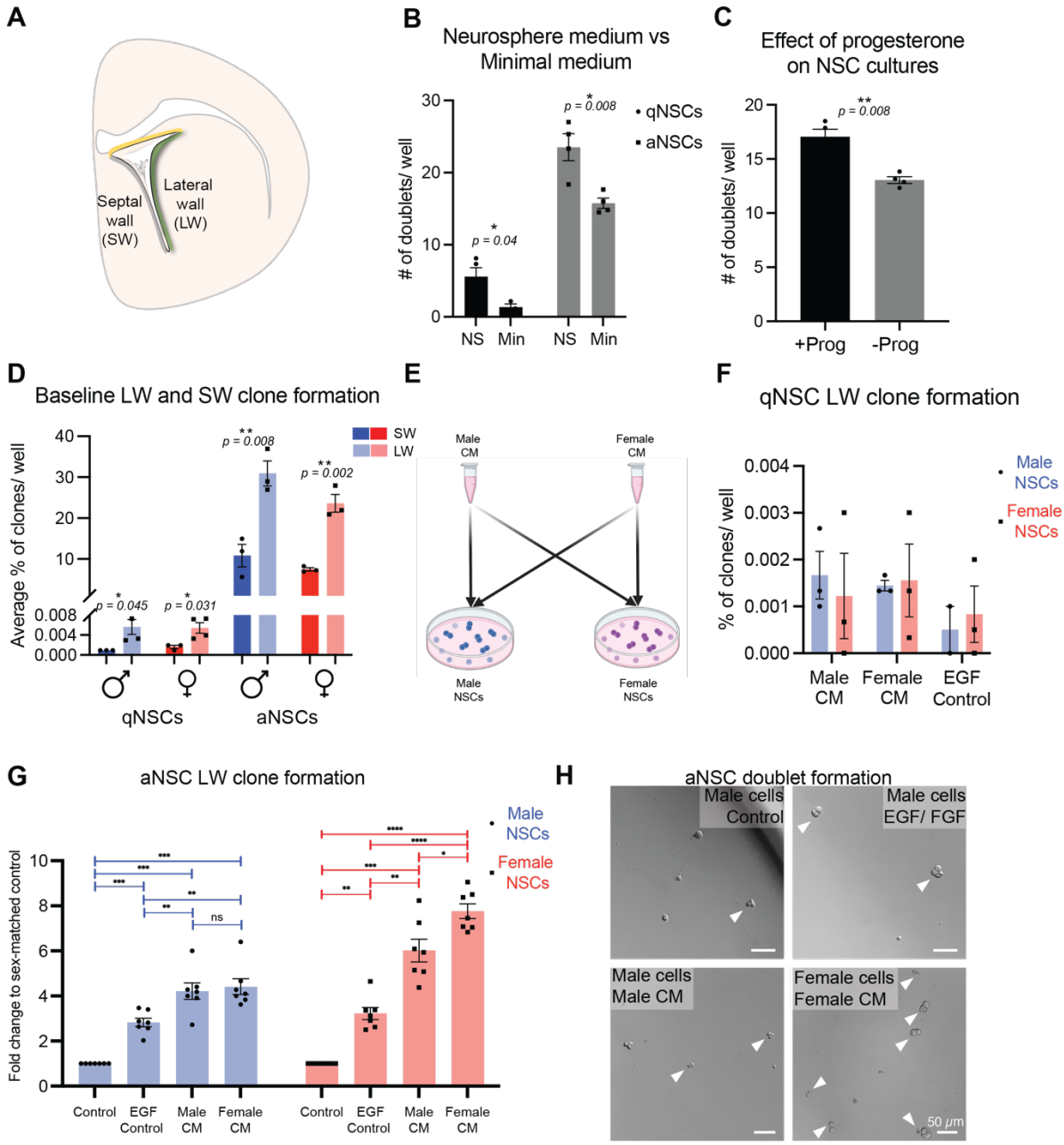

Figure 24: *In vitro* functional experiments of LVChP regulation of V-SVZ NSCs
A) Schema of the lateral (LW, green) and septal (SW, grey) wall. B) Quantification of male qNSCs and aNSCs grown with neurosphere (NS) and minimal (Min) medium. C) Quantification of male aNSCs grown with or without progesterone in minimal medium. D) Quantification of qNSCs and aNSCs purified from the lateral wall (LW) and septal wall (SW). E) Setup for CM experiments F) Quantification of qNSCs grown with EGF control medium and male/ female CM. G) Quantification of aNSCs from the lateral wall (LW) grown with minimal, EGF control, and male and female conditioned medium. Statistics: 2-way ANOVA and Šídák's multiple comparisons test. H) Representative image of male cells grown with control medium (top left), EGF control medium (top right) and male CM (bottom left) and female cells grown with female CM (bottom right).

5.4.3 Sex differences in LVChP ligands

The above experiments show that factors originating from the LVChP regulate the NSCs and that there are sex differences. To identify possible sex differences in ligands expressed in the LVChP, we compared our transcriptome data with a combined list of 4534 ligands and receptors from the CellTalkDB and a ligand gene set from the Harmonizome website [314, 315]. We found that 75% (3334) of the curated ligands and receptors were expressed in the LVChP. Using a statistical threshold of p-value < 0.05, we identified 215 upregulated genes (ligands and receptors) in male or female LVChP. To remove the receptors and focus on differences in LVChP ligands we next compared our list of 215 upregulated ligands and receptors with a curated list of 612 ligands reported to regulate NSCs and found that 72% (443) of these NSC regulating ligands were present in the LVChP, of which 46 were upregulated in male or female LVChP (Figure 25A, B) (see Appendix Table 4).

Notably, several ligands show important sex differences, which may result in sex-specific functional differences in NSC regulation. Of the 46 genes, 17 were upregulated in female and 29 in male LVChP. Ligands upregulated in females included *A2m*, *Hgf*, *Fstl1*, *Ngf*, *Bgn*, *Fn1* and *Fgf2*, while in males *Pdgfa*, *Vegfc*, *Igfbp2*, *Lrg1*, *Shh*, *Nodal* and *Gh* were upregulated (Figure 25B).

5.4.4 Antibody array of male and female LVChP secreted proteins

We next analysed the LVChP secretome (LVChPsec) from male and females to gain insight into the range of factors secreted by the LVChP and to assess any sex differences. LVChPsec from males and females were analysed with antibody arrays containing 111 cytokine antibodies. Of these, 62 were identified across all three independent runs. These 62 proteins were present in both male and female secretome, but with varying levels between the sexes (Figure 25C). While certain proteins exhibited a higher trend in male LVChPsec, namely ICAM-1, E-selectin, CD40, IL-7 and Pentraxin-2, the majority of proteins had higher levels in female LVChPsec. These proteins included amphiregulin, CCL6, DKK-1, IGFBP6, IFNɣ, IL-4, 5, 11, 15, Leptin, MMP2 and 3, Myeloperoxidase, PDGF-BB, Pref-1, Thrombopoietin and VCAM-1 (Figure 25C). This data provides evidence of differences in the cytokines released by male and female LVChP, which may account, at least in part, for the differences observed in the male and female regulation of V-SVZ NSCs by LVCHP-derived factors.

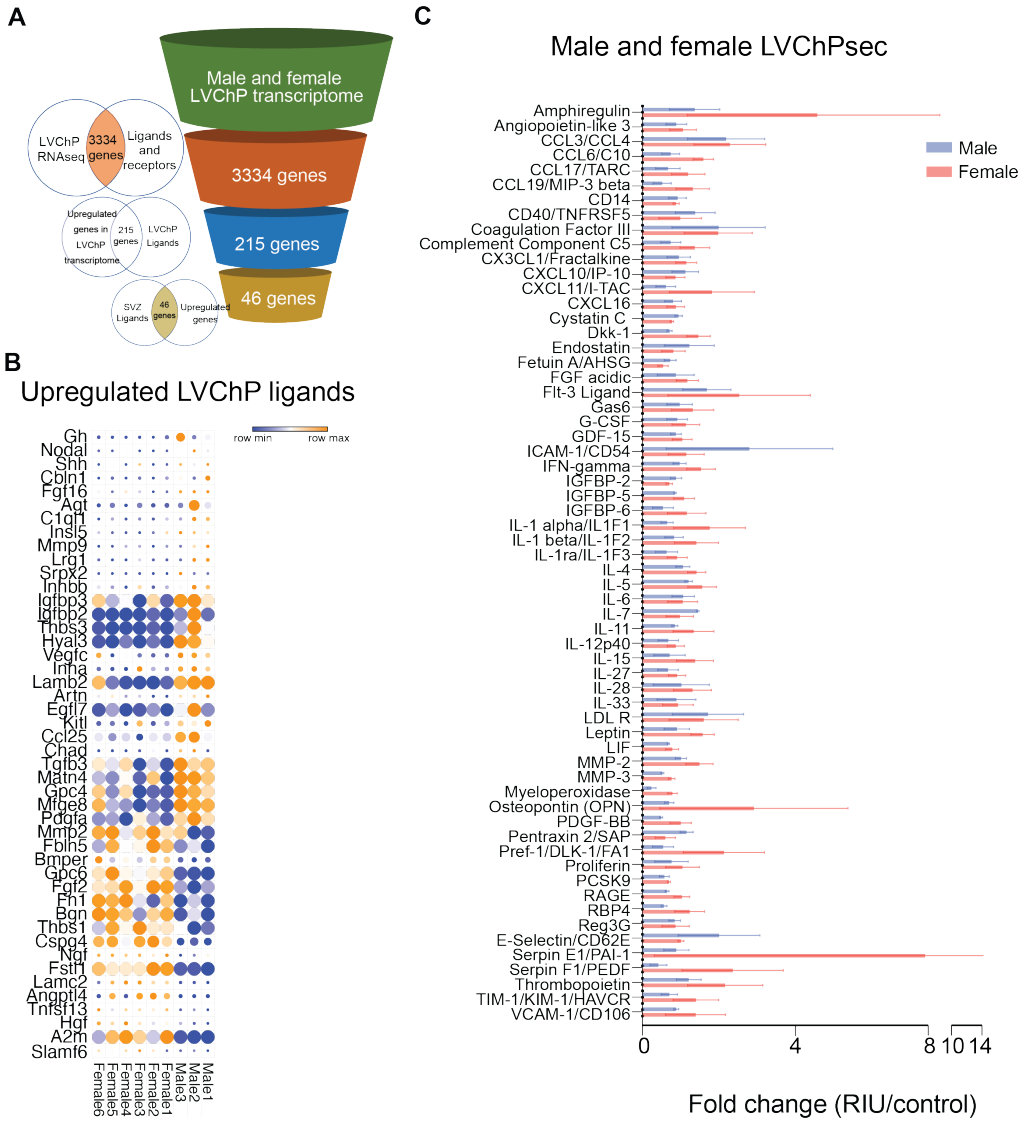

Figure 25: LVChP ligands and secreted factors between sex.
A) The workflow used to identify upregulated ligands between male and female LVChP. B) Heatmap showing the relative gene expression levels for upregulated male and female ligands. The colour map values on the heat map are assigned based on the standard deviation from the row mean. The size of the circles reflect the fpkm gene expression values. Anything over 750fpkm is shown by a circle of the same size. C) Relative protein intensity values for secreted factors detected by antibody array analysis of male (blue) and female (red) LVChP. Data represents the mean of each factor ± SEM. N=3

In summary, the LVChP actively transports and secretes factors that regulate V-SVZ NSCs. Baseline experiments show that the composition of the culture medium influences NSC activation. NSC doublet formation is higher in aNSCs compared to qNSCs and in the lateral wall compared to the septal wall. *In vitro* assays show that both male and female NSCs show increased activation when cultured with LVChP-derived factors. Female NSCs are more sensitive to LVChPsec and show higher activation when cultured with female LVChP-derived factors. Furthermore, transcriptome analysis reveals sex differences in the expression of LVChP ligands. Finally, antibody array analysis of the proteins secreted by the LVChP reveals differences in the levels of several proteins between males and females, which may contribute to the observed sex-specific regulation of aNSCs in the V-SVZ.

5.5 The LVChP and the estrous cycle

Our previous results show important differences between male and female LVChP. Next, we examined the differences in the female LVChP between two phases of the estrous cycle. Since ChP expresses sex hormone receptors, hormones may regulate its function [213-215]. Therefore, we compared the transcriptome and secretome between the estrous and diestrous phases in females.

The estrous phase is associated with higher levels of estrogen and lower progesterone levels, while diestrous phase is associated with lower levels of estrogen and higher progesterone levels (Figure 26A). To assess the estrous cycle, we used the conventional method of tracking the estrous cycle using vaginal swabs. In the vagina of female mice, three types of cells are found whose proportions change during the estrous cycle: nucleated epithelial cells, anucleated keratinised cells and leukocytes. During the proestrous phase, when estrogen levels are high and rising in preparation for mating, there is a high proportion of nucleated epithelial cells. During the estrous phase, the cells are almost completely anucleated and keratinised. During this relatively short window of time, the female is ready to mate. Metestrous phase swabs consist of nucleated and keratinised epithelial cells and leukocytes, while leukocytes dominate in the diestrous phase (Figure 26A, B). To ensure that the mice were in the correct phase, we took daily smears for two cycles (roughly ten days) and then isolated the LVChPs in the estrous and diestrous phases for analysis.

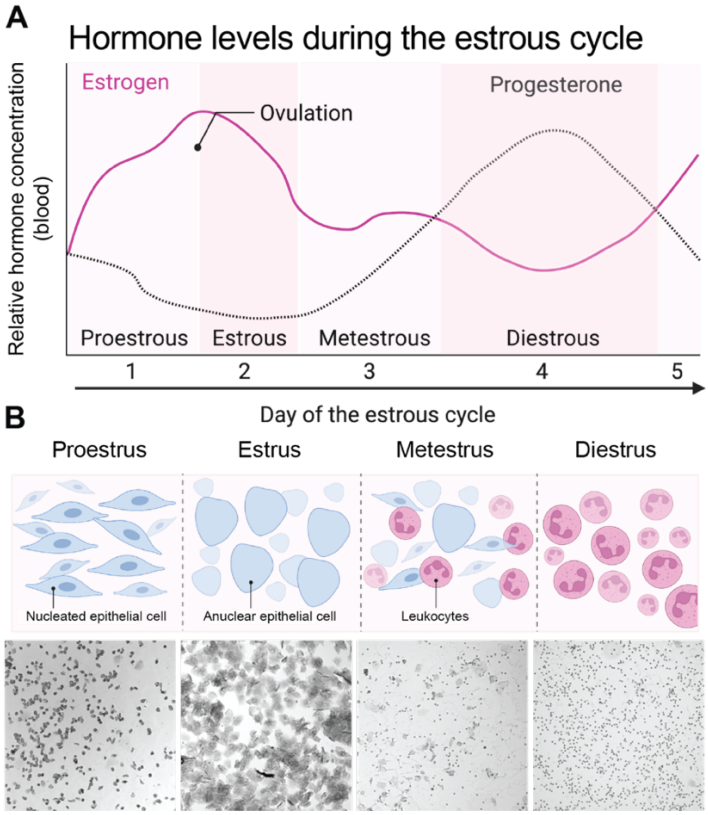

Figure 26: Hormone levels during the estrous cycle.
A) Relative hormone concentration (blood) of estrogen and progesterone during the phases of the estrous cycle. B) Schema and representative images showing vaginal swabs and proportions of cells. Magnification: 10x

5.5.1 LVChP transcriptome changes during the estrous cycle

Comparison of the DEGs of female LVChP in the diestrous and estrous phases revealed differences in their transcriptomes with a total of 192 DEGs between these two phases. In diestrous, genes related to the matrisome (e.g., *Serpina1a*, *Serpina1e*, *Serpina1b*, *Col14a1*, *Col15a1*) showed the greatest differences. Other biological processes enriched in the diestrous phase include metabolic enzymes (*Ces2e*, *Cyp7b1*), apoptosis (*Cflar*) and carriers (*Slc17a8*, *Slc22a19*). In the estrous phase, genes differentially expressed in the processes of transcription (*Ddn*, *Npas4*, *Neurod2*, *Csmd1*, *Tbr1*), ion channels (*Kcnmb4*, *Trpc6*, *Gng13*, *Kcnq5*), synaptic transmission (*Nptx2*, *Nrgn*, *Stx1a*, *Ngef*, *Dok5*) and calcium signalling (*Kif5a*, *Rasa1*, *Cas2*, *Mobp*) as well as signalling processes (*Omp*, *Opalin*, *Scrg1*, *Wnt7b*, *Tafa1*) (Figure 27A, B). STRING plot analysis (using k-means clustering for three clusters) to determine the protein-protein interactions of DEGs revealed clusters comprising processes involved in exocytosis (red), ion channel activity (green) and synaptic transmission (blue) in estrous (Figure 27C), while clusters formed with DEGs from the diestrous phase were not closely associated. These clusters belonged to nicotine addiction (red), endogenous sterols (green) and the ECM (blue) (Figure 27D).

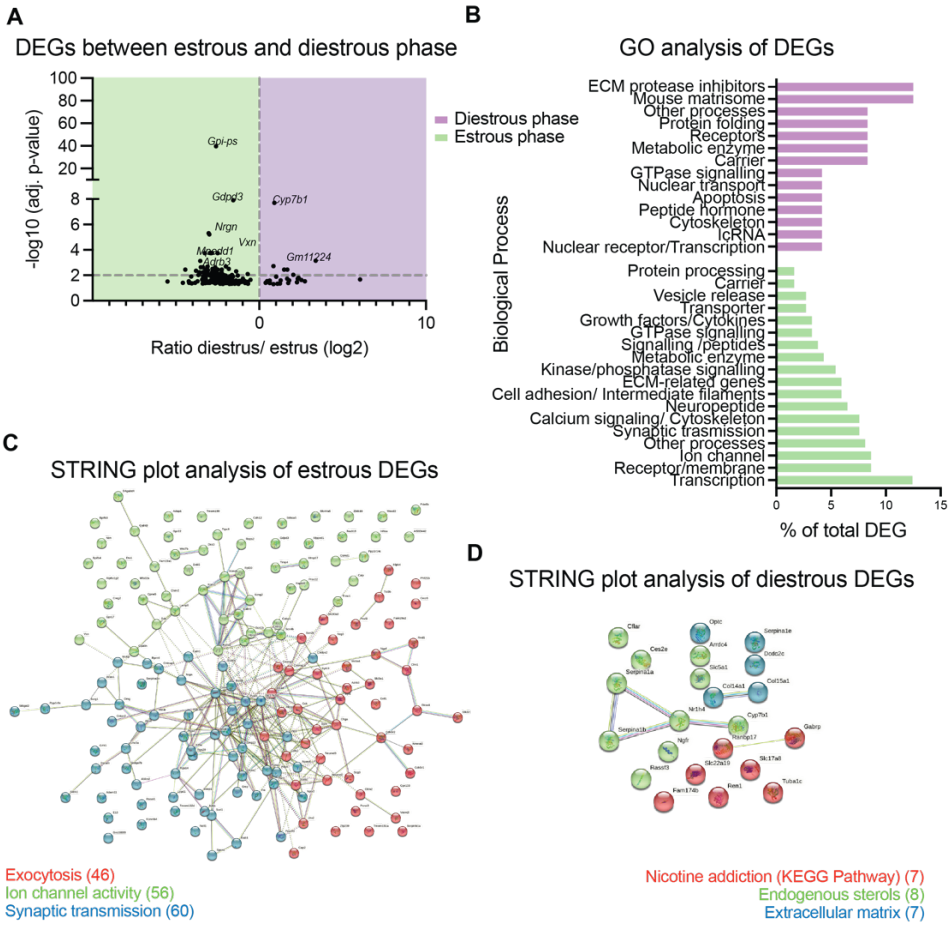

Figure 27: Analysis of DEGs between estrous and diestrous phase.
A) Volcano plot showing the DEGs between estrous (green) and diestrous (purple) B) Analysis of DEGs by biological process. C-D) String plot analysis of DEGS in the estrous phase (C) and DEGs in the diestrous phase (D). Genes underwent k-means clustering into three functional categories based on their association to each other.

5.5.2 Changes in LVChP secretome due to fluctuating sex hormones

To investigate changes in LVChP secretome (LVChPsec) during the estrous cycle, we compared LVChPsec derived from female diestrous phase and female estrous phase using antibody array. Similar to the male and female mixed LVChPsec comparison, 62 out of 111 cytokines and chemokines were detected in both the diestrous and estrous LVChPsec samples. Intriguingly, only Leptin and PDGF-BB showed slightly higher levels in diestrous compared to estrous LVChPsec, while all other proteins showed either higher levels in estrous or similar levels in both phases. Proteins that were higher in estrous LVChPsec included members of the CCL family (CCL6, 17, 19), fractalkine, CXCL chemokines (CXCL10, 11, 16), cytostatin C, Flt-3 ligand, IFNɣ, IGFBP2 and Thrombopoietin. These results suggest dramatic changes in secretome throughout the estrous cycle (Figure 28).

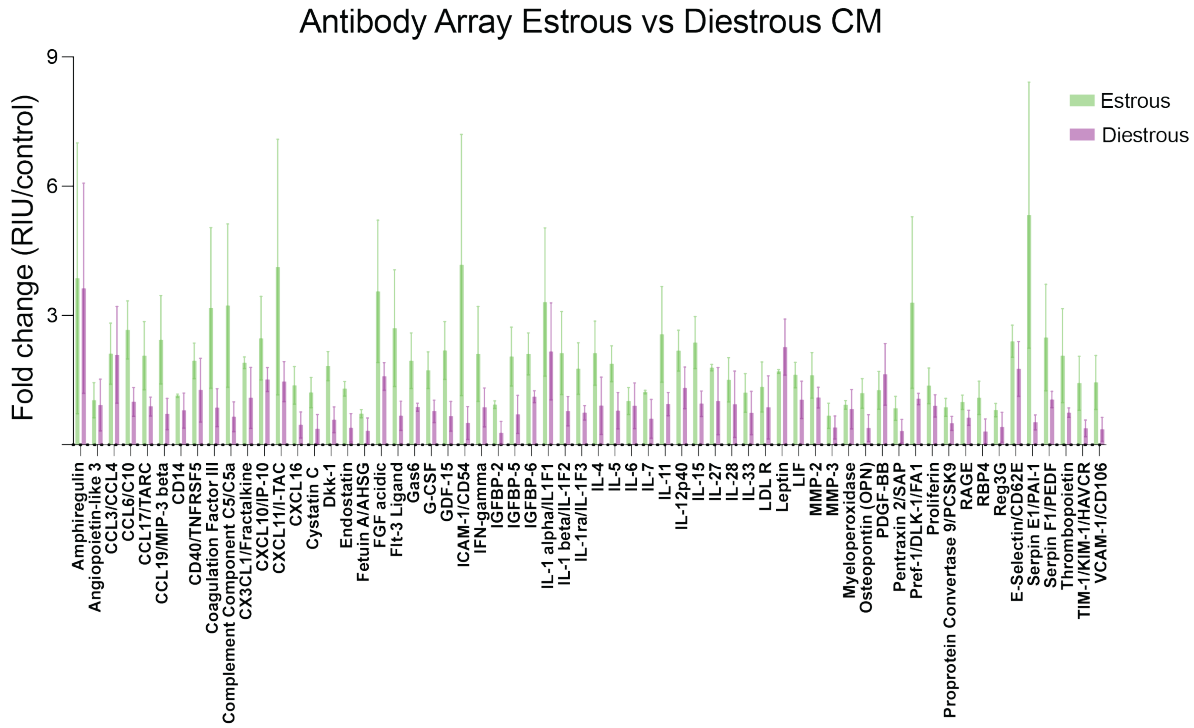

Figure 28: Antibody array of estrous and diestrous LVChPsec
Relative protein intensity values for secreted factors detected by antibody array analysis of female estrous (green) and diestrous (purple) LVChP. Data represents the mean of each factor ± SEM. N=3

5.5.3 Macrophages and the estrous cycle

As shown earlier, a higher number of macrophages were counted in the female LVChP as compared to males (Figure 18F). Macrophages express sex hormone receptors and may thus be modulated by them [316]. In order to determine if macrophage numbers change during the estrous cycle, we quantified the total number of macrophages (IBA1$^+$) and stromal and epiplexus macrophages in estrous and diestrous phases. The total number of IBA1$^+$ macrophages and stromal and epiplexus macrophages showed no significant difference in diestrous or estrous females (Figure 29A). Quantification of MRC1 (Figure 29B) and TMEM119 (Figure 29C) in female mice also showed no statistically significant differences between the diestrous and estrous phases.

Interestingly, despite no change in the number of macrophages, comparison of macrophage-associated genes in females in estrous and diestrous phase, as previously done for males and females (Figure 23), revealed marked differences in macrophage gene expression, with estrous and diestrous females clustering separately (Figure 29D). Of the 149 upregulated macrophage-associated genes in either estrous and diestrous, 80 were upregulated in estrous and 69 in diestrous (Figure 29D). Thus, rather than changing LVChP macrophage numbers, the binding of estrogen and progesterone to their respective receptors could lead to changes in the function and activity of macrophages during the estrous cycle.

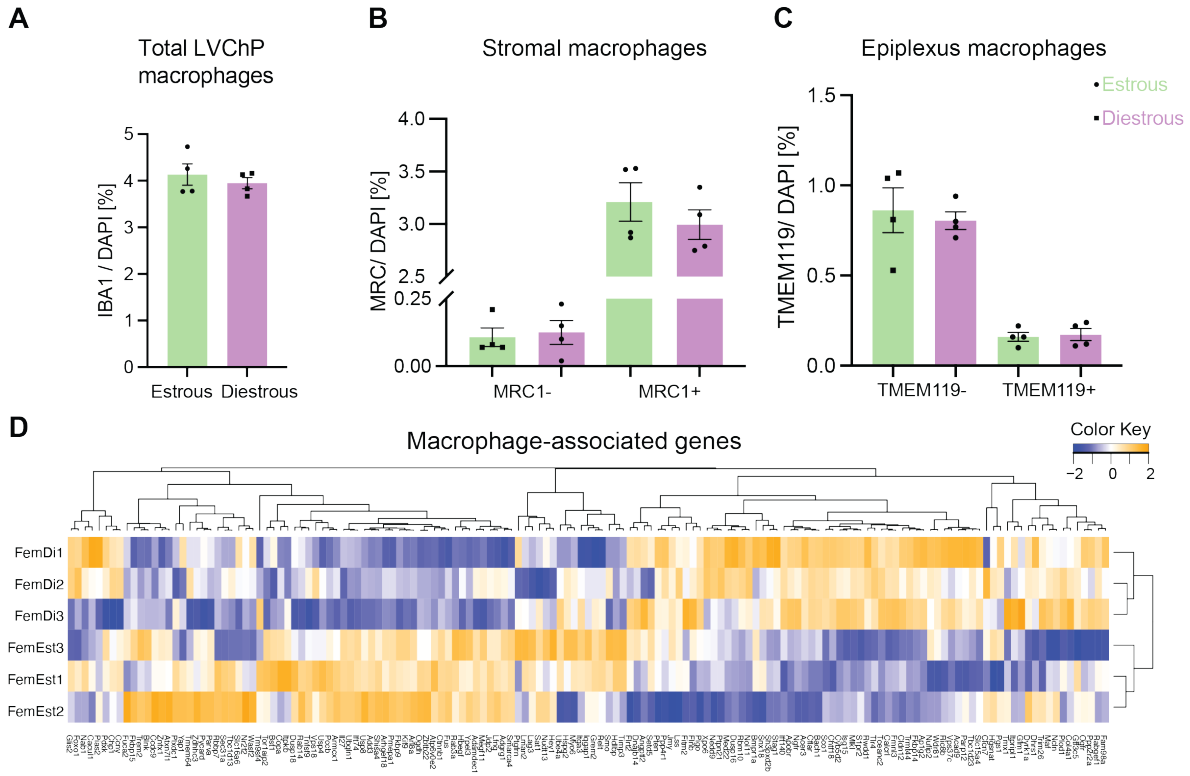

Figure 29: Differences in LVChP macrophages during the estrous cycle.
A) Quantification of the proportion of IBA1 cells per total cells (DAPI) in female estrous and diestrous LVChP cross-sections. B) Quantification of the proportion of MRC1-positive or negative and C) TMEM119-positive or negative cells per total cells (DAPI) in female estrous and diestrous LVChP cross-sections. D) Heatmap showing upregulated macrophage-associated genes in the female LVChP Abbreviations: FemDi = Female Diestrous, FemEst = Female Estrous

In summary, our results suggest that the LVChP responds to changes in sex hormone levels during the estrous cycle. Transcriptome analysis of the LVChP in estrous and diestrous revealed DEGs involved in diverse biological functions. Although analysis of macrophage numbers did not reveal differences between the two phases, there were clear differences in the expression of macrophage-associated genes. In addition, antibody analysis of LVChP CM from the estrous and diestrous phases suggested differences in protein secretion. These results suggest that while there were no detectable cellular differences between macrophages, the LVChP appears to be sensitive to changes in sex hormone levels at the transcriptional and secretory levels, supporting the hypothesis that the LVChP is a dynamic hub that responds rapidly to changes in its environment.

6 Developing tools to study the LVChP

There have been several limitations in the study of the LVChP, including its complex folding and the ability to obtain viable single cells without favouring a particular cell type in the adult LVChP. We have developed methods to overcome these limitations. These include creating a dissociation protocol for dissociating adult LVChP into viable single cells for molecular characterisation, developing methods for immunostaining whole mount explants, and optimising conditioning times to obtain the most suitable LVChPsec for our *in vitro* functional experiments and proteomic analyses.

6.1 Protocol for immunostainings of LVChP whole mount explants

The LVChP is commonly studied using coronal cross-sections. However, this is challenging due to the high degree of folding, which would require examining large numbers of cross-sections across its span (5-7mm). To better visualise the spatial distribution and quantify cells, we optimised a technique for immunostaining adult LVChP whole mount explants that provides spatial information on different cell types such as macrophages, pericytes, epithelial cells and blood vessels (Figures 11, 19). The intact LVChP is harvested from the brain and then unfolded to obtain a flat two-dimensional tissue. By using whole mount immunostaining, spatial resolution of specific cell locations along the dorsal-ventral and rostral-caudal axes of the LVChP can be achieved. This allows for a more comprehensive study of the LVChP while circumventing the complexity associated with its folded nature (Figure 30).

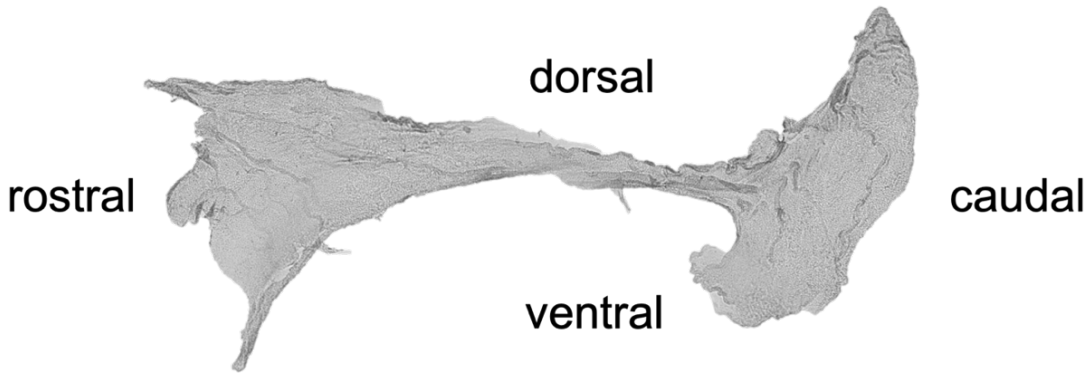

Figure 30: Whole mount LVChP explants
Whole mount preparation of the LVChP depicting the dorsal-ventral and rostral-caudal orientation of the tissu.e

I tested various methods and conditions to optimise immunostaining of whole mount preparations of the LVChP. Fixation times ranging from 10 to 120 minutes were tested. No significant difference was observed between 30 and 120 minutes of fixation for immunostainings of the vasculature and macrophages, therefore 30 minutes was chosen as the fixation time for subsequent experiments. However, this should be optimised for each antibody. As the LVChP is a tissue that binds readily to substances in its environment, background staining in whole mount preparations was often high due to non-specific binding. To alleviate this problem, different blocking solutions were tested using normal donkey serum (NDS), bovine serum albumin (BSA) and Tris-HCl. When comparing a 10% BSA blocking with a 10% NDS blocking (Figure 31A), a clear difference in staining intensity was observed, with the BSA-blocked tissue showing a higher staining intensity. For this reason, subsequent whole mount preparations were blocked with 10% BSA. To determine the optimal BSA concentration that minimised background signal, various concentrations were tested from 1% to 10% (not shown here). Blocking with 10% BSA and then switching to 3% BSA during incubation of the primary antibody gave the best signal-to-noise ratio. Other parameters, such as different concentrations of Triton X-100 and Saponin, as well as the duration of incubation with secondary antibodies were also tested. Depending on the antibody used, either Triton X-100 or Saponin are the better permeabilising agents. Specifically, stromal labelling requires Triton X-100 as it allows better permeabilization into the LVChP tissue (data not shown).

A crucial step for high-quality whole mount immunostaining was to obtain a flat LVChP tissue when mounting. Several methods were tried, including fixing the tissue on agarose-coated slides using small pins, staining the tissue first and then mounting, and staining under floating conditions followed by mounting. However, mounting the tissue on agarose-coated slides caused the buffer to leak through the agarose and the tissue to dry out. Staining after mounting showed limited antibody penetration from only one side of the tissue, particularly in the stromal compartment. In contrast, staining under floating conditions allowed antibody penetration into both sides of the tissue, resulting in better staining of blood vessels (CD31) and macrophages (IBA1) in the tissue (Figure 31B). Therefore, the LVChP was stained under floating conditions and subsequently mounted on glass slides for analysis.

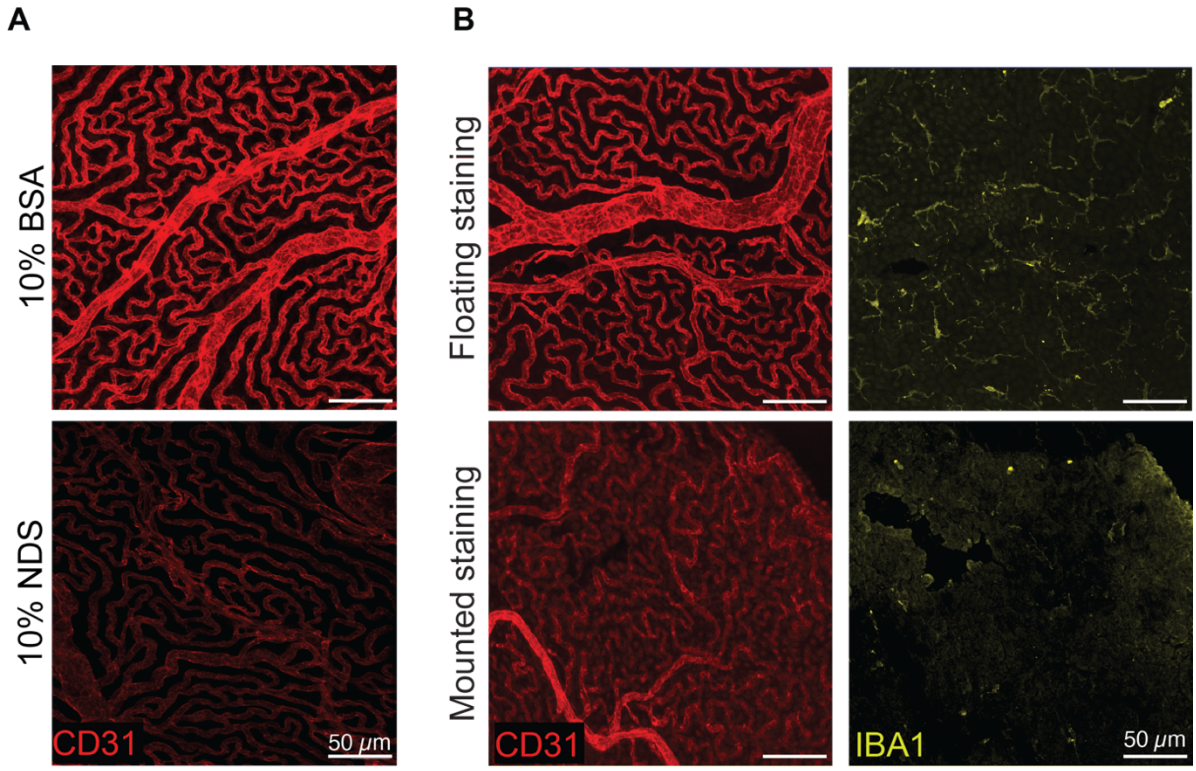

Figure 31: Testing different conditions in whole mount preparations.
A) Representative image immunostained for CD31 (red). Top: Tissue blocking with 10% BSA (bovine serum albumin). Bottom: Tissue blocking with 10% NDS (normal donkey serum). B) Representative images immunonstained with CD31 (red) and IBA1 (yellow). Top: Tissue stained in floating conditions. Bottom: Tissue stained in mounted conditions.

The full protocol for whole mount immunostainings is documented in the Materials and Methods section (section 8) of this thesis. Within the scope of this thesis, whole mount immunostainings were employed to compare blood vessel architecture (section 5.1.1) and macrophage distribution (section 5.3.2) between the sexes.

6.2 Optimising conditions for preparation of LVChP CM

The LVChP is an important niche component of the V-SVZ, and LVChP-derived factors have been shown to regulate NSCs both *in vitro* and *in vivo* [15]. Previous studies have reported the harvesting of conditioned medium (CM) from LVChP explants. Briefly, LVChP explants are isolated from the brains of adult mice and placed in a transwell insert containing medium and incubated at 37°C. After incubation, the transwell is removed and the CM in the well is harvested for further use (Figure 32A).

We aimed to optimise this method for our *in vitro* functional experiments and proteomic analyses of LVChP CM from male and female samples. The main parameters tested included the number of explants per insert, the duration of conditioning in the incubator, the type of transwell insert used (coated or uncoated) and the choice of medium. As described in the results, we tested neurosphere medium and a minimal medium (Figure 25B) and also

examined the effect of conditioning with or without progesterone, a sex hormone known to play a role in LVChP secretion and osmoregulation [213, 217]. To determine the timing of conditioning, proteomic analysis was performed on CM conditioned over a time-course of 2, 4, 6 and 24 hours to determine the optimal conditioning duration to capture as many secreted factors as possible without compromising LVChP viability (Figure 32B). Our mass spectrometry analysis revealed that several peptides, including coronin 1c (CORO1C), stromal cell-derived factor 2 like 1 (SDF2L1), superoxide dismutase 2 (SOD2), CC motif chemokine ligand 2 (CCL2) and prostaglandin reductase 2 (PTGR2), were secreted only after an incubation period of at least four hours (Figure 32B). Minimal differences were observed between the 4- and 6-h conditioning intervals, while fewer peptides were detected overall after 24-h conditioning. Importantly, no differences in clone formation were observed between 4 and 6 hours of conditioning (data not shown).

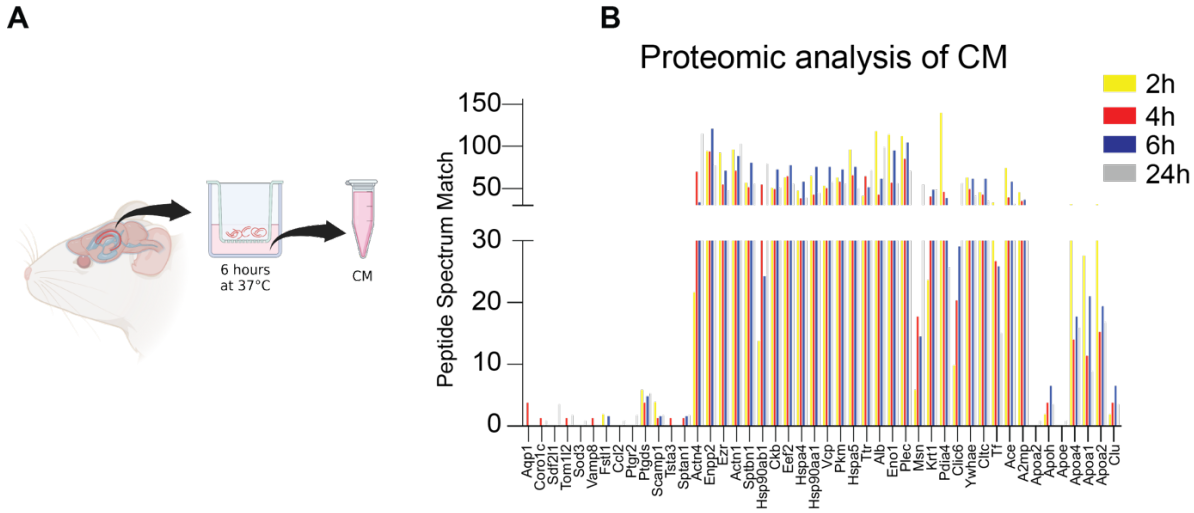

Figure 32: Preparation and proteomic analysis of LVChP CM.
A) Schema showing how CM is prepared and B) A selected number of peptides from the proteomic analysis of CM over a time course ranging from 2h to 24h.

In summary, to obtain CM for our *in vitro* experiments and for proteomic comparison of male and female LVChP-derived factors, 5 LVChPs are added per insert and incubated for six hours at 37°C in non-collagen-coated inserts containing minimal medium without progesterone. After incubation, the transwell is removed, the medium is harvested and progesterone is added to the harvested CM.

6.3 Establishing a cell dissociation protocol for adult LVChP single cell analysis

The rich ECM, tight junctions between epithelial cells and variety of cell types in the LVChP pose a challenge to the successful dissociation of this tissue. While dissociation protocols for ChPs have been published, these have primarily focused on isolating specific cell types and have had difficulty obtaining viable single LVChP cells without cell type bias [13, 44, 317, 318]. To optimise the dissociation protocol for adult LVChP and obtain viable cells without bias for a particular cell type, an extensive array of enzymes was systematically tested with different incubation sequences, concentrations and lengths. In addition, different strainer sizes, pipetting techniques and volumes were thoroughly evaluated during manual trituration to ensure optimal yield. After dissociation, live staining was performed to confirm the preservation of each cell type and the viability of the cells. Flow cytometric analyses confirmed the preservation of the major cell types in the dissociated LVChP cells and confirmed the robustness and reliability of the optimised dissociation protocol (Figure 33, 34A-C).

In Table 1, a comprehensive list of the various parameters employed and tested to optimise the dissociation of the LVChP is presented. Enzymes such as Collagenase II, TrypIE Express, Pronase and Trypsin were tested in the experiments, with varying concentrations and incubation times examined for each enzyme. Additionally, combinations of multiple enzymes were evaluated. In general, the longer the incubation of enzymes, the more cell death was observed. Trypan blue was used to determine cell viability. For each individual round, the total cell number was counted and cells plated to see if dissociation into single cells was successful.

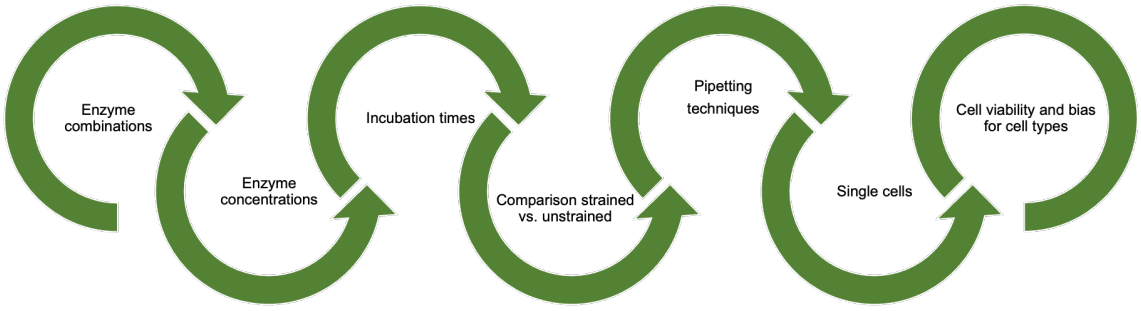

Figure 33: Workflow for dissociation of the LVChP into single cells

Table 1: Parameters tested for dissociation of LVChP into single cells.
From left to right: conditions tested per dissociation (changes in red), number of cells/ mL obtained, percentage of single cells, percentage of viable cells and comments regarding the dissociation and flow analysis.

Condition	# of cells/mL	% of single cells	% of viable cells	Comments
Collagenase II (5mg/mL) + 1x TrypIE strained	152500	98.4%	93%	Few cells
Collagenase II (5mg/mL) + 1x TrypIE unstrained	132500	94.3%	98%	Few cells
Collagenase II (5mg/mL) + 2x TrypIE strained	325000	98.5%	92%	
Collagenase II (5mg/mL) + 2x TrypIE unstrained	260000	98.1%	98%	
Pronase (1mg/mL) + 5x Trypsin 0.0025% strained	80000	90.6%	100%	Few cells, many aggregates
Pronase (1mg/mL) + 5x Trypsin 0.0025% unstrained	62500	92.0%	100%	Few cells, many aggregates
Pronase (4mg/mL) + 5x Trypsin 0.0025% strained	77500	80.6%	100%	Few cells, many aggregates
Pronase (4mg/mL) + 5x Trypsin 0.0025% unstrained	77500	93.5%	97%	
Collagenase II (5mg/mL) + 1x TrypIE strained	217500	95.4%	100%	
Collagenase II (5mg/mL) + 1x TrypIE unstrained	142500	96.5%	100%	
Collagenase II (5mg/mL) + 2x TrypIE strained	255000	100.0%	93%	
Collagenase II (5mg/mL) + 2x TrypIE unstrained	160000	100.0%	98%	
Pronase (1mg/mL) + 1x Trypsin 0.0025% strained	142500	98.2%	98%	
Pronase (1mg/mL) + 1x Trypsin 0.0025% unstrained	232500	100.0%	100%	
Pronase (2mg/mL) + 5x Trypsin 0.0025% strained	135000	98.1%	93%	Dead cells
Pronase (2mg/mL) + 5x Trypsin 0.0025% unstrained	92500	100.0%	100%	
Collagenase (5mg/mL) 40 minutes strained	607500	95.9%	95%	Pericytes lost
Collagenase (5mg/mL) 40 minutes unstrained	452500	97.2%	97%	Pericytes lost
Collagenase (5mg/mL) 20min + Pronase (1mg/mL) 25 min strained	375000	93.3%	95%	Several aggregates
Collagenase (5mg/mL) 20min + Pronase (1mg/mL) 25 min unstrained	462500	94.6%	98%	Several aggregates
Pronase (1mg/mL) + 1x TrypIE strained	180000	100.0%	94%	
Pronase (1mg/mL) + 1x TrypIE unstrained	157500	98.4%	94%	
Collagenase (5mg/mL) 30 minutes strained	585000	96.6%	98%	
Collagenase (5mg/mL) 30 minutes unstrained	505000	95.5%	97%	
Collagenase (5mg/mL) 20min + Pronase (1mg/mL) 25 min strained	487500	97.9%	99%	Pericytes lost
Collagenase (5mg/mL) 20min + Pronase (1mg/mL) 25 min unstrained	345000	94.9%	99%	Several aggregates
Collagenase (5mg/mL) 30 minutes strained - FACS P1000	73264	93.9%	data missing	Few cells, many aggregates
Collagenase (5mg/mL) + Pronase (1mg/mL) 25 min strained - FACS P1000	75548	95.0%	97.1%	Few cells, many aggregates
Collagenase (5mg/mL) + Pronase (1mg/mL) 25 min strained - FACS P1000 + P200	67676	88.5%	98.7%	Few cells, many aggregates
Collagenase (5mg/mL) + Pronase (1mg/mL) 25 min strained - FACS P1000 + P200	32795	83.2%	94.0%	Few cells, many aggregates
Collagenase (5mg/mL) + Pronase (1mg/mL) 25 min strained - FACS P1000 + Pasteur	29505	82.0%	94.6%	Few cells, many aggregates
Pronase (2mg/mL) 10 minutes strained	232500	97.0%	98.0%	
Pronase (1mg/mL) 10 minutes strained	247500	90.1%	86.8%	Many dead cells
Pronase (1.5 mg/mL) 30 minutes strained	227500	94.6%	95.7%	
Collagenase (5mg/mL) + Pronase (2mg/mL) 10 min strained P1000	370000	99.98%	99.97%	
Collagenase (5mg/mL) + Pronase (1mg/mL) 10 min strained Pasteur	465000	99.96%	99.98%	Large cells lost
Collagenase (5mg/mL) 20min + Pronase (2mg/mL) 10min sequentially	422500	96.4%	95.9%	
Collagenase (5mg/mL) 20min + Pronase (2mg/mL) 10min combined	360000	88.9%	91.7%	Reduced number of pericytes
Collagenase (5mg/mL) 20min + Pronase (2mg/mL) 10min sequentially + Accutase	382500	98.0%	96.1%	
Collagenase (5mg/mL) 20min + Pronase (2mg/mL) 10min combined + Accutase	455000	91.8%	97.3%	Many aggregates
Collagenase (5mg/mL) 20min + Pronase (2mg/mL) 10 min - 1 ChP	75000	100.0%	100.0%	
Collagenase (5mg/mL) 20min + Pronase (2mg/mL) 10 min - 2 ChP	145000	100.0%	96.6%	
Collagenase (5mg/mL) 20min + Pronase (2mg/mL) 10 min - 3 ChP	277500	99.1%	98.2%	
Collagenase (5mg/mL) 20min + Pronase (2mg/mL) 10 min - 4 ChP	330000	97.7%	97.7%	
Collagenase (5mg/mL) 20min + Pronase (2mg/mL) 10 min - 5 ChP	312500	98.4%	99.2%	

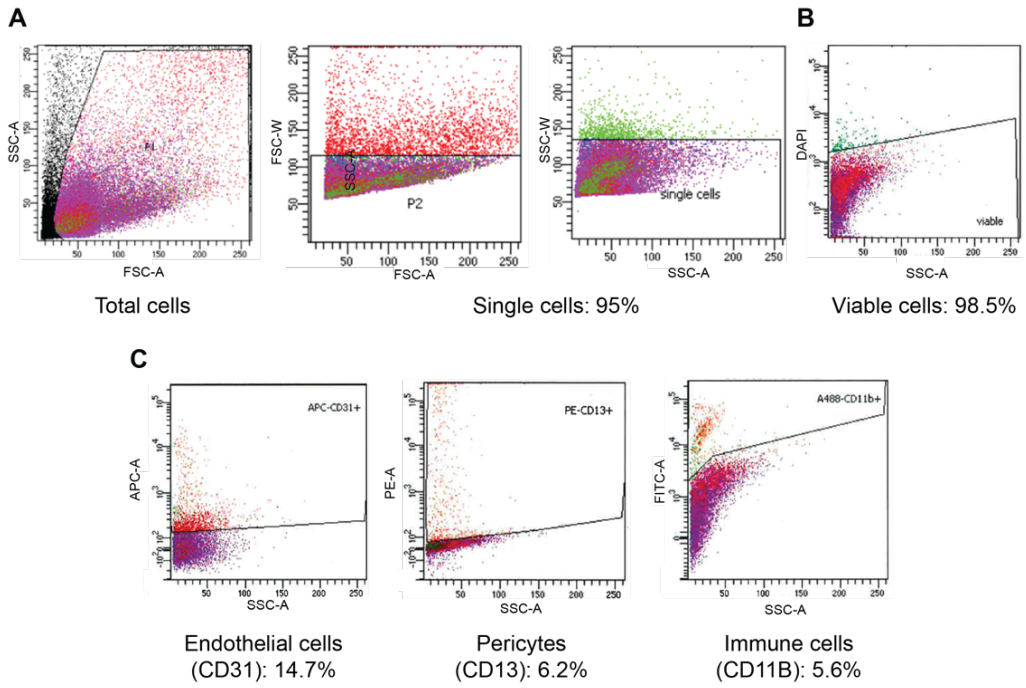

Figure 34: Flow analysis of dissociated LVChP.
A) Dissociation with Collagenase II (5mg/mL) 20 minutes + Pronase (1mg/mL) 10 minutes and strained with a 40µm strainer. B) Cell viability C) FACS plots for endothelial cells (CD31), pericytes (CD13) and immune cells (CD11B).

Sequential incubation of the enzymes is more effective than simultaneous incubation. In Figure 35A, cells were subjected to simultaneous enzyme digestion of collagenase II (5mg/mL) and pronase (2mg/mL) for 20 minutes. In Figure 35A', LVChP cells were incubated sequentially with collagenase (5mg/mL) for 20 minutes, followed by pronase (1mg/mL) for 25 minutes. Finally, in Figure 35A'', the enzymatic digestion of LVChP cells was incubated with collagenase (5mg/mL) for 20 minutes followed by a shorter incubation with pronase (1mg/mL) for 10 minutes. The percentage of CD13+ cells (a pericyte marker) varied significantly depending on the enzymatic digestion method used. This highlights the importance of selecting enzyme combinations, concentrations and incubation times for the analysis of the different desired LVChP cell types. This dissociation method allows us to retain high viability of LVChP cells and captures most of the reported cell populations.

Importantly, we found that tailoring the dissociation parameters to the specific cell type of interest, particularly immune cells, could be beneficial. Using our dissociation protocol (Doetsch protocol), we achieved excellent cell viability (92.3%) while maintaining different cell populations. However, only a small proportion (0.91%) were macrophages.
In contrast, when using a previously reported immune cell protocol (Baruch protocol [317]), we observed lower viability (70.2%) but a higher proportion of macrophages (6.96%) (Figure 35C). Given the enrichment of immune cells with the Baruch method, we used this dissociation protocol for our comparative analyses of immune cells (including dendritic cells, T cells, B cells and stromal and epiplexus macrophages (section 6.3.1).

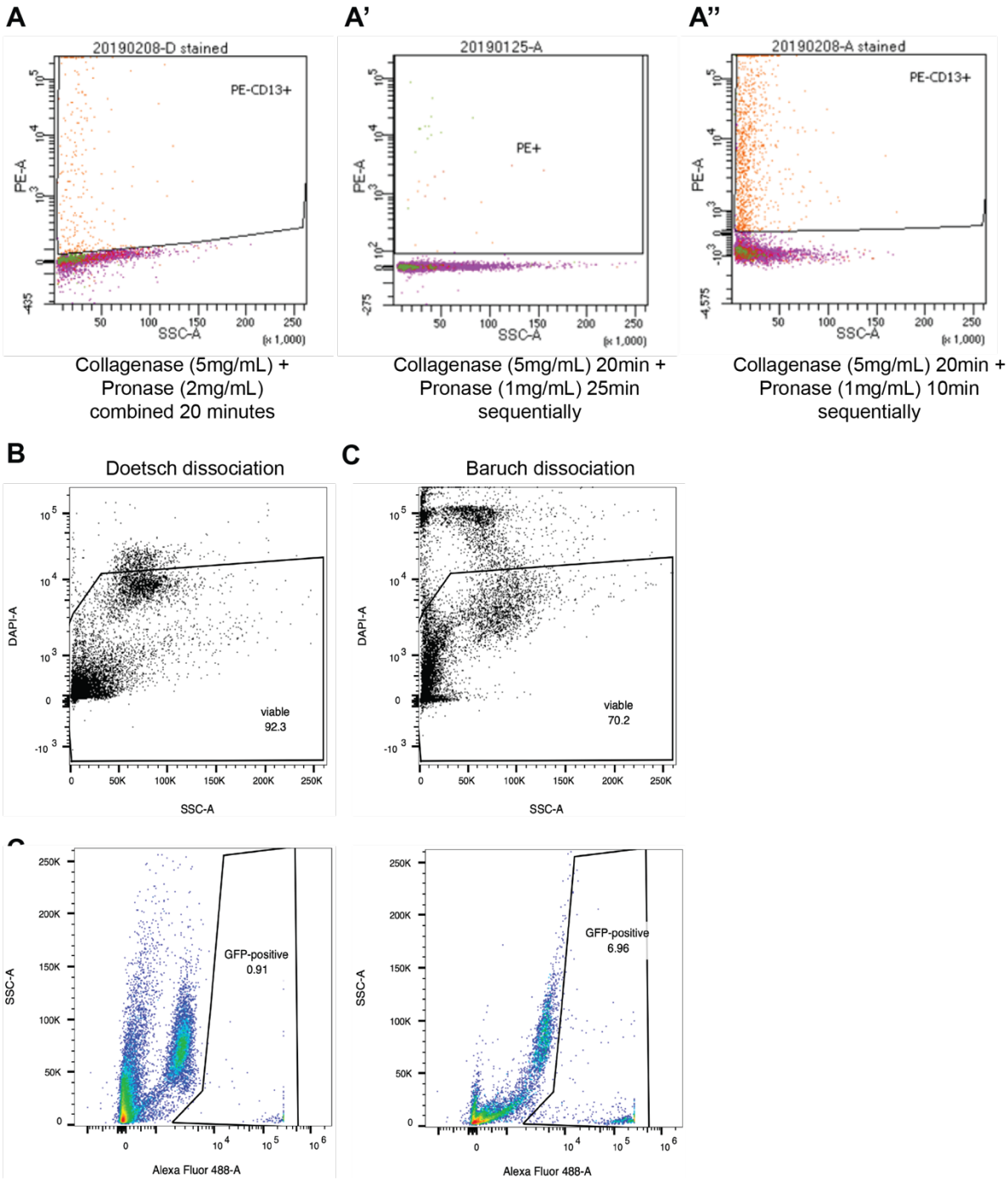

Figure 35: Dissociation of the LVChP into single cells.
A-A'') Different dissociations tested. Dissociations were as follows: A) collagenase II (5mg/mL) + pronase (2mg/mL) for 20 minutes combined, A') collagenase II (5mg/mL) for 20 minutes + pronase (1mg/mL) for 25 minutes sequentially, A'') collagenase II (5mg/mL for 20 minutes + pronase (1mg/mL) for 10 minutes sequentially; B-C) depict the comparison between the Doetsch (B) and Baruch (C) dissociation methods. Viability in the Doetsch protocol is 92.3%, while the Baruch protocol is 70.2%, flow cytometry analysis for macrophages (Alexa Fluor 488-positive) was 0.91% using the Doetsch protocol and 6.96% using the Baruch protocol

6.3.1 Flow Cytometry for LVChP cell types

LVChP samples were subjected to flow cytometry analysis to assess the distribution of different cell types, including fibroblasts (FAP), pericytes (CD13), endothelial cells (CD31), immune cells such as T cells (CD3), B cells (CD19), dendritic cells (CD11c), epiplexus cells (P2RY12) and macrophages (CX3CR1). Our results show no significant differences in the abundance of any particular cell type between male and female LVChP (Figure 36A, B). There were slightly higher proportions of fibroblasts in females, while males had higher proportions of pericytes (Figure 36A). However, these findings warrant further analysis. In the immune cell population, the epiplexus cells had higher proportions in males than females, supporting the IHC stainings described previously. Also, CX3CR1 showed higher proportions in females than males (Figure 36B, B').

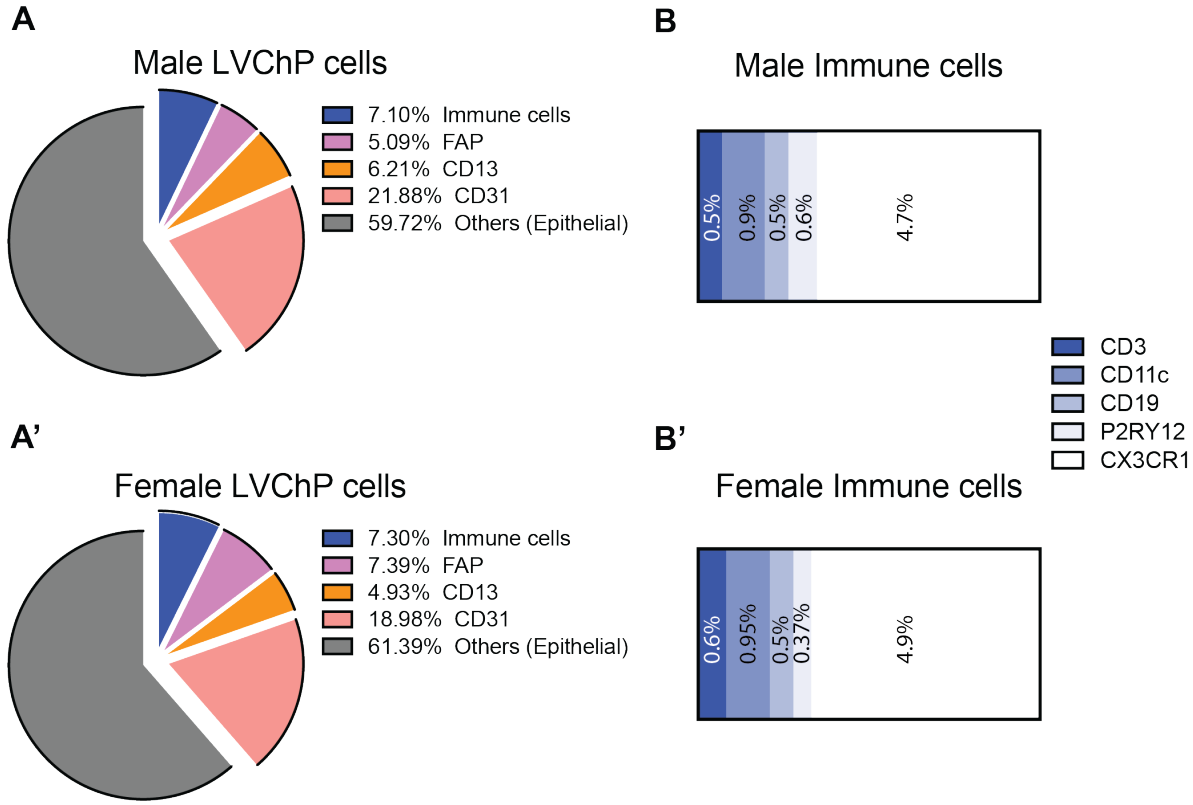

Figure 36: Flow cytometry for LVChP cell types.
A, A') Proportions of cells in A) male and A') female LVChP. B,B') Proportion of immune cells in B) male and B') female LVChP. N = 6

7 Discussion

7.1 Conclusions

The lateral ventricle choroid plexus is a central hub in the CNS responsible for regulating brain homeostasis by integrating and responding to a variety of signalling moieties. Impaired function can lead to severe CNS disorders, including neurodegenerative diseases. Several CNS disorders have a sex prevalence, highlighting the importance of studying and understanding the differences between males and females in the clinical setting. The findings in this thesis have greatly improved our understanding of the LVChP in healthy male and female mice. In **section 5.2**, we examined the transcriptomic differences in LVChP between males and females. Our analyses revealed multiple DEGs in both sexes involved in different biological functions. This data suggests that sex differences may result in varying LVChP functions as well. Our transcriptome analyses led us to next examine macrophages in the LVChP (**section 5.3**), where we found higher numbers of macrophages in females compared to males with differences in macrophage subpopulations and macrophage gene expression between the sexes. In **section 5.4**, we examined the differences in LVChP secretome between the sexes. Our *in vitro* experiments combined with our proteomic analysis of male and female CM revealed differences in secreted factors between the sexes, indicating differential regulation of V-SVZ NSCs *in vitro*.

In **section 5.5**, we examined the effects of the estrous cycle on the female LVChP transcriptome, secretome and LVChP macrophages. ENRICHR analysis of DEGs between the estrous and diestrous phases showed striking changes in LVChP expression during the estrous cycle. Finally, **section 6** describes the various methods and protocols that have been optimised and used to facilitate the analyses described in this thesis and ongoing research in the laboratory. These include dissociation of the LVChP into single cells for FACS analyses and single cell RNA sequencing, immunostaining for whole mount preparations to investigate the spatial distribution of proteins and cell types in the LVChP, and optimising CM for LVChP-derived factors. Overall, this thesis highlights the involvement of the strategically located LVChP in numerous fundamental biological processes that contribute to the proper functioning of the CNS.

To understand the impact of sex differences on the LVChP and its essential role in the CNS, we performed a comparative analysis of the transcriptome and secretome of the male and female LVChP. Our transcriptome analyses revealed the presence of DEGs associated with a variety of interesting biological processes, including immune responses, modulation of the ECM, chemical detoxification and clearance mechanisms and LVChP secretome differences between sex (Figure 13, 14), which was supported by our secretome analyses and immunostainings in the LVChP. In the next pages, I will discuss the functional implications of our findings.

Sex differences in the LVChP immune landscape

The ChP is an immunological niche at the interface between the blood and the CSF that harbours different types of immune cells such as T cells and macrophages [13, 317]. The ChP responds differentially to acute and recurrent peripheral inflammation and senses changes in the blood and CSF to trigger an inflammatory response [121, 123]. Our transcriptome and CM proteome data highlight that cytokine and chemokine signalling pathways are predominant in both male and female LVChP, with an important enrichment in genes related to the immune response and immune-related pathways in the female LVChP transcriptome (Figures 13, 14, 25).

These results are in line with the fact that females have a stronger innate and adaptive immune response than males, resulting in more rapid clearance of pathogens. However, this trait is also associated with increased susceptibility to inflammatory and autoimmune diseases [292]. The X chromosome contains numerous genes that regulate immune function and are largely responsible for sex differences in the development of immune-related diseases [319]. These genes include Toll-like receptors (TLR7 and TLR8) and cytokine receptors (e.g., IL2RG) [320, 321]. In addition, women with Turner syndrome (with only one X chromosome or have major X chromosome deletions) have lower IgG and IgM levels and fewer T and B cells compared to XX women, highlighting the importance of the X chromosome in the immune response [322]. In the female LVChP, DEGs associated with the immune system included *A2m*, *Cx3cr1* and *Csf1r*, while DEGs in males included *Bst2*, *Apoe* and *Ly6a* (Figure 14, Appendix Table 2). *A2m* plays a role in the immune response by binding and inhibiting cytokines, thereby exerting anti-inflammatory effects. Moreover, it has been linked to AD due to its role in mediating clearance and degradation of amyloid β [301]. *Bst2* is an interesting immune-related gene that is differentially expressed in male LVChP and has been linked to viral immunity [305]. Females have been shown to be more susceptible to viral infections such as cytomegalovirus, HIV and influenza A virus [323]. Since *Bst2* is involved in trapping viruses in the ChP, it is possible that its higher expression in males is more effective in limiting the entry of virions into the CNS than in females. *Apoe* is another gene that is heavily involved in the immune system. It reportedly acts in suppressing T-cell proliferation, regulating macrophages, presenting lipid

antigens to natural killer cells and modulating inflammation [324]. Interestingly, *Apoe* is highly expressed in epiplexus macrophages (data not shown). This is in agreement with the transcriptomic profiling of epiplexus cells showing that genes involved in lipid metabolism are upregulated [44, 281].

CX3CR1 and CSF1R are widely recognised markers of macrophages, with Cx3cr1 binding neurotactin and playing an essential role in the recruitment of T cells and monocytes and in the regulation of adhesion and migration functions [325]. *Csf1r*, is responsible for macrophage differentiation and regulation of macrophage functions [326]. Our studies of macrophages in the LVChP have revealed interesting differences in numbers of stromal and epiplexus compartments between sexes. Notably, females had higher numbers of macrophages in the LVChP, with stromal macrophages enriched in females, while males had more epiplexus cells overall (Figure 18-22). To our knowledge, this is the first report to indicate significant sex-related differences in LVChP cell types between the sexes. Single-cell studies have recently expanded our understanding of LVChP macrophages by identifying specific genes expressed in either stromal or epiplexus macrophages, revealing their transcriptional differences [44, 269].

Our investigation of epiplexus cells also showed a higher abundance of TMEM119^{-} epiplexus macrophages, whereas females displayed a higher number of TMEM119^{+} epiplexus macrophages (Figure 22C, D). Our analysis of the gene expression profiles associated with these distinct populations unequivocally suggest different functional characteristics (Figure 22 E-G). TMEM119^{-} macrophages, making up the larger fraction of the total epiplexus cell population, are enriched in genes linked to granzymes, implicating their involvement in phagocytic processes. This is consistent with reports in the literature showing that one of the main described functions of epiplexus cells is phagocytosis [327]. On the other hand, TMEM119^{+} macrophages express genes associated with cytokine and chemokine signalling, indicative of their role in immunosurveillance and recruitment of other immune cells (Figure 22G). Nevertheless, the underlying reasons for these sex-based differences in epiplexus macrophage populations remain elusive and require further investigation. The same analysis for stromal macrophages (MRC1^{+} IBA1^{+} cells) revealed that a significant proportion of genes associated with these cells are involved in the regulation of host defence mechanisms, complement pathway activation, synapse pruning and regulation of immune cell chemotaxis (data not shown). Notably, these functions include both pro- and anti-inflammatory processes. Immunostaining of whole mount explants for IBA1 allowed us to observe interesting differences in stromal macrophage morphology between the sexes (Figure 19E, E'). Morphology is often associated with macrophage activation and function [328]. While the concept of activation states of M1 and M2 macrophages remains controversial in the field, I will use this classic polarisation to explain the correlation between macrophage morphology and activation/function. M1 macrophages typically have a large, round and amoeboid

appearance and are known to be more phagocytic and pro-inflammatory. Their morphology allows them to rapidly migrate to where they are needed [329, 330]. In contrast, stellate M2 macrophages are associated with a pro-healing and anti-inflammatory phenotype, and their stellate morphology allows them to be more sensitive to their environment [331]. However, this correlation between macrophage function and morphology does not apply in every case [332]. To illustrate this point, our transcriptome analysis of macrophage-associated genes, together with our immunostaining data, has shown that only a small subset of these genes are classical M2 genes (Figure 23A). However, the vast majority (96%) of stromal macrophages of both sexes express CD206 (MRC1), a marker commonly associated with M2 macrophages, highlighting the challenge of making assumptions based on markers alone (Figure 20C).

Our investigation of immune signalling revealed further differences between cytokine and chemokine signalling and secretion between male and female LVChP (Figure 25C). In particular, higher levels of these immunomodulatory factors were found in the female CM. This observation is consistent with our overarching findings that the female LVChP exhibit enhanced immune responses, which may be important in the context of various CNS pathologies. An example of this is *A2m*, a female DEG, which has been shown to mediate the clearance and degradation of amyloid β in the CSF. Importantly, decrease of A2M increases the risk for AD [333].

Finally, sex-specific differences in immune response are known to vary across life stages and may be influenced by age and reproductive status [292]. Mouse macrophages have been found to express sex hormone receptors that can influence macrophage functions such as phagocytosis and chemokine expression [334-336]. Indeed, removal of gonads in male or female mice has been shown to alter the expression of chemokines, adhesion molecules and cytokine transcripts, which have different basal levels between the sexes, with female ovariectomy having a more pronounced effect on genes related to immune surveillance compared to male gonadectomy [147, 212]. In our study, it remains unclear whether all subpopulations of macrophages in the LVChP express sex hormone receptors. While we did not find differences in macrophage numbers between the estrous and diestrous phases (Figure 29A-C), our transcriptome analyses revealed distinct differences in gene expression during these phases (Figure 29D, Appendix Table 7), suggesting that macrophages are sensitive to fluctuations in sex hormones, which may lead to differential functions and secretomes. Indeed, our proteomic analysis of the LVChPsec reveal differences in cytokines (IL5, IL7, IL15) and chemokines (CXCL1, CXCL16) in females during the estrous and diestrous phases, further supporting this assumption (Figure 28). Further analyses of macrophage subpopulations and their functions during the estrous cycle will shed light on this unknown connection.

The differential secretome of male and female LVChP and its functional effect on V-SVZ NSCs

It has been previously reported that the LVChP is a source of several factors that regulate the behaviour of V-SVZ NSCs [15]. Moreover, adult female mice have a 30% higher CSF production than age-matched males, suggesting that the total turnover of factors present in the CSF is higher in females. Furthermore, CSF production decreases with physiological ageing, which is further reduced in aged mice overexpressing amyloid β [209].

Given these sex-dependent differences in LVChP secretion, it is reasonable to speculate that the differences observed in our *in vitro* cultures may be due, at least in part, to the higher secretory capacity of females compared to males. This could lead to a higher concentration of LVChP-derived factors reaching the NSCs in females. However, it is important to note that the factors secreted in by the LVChP may also differ between the sexes.

Our proteomic analysis of male and female LVChPsec using antibody arrays may support the first hypothesis, as it reveals differences in the concentration of several secreted factors, including immunomodulatory (cytokines and chemokines), proliferative (e.g., G-CSF, PDGFB) and hormones (e.g., leptin) (Figure 25C). However, further investigation using Mass Spectrometry analysis of male and female LVChPsec are needed to shed more light on this aspect.

Our ligand analysis of the transcriptome of male and female LVChP revealed a variety of potentially secreted factors that were upregulated in either males or females. These include growth factors (*Gh*, *Igfbp2*, *Ngf*, *Hgf*), immunomodulatory factors (*A2m*) and ECM factors (*Fn1*) (Figure 25B). Each of these ligands has previously been reported to be involved in the regulation of V-SVZ NSCs or its niche (Figure 37) [337-339]. For example, PDGFRα has been observed in intraventricular oligodendrocyte progenitor cells (OPCs) located above the ependymal layer which are bathed by CSF. The emergence of these cells occurs around postnatal day 5 and coincides with an increase in PDGFAA ligand within the LVChP [106].

In addition, A2M, ITIH5 and APOE have been detected in CSF [340, 341]. Interestingly, *Gpat3*, which is enriched in the female LVChP, and *Apoe* and *Gh*, which are enriched in the male LVChP, are involved in lipid signalling, which is emerging as another important regulator of NSCs [342]. For example, *Gpat3* is involved in the synthesis of lipophosphatidic acid (LPA), which has been shown to play an important role in brain development and neurogenesis in the dentate gyrus [343].

The limitation of the antibody array analysis of the LVChP secretome is the limited number of proteins assayed (111). Nevertheless, we were able to identify many ligands including IGFBP2, IGFBP4 and HGF, with different levels of IGFBP2 in female and male LVChPsec (Figure 25C). Our results suggest that the LVChP plays a role in regulating NSCs and that differences in the LVChP secretome between the sexes lead to differential effects on NSCs *in vitro* (Figure 24). Examination of the expression of receptors in NSCs known to serve as binding sites for ligands from the LVChP reveals their presence in activated NSCs, suggesting possible regulation by these specific ligands (Figure 37). It will be interesting to see how these differences in ligand expression may contribute to the observed differences in NSCs in males and females in the V-SVZ [95].

Finally, our analysis of secreted factors during the estrous and diestrous phases of the estrous cycle suggests that sex hormones may also play a role in regulation of the LVChP secretome (Figure 29). We also show that NSCs respond to progesterone in culture (Figure 24C). Since the LVChP expresses receptors for progesterone, its secretome could also be modulated by progesterone. It would be interesting to investigate how sex hormones such as progesterone, estrogen, and testosterone modulate the LVChP secretome in different ways.

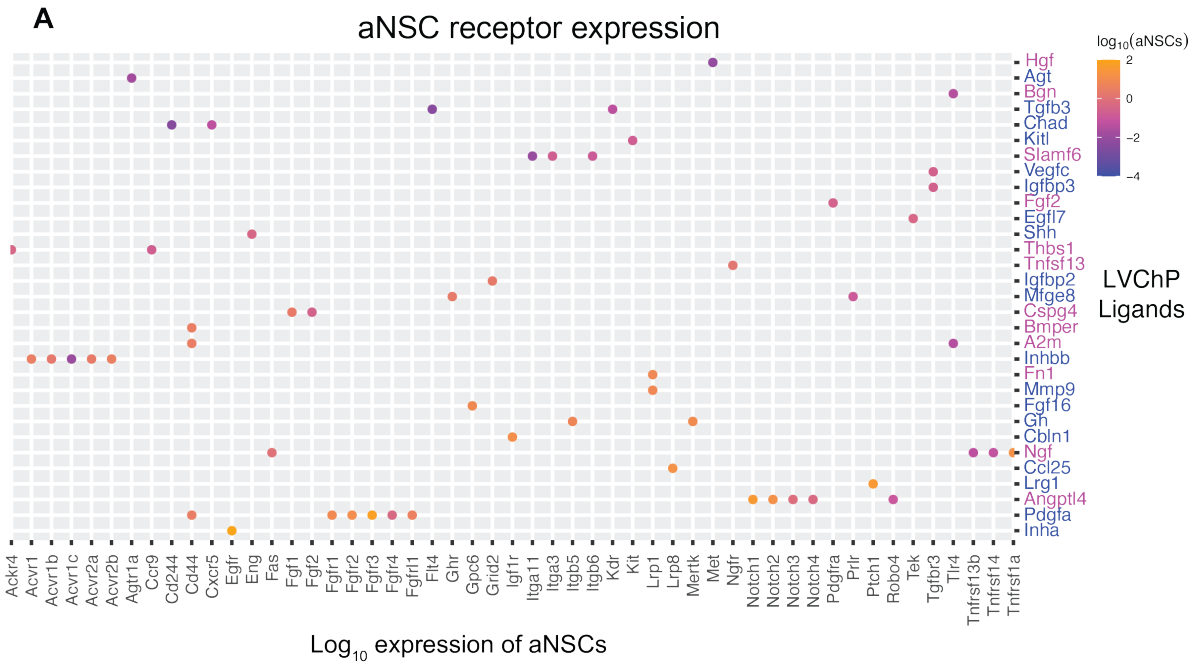

Figure 37: Expression of ChP-ligand receptors in V-SVZ NSCs.
Fpkm values of receptors in aNSCs (x-axis) in a log10 scale. Expression of ligands upregulated in male (blue) and female (magenta) LVChP (y-axis).

The LVChP matrisome composition is sex-dependent

The LVChP contains a rich ECM and ChP-derived ECM molecules are present in the CSF [344]. The ECM is involved in the structural support of cells and tissues, but it also releases and regulates growth factors and other bioactive molecules [345]. The composition of the ECM is dynamic and some components, such as matrix metalloproteinases, can be used as biomarkers of CNS damage (e.g., traumatic brain injury) [346]. Moreover, impairment of the ECM in the ChP disrupts ECM-cytoskeleton interactions and consequently leads to loss of ChP epithelial cell polarisation, highlighting the importance of an intact ECM for the ChP [347]. Although the ECM plays a central role in regulating LVChP structure and various signalling cascades, the role of the ECM in the LVChP is still very poorly understood and requires further investigation.

Interestingly, our GSEA analysis revealed enriched gene sets related to cell matrix and adhesion in the female LVChP (Figure 13). Upon closer inspection, we identified several female DEGs associated with the mouse matrisome (Figure 14). ITIH5 is a proteoglycan involved in binding and stabilising the ECM, thereby ensuring the maintenance of ECM integrity [348]. Other DEGs in the female LVChP, such as collagen 6a3 (*Col6a3*), nephronectin (*Npnt*), follastatin like 1 (*Fstl1*) and glypican 6 (*Gpc6*) are either part of the core matrisome or involved in its regulation [349]. Interestingly, binding of A2M to collagens leads to increased migration of macrophages [350]. A previous study examining the expression of ECM-related genes between the sexes and their correlation with tissue stiffness in the cerebral cortex found that females have higher expression of ECM-related genes and are 9% stiffer than males [351].

In addition, our proteomic analysis of CM, showed that female CM has higher levels of matrix metallopeptidase 2 and 3 (MMP2 and MMP3). MMPs are involved in ECM degradation and their expression can be controlled by inflammatory cytokines. The higher MMP levels in the female LVChP may be related to the accumulation of cytokines in the female LVChP compared to the male LVChP. Furthermore, increased MMP levels have been shown to lead to the opening of BCSFB in AD due to increased TNFα signalling [352]. The higher basal MMP secretion in females could lead to a leakier BCSFB, which could be related to the higher CSF production in females compared to males [209]. Notably, one of the DEGs in males was *Hyal3*, an enzyme that degrades hyaluronan, a major component of the ECM that regulates its structure as well as cell proliferation, migration and differentiation [353]. The significant upregulation of *Hyal3* in the male LVChP may be correlated with a weaker ECM in the LVChP. Additionally, a recent study has shown that *Hyal3* is one of the 47 genes predicted to be a involved in causing Attention-deficit hyperactivity disorder (ADHD) [354] showing the need to study the LVChP matrisome and comparing it between the sexes.

The identification of these DEGs prompted us to investigate the ECM of the LVChP. Notably, the expression of core ECM genes in the LVChP was overall higher in females than in males (Figure 38A). In addition, GSEA focused on matrisome genes revealed a significant enrichment of ECM components in the female LVChP (Figure 38B). Furthermore, a look at our proteomic analysis of male and female LVChP by mass spectrometry showed that this sex-specific difference is maintained in the proteome of females (Figure 38C). Preliminary results of immunostaining with the glycoprotein laminin in male and female brain coronal sections also showed higher levels in the female LVChP (Figure 38D). Taken together, these results highlight differences in the composition of the matrisome in male and female LVChP, confirmed by different expression patterns of genes and proteins. Consequently, these results suggest that these differences in the functions of the ECM between the sexes. However, this needs to be further explored.

Collagen turnover has been shown to vary with age and hormonal changes in other tissues [355]. Estrogens appear to promote maturation and expression of ECM proteins in female smooth muscle progenitor cells [356]. Analysis of estrous and diestrous DEGs revealed an enrichment of matrisome-associated genes in the diestrous phase, including serpins (*Serpina1e*, *Serpina1a*, *Serpina1b*) and collagens (*Col15a1*, *Col14a1*) (Figure 27). Our antibody array for the estrous and diestrous phases CM showed higher MMP concentrations in the estrous compared to the diestrous phase (Figure 29). It would be interesting to study how the estrous cycle modulates LVChP composition and function.

Finally, fibroblasts are an important cell type involved in the regulation of the ECM by secreting ECM proteins to provide structural support to the tissue and additional signalling cues [357]. Our flow cytometric analysis of LVChP cell types revealed differences in the percentage of fibroblasts in female compared to male LVChP, with higher percentages in the female LVChP (Figure 36A, A'). One could speculate that this could result in a greater baseline production of ECM molecules in the female LVChP. Since the ECM plays a crucial role in various cellular processes such as adhesion, communication and signal transduction, sex differences could lead to different functions of the LVChP [358]. Future analyses of the LVChP ECM with atomic force microscopy could reveal correlations with the ECM and LVChP folding. Further, several neurodegenerative diseases including AD, MS and PD show exacerbating changes in ECM components leading to brain dysfunction [359-361]. These findings open up exciting avenues for further research into sex differences in the LVChP matrisome.

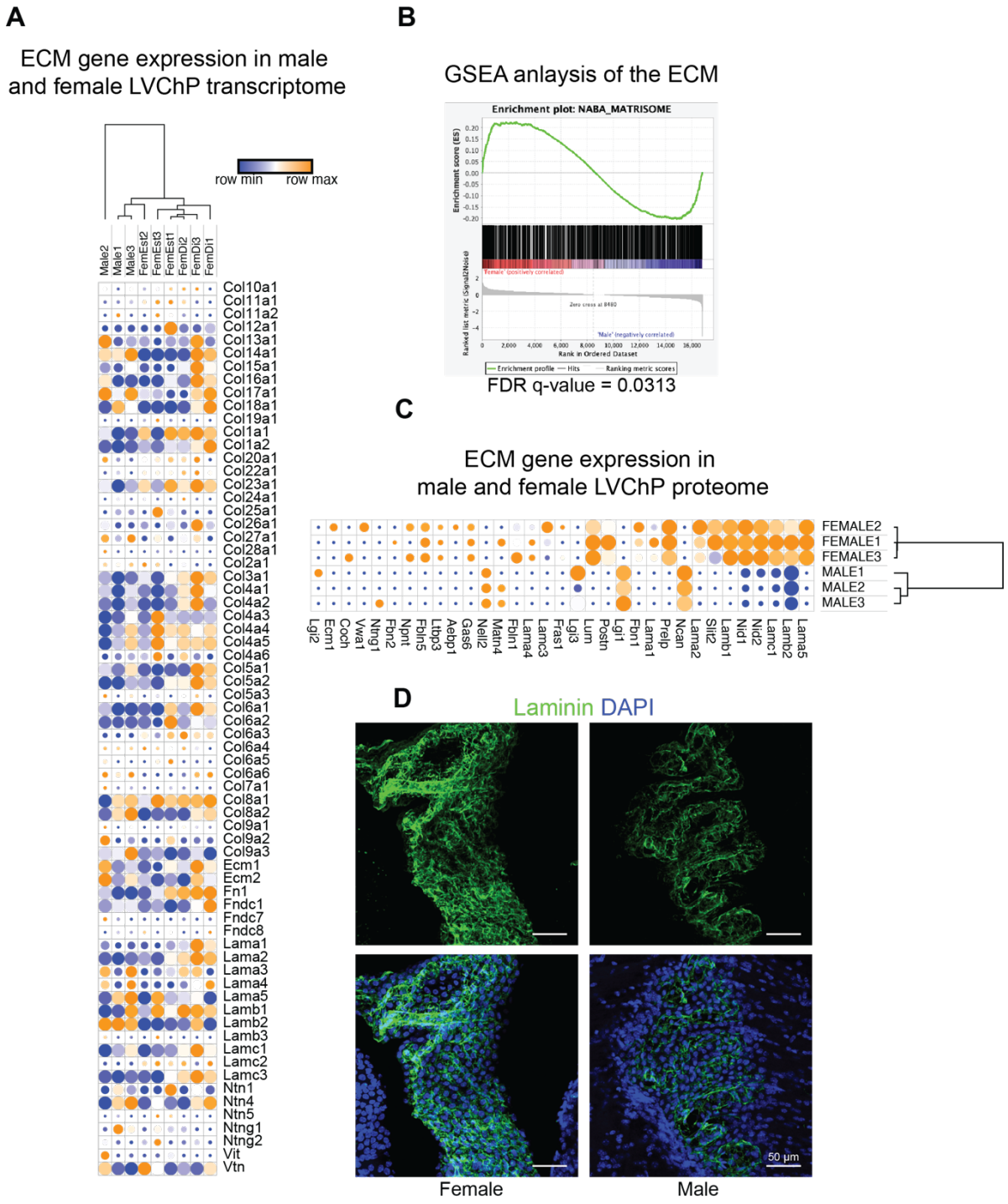

Figure 38: Differences in the LVChP ECM between the sexes
A) Heatmap showing expression of ECM-related core genes in females and males. B) GSEA analysis of the ECM in males and females. C) Heatmap showing expression of ECM-related genes in the proteome of male and female LVChP. D) Representative image of the ECM in males and females. Cross-sections were immunostained with a pan-laminin antibody (green) and DAPI (blue).

Increased detoxification and clearance in female LVChP

Efficient and timely elimination of xenobiotics, toxic metabolites and products from the brain is essential for the maintenance of homeostasis and normal brain function. In addition, the brain generates reactive oxygen species (ROS) due to its high cerebral oxygen consumption. While ROS play a crucial role in neurogenesis, neuronal polarisation and maturation during development, their levels need to be tightly regulated due to the potentially harmful effects they can have on the CNS [301].

A central role of the ChPs are to facilitate the removal of ROS, xenobiotics, metabolites and cellular debris from the brain through various clearance mechanisms. These mechanisms include bulk CSF flow clearance, transportation of compounds from the CSF through the BCSFB and ChP stroma into the bloodstream for elimination, and also detoxification processes within ChP epithelial cells [145, 362]. The constant turnover of CSF results in bulk and non-selective removal of solutes and macromolecules. A recent study has shown that the rate of CSF turnover is higher in female mice [209], suggesting a potentially greater removal of xenobiotics and implying a higher level of overall detoxification as a result of increased CSF flow in females.

The epithelial cells of the ChP express various membrane transporters that actively transport substances from the CSF into the blood. These transporters mainly belong to the ATP-binding cassette (ABC) and solute carrier (Slc) families [363]. In addition, the ChP has a third detoxification pathway in which toxic xenobiotics are enzymatically converted into less reactive and more hydrophilic compounds in the epithelial cells of the LVChP by phase I and II enzymes [145]. Of note, our GSEA of male and female LVChP revealed an enrichment of gene sets related to the response of the ChP to ROS, peroxidases and other chemical compounds in females (Figure 13A, and Appendix Table 3). This further suggests that the LVChP may play a more active role in detoxification in females compared to males. Interestingly, our DEG transcriptomic analysis support this hypothesis, as several female DEGs were associated with detoxification and drug metabolism, including *A2m*, *Cpxm2*, N-acetyltransfease 8b pseudogene (*Cml2*), glutathione transferase 3 (*Gsta3*) and various crystallins (Figure 14). A2M plays multiple roles in eliminating potentially dangerous compounds, including targeting aggregation-prone proteins, interacting with stress proteins and facilitating their degradation through receptor-mediated transport and recognition of misfolded proteins, followed by their transport to lysosomes for degradation (Figure 14) [364, 365].

GSTA3 is a membrane-bound form of glutathione S-transferase that plays an important role in cellular defence against toxic and pharmacologically active electrophilic compounds [366]. In addition, several crystallins are differentially expressed in the female LVChP. Crystallins, traditionally known for their structural role in the lens, have been shown to act as chaperones in stress regulation [367]. In addition, α-crystallins have demonstrated the ability to prevent

stress-induced protein aggregation *in vitro* [368]. The ChP could use crystallins in a similar way, possibly secreting them into the CSF to protect nearby cells from the effects of protein aggregates. Elevated concentrations of α-crystallin have been detected in CSF, especially in patients with MS [369].

In summary, our transcriptomic analysis of male and female LVChP reveals remarkable differences in response to xenobiotic compounds involving drug metabolism, clearance of protein aggregates and oxidative stress. Based on these findings, further studies focusing on the specific pathways involved in the elimination of these compounds are needed to validate our findings. These findings could help identify sex-specific metabolic pathways and targets that could be used to improve the degradation of these compounds in the context of disease.

7.2 Outlook

Assessing choroid plexus heterogeneity and sex differences using transcriptomic approaches

There is heterogeneity within the LVChP. The vasculature exhibits arterio-venous zonation [13] and epithelial cell heterogeneity has also been described [370, 371], but the functional implications thereof are unknown. In this thesis, I have shown that epiplexus macrophages are also heterogeneous in their gene expression, suggesting different functions. Furthermore, regional diversity within the LVChP may lead to spatial differences in the LVChP secretome, which could have significant functional implications for NSCs in the different regions and domains of the V-SVZ.

We have used a number of approaches to gain a comprehensive understanding of sex differences in the LVChP, including bulk RNA sequencing, proteomic analysis using mass spectrometry and antibody arrays of factors secreted by the LVChP, and flow cytometry analysis to identify different cell types within the LVChP. Our work to dissociate the LVChPs of males and females into single viable cells has paved the way for the study of the transcriptome at the single cell level by single cell RNA sequencing. This approach is important because the high number of epithelial cells within the LVChP may have masked changes in less abundant cell populations in our bulk RNA sequencing results. In addition, validation of protein expression in ChP tissue at the cellular level has proven difficult. Therefore, examining gene expression of male and female LVChP at the single cell level may reveal subtle changes that have remained undetected. Our established method for obtaining single cells is currently being used to investigate further differences between cell types and their functions, with the aim of exploring heterogeneity within the LVChP and making a comparison between the sexes. Two cell types of interest for further sex-specific comparison are pericytes and fibroblasts. Our flow cytometric analysis has suggested possible differences in the abundance of these highly secretory cells between the sexes. Single-cell analysis will reveal differences in their populations, gene expression and consequently their functions in males and females.

Another step to study LVChP heterogeneity will be spatial transcriptomics, which links the relationships between cell type and gene expression to their spatial distribution in the ChP. Applying spatial transcriptomics to male and female LVChP samples could provide valuable insights into the heterogeneity of LVChP macrophages, particularly with regard to differential expression of markers in subpopulations and their spatial morphology. This additional spatial information has the potential to reveal differential functions between the sexes.

In addition, the CNS contains four ChPs, each located in one of the brain ventricles. In this thesis, we have focused on the LVChPs. The LVChPs are often chosen for study due to their proximity to the NSCs in the V-SVZ. This allows for better comparability of our study with the existing literature. However, the ChPs of the 3V and 4V in adults have been poorly studied. Studies in rodents have shown transcriptional, cellular and secretory heterogeneity between the different ChPs [3, 13, 372]. In particular, epithelial cells have shown marked regionalisation, suggesting the likelihood of differences in the ChP secretome between different ChPs [373]. Furthermore, a comparison of matrisome gene expression in fibroblasts in a recent single nuclear RNA sequencing study revealed that their gene expression varies between ChPs in different ventricles, suggesting differences in fibroblast functions [13]. Therefore, it will be necessary to extend the analysis of male and female ChPs to include the 3VChP and 4VChP.

Studying sex chromosome and sex hormone differences using the four core genotype mouse model

The four core genotype (FCG) mouse model is an approach used to investigate the influence of the sex chromosomes (XX and XY) and the effects of ovarian and testicular secretion (sex hormones) on phenotype [374, 375]. Studies using the FCG model have revealed differences in behaviours, gene expression and susceptibility to diseases between XX and XY mice that are not mediated by gonadal hormones.

To establish the FCG model, the testis-determining region *Sry* is deleted from the Y chromosome (indicated as Y-) [376], and an *Sry* transgene is inserted onto an autosome in the same mouse (indicated below as *Sry*+) [377]. This results in mice in which the sex chromosome complement is uncoupled from the animal's gonadal sex.

The FCG model enables the comparison of two aspects: first the difference in phenotypes caused by sex chromosome complement (XX vs XY), and second the differential effects resulting from ovarian and testicular secretion (sex hormones) (Figure 39). Implementing the FCG mouse model in our studies would yield valuable insights, enabling us to discern whether the observed differences are attributed to variations in sex chromosomes or fluctuations in sex hormone levels. In addition, it would be very interesting to compare the male and female LVChP during pre-pubertal stages and aged mice before sex hormones become active in pups or when sex hormones gradually decline at around 17-18 months of age [378]. This would allow us to investigate whether there are intrinsic differences in the LVChP cells, transcriptome and secretome that are independent of sex hormone regulation. A comparison between young and aged LVChP has shown that the transcriptome and secretome change significantly with age, including the upregulation of signalling pathways related to immune response and inflammation [15]. However, it remains to be clarified whether these changes are seen in both male and female mice and whether or how they differ in these contexts.

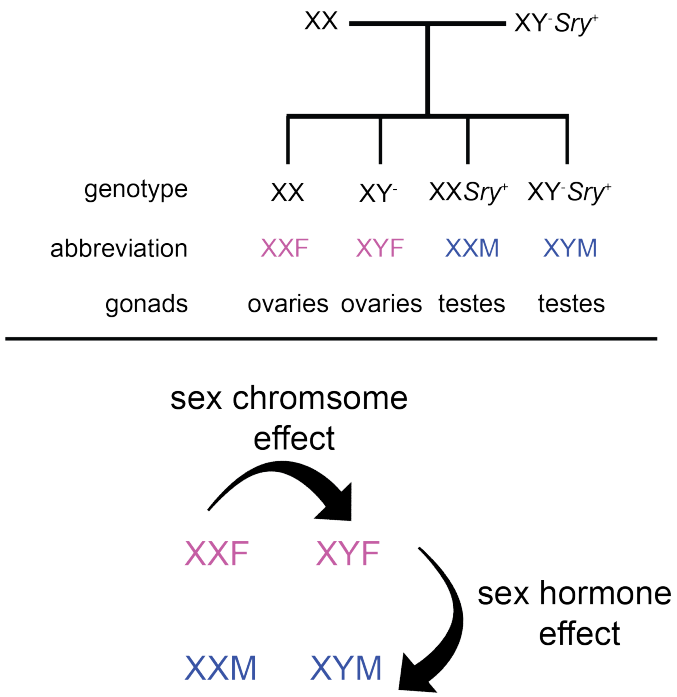

Figure 39: The four core genotype (FCG) mouse model.
Abbreviations: F = female, M = male, Image adapted from Arnold et al. 2012, Front. Neuroendocrinol.

7.3 Closing remarks

The present study has provided a comprehensive insight into sex differences in the structural, cellular and molecular organisation of the LVChP. Exploration of sex-specific molecular signatures has highlighted the central role of sex in regulating the function of this brain structure. Our findings prompt a new look at the described functions of the LVChP and the need to compare sex differences thereof. Further, the identification of differential gene expression, protein regulation and cellular signalling pathways has paved the way for a deeper understanding of the sexually distinct nature of the LVChP. The importance of studying sex differences in all tissues cannot be overstated as it becomes increasingly clear that these differences have clinical implications. The ultimate goal of understanding sex differences in the LVChP and the brain is to provide personalised, sex-tailored treatments for CNS disorders. The first step towards realising this vision is a thorough understanding of the fundamental sex differences in the LVChP. This research has laid the foundation for further investigations aimed at unravelling the complexity of sex differences in the brain and has provided valuable insights that will undoubtedly set the course of future scientific investigations in this field.

Contributions

The results in this thesis were produced in close collaboration with Violeta Silva-Vargas. Violeta conducted the antibody array experiment and subsequently analysed the obtained data. Additionally, she provided assistance in performing GSEA and ENRICHR analysis, as well as *in vitro* culture and flow cytometry experiments. Thomas Sakoparnig performed the alignment and ran the DESeq2 pipeline of the male and female RNA sequencing data, and Karol Kaiser performed the immunostaining for TMEM119 and P2RY12 in cross sections.

8 Material and Methods

8.1 Animal use

Two- to four-month-old male and female CD1 mice (Charles River Labs, Strain 022), *h*GFAP::GFP mice (Jackson Laboratory) and CX3CR1-GFP (Jackson Laboratory, Cat# 005582) mice were used for our experiments. All mice were housed in a 12:12h dark/light cycle with ad libitum access to food. The experiments were done in accordance with the license 2859 approved by the veterinary office of canton Basel-Stadt.

Estrous tracking

To track the estrous cycle in females, vaginal swabs were taken for 10 days as described by Ajayi et al. [199]. For this, the animal was restrained and vaginal cells were flushed by gently adding a small amount of sterile saline using a transfer pipette. The liquid was released into the vagina slowly and drawn back into the tip twice. The liquid was then added to a glass slide and checked under the light microscope at 10x magnification. The proportions of the vaginal cells enabled estimation of the estrous cycle (see section 5.5)

8.2 Tissue preparation for immunohistochemistry and fluorescent RNA *in situ* hybridization

Cryopreservation of mouse brains for cross-sectioning

For coronal sections, mice were deeply anaesthetised by intraperitoneal injection of Esconarkon. Subsequently, they were perfused with 0.9% saline followed by ice-cold 4% paraformaldehyde (PFA, Electron Microscopy Sciences) in 0.1M phosphate buffer. The brains were then postfixed in 4% PFA for 24 hours at 4°C, followed by washing with 1X phosphate-buffered saline (PBS). The brains were transferred to a 15 mL Falcon tube containing a 15% sucrose solution and allowed to sink to the bottom of the tube over several hours. Afterwards, the brains were further incubated overnight in a 30% sucrose solution. The next day, the brains were embedded in OCT compound and frozen at -80°C until use. OCT-embedded brains were coronally sectioned at 12 µm thickness using a cryostat (Leica CM30505).

Whole mount LVChP preparation

Mice were sacrificed with carbon dioxide and both lateral ventricle choroid plexuses were dissected from the brain. Whole ChP from the lateral walls were harvested using forceps and microsurgery scalpels. A bilateral cut was made along the midline to separate the brain into two hemispheres. Each hemisphere was stabilised with forceps and the ventricle was exposed [107]. The LVChP was carefully separated from the hippocampus/ fornix using forceps. The LVChPs were fixed in ice-cold 4% PFA for 30 minutes followed by washes in 1X PBS and stored until used.

8.3 Immunohistochemistry

Immunostaining of coronal cryosections

Sections were thawed and washed in 1X PBS, afterwards sections were boiled for 15 minutes at 100°C in antigen retrieval solution (DAKO). Sections were then washed and permeabilised in PBST (1X PBS supplemented with 0.5% Tween-20), followed by blocking in PBTA (1X PBS supplemented with 5% donkey serum, 0.3% Triton X-100 and 1% BSA [fatty acid free, Sigma, Cat#A7030]). Sections were then incubated in primary antibodies in PBTA at 4°C overnight. After washing in PBST, sections were incubated with the secondary antibodies in PBTA for 1 hour at room temperature, washed in PBST again and counterstained with 4', 6-diamidino-2-phenylindole (DAPI). Slides were then mounted with Aqua-Poly/ Mount (Polysciences #18606-20).

Immunostaining of whole mount preparations

The whole mounts were permeabilised and blocked with 1X PBS containing 10% BSA and 0.2% TX-100 for 2 hours at room temperature. Primary antibodies were incubated overnight at 4°C in 1X PBS containing 3% BSA and 0.2% TX-100, followed by secondary incubation for 2 hours at room temperature in the same solution. Whole mounts were then counterstained with DAPI and mounted on slides using Aqua-Poly/Mount.

Antibodies

The following antibodies and dyes were used for immunostainings: anti-AQP1 (mouse, 1:200, Santa Cruz, sc-55466), anti-actin α-smooth muscle-Cy3 (mouse, 1:200, Sigma, Cat#C6198), anti-CSFR1 (sheep, 1:250, bio-techne, Cat#AF3818), DAPI (1:500, Invitrogen, Cat#D1306), anti-IBA1 (goat, 1:200, Abcam, Cat#ab5076), anti-GFP (chick, 1:250, Aves Labs, Cat#GFP-1020), anti-IBA1 (rabbit, 1:250, IGZ Instruments AG (Fujifilm), Cat#019-19741), anti-LAMININ (rabbit, 1:250; NovusBio, Cat#NB300-144), anti-MRC1 (rabbit, 1:200, Abcam, Cat#ab64693), anti-P2RY12 (rabbit, 1:250, Alomone Labs, Cat#APR-012), anti-PECAM1/CD31 (rat, 1:200, BD Pharmington, Cat#550274), anti-TMEM119 (rabbit, 1:100, Abcam, Cat#ab209064). All secondary antibodies used (from Invitrogen and Jackson ImmunoResearch) were raised in donkey and conjugated to Alexa Fluor 488, Alexa Fluor 568, Alexa Fluor 647 or Cy3. They were reconstituted as advised by the manufacturers and used at a dilution of 1:600.

The following antibodies and dyes were used for FACS: P2RY12-PE (1:100, Alomone Labs, Cat#APR-020-PE), CD31-PeCy7 (1:100, Biolegend, Cat#102418), CD13-PE (1:100, Biolegend, Cat#164004), CD11B-A488 (1:100, ThermoFisher, Cat#53-0112-82), CD3-A700 (1:100, Biolegend, Cat#100216), CD19-A700 (1:100, ThermoFisher, Cat#56-0193-82), FAP-647 (1:100, RnDSystems, Cat#FAB3715R-100UG), DAPI (1:500, Invitrogen, Cat#D1306)

8.4 Fluorescent *in situ* hybridization (FISH)

RNAscope protocol

The FISH was performed according to the manufacturer's protocol (ACD, Biotechne, acdbio.com). Slides were washed in 1X PBS and baked for 30min at 60°C followed by fixation in 4% PFA for 15min at 4°C. After washing in PBS, sections were dehydrated in 50%, 70% and 2x in 100% EtOH for 5min each. Sections were then incubated treated with peroxidase (RNAscope Multiplex Fluorescent Assay Kit (Advanced Cell Diagnostics)) for 10min at room temperature followed by antigen retrieval (Cat#322000) in a steamer at 100°C for 10min. Sections were washed with MilliQ dH2O, and permeabilized for 25min in Protease Plus (Cat. 322330) at 40°C. After washing in dH2O, slides were incubated with the preheated (40°C) probes for 2 hours at 40°C. Sections were washed in wash buffer and stored in 5X SSC (Sigma-Aldrich, Cat#S6639-1L)) overnight at room temperature.

The next day slides underwent signal amplification (RNAscope Multiplex Fluorescent Detection Reagents v2, Cat#323110), incubating in RNAscope Amp-1 (30min, 40°C), AMP-2 (30min, 40°C) and RNAscope AMP-3 (15min, 40°C). Slides were then incubated in RNAscope Multiplex FL v2 HRP-C1 for 15min, at40°C, washed and the TSA 520 fluorophore (7523/1 KIT) diluted in TSA buffer (1:5000, 322810) against the C1 probe was incubated for 30min at 40°C, washed and then incubated with RNAscope Multiplex FL v2 HRP blocker for 15min, 40°C. After 2 washes in wash buffer, either the RNAscope Multiplex FL v2 HRP-C2 or RNAscope Multiplex FL v2 HRP-C3 (depending on the probe) were added to the slide and incubated for 15 min at 40°C, followed by washes and incubation with the TSA 650 fluorophore (7527/1 KIT) diluted in TSA buffer (1:5000) for 30min at 40°C. After washing, RNAscope Multiplex FL v2 HRP blocker was added to the slide and incubated for 15min at 40°C followed by washes. Finally, sections were stained for DAPI for 30s and mounted in Aqua-Poly/Mount (Polysciences).

Probes used for RNAscope

Following probes were used in this thesis: A2m (C1, acdbio, 853411), Bst2 (C2, acdbio, 502401-C2), Bscl2 (C2, acdbio, 1222851-C2), Cpxm2 (C1, acdbio, 559751), Itih5 (C1, acdbio, 460971), Syne1 (C3, acdbio, 316511-C3)

8.5 Fluorescent activated cell sorting (FACS)

Dissociation and FACS purification of the LVChP

The LVChP was isolated with forceps under a stereotactic microscope, followed by two short washes in 1X PBS. Then plexuses were incubated in Hank's Balanced Salt Solution (HBSS) supplemented with collagenase II (5mg/mL) for 15min at 37°C and flicked every 5min. Following incubation, the cell suspension was pipetted up and down 50x with a P1000 pipette (set to 750µl) followed by centrifugation at 1300rpm for 3min at 4°C. The resulting supernatant was collected in an eppendorf tube containing fetal bovine serum (FBS) and placed on ice, while the remaining cell pellet was treated with PBS supplemented with pronase (2mg/mL) and DNAse I (0.5µg/mL) for 10 min at 37°C and flicked every 5min. Following enzyme treatment, the cell suspension was manually dissociated using a P1000 (25X), followed by pipetting with a P200 pipette (75X). FBS, FACS buffer (HBSS supplemented with 1% BSA and 0.1% glucose) and the collectedsupernatant were added to the suspension and filtered through a 40µm nylon cell strainer (VWR, Cat#302024). After centrifugation at 1300rpm for 5min, the supernatant was discarded and the cell pellet was resuspended in the desired volume of FACS buffer. CD16/32 (TruStain, Biolegend, Cat#101320) was added to block FC receptors at a concentration of 1:250 and incubated in the dark on ice for 10min. Subsequently, conjugated antibodies, diluted in FACS buffer, were added to the cell suspension and incubated on ice for 10min. After incubation, FACS buffer was added and the suspension was centrifuged at 1300rpm for 5min. The supernatant was removed, and the cell pellet was resuspended in FACS buffer. Finally, DAPI was added to the cell suspension. Gates were set manually using isotype control samples (all samples) and FMO controls (for the CX3CR1, P2RY12 analysis). Data was analysed with FlowJo (version 9.0.1.11) data analysis software.

Dissociation and FACS purification of LVChP immune cells

For FACS analysis of LVChP immune cells, mice were deeply anaesthetised by intraperitoneal injection of Esconarkon. Subsequently, they were perfused with 1X phosphate buffered saline (PBS) and the LVChP was isolated with forceps under a stereotactic microscope. Tissues were incubated at 37°C for 45 minutes in PBS containing 400U/mL collagenase type IV (Worthington Biochemical) followed by manual homogenization by pipetation. After centrifugation at 1300rpm for 5min, the supernatant was discarded and the cell pellet was resuspended in the desired volume of FACS buffer. CD16/32 (TruStain, Biolegend, Cat#101320) was added to block FC receptors at a concentration of 1:250 and incubated in the dark on ice for 10min. Subsequently, conjugated antibodies, diluted in FACS buffer, were added to the cell suspension and incubated on ice for 10min. After incubation, FACS buffer was added and the suspension was centrifuged at 1300rpm for 5min. The supernatant was removed, and the cell pellet was resuspended in FACS buffer. Finally, DAPI was added to the

cell suspension. Gates were set manually using isotype control samples (all samples) and FMO controls (for the CX3CR1, P2RY12 analysis). Data was analysed with FlowJo (version 9.0.1+11) data analysis software.

FACS purification of V-SVZ NSCs

qNSCs and aNSCs were FACS purified from the V-SVZ of 2-3 month old *h*GFAP::GFP (Jackson Laboratory), or CD1 mice (Charles River) as previously described [107, 379].

The V-SVZs from 2-4 month old heterozygous *h*GFAP::GFP mice (Jackson Laboratory) or wildtype CD-1 mice (Charles River), were digested with papain (Worthington, 1200 units per 5 mice, 10min at 37°C) in PIPES solution [120mM NaCl, 5mM KCl, 50mM PIPES (Sigma), 0.6% glucose, 1x Antibiotic/ Antimycotic (Gibco), and phenol red (Sigma) in water, pH adjusted to 7.6] and then mechanically dissociated into single cells after addition of ovomucoid (Worthington, 0.7mg per 5 mice) and DNAse (Worthington 1000 units per 5 mice). To remove myelin, the cell suspension was centrifuged for 10min at 4°C without brake in 22% Percoll (Sigma). Cells were stained in three steps. Cells were first incubated with PE-conjugated rat anti-mCD24 (1:500, BD Pharmington) and biotinylated rat anti-mCD133 (1:300, clone 13A4, eBioscience) for 20min on ice. After centrifugation at 1300rpm for 5min, the cells were incubated with Streptavidin Pe-Cy7 (1:500, eBioscience) for 10min on ice. After centrifugation, cells were incubated with A647-conjugated EGF (1:300, Molecular Probes) for 15min and washed by centrifugation. All antibodies were diluted in FACS buffer (1% BSA, 0.1% glucose HBSS solution). DAPI was used to assess cell viability (1:1000, Sigma). Cell populations were isolated using the Aria Fusion and were collected in Neurosphere medium (NSM) [DMEM/F12 (Life Technologies) supplemented with 0.6% glucose (Sigma), 1x Hepes (Life Technologies), 1x Insulin-Selenium-Transferrin (Life Technologies), N-2 (Life Technologies), and B-27 supplement (Life Technologies). Gates were set manually using single-color control samples and FMO controls.

8.6 Molecular analyses

8.6.1 Bulk RNA sequencing of male and female LVChP

LVChPs from males, females in diestrous phase and females in estrous phase were isolated in triplicate for transcriptome analysis. RNA was extracted using the RNeasy Plus Micro Kit (Qiagen, Cat#74034) according to the manufacturer's instructions. RNA sequencing was done by paired end sequencing with Illumina NovaSeq 6000 V3.4.4. STAR was used to align the raw reads to the mm10 transcriptome and count the reads per gene [380]. DESeq2 (v1.22.2) was used to determine differential expression and normalisation of the gene-wise count data. Genes with an adjusted p-value lower than 0.05 were considered differentially expressed [381].

Gene set enrichment analysis (GSEA) of adult male and female LVChP transcriptome

The transcriptome data from male and female LVChP was used to perform Gene Set Enrichment Analysis (GSEA) with the following parameters:

- Gene set database: Biological processes; ftp.broadinstitute.org://pub/gsea/gene_sets/c5.go.bp.v2022.1.Hs.symbols.gmt
- Number of permutations: 1000
- Permutation type: gene_set
- Chip platform: ftp.broadinstitute.org://pub/gsea/annotations_versioned/Mouse_Gene_Symbol_Remapping_Human_Orthologs_MSigDB.v2023.1.Hs.chip

GSEA performed on the entire LVChP RNAseq data to identify significant differences in biological processes between the sexes. Gene sets with a false discovery rate (FDR) of less than 25% were considered statistically significant. Enriched gene sets were manually summarised into global biological processes and documented in Table 3.

To analyse enriched gene sets associated with neurodegenerative diseases, the online mouse gene set database was searched for known neurodegenerative diseases (https://www.gsea-msigdb.org/gsea/msigdb/mouse/genesets.jsp).

The relevant gene sets were downloaded and used for this enrichment analysis (Figure 14).

Analysis of the DEGs between male and female LVChP

Script to generate a heatmap of the DEGs between male and female. The same script was used to generate a heatmap of the DEGs between female diestrous and estrous samples with the variation line 6 (degED <-- read.csv("condition_Diestrous2021_Estrous2021.csv", sep = ","):

R-script for DEG heatmap:

```
install.packages("gplots")
library(gplots)
counts <- read.csv("RNAseq3_2021.csv", sep = ",")
degMF <- read.csv("condition_Male2021_Female2021.csv", sep = ",")
deg <- counts[counts$Gene_name %in% degMF$X,]
matrix_deg<- data.matrix(deg[,2:10])
row.names(matrix_degMF) <- deg$Gene_name
dist.pear <- function(x) as.dist(1-cor(t(x))/2)
hclust.wd2 <- function(x) hclust(x, method="ward.D2")
my_palette <- colorRampPalette(c("blue", "white","orange"))(n = 100)
heatmap.2(matrix_deg,
        key.title = "Male vs Female LVChP DEG",
        main = "Male vs Female LVChP DEG",
        labRow = deg$Gene_name,
        col=my_palette,
        trace="none",
        density.info = "none",
        distfun=dist.pear,
        hclustfun=hclust.wd2,
        srtCol = 45,
        cexRow = 0.25,
        cexCol = 0.5,
        scale="row")
```

ENRICHR GO process analysis of DEGs

The ENRICHR tool was used to investigate the gene ontology (GO) processes enriched of differentially expressed genes (DEGs) [382-384]. Specifically, we assessed the GO biological processes (BPs), OMIM disease processes and Descartes Cell Types and Tissue 2021 processes using the DEGs identified in the LVChP between males and females. Processes were ranked based on the combined enrichment score, and only processes with combined scores greater than 50 were considered. Subsequently, the list of BPs was manually curated into global BPs for both sexes. The percentage of these global BPs relative to the total BPs was then calculated and presented in the form of a bar chart, with the corresponding genes listed next to the bar charts. In addition, the same DEGs were used for the ENRICHR cell type analysis of the female and male DEGs.

Gene network analysis

Gene networks in Figure 14 were obtained with the STRING software [385], using the differentially expressed gene between male and female LVChP, and applying k-means clustering on network components.

Volcano plot of DEGs

To visualise the DEGs in Figure 15, the negative log10 of the adjusted p-value was calculated and plotted for the y-axis, the x-axis was plotted by calculating the log2 ratio of averaged male/ female fragments per kilobase of transcript per million mapped reads (fpkm) values.

Macrophage-associated gene expression

To investigate macrophage-associated genes upregulated in male or female LVChP, a gene set list of 2209 genes from the Ma'ayan laboratory was used. (Source: https://maayanlab.cloud/Harmonizome/gene_set/macrophage/BioGPS+Mouse+Cell+Type+and+Tissue+Gene+Expression+Profiles) [314]. Using our male and female and female diestrous and estrous RNAseq datasets, macrophage-associated genes were identified with a p-value < 0.05 and a fold change > 1.5 between male and female LVChP and between estrous phase. Male and female upregulated macrophage genes were subjected to ENRICHR analysis to identify enriched GO biological processes.

R-script for the heatmap of upregulated macrophage genes: The same script with altered dataframes were used for the upregulated estrous/ diestrous macrophage genes.

```
install.packages("gplots")
install.packages("tidyverse")
install.packages("car")
install.packages("devtools")

library(gplots)              #heatmap plotting
library(tidyverse)           # data manipulation
```

```
library(cluster)  # clustering algorithms
counts <- read.csv("RNASeq3_MvF_upregulated.csv", sep = ",")
Macrophages_RNAseq3 <- read.csv("Macrophage_GeneList.csv", sep = ",")
Macrophage_genes_counts <- counts[counts$Gene_name %in% Macrophages_RNAseq3$Gene,]
row.names(Macrophage_genes_counts) <- Macrophage_genes_counts $Gene_name
Macrophage_genes_counts <- Macrophage_genes_counts [,-1]
Data.log.scale <- scale(log10(Macrophage_genes_counts + 1))
y <- as.matrix(Data.log.scale)
hr <- hclust(as.dist(1 - cor(t(y), method = "pearson")), method = "complete")
hc <- hclust(as.dist(1 - cor(y, method = "spearman")), method = "complete")
mycl <-  cutree(hr, h = max(hr$height) / 1.01)
mycolhc <-   rainbow(length(unique(mycl)), start = 0.1, end = 0.9)
mycolhc <- mycolhc[as.vector(mycl)]
cluster <- as.matrix(mycl)
my_palette <- colorRampPalette(c("blue", "white","orange"))(n = 100)
heatmap.2(
  y,
  Rowv = as.dendrogram(hr),
  Colv = as.dendrogram(hc),
  col = my_palette,
  density.info = "none",
  trace = "none",
  dendrogram = "both",
  scale = "row",
  labRow = NULL,
  labCol = NULL,
  main = "Upregulated macrophage genes MvF",
  margins = c(5, 10),
  cexRow = 0.1,
  RowSideColors = mycolhc
)
```

The list of genes is found in Appendix Table 6 (Male versus Female) and Table 7 (Estrous versus Diestrous).

Ligand analysis

To investigate the ligands that are upregulated in male or female LVChP, two gene set lists were merged for a total of 4534 ligands. The gene sets originated from the Ma'ayan Lab Harmonizome website [314] (Source: https://maayanlab.cloud/Harmonizome/gene_set/ligand/GeneRIF+Biological+Term+Annotations) and CellTalkDB [315].

This list of 4534 ligands were compared to our RNAseq data from male and female LVChP. Of these, 3334 ligands were expressed in our dataset. Next, we manually curated a list of 612 ligands and ECM molecules previously reported to interact with and regulate the V-SVZ NSCs. Comparison of this list to our LVChP expressed ligands revealed expression of 612 V-SVZ-associated ligands in our dataset. Of these 612 ligands 46 were upregulated (p-value < 0.05) in male or female LVChP. A heat map showing the expression of these genes was plotted using Morpheus (source: https://software.broadinstitute.org/morpheus/). The size of the circles reflected the fpkm gene expression values. Any gene with an expression over 750 fpkm was shown by a full circle (Figure 25).

To compare the expression of V-SVZ aNSCs (Figure 37), the transcriptome data from Codega et al was used [107]. The log10 averaged expression of aNSCs was calculated and plotted in a ball plot, showing their interaction with LVChP ligands. For this, the LVChP ligands with their corresponding receptors were manually identified and saved as a csv file (receptor_expression_comparison.csv), as used below.

The following R script was used:

```
library(ggplot2)
library(dplyr)

ligands_df <- read.csv("Ligands_upregulated_MvF.csv", header = TRUE)
receptors_df <- read.csv("receptor_expression_comparison.csv", header = TRUE)

merged_df <- merge(ligands_df, receptors_df, by = "Receptor")
geom_point(aes(color = qNSCs, shape = "qNSCs"), size = 1) +
  geom_point(aes(color = aNSCs, shape = "aNSCs"), size = 1) +
  scale_color_gradientn(colors = c("blue", "white", "red"), name = "Expression",
                        breaks = c(0, 1), labels = c("Low", "High"),
                        guide = guide_legend(override.aes = list(shape = c(16, 17)))) +
  labs(title = "Receptor-ligand interaction with expression in qNSCs and aNSCs",
       x = "Ligand", y = "Receptor") +
  guides(shape = FALSE)
merged_data <- merge(ligands_df, receptors_df, by= "Receptor")
merged_data <- merged_data %>%
  filter(!is.na(qNSCs) & is.numeric(aNSCs) & aNSCs > 0) %>%
  mutate(Ligand = factor(Ligand, levels = unique(Ligand[order(log10(aNSCs), decreasing = TRUE)])),
```

```
      Receptor = factor(Receptor)) # Convert Receptor to a factor

ggplot(merged_data, aes(x = Ligand, y = Receptor, fill = log10(aNSCs))) +
  geom_point(shape = 21, size = 2) +
  scale_fill_gradient(low = "blue", high = "orange", limits = c(-4, 2),
                      breaks = seq(-4, 2, 2), na.value = "orange",
                      name = expression(log[10]("aNSCs"))) +
  labs(title = "Receptor Expression in aNSCs",
       x = "Ligand", y = expression("Receptor"~log[10]~"Expression")) +
  scale_y_discrete(limits = rev(levels(merged_data$Receptor)),
                   labels = rev(levels(merged_data$Receptor)), # Reverse the order of levels and labels
                   expand = c(0, 0.05)) +
  theme(axis.text.y = element_text(margin = margin(r = 5)))
```

Single cell dataset analysis of TMEM119+ and TMEM119- macrophages

The single-cell dataset published by van Hove et al. 2019 was used to examine genes associated with $TMEM119^{+}$ and $TMEM119^{-}$ macrophages [44]. To achieve this, all stromal cells expressing MRC1 were excluded from the dataset. Subsequently, the remaining epiplexus cells ($MRC1^{-}$) were divided into two populations: $TMEM119^{+}$ and $TMEM119^{-}$. The genes associated with each population were subjected to ENRICHR analysis to identify enriched GO biological processes (see section 8.6.1). A volcano plot of these was generated according to the methods described in section 8.6.1.

ECM analysis

To obtain ECM-related genes, we compiled a gene list of 69 collagens and laminins. The list of genes was compared to our RNAseq data from male and female LVChP using R Studio:

```
counts <- read.csv("RNAseq3_MvF_total.csv", sep = ",")
Matrisome <- read.csv("Manual_Matrisome2.csv", sep = ",")
Matrisome_RNAseq <- counts[counts$Gene_name %in% Matrisome$Gene,]
write.csv(Matrisome_RNAseq,Matrisome_RNAseq3.csv', row.names=TRUE)
```

8.6.2 Proteomic analyses

Antibody arrays of LVChPsec

Male, female estrous, female diestrous and female pooled (estrous and diestrous pooled) CM samples were prepared as described in section 8.6.3.1.3. For antibody array analysis the proteome profiler mouse XL cytokine array (R&D systems, Cat#ARY028) was used. All buffers were supplied in the kit. The antibody array was performed according to the manufacturer's instruction. Relative levels of the different proteins were calculated based on densitometry and presented as a fold change ratio to the control sample (unconditioned medium). The antibody array was performed three times with different male, female mixed, female estrous and female diestrous samples.

Mass Spectrometry and TMT labelling of CM (1) and of the LVChP proteome (2)

Peptide fractions of whole male and female LVChP explants (2) or combined male and female CM conditioned for 2h, 4h, 6h and 24h (1) were extracted using lysis buffer (1% sodium deoxycholate, 10mM TCEP, 100mM Tris pH8.5) in a Bioruptor. BCA assay was performed to measure the protein concentration according to the manufacturer's instructions (ThermoFisher, Cat#23227). Proteins were subsequently digested using trypsin (0.5µg/mL) in a final enzyme/ protein ratio of 1:50 and digested at 37°C overnight. After incubation, samples were prepared for solid phase extraction by addition of 5% TFA (Pierce/ Thermo, Cat#28904), then washed, desalted using the Tecan A200 and dried. Solid phase extraction (SDB-RPS purification) was performed and stored at -20°C until use. For TMT labelling of peptide samples 10µg of total protein was used. The dried peptides were dissolved in 20µl HPLC-A buffer using ultrasonication and then spun down for 30s at 1000rpm. Samples were then dissolved in labelling buffer using the same procedure and ProtMix was added to the samples. Then TMT pro reagent (Thermo, Pierce) was added to the samples and incubated for 1h at 25°C at 500rpm in a Thermomixer. Reaction was stopped and 5% TFA was added to samples. For solid phase extraction of TMT labelled peptides (C18 purification) BioPureSPN MACRO SPE columns were used. The columns were conditioned with acetonitrile and equilibrated 2x with 0.1% TFA. Samples were loaded and the flow-through collected in 2mL Eppendorf tubes. Columns were washed 3x with 5% acetonitrile/ 95% water (v/v) and 0.1% TFA.

Peptides were eluted into new 2mL Eppendorf tubes using 50% acetonitrile/ 50% water (v/v), 0.1% TFA. Peptides were then analysed by the Proteomics Core Facility of the Biozentrum, University of Basel.

ECM analysis of male and female LVChP proteome

Male and female matrisome genes were plotted in a heatmaps using Morpheus https://software.broadinstitute.org/morpheus. Hierarchical clustering was performed using a one minus Pearson correlation and circles were displayed with a threshold set to 0.0001. All values above this threshold are shown with full circles.

qPCR analysis of expression of DEG between male and female LVChPs

RNA was extracted from LVChP using the RNeasy Plus Micro Kit (Qiagen, Cat#74034) according to the manufacturer's protocol. Subsequently, the cDNA was generated with the Promega kit (Cat#3802). Quantitative polymerase chain reaction (qPCR) was performed using SYBR green (Roche) for detection on a Light Cycler Instrument II (Roche) according to the manufacturer's instructions. Each gene and sample were analysed in triplicate. The thermocycling programme consisted of an initial incubation at 95°C for 10 minutes, followed by 40 cycles at 95°C for 15 seconds and 60°C for 1 minute.

ΔCT values were calculated for each gene of interest in each sample, using Rpl13a as the reporter gene. The relative change in expression level of the analysed gene (ΔCT) was determined by subtracting the gene expression levels in the male and female LVChP from the gene expression level of the housekeeping gene Rpl13a. Then, the ratio between the gene expression of Rpl13a and the gene of interest in the male and female LVChP was calculated using the following formula: $2^{-\Delta\Delta CT}$.

The results were expressed as relative fold enrichment compared to the expected input for male/female DEGs. This means that if a gene was upregulated in males based on transcriptomic data, qPCR results were calculated as a fold change compared to males, for genes upregulated in females the results were calculated as a fold change compared to females. Sequences of primers are as follows:

Gene	**Primer name**	**Sequence (5' → 3')**	**Length**
A2m	A2m forward A2m reverse	AGATGGTGAGATTTCGTGTTGTC ACGGTCCTGCCTGATTCTGTA	220bp
Gpat3	Gpat3 forward Gpat3 reverse	GGCCTTCGGATTATCCCTGG CTTGGGGGCTCCTTTCTGAA	100bp
Bst2	Bst2 forward Bst2 reverse	AGCATCCAAGGAACCCACAC CAGCATCCCAAGGGCTCTG	179bp
Hyal3	Hyal3 forward Hyal3 reverse	TCTGTGGTATGGAATGTACCCT TTTTGGCCGTGAAAATGTTGG	113bp
Rpl13a	Rpl13a forward Rpla13a reverse	AGCCTACCAGAAAGTTTGCTTAC GCTTCTTCTTCCGATAGTGCATC	129bp
C1qtnf12	C1qtnf12 forward C1qtnf12 reverse	ATTACCACGTCCAACCGTGAG GGCCACGACACCGTTTTCT	145bp

8.7 Image acquisition and quantification

Image acquisition

Images were acquired using the Olympus confocal spinning disk microscopes SpinSR (CSU-W1) and SpinD (CSU-W1). For both, a UPL S APO 30x/ 1.05NA objective in combination with Silicon oil was used. Tile scans of the entire LVChP in cross-sections and whole mounts were acquired, with z-stacks encompassing the entire thickness of the tissue in cross-sections and whole mounts. Individual z step sizes were 0.41-1µm, depending on the staining. Images of the same immunostainings were acquired on the same microscope with the same laser power and exposure. Individual tiles acquired on the SpinSR and SpinD were stitched using the Fiji plugin *recursive Olympus vsi stitcher* provided by the local imaging core facility (IMCF). Images of cultured V-SVZ cells were taken with the Leica DMi8 system at 10x.

8.7.1 Image quantifications

LVChP cell density

To measure cell density in cross-sections, the number of cells (visualised by DAPI staining) was quantified using QuPath version 2.3 and the volume of the tissue was calculated by drawing around the tissue and multiplying it by the thickness of the tissue. The number of cells was then divided by the volume obtained. The applied cell detection parameters in QuPath were the following:

Set up parameter:

Requested pixel size = 0.5µm

Nucleus parameter:

Background radius = 8µm

Median filter radius = 0µm

Sigma: 1.5µm

Minimum area: 10µm^2

Maximum area: 400µm^2

Intensity Parameters:

The threshold was adjusted manually for each section until the results were satisfying.

Quantification of cell density in whole mount preparations of the LVChP was performed using Cellpose [297] via automatic quantification of DAPI and the LVChP volume. In this approach, all cells in the LVChP were counted based on DAPI staining and volume was measured using individual thresholds for the tissues by using another channel (in this case IBA1 staining). Cell density was calculated as done previously.

Analysis of cross-section immunostainings

Maximum intensity projections were used to quantify the coronal cross sections. The number of IBA1-, MRC1-, P2RY12- and TMEM119-positive cells in the different sections was counted using the *cell counter* plugin in ImageJ. The total number of cells per LVChP cross-section was determined using DAPI staining in QuPath2.3 as described above. The proportions of positive cells per DAPI (cells/DAPI) and positive cells per total IBA1-positive cells (cells/IBA1) were then calculated for each cross-section. Quantifications involved the comparison of between four and eight mice. For each individual mouse, an average of five coronal sections spanning the rostro-caudal axis was considered. The total number off macrophages per coronal section along the dorsal-ventral axis was quantified.

Analysis of whole mount immunostainings

The number of $IBA1^+$ cells was counted using the *cell counter* plugin in ImageJ. Volumetric measurement of LVChP tissue was performed using surface rendering in Imaris. For regional quantification, the LVChP was divided into head (rostral), middle and tail (caudal) regions, and three to four tiles were quantified in each region in three female and four male samples, respectively. $IBA1^+$ cells with different morphologies were manually counted using the *cell counter* plugin and LVChP tissue volume was measured in Imaris as previously described. All whole mount quantifications are presented as densities (number of cells/mm^3). The association of macrophages with blood vessels was quantified based on the presence of at least one macrophage process in direct contact with the vasculature, leading to the formation of podocyte-like areas.

8.8 *In vitro* experiments

8.8.1 Medium composition

Neurosphere and N2 medium

Neurosphere medium consisted of DMEM/F12 medium supplemented with 0.6% glucose (Sigma), 1x Hepes (Life Technologies), 1x Insulin-Selenium-Transferrin (Life Technologies), N-2 (Life Technologies), and B-27 supplement (Life Technologies).

Minimal and EGF control medium

Minimal medium was prepared according to the control medium published by Ferrón et al. 2007 [386]. It consists of DMEM/F12 medium supplemented with 0.6% glucose (Sigma), 0.1% NaHCO3 (Sigma), 5mM Hepes (Sigma), 2mM L-Glutamine (Gibco BRL), 50U/mL penicillin/ streptomycin (Gibco) and 1X hormone mix (10x) [DMEM/F12 supplemented with 0.5% glucose, 0.09% NaHCO3, 4mM Hepes, 0.8mg/mL apo-t-transferrin (Sigma), 0.02mg/mL insulin (bovine, Sigma), 90µg/mL putrescine (Sigma), 160nM progesterone (Sigma) and 240nM Na2SeO3 (Sigma)].

EGF control medium consists of minimal medium supplemented with 20ng/mL EGF (human recombinant, GibcoBRL) and 10ng/mL FGF2 (human recombinant, Sigma).

LVChP Conditioned Medium (CM)

To prepare LVChP CM (LVChPsec), 5 dissected LVChP were cultured in a transwell (Corning, Cat#3470) containing minimal medium without addition of progesterone for 6 hours at 37°C. The transwell containing the LVChPs was then removed and the medium collected from the well plate. Next, progesterone, at a final concentration of 160nM, was added to the harvested CM and the CM was used either directly or stored at -80°C for later use [15].

8.8.2 In vitro NSC cultures

After FACS purification of qNSCs and aNSCs, cells were centrifuged at 1300 rpm for 10 min at 4°C and then resuspended in minimal medium. Cell number and viability were determined at the time of plating using a haemocytometer and Vybrant Dye staining (1:1000, Invitrogen). qNSCs and aNSCs were plated out at a density of 1 cell/µl (aNSC) or 10 cells/µl (qNSC) in male or female LVChP CM, minimal medium, or neurosphere medium. Cells were cultured in ultra-low attachment 96-well plates (Corning, Cat#3474) at 37°C and 5% CO2 with 10% O2 as previously described by Silva-Vargas et al. 2016 [15]. Activated clones (doublets) were counted two days after seeding for aNSCs or four days after seeding for qNSCs. For our comparison of neurosphere versus minimal medium and cultures grown with or without progesterone, male aNSCs were used (Figure 24B, C). To study the baseline formation of clones, qNSCs and aNSCs of male and female cells from the lateral and septal wall were

purified by FACS and cultured in neurosphere medium. For the experiments with male and female CM, male and female NSCs were purified by FACS and cultured in sex-matched or sex-swapped LVChPsec or control medium with or without mitogens (Figure 24D, F, G).

8.9 Statistical analysis

Statistical analyses and graphs were performed using GraphPad Prism software (version 7) Significance was established using two-tailed student's *t*-tests for pair-wise comparisons. 2-way ANOVA was used to assess the effect of male and female CM cultured with sex-matched or sex-swapped NSCs, followed by Šídák's multiple comparisons test (Figure 24G). In Figure 14, significance was calculated using the adjusted p-value <0.05. In Figures 20, 24B, C, D, F and 26, two-tailed student's t-tests with a p-value <0.05 were considered upregulated. Significance was established at *p<0.05, **p<0.01, ***p<0.001, and ****p<0.0001. Error bars indicate the standard error of the mean (SEM).

9 Appendix

Table 2: Male and female LVChP DEGs.
Table showing log2FC (fold change) Male/ Female and adjusted p-value of DEGs.

Gene	log2FoldChange Male/Female	Adjusted p-value
Cryba1	-6.94	2.40E-07
Crygd	-6.81	2.65E-04
Gm42436	-5.36	1.57E-02
Xist	-5.06	4.25E-08
Crx	-4.87	1.76E-02
Prph2	-4.58	4.64E-04
Rp1	-4.38	4.63E-02
Nrl	-4.26	9.67E-03
B4galnt3	-4.24	3.00E-04
Crybb2	-4.16	6.29E-12
Crygb	-3.73	6.13E-08
Cryaa	-3.44	5.04E-12
Crygc	-3.22	1.80E-02
Nat8f2	-3.08	4.59E-02
Cryba2	-3.06	3.21E-02
Gm14681	-2.79	3.08E-02
Crygs	-2.56	1.01E-04
Cryba4	-2.46	1.21E-04
Gnat1	-2.35	3.38E-07
Rho	-2.29	4.38E-05
Cpxm2	-2.24	1.07E-17
Ceacam16	-2.01	3.00E-04
Gpat3	-1.93	3.15E-02
Adam7	-1.64	2.50E-02
A2m	-1.64	4.27E-07
Itih5	-1.26	1.80E-02
Kdm6a	-1.19	1.40E-05
Cubn	-1.15	2.36E-02
Ehf	-1.12	3.00E-02
Ddx3x	-1.01	1.12E-02
Zfp955a	-1.00	1.01E-03
5930430L01Rik	-0.98	1.69E-02
Vav1	-0.97	3.28E-02
Vamp7-ps	-0.97	6.42E-05
Mpeg1	-0.96	1.16E-02
Adgre1	-0.95	3.77E-05
Cfh	-0.91	1.01E-02
Laptm5	-0.88	2.02E-03
Slc9a9	-0.83	2.01E-04
Col6a3	-0.80	1.56E-02
Kdm5c	-0.79	3.41E-03
Eif2s3x	-0.79	1.89E-06
Cdh11	-0.77	9.89E-03
Gsta3	-0.76	2.82E-02
Cx3cr1	-0.74	1.69E-02
5530601H04Rik	-0.74	1.25E-03
Mrc2	-0.74	1.12E-02
Plag1	-0.73	4.04E-02
Fstl1	-0.73	2.34E-05
Abtb2	-0.70	3.16E-02
Pag1	-0.69	3.28E-02
Prlr	-0.68	2.57E-02
Arhgdib	-0.67	6.08E-03
Tc2n	-0.67	5.77E-03
Npnt	-0.67	8.44E-05
Cspg4	-0.66	2.79E-04
Spire2	-0.66	3.28E-02
Irf5	-0.65	3.28E-02
Rrh	-0.64	1.24E-02
Wipf1	-0.61	3.82E-02

Csf1r	-0.61	3.40E-02
Ammecr1	-0.57	1.24E-02
Gln-ps1	-0.56	4.95E-02
Pbdc1	-0.53	2.23E-02
Fgf2	-0.50	4.34E-02
Tmem229b	-0.48	2.54E-02
Zfp275	-0.48	4.46E-02
Fam167a	-0.46	3.28E-02
Rapgef3	-0.45	4.70E-02
Gpc6	-0.45	8.81E-03
Niban1	-0.41	1.76E-02
Plagl2	-0.39	1.29E-02
Me3	-0.29	4.01E-02
Pdzrn3	-0.29	3.16E-02
Afap1	-0.25	3.16E-02
Tmem9	0.24	2.42E-02
Gaa	0.24	1.42E-02
Tmed3	0.27	8.55E-03
Npdc1	0.36	1.01E-03
P3h4	0.37	3.16E-02
Apmap	0.38	6.52E-03
Praf2	0.38	3.21E-02
Pld3	0.39	3.17E-03
Syne1	0.39	2.83E-02
Aga	0.39	1.70E-02
Bscl2	0.40	1.42E-02
Leng8	0.40	3.28E-02
Hmgn5	0.42	3.28E-02
Mbd6	0.44	2.60E-02
Sirt7	0.46	3.28E-02
C1qtnf12	0.55	7.22E-03
Hyal3	0.56	4.40E-04
Thbs3	0.57	1.15E-02
C130074G19Rik	0.57	5.46E-03
Uba5	0.57	3.65E-05
Necab3	0.62	3.33E-02
Spag1	0.62	6.52E-03
Abhd3	0.64	1.15E-02
Spint2	0.69	2.63E-02
Hspb6	0.75	3.28E-02
Apoe	0.76	4.53E-02
Epcam	0.83	1.56E-02
Wdr66	0.84	3.13E-03
Ly6a	0.94	3.60E-02
Cpne7	0.99	3.16E-02
Pdzk1ip1	1.17	1.41E-02
Bst2	1.18	2.74E-03
Mill2	1.24	3.18E-06
Ttll6	1.28	3.21E-03
Nnat	1.32	1.48E-02
Tmem252	1.54	4.01E-02
Rab37	1.91	4.48E-02
Gh	2.31	6.70E-03
Slc35d3	2.46	3.33E-02
Pomc	3.09	4.03E-08
Uty	6.26	1.38E-99
Gm29650	8.89	2.13E-17
Eif2s3y	11.01	2.64E-33
Kdm5d	12.88	8.58E-48
Ddx3y	14.47	1.47E-56

Table 3: GSEA analysis of male and female LVChP transcriptome
Gene ontology of biological processes (GOBP) enriched in male and female LVChP (left) and manual categorization into biological processes (right).

Male GOBP	Biological Process
GOBP_ANTIGEN_PROCESSING_AND_PRESENTATION_OF_ENDOGENOUS_PEPTIDE_ANTIGEN	Antigen Processing
GOBP_ANTIGEN_PROCESSING_AND_PRESENTATION_OF_PEPTIDE_ANTIGEN_VIA_MHC_CLASS_I	Antigen Processing
GOBP_AXONEMAL_DYNEIN_COMPLEX_ASSEMBLY	Axoneme/ Dynein complex
GOBP_INNER_DYNEIN_ARM_ASSEMBLY	Axoneme/ Dynein complex
GOBP_OUTER_DYNEIN_ARM_ASSEMBLY	Axoneme/ Dynein complex
GOBP_REGULATION_OF_MICROTUBULE_BASED_MOVEMENT	Axoneme/ Dynein complex
GOBP_AXONEME_ASSEMBLY	Axoneme/ Dynein complex
GOBP_NEGATIVE_REGULATION_OF_VASCULAR_ENDOTHELIAL_GROWTH_FACTOR_PRODUCTION	Developmental Processes
GOBP_EPITHELIAL_CELL_FATE_COMMITMENT	Developmental Processes
GOBP_DIENCEPHALON_DEVELOPMENT	Developmental Processes
GOBP_PROXIMAL_DISTAL_PATTERN_FORMATION	Developmental Processes
GOBP_NEUROEPITHELIAL_CELL_DIFFERENTIATION	Developmental Processes
GOBP_HYPOTHALAMUS_DEVELOPMENT	Developmental Processes
GOBP_INTERMEDIATE_FILAMENT_ORGANIZATION	Intermediate filament organization
GOBP_PEPTIDYL_GLUTAMIC_ACID_MODIFICATION	Metabolism
GOBP_NUCLEOSIDE_TRIPHOSPHATE_BIOSYNTHETIC_PROCESS	Metabolism
GOBP_ATP_SYNTHESIS_COUPLED_ELECTRON_TRANSPORT	Mitochondria/ Oxidative Phosphorylation
GOBP_MITOCHONDRIAL_ELECTRON_TRANSPORT_NADH_TO_UBIQUINONE	Mitochondria/ Oxidative Phosphorylation
GOBP_PROTON_MOTIVE_FORCE_DRIVEN_ATP_SYNTHESIS	Mitochondria/ Oxidative Phosphorylation
GOBP_NADH_DEHYDROGENASE_COMPLEX_ASSEMBLY	Mitochondria/ Oxidative Phosphorylation
GOBP_MITOCHONDRIAL_RESPIRATORY_CHAIN_COMPLEX_ASSEMBLY	Mitochondria/ Oxidative Phosphorylation
GOBP_OXIDATIVE_PHOSPHORYLATION	Mitochondria/ Oxidative Phosphorylation
GOBP_RESPIRATORY_ELECTRON_TRANSPORT_CHAIN	Mitochondria/ Oxidative Phosphorylation
GOBP_ATP_BIOSYNTHETIC_PROCESS	Mitochondria/ Oxidative Phosphorylation
GOBP_MANNOSYLATION	Post-translational modification
GOBP_PROTEIN_DEMETHYLATION	Post-translational modification
GOBP_PEPTIDYL_PROLINE_MODIFICATION	Post-translational modification
GOBP_AMYLOID_PRECURSOR_PROTEIN_BIOSYNTHETIC_PROCESS	Post-translational modification
GOBP_ONE_CARBON_COMPOUND_TRANSPORT	Transport/ Secretion
GOBP_EXTRACELLULAR_TRANSPORT	Transport/ Secretion
GOBP_POSITIVE_REGULATION_OF_CALCIUM_ION_DEPENDENT_EXOCYTOSIS	Transport/ Secretion
Female GOBP	**Biological Process**
GOBP_CATECHOL_CONTAINING_COMPOUND_METABOLIC_PROCESS	Biosynthesis of signaling macromolecules
GOBP_DOPAMINE_METABOLIC_PROCESS	Biosynthesis of signaling macromolecules
GOBP_NITRIC_OXIDE_SYNTHASE_BIOSYNTHETIC_PROCESS	Biosynthesis of signaling macromolecules
GOBP_POSITIVE_REGULATION_OF_NITRIC_OXIDE_SYNTHASE_BIOSYNTHETIC_PROCESS	Biosynthesis of signaling macromolecules
GOBP_POSITIVE_REGULATION_OF_SMALL_MOLECULE_METABOLIC_PROCESS	Biosynthesis of signaling macromolecules
GOBP_REGULATION_OF_CATECHOLAMINE_METABOLIC_PROCESS	Biosynthesis of signaling macromolecules
GOBP_TRANSFORMING_GROWTH_FACTOR_BETA_PRODUCTION	Biosynthesis of signaling macromolecules
GOBP_VITAMIN_BIOSYNTHETIC_PROCESS	Biosynthesis of signaling macromolecules
GOBP_VITAMIN_D_METABOLIC_PROCESS	Biosynthesis of signaling macromolecules
GOBP_CARBOHYDRATE_CATABOLIC_PROCESS	Carbohydrate metabolism
GOBP_CELLULAR_CARBOHYDRATE_METABOLIC_PROCESS	Carbohydrate metabolism
GOBP_MONOSACCHARIDE_CATABOLIC_PROCESS	Carbohydrate metabolism
GOBP_POSITIVE_REGULATION_OF_CARBOHYDRATE_METABOLIC_PROCESS	Carbohydrate metabolism

GOBP_POSITIVE_REGULATION_OF_CELLULAR_CARBOHYDRATE_METABOLIC_PROCESS	Carbohydrate metabolism
GOBP_POSITIVE_REGULATION_OF_CELLULAR_CATABOLIC_PROCESS	Carbohydrate metabolism
GOBP_POSITIVE_REGULATION_OF_GLUCOSE_METABOLIC_PROCESS	Carbohydrate metabolism
GOBP_POSITIVE_REGULATION_OF_GLYCOLYTIC_PROCESS	Carbohydrate metabolism
GOBP_REGULATION_OF_CARBOHYDRATE_CATABOLIC_PROCESS	Carbohydrate metabolism
GOBP_REGULATION_OF_GLYCOLYTIC_PROCESS	Carbohydrate metabolism
GOBP_ANOIKIS	Cell matrix/ Adhesion
GOBP_CELL_ADHESION_MEDIATED_BY_INTEGRIN	Cell matrix/ Adhesion
GOBP_CELL_CELL_ADHESION_MEDIATED_BY_INTEGRIN	Cell matrix/ Adhesion
GOBP_CELL_JUNCTION_DISASSEMBLY	Cell matrix/ Adhesion
GOBP_CELL_MATRIX_ADHESION	Cell matrix/ Adhesion
GOBP_CELL_SUBSTRATE_ADHESION	Cell matrix/ Adhesion
GOBP_COLLAGEN_FIBRIL_ORGANIZATION	Cell matrix/ Adhesion
GOBP_EPITHELIAL_CELL_CELL_ADHESION	Cell matrix/ Adhesion
GOBP_HOMOTYPIC_CELL_CELL_ADHESION	Cell matrix/ Adhesion
GOBP_INTEGRIN_ACTIVATION	Cell matrix/ Adhesion
GOBP_INTEGRIN_MEDIATED_SIGNALING_PATHWAY	Cell matrix/ Adhesion
GOBP_POSITIVE_REGULATION_OF_CELL_ADHESION	Cell matrix/ Adhesion
GOBP_POSITIVE_REGULATION_OF_CELL_ADHESION_MEDIATED_BY_INTEGRIN	Cell matrix/ Adhesion
GOBP_POSITIVE_REGULATION_OF_CELL_CELL_ADHESION	Cell matrix/ Adhesion
GOBP_REGULATION_OF_CELL_ADHESION_MEDIATED_BY_INTEGRIN	Cell matrix/ Adhesion
GOBP_REGULATION_OF_CELL_CELL_ADHESION	Cell matrix/ Adhesion
GOBP_REGULATION_OF_INTEGRIN_ACTIVATION	Cell matrix/ Adhesion
GOBP_CYTOSOLIC_TRANSPORT	Cellular and membrane transport
GOBP_ENDOSOMAL_TRANSPORT	Cellular and membrane transport
GOBP_FATTY_ACID_TRANSMEMBRANE_TRANSPORT	Cellular and membrane transport
GOBP_IMPORT_INTO_NUCLEUS	Cellular and membrane transport
GOBP_LATE_ENDOSOME_TO_LYSOSOME_TRANSPORT	Cellular and membrane transport
GOBP_LYSOSOMAL_TRANSPORT	Cellular and membrane transport
GOBP_MAGNESIUM_ION_TRANSPORT	Cellular and membrane transport
GOBP_MEMBRANE_INVAGINATION	Cellular and membrane transport
GOBP_NEGATIVE_REGULATION_OF_PROTEIN_LOCALIZATION_TO_NUCLEUS	Cellular and membrane transport
GOBP_NEGATIVE_REGULATION_OF_SODIUM_ION_TRANSMEMBRANE_TRANSPORT	Cellular and membrane transport
GOBP_POSITIVE_REGULATION_OF_PROTEIN_LOCALIZATION_TO_CELL_SURFACE	Cellular and membrane transport
GOBP_POTASSIUM_ION_IMPORT_ACROSS_PLASMA_MEMBRANE	Cellular and membrane transport
GOBP_PROSTAGLANDIN_TRANSPORT	Cellular and membrane transport
GOBP_PROTEIN_LOCALIZATION_TO_ENDOSOME	Cellular and membrane transport
GOBP_PROTEIN_LOCALIZATION_TO_GOLGI_APPARATUS	Cellular and membrane transport
GOBP_PROTEIN_LOCALIZATION_TO_MICROTUBULE_ORGANIZING_CENTER	Cellular and membrane transport
GOBP_REGULATION_OF_FATTY_ACID_TRANSPORT	Cellular and membrane transport
GOBP_REGULATION_OF_ORGANIC_ACID_TRANSPORT	Cellular and membrane transport
GOBP_RETROGRADE_TRANSPORT_ENDOSOME_TO_GOLGI	Cellular and membrane transport
GOBP_VACUOLAR_TRANSPORT	Cellular and membrane transport
GOBP_VESICLE_MEDIATED_TRANSPORT_BETWEEN_ENDOSOMAL_COMPARTMENTS	Cellular and membrane transport
GOBP_AMYLOID_BETA_CLEARANCE	Cellular and membrane transport
GOBP_LIPID_IMPORT_INTO_CELL	Cellular and membrane transport
GOBP_OVULATION_CYCLE	Developmental processes
GOBP_BRAIN_MORPHOGENESIS	Developmental processes
GOBP_MONONUCLEAR_CELL_DIFFERENTIATION	Developmental processes
GOBP_NEGATIVE_REGULATION_OF_VASCULAR_ASSOCIATED_SMOOTH_MUSCLE_CELL_MIGRATION	Developmental processes
GOBP_OVULATION_CYCLE_PROCESS	Developmental processes
GOBP_POSITIVE_REGULATION_OF_SMOOTH_MUSCLE_CONTRACTION	Developmental processes
GOBP_SENSORY_PERCEPTION_OF_SMELL	Developmental processes
GOBP_SEX_DETERMINATION	Developmental processes
GOBP_SMOOTH_MUSCLE_CELL_MIGRATION	Developmental processes
GOBP_ADIPOSE_TISSUE_DEVELOPMENT	Developmental processes
GOBP_BIOMINERALIZATION	Developmental processes
GOBP_BONE_RESORPTION	Developmental processes
GOBP_CENTRAL_NERVOUS_SYSTEM_NEURON_AXONOGENESIS	Developmental processes
GOBP_COCHLEA_MORPHOGENESIS	Developmental processes
GOBP_CORONARY_VASCULATURE_DEVELOPMENT	Developmental processes
GOBP_CORONARY_VASCULATURE_MORPHOGENESIS	Developmental processes
GOBP_ECTOPIC_GERM_CELL_PROGRAMMED_CELL_DEATH	Developmental processes

GOBP_FIBROBLAST_MIGRATION	Developmental processes
GOBP_GLIAL_CELL_ACTIVATION	Developmental processes
GOBP_GLIAL_CELL_MIGRATION	Developmental processes
GOBP_HAIR_FOLLICLE_MATURATION	Developmental processes
GOBP_HEPATOCYTE_APOPTOTIC_PROCESS	Developmental processes
GOBP_MAINTENANCE_OF_GASTROINTESTINAL_EPITHELIUM	Developmental processes
GOBP_METANEPHRIC_GLOMERULUS_DEVELOPMENT	Developmental processes
GOBP_MODULATION_OF_PROCESS_OF_ANOTHER_ORGANISM	Developmental processes
GOBP_MUSCLE_CELL_PROLIFERATION	Developmental processes
GOBP_NEGATIVE_REGULATION_OF_SMOOTH_MUSCLE_CELL_MIGRATION	Developmental processes
GOBP_OSTEOCLAST_DIFFERENTIATION	Developmental processes
GOBP_PODOSOME_ASSEMBLY	Developmental processes
GOBP_POSITIVE_REGULATION_OF_CELL_ACTIVATION	Developmental processes
GOBP_POSITIVE_REGULATION_OF_ERYTHROCYTE_DIFFERENTIATION	Developmental processes
GOBP_POSITIVE_REGULATION_OF_FIBROBLAST_MIGRATION	Developmental processes
GOBP_POSITIVE_REGULATION_OF_G1_S_TRANSITION_OF_MITOTIC_CELL_CYCLE	Developmental processes
GOBP_POSITIVE_REGULATION_OF_MITOTIC_CELL_CYCLE	Developmental processes
GOBP_POSITIVE_REGULATION_OF_MITOTIC_CELL_CYCLE_PHASE_TRANSITION	Developmental processes
GOBP_POSITIVE_REGULATION_OF_MORPHOGENESIS_OF_AN_EPITHELIUM	Developmental processes
GOBP_POSITIVE_REGULATION_OF_MYELINATION	Developmental processes
GOBP_POSITIVE_REGULATION_OF_NERVOUS_SYSTEM_PROCESS	Developmental processes
GOBP_POSITIVE_REGULATION_OF_OSTEOCLAST_DIFFERENTIATION	Developmental processes
GOBP_POSITIVE_REGULATION_OF_SMOOTH_MUSCLE_CELL_PROLIFERATION	Developmental processes
GOBP_POSITIVE_REGULATION_OF_SPROUTING_ANGIOGENESIS	Developmental processes
GOBP_POSITIVE_REGULATION_OF_VASCULAR_ASSOCIATED_SMOOTH_MUSCLE_CELL_PROLIFERATION	Developmental processes
GOBP_POSITIVE_REGULATION_OF_VASCULATURE_DEVELOPMENT	Developmental processes
GOBP_REGULATION_OF_BONE_REMODELING	Developmental processes
GOBP_REGULATION_OF_EXTRINSIC_APOPTOTIC_SIGNALING_PATHWAY_VIA_DEATH_DOMAIN_RECEPTORS	Developmental processes
GOBP_REGULATION_OF_GLIAL_CELL_MIGRATION	Developmental processes
GOBP_REGULATION_OF_KERATINOCYTE_DIFFERENTIATION	Developmental processes
GOBP_REGULATION_OF_MORPHOGENESIS_OF_AN_EPITHELIUM	Developmental processes
GOBP_REGULATION_OF_OSTEOCLAST_DIFFERENTIATION	Developmental processes
GOBP_SENSORY_ORGAN_MORPHOGENESIS	Developmental processes
GOBP_SENSORY_SYSTEM_DEVELOPMENT	Developmental processes
GOBP_SKELETAL_MUSCLE_CELL_PROLIFERATION	Developmental processes
GOBP_STRIATED_MUSCLE_CELL_APOPTOTIC_PROCESS	Developmental processes
GOBP_TELENCEPHALON_GLIAL_CELL_MIGRATION	Developmental processes
GOBP_TONGUE_DEVELOPMENT	Developmental processes
GOBP_TOOTH_MINERALIZATION	Developmental processes
GOBP_VASCULAR_ASSOCIATED_SMOOTH_MUSCLE_CELL_MIGRATION	Developmental processes
GOBP_EPIGENETIC_REGULATION_OF_GENE_EXPRESSION	Gene expression
GOBP_GENE_SILENCING_BY_RNA	Gene expression
GOBP_HISTONE_H4_K5_ACETYLATION	Gene expression
GOBP_NUCLEAR_TRANSCRIBED_MRNA_POLY_A_TAIL_SHORTENING	Gene expression
GOBP_POSITIVE_REGULATION_OF_PROTEIN_MODIFICATION_BY_SMALL_PROTEIN_CONJUGATION_OR_REMOVAL	Gene expression
GOBP_REGULATION_OF_NUCLEAR_TRANSCRIBED_MRNA_POLY_A_TAIL_SHORTENING	Gene expression
GOBP_TRANSLATIONAL_TERMINATION	Gene expression
GOBP_DOSAGE_COMPENSATION	Homeostasis
GOBP_ENERGY_HOMEOSTASIS	Homeostasis
GOBP_POSITIVE_REGULATION_OF_CELL_CYCLE_G1_S_PHASE_TRANSITION	Homeostasis
GOBP_PROGRAMMED_CELL_DEATH_INVOLVED_IN_CELL_DEVELOPMENT	Homeostasis
GOBP_SODIUM_ION_HOMEOSTASIS	Homeostasis
GOBP_ACTIVATION_OF_IMMUNE_RESPONSE	Immune regulation
GOBP_ACTIVATION_OF_INNATE_IMMUNE_RESPONSE	Immune regulation
GOBP_ADAPTIVE_IMMUNE_RESPONSE	Immune regulation
GOBP_ALPHA_BETA_T_CELL_ACTIVATION	Immune regulation
GOBP_ALPHA_BETA_T_CELL_DIFFERENTIATION	Immune regulation
GOBP_ALPHA_BETA_T_CELL_PROLIFERATION	Immune regulation
GOBP_ANTIGEN_RECEPTOR_MEDIATED_SIGNALING_PATHWAY	Immune regulation
GOBP_B_CELL_ACTIVATION	Immune regulation
GOBP_B_CELL_DIFFERENTIATION	Immune regulation
GOBP_B_CELL_HOMEOSTASIS	Immune regulation

GOBP_B_CELL_PROLIFERATION	Immune regulation
GOBP_B_CELL_RECEPTOR_SIGNALING_PATHWAY	Immune regulation
GOBP_CD4_POSITIVE_ALPHA_BETA_T_CELL_ACTIVATION	Immune regulation
GOBP_CD4_POSITIVE_ALPHA_BETA_T_CELL_DIFFERENTIATION	Immune regulation
GOBP_CELL_ACTIVATION_INVOLVED_IN_IMMUNE_RESPONSE	Immune regulation
GOBP_CELL_KILLING	Immune regulation
GOBP_CELLULAR_DEFENSE_RESPONSE	Immune regulation
GOBP_CELLULAR_RESPONSE_TO_VIRUS	Immune regulation
GOBP_CHEMOKINE_PRODUCTION	Immune regulation
GOBP_CYTOKINE_PRODUCTION_INVOLVED_IN_IMMUNE_RESPONSE	Immune regulation
GOBP_CYTOKINE_PRODUCTION_INVOLVED_IN_INFLAMMATORY_RESPONSE	Immune regulation
GOBP_CYTOPLASMIC_PATTERN_RECOGNITION_RECEPTOR_SIGNALING_PATHWAY	Immune regulation
GOBP_DEFENSE_RESPONSE_TO_BACTERIUM	Immune regulation
GOBP_DEFENSE_RESPONSE_TO_SYMBIONT	Immune regulation
GOBP_DENDRITIC_CELL_CYTOKINE_PRODUCTION	Immune regulation
GOBP_DETECTION_OF_ABIOTIC_STIMULUS	Immune regulation
GOBP_DETECTION_OF_BIOTIC_STIMULUS	Immune regulation
GOBP_DETECTION_OF_OTHER_ORGANISM	Immune regulation
GOBP_ESTABLISHMENT_OF_LYMPHOCYTE_POLARITY	Immune regulation
GOBP_EXTRINSIC_APOPTOTIC_SIGNALING_PATHWAY	Immune regulation
GOBP_EXTRINSIC_APOPTOTIC_SIGNALING_PATHWAY_VIA_DEATH_DOMAIN_RECEPTORS	Immune regulation
GOBP_FC_EPSILON_RECEPTOR_SIGNALING_PATHWAY	Immune regulation
GOBP_FC_GAMMA_RECEPTOR_SIGNALING_PATHWAY	Immune regulation
GOBP_FC_RECEPTOR_MEDIATED_STIMULATORY_SIGNALING_PATHWAY	Immune regulation
GOBP_FC_RECEPTOR_SIGNALING_PATHWAY	Immune regulation
GOBP_GAMMA_DELTA_T_CELL_ACTIVATION	Immune regulation
GOBP_GRANULOCYTE_ACTIVATION	Immune regulation
GOBP_GRANULOCYTE_CHEMOTAXIS	Immune regulation
GOBP_GRANULOCYTE_MACROPHAGE_COLONY_STIMULATING_FACTOR_PRODUCTION	Immune regulation
GOBP_GRANULOCYTE_MIGRATION	Immune regulation
GOBP_HEMATOPOIETIC_STEM_CELL_PROLIFERATION	Immune regulation
GOBP_IMMUNE_RESPONSE_REGULATING_CELL_SURFACE_RECEPTOR_SIGNALING_PATHWAY	Immune regulation
GOBP_IMMUNE_RESPONSE_REGULATING_CELL_SURFACE_RECEPTOR_SIGNALING_PATHWAY_INVOLVED_IN_PHAGOCYTOSIS	Immune regulation
GOBP_IMMUNE_RESPONSE_REGULATING_SIGNALING_PATHWAY	Immune regulation
GOBP_IMMUNOGLOBULIN_PRODUCTION	Immune regulation
GOBP_IMMUNOLOGICAL_SYNAPSE_FORMATION	Immune regulation
GOBP_INFLAMMASOME_COMPLEX_ASSEMBLY	Immune regulation
GOBP_INNATE_IMMUNE_RESPONSE_ACTIVATING_SIGNAL_TRANSDUCTION	Immune regulation
GOBP_INTERFERON_ALPHA_PRODUCTION	Immune regulation
GOBP_INTERFERON_BETA_PRODUCTION	Immune regulation
GOBP_LEUKOCYTE_ACTIVATION_INVOLVED_IN_INFLAMMATORY_RESPONSE	Immune regulation
GOBP_LEUKOCYTE_CELL_CELL_ADHESION	Immune regulation
GOBP_LEUKOCYTE_DEGRANULATION	Immune regulation
GOBP_LEUKOCYTE_MEDIATED_CYTOTOXICITY	Immune regulation
GOBP_LEUKOCYTE_MEDIATED_IMMUNITY	Immune regulation
GOBP_LEUKOCYTE_PROLIFERATION	Immune regulation
GOBP_LYMPHOCYTE_ACTIVATION_INVOLVED_IN_IMMUNE_RESPONSE	Immune regulation
GOBP_MACROPHAGE_ACTIVATION	Immune regulation
GOBP_MACROPHAGE_ACTIVATION_INVOLVED_IN_IMMUNE_RESPONSE	Immune regulation
GOBP_MACROPHAGE_MIGRATION	Immune regulation
GOBP_MAST_CELL_ACTIVATION	Immune regulation
GOBP_MAST_CELL_MEDIATED_IMMUNITY	Immune regulation
GOBP_MYD88_DEPENDENT_TOLL_LIKE_RECEPTOR_SIGNALING_PATHWAY	Immune regulation
GOBP_MYELOID_CELL_ACTIVATION_INVOLVED_IN_IMMUNE_RESPONSE	Immune regulation
GOBP_MYELOID_CELL_DIFFERENTIATION	Immune regulation
GOBP_MYELOID_LEUKOCYTE_ACTIVATION	Immune regulation
GOBP_MYELOID_LEUKOCYTE_CYTOKINE_PRODUCTION	Immune regulation
GOBP_MYELOID_LEUKOCYTE_MEDIATED_IMMUNITY	Immune regulation
GOBP_NATURAL_KILLER_CELL_ACTIVATION	Immune regulation
GOBP_NATURAL_KILLER_CELL_ACTIVATION_INVOLVED_IN_IMMUNE_RESPONSE	Immune regulation
GOBP_NEGATIVE_REGULATION_OF_B_CELL_ACTIVATION	Immune regulation
GOBP_NEGATIVE_REGULATION_OF_B_CELL_PROLIFERATION	Immune regulation
GOBP_NEGATIVE_REGULATION_OF_CD4_POSITIVE_ALPHA_BETA_T_CELL_ACTIVATION	Immune regulation

GOBP_NEGATIVE_REGULATION_OF_CELL_ACTIVATION	Immune regulation
GOBP_NEGATIVE_REGULATION_OF_IMMUNE_EFFECTOR_PROCESS	Immune regulation
GOBP_NEGATIVE_REGULATION_OF_IMMUNE_SYSTEM_PROCESS	Immune regulation
GOBP_NEGATIVE_REGULATION_OF_INFLAMMATORY_RESPONSE_TO_ANTIGENIC_STIMULUS	Immune regulation
GOBP_NEGATIVE_REGULATION_OF_INTERLEUKIN_2_PRODUCTION	Immune regulation
GOBP_NEGATIVE_REGULATION_OF_LEUKOCYTE_CELL_CELL_ADHESION	Immune regulation
GOBP_NEGATIVE_REGULATION_OF_LYMPHOCYTE_ACTIVATION	Immune regulation
GOBP_NEGATIVE_REGULATION_OF_TOLL_LIKE_RECEPTOR_SIGNALING_PATHWAY	Immune regulation
GOBP_NEUROINFLAMMATORY_RESPONSE	Immune regulation
GOBP_NEUTROPHIL_ACTIVATION_INVOLVED_IN_IMMUNE_RESPONSE	Immune regulation
GOBP_NEUTROPHIL_CHEMOTAXIS	Immune regulation
GOBP_NUCLEOTIDE_BINDING_OLIGOMERIZATION_DOMAIN_CONTAINING_2_SIGNALING_PATHWAY	Immune regulation
GOBP_PATTERN_RECOGNITION_RECEPTOR_SIGNALING_PATHWAY	Immune regulation
GOBP_POSITIVE_REGULATION_OF_B_CELL_ACTIVATION	Immune regulation
GOBP_POSITIVE_REGULATION_OF_B_CELL_DIFFERENTIATION	Immune regulation
GOBP_POSITIVE_REGULATION_OF_CHEMOKINE_PRODUCTION	Immune regulation
GOBP_POSITIVE_REGULATION_OF_CYTOKINE_PRODUCTION	Immune regulation
GOBP_POSITIVE_REGULATION_OF_CYTOKINE_PRODUCTION_INVOLVED_IN_IMMUNE_RESPONSE	Immune regulation
GOBP_POSITIVE_REGULATION_OF_CYTOKINE_PRODUCTION_INVOLVED_IN_INFLAMMATORY_RESPONSE	Immune regulation
GOBP_POSITIVE_REGULATION_OF_GRANULOCYTE_CHEMOTAXIS	Immune regulation
GOBP_POSITIVE_REGULATION_OF_HEMOPOIESIS	Immune regulation
GOBP_POSITIVE_REGULATION_OF_IMMUNE_EFFECTOR_PROCESS	Immune regulation
GOBP_POSITIVE_REGULATION_OF_INNATE_IMMUNE_RESPONSE	Immune regulation
GOBP_POSITIVE_REGULATION_OF_INTERFERON_ALPHA_PRODUCTION	Immune regulation
GOBP_POSITIVE_REGULATION_OF_INTERFERON_BETA_PRODUCTION	Immune regulation
GOBP_POSITIVE_REGULATION_OF_LEUKOCYTE_ADHESION_TO_VASCULAR_ENDOTHELIAL_CELL	Immune regulation
GOBP_POSITIVE_REGULATION_OF_LEUKOCYTE_CELL_CELL_ADHESION	Immune regulation
GOBP_POSITIVE_REGULATION_OF_LEUKOCYTE_CHEMOTAXIS	Immune regulation
GOBP_POSITIVE_REGULATION_OF_LEUKOCYTE_DEGRANULATION	Immune regulation
GOBP_POSITIVE_REGULATION_OF_LEUKOCYTE_MEDIATED_IMMUNITY	Immune regulation
GOBP_POSITIVE_REGULATION_OF_LYMPHOCYTE_DIFFERENTIATION	Immune regulation
GOBP_POSITIVE_REGULATION_OF_MACROPHAGE_ACTIVATION	Immune regulation
GOBP_POSITIVE_REGULATION_OF_MACROPHAGE_CHEMOTAXIS	Immune regulation
GOBP_POSITIVE_REGULATION_OF_MACROPHAGE_MIGRATION	Immune regulation
GOBP_POSITIVE_REGULATION_OF_MYELOID_CELL_DIFFERENTIATION	Immune regulation
GOBP_POSITIVE_REGULATION_OF_MYELOID_LEUKOCYTE_CYTOKINE_PRODUCTION_INVOLVED_IN_IMMUNE_RESPONSE	Immune regulation
GOBP_POSITIVE_REGULATION_OF_MYELOID_LEUKOCYTE_DIFFERENTIATION	Immune regulation
GOBP_POSITIVE_REGULATION_OF_MYELOID_LEUKOCYTE_MEDIATED_IMMUNITY	Immune regulation
GOBP_POSITIVE_REGULATION_OF_NATURAL_KILLER_CELL_MEDIATED_IMMUNITY	Immune regulation
GOBP_POSITIVE_REGULATION_OF_NIK_NF_KAPPAB_SIGNALING	Immune regulation
GOBP_POSITIVE_REGULATION_OF_PATTERN_RECOGNITION_RECEPTOR_SIGNALING_PATHWAY	Immune regulation
GOBP_POSITIVE_REGULATION_OF_PRODUCTION_OF_MOLECULAR_MEDIATOR_OF_IMMUNE_RESPONSE	Immune regulation
GOBP_POSITIVE_REGULATION_OF_RESPONSE_TO_BIOTIC_STIMULUS	Immune regulation
GOBP_POSITIVE_REGULATION_OF_TUMOR_NECROSIS_FACTOR_SUPERFAMILY_CYTOKINE_PRODUCTION	Immune regulation
GOBP_POSITIVE_REGULATION_OF_VIRAL_GENOME_REPLICATION	Immune regulation
GOBP_PRODUCTION_OF_MOLECULAR_MEDIATOR_INVOLVED_IN_INFLAMMATORY_RESPONSE	Immune regulation
GOBP_PRODUCTION_OF_MOLECULAR_MEDIATOR_OF_IMMUNE_RESPONSE	Immune regulation
GOBP_REGULATION_OF_ALPHA_BETA_T_CELL_ACTIVATION	Immune regulation
GOBP_REGULATION_OF_ANTIGEN_PROCESSING_AND_PRESENTATION	Immune regulation
GOBP_REGULATION_OF_B_CELL_ACTIVATION	Immune regulation
GOBP_REGULATION_OF_B_CELL_DIFFERENTIATION	Immune regulation
GOBP_REGULATION_OF_B_CELL_PROLIFERATION	Immune regulation
GOBP_REGULATION_OF_CD4_POSITIVE_ALPHA_BETA_T_CELL_ACTIVATION	Immune regulation
GOBP_REGULATION_OF_CD4_POSITIVE_ALPHA_BETA_T_CELL_DIFFERENTIATION	Immune regulation
GOBP_REGULATION_OF_CD8_POSITIVE_ALPHA_BETA_T_CELL_ACTIVATION	Immune regulation
GOBP_REGULATION_OF_CELL_KILLING	Immune regulation
GOBP_REGULATION_OF_DEFENSE_RESPONSE_TO_BACTERIUM	Immune regulation

GOBP_REGULATION_OF_GRANULOCYTE_CHEMOTAXIS	Immune regulation
GOBP_REGULATION_OF_HEMOPOIESIS	Immune regulation
GOBP_REGULATION_OF_HUMORAL_IMMUNE_RESPONSE	Immune regulation
GOBP_REGULATION_OF_IMMUNE_EFFECTOR_PROCESS	Immune regulation
GOBP_REGULATION_OF_IMMUNOGLOBULIN_PRODUCTION	Immune regulation
GOBP_REGULATION_OF_INFLAMMATORY_RESPONSE_TO_ANTIGENIC_STIMULUS	Immune regulation
GOBP_REGULATION_OF_INNATE_IMMUNE_RESPONSE	Immune regulation
GOBP_REGULATION_OF_LEUKOCYTE_CHEMOTAXIS	Immune regulation
GOBP_REGULATION_OF_LEUKOCYTE_DEGRANULATION	Immune regulation
GOBP_REGULATION_OF_LEUKOCYTE_DIFFERENTIATION	Immune regulation
GOBP_REGULATION_OF_LEUKOCYTE_MEDIATED_CYTOTOXICITY	Immune regulation
GOBP_REGULATION_OF_LEUKOCYTE_MEDIATED_IMMUNITY	Immune regulation
GOBP_REGULATION_OF_LEUKOCYTE_PROLIFERATION	Immune regulation
GOBP_REGULATION_OF_LYMPHOCYTE_DIFFERENTIATION	Immune regulation
GOBP_REGULATION_OF_MACROPHAGE_ACTIVATION	Immune regulation
GOBP_REGULATION_OF_MACROPHAGE_CHEMOTAXIS	Immune regulation
GOBP_REGULATION_OF_MACROPHAGE_MIGRATION	Immune regulation
GOBP_REGULATION_OF_MYELOID_LEUKOCYTE_MEDIATED_IMMUNITY	Immune regulation
GOBP_REGULATION_OF_NEUTROPHIL_ACTIVATION	Immune regulation
GOBP_REGULATION_OF_NEUTROPHIL_CHEMOTAXIS	Immune regulation
GOBP_REGULATION_OF_NEUTROPHIL_MIGRATION	Immune regulation
GOBP_REGULATION_OF_NLRP3_INFLAMMASOME_COMPLEX_ASSEMBLY	Immune regulation
GOBP_REGULATION_OF_PATTERN_RECOGNITION_RECEPTOR_SIGNALING_PATHWAY	Immune regulation
GOBP_REGULATION_OF_PRODUCTION_OF_MOLECULAR_MEDIATOR_OF_IMMUNE_RESPONSE	Immune regulation
GOBP_REGULATION_OF_RESPONSE_TO_BIOTIC_STIMULUS	Immune regulation
GOBP_REGULATION_OF_T_CELL_ACTIVATION	Immune regulation
GOBP_REGULATION_OF_T_HELPER_1_TYPE_IMMUNE_RESPONSE	Immune regulation
GOBP_REGULATION_OF_TOLL_LIKE_RECEPTOR_SIGNALING_PATHWAY	Immune regulation
GOBP_RESPONSE_TO_MOLECULE_OF_BACTERIAL_ORIGIN	Immune regulation
GOBP_T_CELL_ACTIVATION_INVOLVED_IN_IMMUNE_RESPONSE	Immune regulation
GOBP_T_CELL_CHEMOTAXIS	Immune regulation
GOBP_T_CELL_DIFFERENTIATION	Immune regulation
GOBP_CHOLESTEROL_STORAGE	Lipid metabolism
GOBP_LIPOPROTEIN_LOCALIZATION	Lipid metabolism
GOBP_POSITIVE_REGULATION_OF_FATTY_ACID_OXIDATION	Lipid metabolism
GOBP_POSITIVE_REGULATION_OF_FATTY_ACID_TRANSPORT	Lipid metabolism
GOBP_POSITIVE_REGULATION_OF_LIPID_CATABOLIC_PROCESS	Lipid metabolism
GOBP_POSITIVE_REGULATION_OF_LIPID_KINASE_ACTIVITY	Lipid metabolism
GOBP_POSITIVE_REGULATION_OF_LIPID_METABOLIC_PROCESS	Lipid metabolism
GOBP_REGULATION_OF_FATTY_ACID_BETA_OXIDATION	Lipid metabolism
GOBP_REGULATION_OF_FATTY_ACID_OXIDATION	Lipid metabolism
GOBP_REGULATION_OF_LIPASE_ACTIVITY	Lipid metabolism
GOBP_REGULATION_OF_LIPID_KINASE_ACTIVITY	Lipid metabolism
GOBP_TRIGLYCERIDE_CATABOLIC_PROCESS	Lipid metabolism
GOBP_TRIGLYCERIDE_METABOLIC_PROCESS	Lipid metabolism
GOBP_HEAT_GENERATION	Metabolism
GOBP_POSITIVE_REGULATION_OF_NUCLEOTIDE_METABOLIC_PROCESS	Metabolism
GOBP_REGULATION_OF_SECONDARY_METABOLIC_PROCESS	Metabolism
GOBP_RESPIRATORY_BURST	Metabolism
GOBP_POSITIVE_REGULATION_OF_REACTIVE_OXYGEN_SPECIES_BIOSYNTHETIC_PROCESS	Oxidative stress
GOBP_POSITIVE_REGULATION_OF_REACTIVE_OXYGEN_SPECIES_METABOLIC_PROCESS	Oxidative stress
GOBP_REACTIVE_OXYGEN_SPECIES_BIOSYNTHETIC_PROCESS	Oxidative stress
GOBP_REACTIVE_OXYGEN_SPECIES_METABOLIC_PROCESS	Oxidative stress
GOBP_REGULATION_OF_REACTIVE_OXYGEN_SPECIES_BIOSYNTHETIC_PROCESS	Oxidative stress
GOBP_REGULATION_OF_REACTIVE_OXYGEN_SPECIES_METABOLIC_PROCESS	Oxidative stress
GOBP_REGULATION_OF_RESPONSE_TO_REACTIVE_OXYGEN_SPECIES	Oxidative stress
GOBP_REGULATION_OF_SUPEROXIDE_METABOLIC_PROCESS	Oxidative stress
GOBP_SUPEROXIDE_ANION_GENERATION	Oxidative stress
GOBP_SUPEROXIDE_METABOLIC_PROCESS	Oxidative stress
GOBP_PHAGOCYTOSIS	Phagocytosis/ Autophagy
GOBP_POSITIVE_REGULATION_OF_PHAGOCYTOSIS	Phagocytosis/ Autophagy
GOBP_PHAGOCYTOSIS_RECOGNITION	Phagocytosis/ Autophagy
GOBP_POSITIVE_REGULATION_OF_AUTOPHAGY	Phagocytosis/ Autophagy

GOBP_POSITIVE_REGULATION_OF_CELL_KILLING	Phagocytosis/ Autophagy
GOBP_POSITIVE_REGULATION_OF_MACROAUTOPHAGY	Phagocytosis/ Autophagy
GOBP_REGULATION_OF_PHAGOCYTOSIS	Phagocytosis/ Autophagy
GOBP_INOSITOL_LIPID_MEDIATED_SIGNALING	Phospho-inositol / Phospholipase
GOBP_INOSITOL_PHOSPHATE_BIOSYNTHETIC_PROCESS	Phospho-inositol / Phospholipase
GOBP_INOSITOL_PHOSPHATE_METABOLIC_PROCESS	Phospho-inositol / Phospholipase
GOBP_PHOSPHATIDYLINOSITOL_3_PHOSPHATE_BIOSYNTHETIC_PROCESS	Phospho-inositol / Phospholipase
GOBP_PHOSPHATIDYLINOSITOL_METABOLIC_PROCESS	Phospho-inositol / Phospholipase
GOBP_PHOSPHATIDYLINOSITOL_PHOSPHATE_BIOSYNTHETIC_PROCESS	Phospho-inositol / Phospholipase
GOBP_PHOSPHOLIPASE_C_ACTIVATING_G_PROTEIN_COUPLED_RECEPTOR_SIGNALING_PATHWAY	Phospho-inositol / Phospholipase
GOBP_POSITIVE_REGULATION_OF_LIPASE_ACTIVITY	Phospho-inositol / Phospholipase
GOBP_POSITIVE_REGULATION_OF_PHOSPHOLIPASE_ACTIVITY	Phospho-inositol / Phospholipase
GOBP_REGULATION_OF_INOSITOL_PHOSPHATE_BIOSYNTHETIC_PROCESS	Phospho-inositol / Phospholipase
GOBP_REGULATION_OF_PHOSPHATIDYLINOSITOL_3_KINASE_ACTIVITY	Phospho-inositol / Phospholipase
GOBP_REGULATION_OF_PHOSPHOLIPASE_ACTIVITY	Phospho-inositol / Phospholipase
GOBP_REGULATION_OF_PHOSPHOLIPASE_C_ACTIVITY	Phospho-inositol / Phospholipase
GOBP_REGULATION_OF_PHOSPHOLIPID_METABOLIC_PROCESS	Phospho-inositol / Phospholipase
GOBP_DEPHOSPHORYLATION	Phosphorylation
GOBP_PEPTIDYL_SERINE_MODIFICATION	Phosphorylation
GOBP_PEPTIDYL_THREONINE_MODIFICATION	Phosphorylation
GOBP_PHOSPHATIDYLINOSITOL_DEPHOSPHORYLATION	Phosphorylation
GOBP_POSITIVE_REGULATION_OF_DEPHOSPHORYLATION	Phosphorylation
GOBP_POSITIVE_REGULATION_OF_PHOSPHATASE_ACTIVITY	Phosphorylation
GOBP_POSITIVE_REGULATION_OF_PHOSPHOPROTEIN_PHOSPHATASE_ACTIVITY	Phosphorylation
GOBP_PROTEIN_AUTOPHOSPHORYLATION	Phosphorylation
GOBP_REGULATION_OF_DEPHOSPHORYLATION	Phosphorylation
GOBP_REGULATION_OF_PHOSPHATASE_ACTIVITY	Phosphorylation
GOBP_CAMERA_TYPE_EYE_MORPHOGENESIS	Phototransduction
GOBP_CAMERA_TYPE_EYE_PHOTORECEPTOR_CELL_DIFFERENTIATION	Phototransduction
GOBP_DETECTION_OF_LIGHT_STIMULUS	Phototransduction
GOBP_DETECTION_OF_VISIBLE_LIGHT	Phototransduction
GOBP_EMBRYONIC_EYE_MORPHOGENESIS	Phototransduction
GOBP_PHOTOTRANSDUCTION	Phototransduction
GOBP_PHOTOTRANSDUCTION_VISIBLE_LIGHT	Phototransduction
GOBP_RESPONSE_TO_LIGHT_INTENSITY	Phototransduction
GOBP_RETINA_MORPHOGENESIS_IN_CAMERA_TYPE_EYE	Phototransduction
GOBP_CELLULAR_RESPONSE_TO_ACID_CHEMICAL	Response to chemical compounds
GOBP_CELLULAR_RESPONSE_TO_ALCOHOL	Response to chemical compounds
GOBP_CELLULAR_RESPONSE_TO_ATP	Response to chemical compounds
GOBP_CELLULAR_RESPONSE_TO_GLUCOSE_STARVATION	Response to chemical compounds
GOBP_CELLULAR_RESPONSE_TO_KETONE	Response to chemical compounds
GOBP_CELLULAR_RESPONSE_TO_LOW_DENSITY_LIPOPROTEIN_PARTICLE_STIMULUS	Response to chemical compounds
GOBP_CELLULAR_RESPONSE_TO_OXYGEN_RADICAL	Response to chemical compounds
GOBP_CELLULAR_RESPONSE_TO_PEPTIDE_HORMONE_STIMULUS	Response to chemical compounds
GOBP_CELLULAR_RESPONSE_TO_PROSTAGLANDIN_E_STIMULUS	Response to chemical compounds
GOBP_CELLULAR_RESPONSE_TO_PROSTAGLANDIN_STIMULUS	Response to chemical compounds
GOBP_REGULATION_OF_RESPONSE_TO_OXIDATIVE_STRESS	Response to chemical compounds
GOBP_RESPONSE_TO_ACID_CHEMICAL	Response to chemical compounds
GOBP_RESPONSE_TO_CORTICOSTEROID	Response to chemical compounds
GOBP_RESPONSE_TO_DEXAMETHASONE	Response to chemical compounds
GOBP_RESPONSE_TO_FATTY_ACID	Response to chemical compounds
GOBP_RESPONSE_TO_HYDROPEROXIDE	Response to chemical compounds
GOBP_RESPONSE_TO_KETONE	Response to chemical compounds
GOBP_RESPONSE_TO_LECTIN	Response to chemical compounds
GOBP_RESPONSE_TO_MAGNESIUM_ION	Response to chemical compounds
GOBP_RESPONSE_TO_MURAMYL_DIPEPTIDE	Response to chemical compounds
GOBP_RESPONSE_TO_PROSTAGLANDIN	Response to chemical compounds
GOBP_RESPONSE_TO_PROSTAGLANDIN_E	Response to chemical compounds
GOBP_RESPONSE_TO_TESTOSTERONE	Response to chemical compounds
GOBP_RESPONSE_TO_TRANSFORMING_GROWTH_FACTOR_BETA	Response to chemical compounds
GOBP_EYE_MORPHOGENESIS	Retinal development
GOBP_EYE_PHOTORECEPTOR_CELL_DEVELOPMENT	Retinal development
GOBP_EYE_PHOTORECEPTOR_CELL_DIFFERENTIATION	Retinal development

GOBP_LENS_DEVELOPMENT_IN_CAMERA_TYPE_EYE	Retinal development
GOBP_LENS_FIBER_CELL_DIFFERENTIATION	Retinal development
GOBP_PHOTORECEPTOR_CELL_DEVELOPMENT	Retinal development
GOBP_PHOTORECEPTOR_CELL_DIFFERENTIATION	Retinal development
GOBP_RETINA_DEVELOPMENT_IN_CAMERA_TYPE_EYE	Retinal development
GOBP_SENSORY_PERCEPTION_OF_LIGHT_STIMULUS	Retinal development
GOBP_BODY_FLUID_SECRETION	Secretion
GOBP_MUCUS_SECRETION	Secretion
GOBP_REGULATION_OF_ICOSANOID_SECRETION	Secretion
GOBP_INTERLEUKIN_1_PRODUCTION	Signaling
GOBP_INTERLEUKIN_10_PRODUCTION	Signaling
GOBP_INTERLEUKIN_12_PRODUCTION	Signaling
GOBP_INTERLEUKIN_17_PRODUCTION	Signaling
GOBP_INTERLEUKIN_2_PRODUCTION	Signaling
GOBP_INTERLEUKIN_6_PRODUCTION	Signaling
GOBP_INTERLEUKIN_8_PRODUCTION	Signaling
GOBP_MACROPHAGE_CYTOKINE_PRODUCTION	Signaling
GOBP_NIK_NF_KAPPAB_SIGNALING	Signaling
GOBP_POSITIVE_REGULATION_OF_INTERLEUKIN_10_PRODUCTION	Signaling
GOBP_POSITIVE_REGULATION_OF_INTERLEUKIN_12_PRODUCTION	Signaling
GOBP_POSITIVE_REGULATION_OF_INTERLEUKIN_17_PRODUCTION	Signaling
GOBP_POSITIVE_REGULATION_OF_INTERLEUKIN_2_PRODUCTION	Signaling
GOBP_POSITIVE_REGULATION_OF_INTERLEUKIN_6_PRODUCTION	Signaling
GOBP_POSITIVE_REGULATION_OF_INTERLEUKIN_8_PRODUCTION	Signaling
GOBP_POSITIVE_REGULATION_OF_MACROPHAGE_CYTOKINE_PRODUCTION	Signaling
GOBP_POSITIVE_REGULATION_OF_TYPE_I_INTERFERON_PRODUCTION	Signaling
GOBP_REGULATION_OF_NIK_NF_KAPPAB_SIGNALING	Signaling
GOBP_TOLL_LIKE_RECEPTOR_2_SIGNALING_PATHWAY	Signaling
GOBP_TOLL_LIKE_RECEPTOR_SIGNALING_PATHWAY	Signaling
GOBP_TUMOR_NECROSIS_FACTOR_SUPERFAMILY_CYTOKINE_PRODUCTION	Signaling
GOBP_TYPE_I_INTERFERON_PRODUCTION	Signaling
GOBP_ACTIVATION_OF_GTPASE_ACTIVITY	Signaling
GOBP_ADENYLATE_CYCLASE_INHIBITING_G_PROTEIN_COUPLED_RECEPTOR_SIGNALING_PATHWAY	Signaling
GOBP_ADENYLATE_CYCLASE_MODULATING_G_PROTEIN_COUPLED_RECEPTOR_SIGNALING_PATHWAY	Signaling
GOBP_ARF_PROTEIN_SIGNAL_TRANSDUCTION	Signaling
GOBP_HIPPO_SIGNALING	Signaling
GOBP_INSULIN_RECEPTOR_SIGNALING_PATHWAY	Signaling
GOBP_INTRACELLULAR_RECEPTOR_SIGNALING_PATHWAY	Signaling
GOBP_JNK_CASCADE	Signaling
GOBP_NEGATIVE_REGULATION_OF_CALCIUM_MEDIATED_SIGNALING	Signaling
GOBP_NEGATIVE_REGULATION_OF_EXTRINSIC_APOPTOTIC_SIGNALING_PATHWAY	Signaling
GOBP_NEGATIVE_REGULATION_OF_SIGNAL_TRANSDUCTION_BY_P53_CLASS_MEDIATOR	Signaling
GOBP_NEGATIVE_REGULATION_OF_TOR_SIGNALING	Signaling
GOBP_NUCLEOTIDE_BINDING_DOMAIN_LEUCINE_RICH_REPEAT_CONTAINING_RECEPTOR_SIGNALING_PATHWAY	Signaling
GOBP_PLATELET_DERIVED_GROWTH_FACTOR_RECEPTOR_SIGNALING_PATHWAY	Signaling
GOBP_POSITIVE_REGULATION_OF_GTPASE_ACTIVITY	Signaling
GOBP_POSITIVE_REGULATION_OF_JNK_CASCADE	Signaling
GOBP_POSITIVE_REGULATION_OF_STRESS_ACTIVATED_PROTEIN_KINASE_SIGNALING_CASCADE	Signaling
GOBP_PURINERGIC_NUCLEOTIDE_RECEPTOR_SIGNALING_PATHWAY	Signaling
GOBP_REGULATION_OF_GTPASE_ACTIVITY	Signaling
GOBP_REGULATION_OF_JNK_CASCADE	Signaling
GOBP_REGULATION_OF_SMALL_GTPASE_MEDIATED_SIGNAL_TRANSDUCTION	Signaling
GOBP_REGULATION_OF_STRESS_ACTIVATED_PROTEIN_KINASE_SIGNALING_CASCADE	Signaling
GOBP_REGULATION_OF_TOR_SIGNALING	Signaling
GOBP_SMALL_GTPASE_MEDIATED_SIGNAL_TRANSDUCTION	Signaling
GOBP_STRESS_ACTIVATED_PROTEIN_KINASE_SIGNALING_CASCADE	Signaling
GOBP_TOR_SIGNALING	Signaling
GOBP_TRANSFORMING_GROWTH_FACTOR_BETA_RECEPTOR_SIGNALING_PATHWAY	Signaling
GOBP_POSITIVE_REGULATION_OF_PROTEIN_POLYUBIQUITINATION	Ubiquitination
GOBP_PROTEIN_AUTOUBIQUITINATION	Ubiquitination
GOBP_PROTEIN_K63_LINKED_DEUBIQUITINATION	Ubiquitination

GOBP_PROTEIN_K63_LINKED_UBIQUITINATION	Ubiquitination
GOBP_PROTEIN_POLYUBIQUITINATION	Ubiquitination
GOBP_REGULATION_OF_PROTEIN_K63_LINKED_UBIQUITINATION	Ubiquitination
GOBP_REGULATION_OF_PROTEIN_POLYUBIQUITINATION	Ubiquitination

Table 4: Ligands upregulated in male and female LVChP.
Upregulated ligands in male and female LVChP shown by log2FC (fold change) (Male/ Female) and p-value.

Gene	Log2FC	P-value
Slamf6	-1.951	0.028
A2m	-1.655	0.007
Hgf	-1.517	0.009
Tnfsf13	-1.258	0.004
Angptl4	-1.162	0.039
Lamc2	-0.961	0.005
Fstl1	-0.746	0.001
Ngf	-0.731	0.005
Cspg4	-0.675	0.001
Thbs1	-0.644	0.037
Bgn	-0.600	0.013
Fn1	-0.579	0.032
Fgf2	-0.512	0.005
Gpc6	-0.460	0.001
Bmper	-0.436	0.012
Fbln5	-0.340	0.040
Mmp2	-0.236	0.041
Pdgfa	0.203	0.008
Mfge8	0.204	0.010
Gpc4	0.219	0.031
Matn4	0.287	0.011
Tgfb3	0.331	0.039
Chad	0.412	0.044
Ccl25	0.417	0.019
Kitl	0.421	0.036
Egfl7	0.422	0.031
Artn	0.462	0.022
Lamb2	0.464	0.005
Inha	0.516	0.041
Vegfc	0.536	0.026
Hyal3	0.548	0.001
Thbs3	0.550	0.005
Igfbp2	0.564	0.038
Igfbp3	0.619	0.047
Inhbb	0.622	0.037
Srpx2	1.063	0.040
Lrg1	1.100	0.018
Mmp9	1.146	0.035
Insl5	1.153	0.012
C1ql1	1.191	0.016
Agt	1.366	0.032
Fgf16	1.599	0.002
Cbln1	1.601	0.028
Shh	1.688	0.047
Nodal	1.819	0.019
Gh	2.297	0.015

Table 5: Estrous and diestrous LVChP DEGs.
Table showing DEGs between estrous and diestrous females. Log2FC (fold change) Diestrous (Di)/ Estrous (Est).

Gene	log2FoldChange Di/Est	Adjusted p-value
Inhba	-5.500819	0.030476
Ddn	-4.58703	0.039566
Vip	-4.44159	0.003591
Cdh12	-4.231232	0.029619
Camk2a	-4.209407	0.039334
Slc30a3	-4.081516	0.012616
Bpifb3	-4.047795	0.043202
Npas4	-3.849626	0.039121
Kcnv1	-3.79562	0.004432
Kif5a	-3.703409	0.030028
Lamp5	-3.64706	0.00943
Cck	-3.592931	0.007667
Bdnf	-3.590593	0.005803
Cacng3	-3.537031	0.000729
Epop	-3.506613	0.002294
Kcnmb4	-3.429409	0.022108
Trpc6	-3.39578	0.044351
Gng13	-3.378174	0.002294
Cpne5	-3.369985	0.00576
Omp	-3.367183	0.012385
Slc44a5	-3.361245	0.029619
St6gal2	-3.291532	0.009517
Mpped1	-3.271158	0.000178
Cabp1	-3.257595	0.00595
Cnksr2	-3.249804	0.040604
Slc17a7	-3.229942	0.040002
Ttc9b	-3.226151	0.003591
Bpifb4	-3.223819	0.017696
Pdyn	-3.216096	0.015848
Tmem121b	-3.178019	0.02494
Kcnj9	-3.138812	0.004432
Kcnq5	-3.123343	0.009566
Smim43	-3.105605	0.002032
St8sia5	-3.099857	0.007901
Rph3a	-3.085953	0.035881
Gpr22	-3.085794	0.008563
Stx1a	-3.081362	0.039334
Neurod2	-3.081155	0.003971
Nrgn	-3.043414	4.96E-06
Vxn	-2.992775	6.13E-06
Nptx2	-2.984183	0.008563
Scrg1	-2.967379	0.038473
AI593442	-2.960408	0.000174
Cbln2	-2.934543	0.010724
Nrg3	-2.914832	0.025065
Cdk5r2	-2.901361	0.029619
Npy	-2.898698	0.000178
Dok5	-2.886407	0.007667
Slitrk1	-2.842872	0.022108
Tbr1	-2.841962	0.000173
Neurod6	-2.827095	0.00576
Cnr1	-2.808182	0.003135
Unc5a	-2.802011	0.012385
Ppp1r14c	-2.798757	0.012604
Creg2	-2.796647	0.005977
Rprml	-2.777024	0.023838
Wnt7b	-2.768259	0.03514
Rasal1	-2.750291	0.012604
Rgs14	-2.656293	0.009517

Sst	-2.652983	0.003135
Cnih3	-2.637747	0.042935
Galnt9	-2.633422	0.002398
Dscam	-2.610294	0.034387
B4galnt4	-2.600088	0.021221
Pex5l	-2.595469	0.005871
Gpi-ps	-2.594145	2.02E-40
Tafa1	-2.593305	0.011448
Foxg1	-2.573625	0.016285
Dab1	-2.568731	0.0135
Adgrd1	-2.551103	0.025773
Hipk4	-2.549032	0.015848
Vstm2l	-2.538501	0.035881
Mmp17	-2.52139	0.007411
Adrb3	-2.492872	0.000178
Tmem132d	-2.491042	0.003591
Gabrd	-2.488941	0.017696
Tmem198	-2.46261	0.010724
Caln1	-2.454643	0.01685
NA	-2.423878	0.025773
Golga7b	-2.423837	0.008278
Kcnc4	-2.410856	0.025773
Wscd2	-2.396931	0.023385
Abcc8	-2.390195	0.025773
Serpina3n	-2.389116	0.009517
Cacna1a	-2.38078	0.025422
Syt5	-2.374558	0.02494
Lypd1	-2.371926	0.039334
Cap2	-2.368335	0.00908
Syt4	-2.356487	0.029619
Tafa2	-2.351811	0.04594
Kcng2	-2.341976	0.039334
Prss12	-2.32895	0.007667
Csmd1	-2.320797	0.029178
Hapln4	-2.314118	0.015496
Gpr17	-2.303824	0.025313
Omg	-2.270936	0.029558
Tmem151a	-2.256615	0.00595
Stk32c	-2.248363	0.025773
Itpka	-2.24561	0.003591
Snca	-2.231825	0.012238
Clstn2	-2.224047	0.044038
Pcnx2	-2.199459	0.025867
Kcna1	-2.190602	0.027015
Diras1	-2.179957	0.04742
Rgs20	-2.174241	0.040604
Pantr1	-2.170974	0.031203
Adam11	-2.16139	0.040524
Pou3f3	-2.15794	0.040827
Rtn4r	-2.155912	0.00908
Ntm	-2.141697	0.024514
Opalin	-2.10487	0.022227
Pvalb	-2.072008	0.023336
Ina	-2.039854	0.040002
Timp4	-2.028712	0.01685
Mobp	-2.025613	0.010506
Caly	-2.011524	0.011448
Rgs4	-2.003623	0.002032
Lhx2	-1.98656	0.040827
Zbtb16	-1.954171	0.027015
Extl1	-1.949844	0.035963
Cdk5r1	-1.897334	0.039334
Zfp239	-1.888686	0.029619
Cntnap1	-1.871487	0.040827

Scg3	-1.866483	0.030549
Nell1	-1.829454	0.027015
Chrm1	-1.829252	0.025867
Reps2	-1.827111	0.035645
Scn1b	-1.822262	0.003135
Adap1	-1.819049	0.035936
Basp1	-1.779371	0.04742
S100b	-1.774288	0.012604
Ablim2	-1.765633	0.017696
Cadps2	-1.758435	0.040524
Slc1a1	-1.756505	0.040002
Tnnc1	-1.754014	0.02494
Spon1	-1.724073	0.035963
Grhl1	-1.668264	0.040002
Chga	-1.64813	0.046725
Gm15541	-1.647393	0.025773
Syt13	-1.63979	0.010219
Phf21b	-1.638833	0.00943
Sorl1	-1.635063	0.015496
Hpca	-1.625701	0.025065
Rpl30	-1.62093	0.040827
Scn2b	-1.606001	0.039334
Satb2	-1.574928	0.012604
Gdpd3	-1.563918	1.26E-08
Rgs7bp	-1.552671	0.039334
Cplx2	-1.468907	0.04594
Scn4b	-1.424732	0.029178
Rnd1	-1.396409	0.025773
Ngef	-1.383323	0.004851
Pde8b	-1.362833	0.040002
Atp6v1g2	-1.360371	0.040785
Ppp1r3c	-1.333447	0.040604
Bcas1	-1.291113	0.010552
Serpinb1a	-1.249732	0.04742
Lin7b	-1.197918	0.027964
Chn1	-1.182915	0.029558
Dtx1	-1.105262	0.032844
Gm10699	-1.066598	0.032964
Snhg14	-0.978072	0.018364
Mfsd2a	-0.864736	0.029178
Mir99ahg	-0.846003	0.040785
Dkk3	-0.698316	0.032957
Nudt19	-0.692687	0.008156
Nmnat2	-0.671542	0.045519
Rtn4	-0.530735	0.022442
Rassf3	0.383427	0.038732
Tuba1c	0.472706	0.029178
Fam174b	0.622344	0.025773
Arrdc4	0.629815	0.040002
Ranbp17	0.84515	0.001916
Cflar	0.847269	0.048565
Cyp7b1	0.906503	1.99E-08
Col15a1	1.019067	0.01275
Slc22a19	1.094808	0.046388
Nr1h4	1.243669	0.044038
Ces2e	1.281138	0.025065
Ngfr	1.491187	0.003591
Gabrp	1.672885	0.018364
Col14a1	1.686223	0.003591
Ren1	1.736057	0.040002
Serpina1b	1.794834	0.025065
NA	2.043597	0.009287
Serpina1e	2.266081	0.035645
Serpina1a	2.303038	0.018861

Dcdc2c	2.36383	0.015848
Slc17a8	2.522702	0.023748
Optc	2.733428	0.029558
Gm11224	3.38603	0.00072
Gm20305	6.050781	0.021221

Table 6: Upregulated male and female macrophage-associated genes.
Table showing upregulated male and female LVChP macrophage-associated genes. Abbreviations: Di: Diestrous, Est: Estrous.

Gene	Male1	Male2	Male3	FemEst1	FemEst2	FemEst3	FemDi1	FemDi2	FemDi3
Kdm5d	1553.6	1406.2	1906.3	0.0	0.0	0.0	1.0	0.0	0.0
Uty	999.9	788.4	1114.3	8.3	9.0	20.6	6.9	18.6	11.5
Xist	199.6	10.7	18.5	3044.2	2552.7	2693.1	2014.0	2375.3	2666.1
Afap1	1328.8	1310.8	1423.3	1583.8	1595.2	1650.4	1656.3	1651.9	1658.5
Adgre1	96.3	88.3	111.2	220.5	170.2	190.4	162.6	205.9	207.1
Tmem9	13538.8	13842.5	14411.2	11131.5	12025.8	11871.3	12035.5	12096.9	12453.3
Plagl2	769.0	709.7	754.9	920.0	970.1	992.6	992.2	1104.6	935.7
Gpr84	20.8	15.5	9.7	28.2	36.9	36.5	29.6	37.2	33.6
Pld3	24069.4	28030.9	23466.6	19125.2	19955.1	20284.6	19290.3	19010.8	19255.2
Irf5	101.5	94.2	76.8	155.8	129.7	135.7	131.0	158.7	151.5
Gclc	1478.9	1473.0	1405.6	1597.9	1593.4	1563.2	1543.0	1581.5	1529.1
Pdha1	10361.3	9096.7	10244.7	11217.7	11770.0	11146.1	11896.6	11583.4	11229.1
Kcnk18	11.3	16.7	24.7	5.0	3.6	4.8	6.9	0.0	2.9
Arsk	197.9	214.7	181.0	169.9	122.5	137.3	145.8	152.8	134.2
Uros	497.3	510.5	576.6	666.3	662.9	620.5	626.7	637.7	591.5
Ercc2	787.2	621.4	723.1	951.5	895.3	861.7	839.5	916.0	963.5
Tfe3	1874.7	1833.2	1780.9	1980.8	2112.2	1948.0	2007.1	1999.3	1969.1
Plekho2	1797.5	1555.3	1749.1	2188.8	2247.4	1917.8	1975.5	2178.0	2112.9
Rps18	50.3	69.2	49.4	41.4	26.1	30.2	36.5	25.2	31.6
Ampd3	407.1	446.1	453.8	559.4	554.0	546.7	647.3	502.8	595.3
Rap2c	802.0	656.0	765.5	948.1	901.6	888.7	960.7	873.5	852.3
Tdrd7	4831.8	4260.3	5098.9	5886.9	5720.6	5675.8	6234.0	5981.3	5242.1
Med9	1225.5	1241.6	1290.8	1331.0	1407.9	1348.1	1374.5	1464.0	1358.5
Abhd17c	690.0	795.5	794.6	878.5	899.8	841.9	960.7	939.2	876.2
Camk2d	3170.5	2724.1	3291.6	3645.9	3388.6	3611.9	3576.7	3539.0	3591.2
Lamc2	34.7	41.7	41.5	73.8	73.0	88.9	91.6	83.0	48.9
Actr2	9191.3	6959.4	9613.4	10816.6	10705.4	10881.0	11553.7	10954.4	10430.5
Slc25a16	3322.4	2695.5	3125.6	3417.1	3712.9	3612.7	3746.1	3516.4	3633.4
Stxbp3	4557.5	4786.3	4830.5	4492.1	4534.3	4254.7	4392.5	4312.8	4272.9
Ccr5	224.8	246.9	242.8	376.3	346.8	363.4	272.9	304.9	382.5
Acrbp	32.1	53.7	43.3	32.3	18.0	22.2	19.7	25.2	25.9
Sardh	849.7	675.1	734.6	844.5	889.0	926.0	889.7	952.5	928.0
Nod2	25.2	31.0	17.7	55.5	53.1	30.9	54.2	64.4	48.9
Vav1	35.6	57.2	41.5	74.6	90.1	83.3	79.8	77.7	123.7
Tbc1d13	2792.1	2200.5	2751.2	3081.5	3082.3	2910.5	3201.3	3243.4	3202.0
Pip5k1b	10539.2	10132.0	10835.4	14188.9	16096.3	15225.4	13136.1	14297.4	11543.5
Maml1	795.0	666.7	723.1	822.2	874.6	803.0	864.1	902.7	834.1
Ctsl	44384.1	56798.8	47918.6	33578.5	32900.6	33865.1	41180.9	33918.0	42958.7
Neu1	5717.9	4934.2	5765.6	4081.8	3244.5	4578.4	3866.3	4330.1	4694.7
Gas7	11204.9	8846.3	10909.5	12389.6	11625.9	13374.2	12871.1	12730.5	12243.4
Grsf1	8668.0	8019.7	9215.2	9575.9	10331.5	9344.1	9993.0	9774.1	9590.7
Plekhn1	64.2	102.6	75.9	26.5	36.9	48.4	54.2	55.8	45.1
Tnks1bp1	7591.8	8639.9	8411.7	7034.8	6797.0	6800.2	6554.3	6979.0	7844.0
Tapbp	9859.7	10819.0	8915.0	7064.6	7781.5	7538.1	8132.7	7948.1	9092.2
Scarf1	263.0	261.2	260.5	227.9	230.6	204.7	173.4	227.2	222.4
Bst2	6282.9	11968.8	7011.4	3129.5	3384.1	2827.2	4910.8	3160.4	5189.4
Csf1r	1317.5	1393.1	1063.9	1864.8	1897.0	2237.6	1752.9	1529.0	2372.7
Mtss1	2888.5	2547.6	2845.7	3032.6	3059.8	2946.2	2975.6	3102.6	3084.1

Pi4k2a	5241.4	5156.0	5245.5	5455.1	5588.2	5408.4	5911.8	5572.2	5560.4
Tmem119	357.6	455.6	200.4	489.0	621.5	632.4	536.0	476.2	649.0
Birc3	231.7	161.0	235.7	243.7	271.1	295.2	281.8	274.3	279.0
Npc2	30560.6	35762.0	36191.4	26186.5	27674.5	27276.8	29789.8	27913.4	31798.7
Pygm	5518.3	5676.1	5063.6	7410.2	8468.8	6098.7	6533.6	7247.4	6954.3
Prrg2	1895.6	2222.0	1923.0	1652.6	1885.3	1488.6	1595.2	1667.2	1690.2
Mocos	182.3	192.0	128.0	236.2	271.1	233.3	282.8	249.7	193.7
Lims1	2169.0	1623.3	2369.8	2742.5	2517.6	2539.9	3066.3	2567.2	2739.0
Ngfr	1914.6	1094.9	2165.8	368.8	236.9	411.0	1009.9	630.3	1257.8
Vmp1	5198.9	6106.6	5909.5	4557.5	4416.4	4691.1	5204.4	4685.4	5287.2
Aqp9	6.9	4.8	3.5	0.8	1.8	4.0	2.0	0.7	0.0
Dnajb12	4441.2	5049.9	4397.9	3818.2	3990.3	3691.3	3752.1	3897.7	4425.3
Med22	2253.1	1756.8	2245.3	2425.9	2371.7	2490.0	2804.2	2682.1	2667.1
Ube2g1	1621.3	1374.0	1471.9	1687.4	1788.9	1579.0	1760.7	1745.6	1671.0
Osbpl5	2505.7	2368.7	2063.4	2656.3	2656.3	2551.8	2807.1	2789.7	2549.1
Nkiras2	1091.9	1034.1	953.6	1148.7	1176.4	1124.4	1121.3	1264.0	1137.0
Prr12	3701.7	4048.0	3603.3	2903.3	3209.4	3132.7	3163.8	3450.0	3569.2
Lgmn	28687.6	28579.5	30402.9	24809.1	24150.8	26691.2	27780.7	25987.8	27469.2
Bsg	304832	396374	334451	254182	298998	248842	280663	273546	296084
Pld4	169.2	220.6	149.2	266.0	344.1	299.9	245.3	258.4	397.9
Steap1	9570.6	15010.1	11251.2	8090.7	7843.7	6460.5	8694.4	5520.4	9173.7
Wasf2	3939.5	3398.0	3966.1	4189.5	4525.3	4111.8	5040.8	4665.5	4698.5
Cx3cr1	676.1	721.6	613.6	970.5	1124.1	1318.8	1057.2	842.2	1503.2
Mzt1	1255.0	954.2	1135.5	1425.5	1334.0	1310.0	1472.0	1341.7	1245.3
Pltp	47306.4	58004.7	47529.2	38865.4	42551.2	35253.7	40681.4	41267.0	46220.2
Neu3	173.6	144.3	174.8	214.7	198.2	215.0	240.4	196.6	182.2
Rab35	2740.0	2406.9	2749.5	2781.4	3087.8	2863.7	3172.7	3160.4	3029.4
Orai1	1967.6	2294.8	2224.1	1523.3	1781.7	1424.3	1939.1	1519.1	1935.6
Chtf18	27.8	10.7	44.1	40.6	48.6	48.4	55.2	51.8	55.6
Nucks1	6151.9	4832.8	5744.4	6449.7	6516.9	6345.5	7143.5	6431.7	6412.7
Ngrn	2200.2	2189.8	2379.5	2558.5	2761.7	2401.9	2479.0	2437.0	2521.3
Arf6	3173.1	2702.7	3277.4	3398.0	3826.4	3274.7	3758.9	3687.8	3591.2
Ppp2cb	3013.4	2497.5	3077.9	3224.0	3296.7	3245.3	3452.5	3252.7	3184.8
Mkrn2	831.5	642.9	747.8	859.5	852.1	900.6	880.9	835.6	838.9
Enox2	371.5	323.2	407.9	491.5	451.3	450.7	442.4	488.9	389.2
Pank1	1563.1	987.6	1531.9	1856.5	1552.0	1815.5	2023.8	1926.3	1847.4
Tnfaip3	118.9	75.1	125.4	141.7	131.5	142.0	163.6	168.7	140.9
Ly6a	639.7	1384.7	1052.5	440.1	601.7	427.7	568.5	483.6	734.4
Vwa5a	3189.6	2787.3	3364.9	3693.1	3832.7	3467.5	4188.5	3567.6	3524.1
Atp6v0b	9913.5	13800.7	11033.1	7910.0	9826.2	9050.5	8693.4	8611.0	9570.6
Mapk6	6189.2	4646.8	6773.0	7082.0	6632.2	7757.1	7730.7	7843.8	7287.9
Ccrl2	71.2	89.5	64.5	39.0	47.7	54.0	40.4	57.1	67.1
Pik3cg	43.4	75.1	54.7	103.6	100.9	79.3	72.9	78.4	107.4
Cd47	3279.0	4045.6	3568.8	3061.6	2933.7	3279.5	3040.7	2809.0	3309.4
Cnppd1	3308.5	3449.3	3346.3	3079.8	3180.5	2729.6	2930.3	2975.7	3247.1
Cdk20	670.0	563.0	623.4	703.6	779.1	641.9	791.2	757.9	731.5
Ypel5	4126.1	4067.1	3430.2	3533.1	3356.2	3185.0	3532.3	3331.8	3343.9
F11r	11899.3	15090.1	13354.4	10966.6	12025.8	10214.5	11463.1	11095.9	11961.5
Plek	418.3	356.6	268.4	450.0	435.1	446.7	424.7	416.5	489.9
Wnt3a	0.0	2.4	1.8	0.0	0.0	0.0	0.0	0.0	0.0
Safb2	1608.3	2062.2	1894.8	1521.7	1661.9	1510.0	1371.5	1626.7	1556.9
Sh3bp2	97.2	102.6	90.1	151.7	168.4	171.4	112.3	156.1	110.2

Yipf7	1.7	2.4	0.0	0.0	0.0	0.0	0.0	0.0	0.0
Havcr2	20.0	37.0	22.1	32.3	53.1	63.5	46.3	40.5	57.5
Naglu	6733.4	6353.5	6121.4	5521.4	5536.0	5413.1	5225.1	5999.3	6230.5
Rab10	4231.1	3702.1	4275.2	4549.2	4609.1	4261.8	4862.5	4456.3	4787.7
Ndufs1	9782.4	9892.3	10222.6	10046.6	10431.5	10793.8	10850.2	10706.6	11104.5
Cttn	9463.0	7162.2	9808.5	10054.9	10320.7	10535.9	11488.7	10816.9	10452.6
Notch3	353.2	412.7	381.4	576.0	459.4	396.7	599.1	583.9	604.0
Erp29	4613.9	6276.0	4963.0	4222.7	4338.0	3452.4	4429.0	3748.2	4397.5
Hexa	6716.9	7215.8	7206.5	5841.3	6381.8	6505.8	6727.7	6064.4	6672.5
Apoe	150825	271801	166648	98644	116109	136025	113138	98822	143028
Map3k2	1448.6	788.4	1699.6	1865.6	1639.4	1902.8	2298.7	2001.3	1968.2
Tmem86b	112.0	120.5	129.8	68.8	109.0	61.9	78.8	85.7	108.3
Nphp3	441.8	441.3	504.2	335.7	301.7	422.1	421.7	388.6	334.6
Ccdc134	636.2	710.9	722.2	582.6	584.6	556.2	545.9	617.1	676.8
Nckap1l	171.8	205.1	143.0	250.3	261.2	330.1	330.1	221.2	423.7
Cd53	98.9	100.2	60.9	146.7	119.8	156.3	138.9	99.6	182.2
Ncln	2865.9	3167.8	3113.2	2520.4	2607.7	2401.1	2775.6	2801.7	2934.5
Fbxw2	2736.6	2495.1	2700.9	2886.7	2896.8	2657.4	2935.2	2912.6	2901.0
Triqk	487.8	375.7	499.7	566.1	591.8	539.6	522.2	498.2	554.1
Ovol1	79.0	110.9	81.2	30.7	87.4	59.5	35.5	46.5	49.9
Ifnar2	3751.2	5115.5	4082.7	3359.1	3488.6	3526.2	3372.7	3205.5	3891.3
Ak3	7990.1	8146.2	8355.2	9557.6	10742.3	8843.4	10757.6	9380.8	8713.5
Lrch4	3.5	1.2	1.8	5.0	4.5	3.2	5.9	3.3	3.8
Tsc22d1	22639.0	23297.0	21630.1	24911.8	24920.9	22392.1	25354.9	24883.2	24484.8
Micall2	389.7	399.6	302.8	271.0	334.2	295.2	296.6	256.4	302.9
Fuca2	15220.0	16722.9	17619.8	11736.5	13624.7	13001.2	15515.6	14131.4	15210.5
Pofut2	3986.4	5463.8	4661.9	3634.3	3716.5	3303.3	3833.8	3527.7	4368.7
Dusp18	7473.7	5923.0	7801.6	8195.1	7895.9	7956.3	9541.7	8871.4	8967.6
Guf1	416.6	385.2	438.8	440.1	448.6	442.0	442.4	435.1	455.4
Ctsc	12318.5	9650.1	14531.3	18309.7	13530.1	17463.0	20004.7	18187.8	14389.9
Shisa4	3489.1	4260.3	3088.5	3074.8	3222.9	2951.0	2741.1	2770.5	2725.5
Mypop	315.1	361.4	219.0	236.2	189.2	222.2	173.4	215.2	238.7
Brox	1082.3	972.1	1102.8	1109.8	1181.8	1122.0	1216.9	1115.2	1190.7
Rdh13	1446.8	1264.3	1535.4	1583.8	1748.3	1544.1	2090.8	1914.3	1778.4
Bloc1s6	1726.3	1524.3	1687.3	1759.5	1815.9	1853.6	1999.2	1804.7	1746.7
Tmem216	821.1	861.1	738.1	702.8	761.1	657.0	590.2	745.9	636.6
Snx20	12.2	0.0	7.1	28.2	14.4	17.5	15.8	13.3	30.7
Chp1	6278.6	3234.6	6012.8	6719.0	6504.3	6712.9	8106.1	7787.4	7259.2
Folr2	69.4	103.8	99.8	73.8	82.0	49.2	48.3	55.1	63.3
Pcsk7	897.4	892.1	932.4	796.5	733.2	809.4	772.5	823.6	913.6
Stard13	5887.2	4520.3	6266.2	6379.2	6551.1	6445.5	6333.6	7212.2	7136.5
Wdr18	2163.7	2329.3	2367.1	2092.7	2067.2	2110.7	2050.4	2278.3	2098.6
Lemd2	1876.5	2120.6	1821.5	1492.7	1734.8	1658.4	1481.9	1536.4	1899.2
Mpeg1	475.6	609.5	540.4	923.3	992.6	1041.1	940.0	788.4	1713.2
Itgam	248.2	157.4	123.6	245.3	313.5	476.1	284.8	263.7	404.6
Wdr91	1387.8	957.7	1219.3	1384.1	1423.2	1625.8	1319.3	1624.0	1504.2
Lair1	39.1	69.2	56.5	76.2	121.6	98.4	59.1	93.7	105.5
Tecr	32847.6	48715.9	31073.1	26534.6	29261.6	22208.8	26929.4	26612.8	30405
Nudt4	5424.5	6147.2	5609.3	7071.3	6658.3	6224.1	6580.9	6859.5	5797.2
Mmp9	52.9	37.0	19.4	21.5	9.0	23.0	23.6	13.9	7.7
a0ra	46.0	70.4	57.4	97.0	80.2	103.9	96.6	79.7	153.4
Klf11	190.9	183.7	166.0	338.1	320.7	283.3	211.8	403.2	217.6

Ctsb	85373.7	109410	95840.7	78014.2	85051.9	82441.3	79338.9	83661.1	90471
Gpr183	19.1	20.3	23.0	35.6	45.9	23.8	43.4	38.5	65.2
Cmpk2	780.3	635.7	685.2	592.6	581.9	648.3	624.7	621.7	639.4
Atp5b	97248.6	84678.2	93454.1	96023.1	103611	95278.3	108506	104997	103975
Nav2	3892.7	3084.3	3922.0	3979.0	3973.2	4468.9	4123.5	4454.3	4251.8
Taf15	2650.6	3606.7	2798.0	2431.7	2659.0	2223.3	2576.6	2272.3	2538.6
Tlr1	20.8	15.5	5.3	22.4	31.5	35.7	24.6	17.9	25.9
Ctsz	13870.3	20013.5	14799.7	12361.4	13522.9	12449.0	12737.1	12370.5	13812
Mpzl2	92.0	145.5	138.6	253.6	249.5	134.9	178.3	221.2	176.4
Tmed5	1203.8	1444.4	1312.9	1153.7	1197.1	1185.5	1177.4	1076.7	1254.0
Tlr7	59.9	32.2	28.3	68.0	65.8	59.5	48.3	55.1	71.9
Glmp	14929.2	20722.0	15332.1	13080.8	14844.3	12852.8	13699.7	14090.9	13707
Slc31a2	1507.6	1942.9	1678.5	1441.3	1444.8	1491.7	1543.0	1349.7	1554.0
Mob1b	6337.6	3763.0	6635.2	7256.9	6659.2	7031.1	8074.6	7724.9	6942.8
Jade1	2430.2	1457.5	2360.1	2612.4	2385.2	2713.7	2913.6	2795.7	2591.3
Foxo3	2632.4	1858.2	2692.9	2832.8	2612.2	3087.4	3181.6	2848.9	3192.4
Gna11	4923.8	4458.3	4316.7	4666.9	4900.1	5065.6	4936.4	5107.2	5059.0
Slc22a17	185974.2	228408.3	186183.3	161937.8	182985.4	143853.8	160629	175815	181198
Ncstn	15487.3	12810.8	16140.0	10937.6	9922.6	12381.5	13709.6	11887.6	13483
Spred1	1966.7	1536.2	2225.0	2415.1	2096.0	2436.0	2541.1	2126.2	2402.5
Ptpn23	5451.5	5747.6	5453.0	4725.8	4696.5	4569.7	4525.5	5285.9	5559.4
Chrnb1	547.7	529.6	489.1	426.8	503.5	468.2	489.7	435.1	484.1
Snx18	2146.4	1496.8	2157.9	2319.8	2124.9	2286.0	2605.2	2389.2	2556.8
Slc35e4	1866.9	1709.1	1876.2	1573.9	1741.1	1652.0	1454.3	1754.9	1569.4
Dse	188.3	225.4	274.6	347.3	284.6	253.9	419.7	321.5	429.5
Tbk1	2122.1	2061.0	2231.2	2252.7	2249.2	2236.8	2458.3	2231.8	2390.0
Cipc	4656.4	3343.1	4587.7	4879.9	4947.8	4886.3	5536.4	5065.4	4730.2
Itih5	966.9	1340.6	1462.1	1560.6	3647.1	3945.2	2084.9	4577.2	2400.6
P2ry2	17.4	9.5	12.4	15.7	18.0	34.9	41.4	27.2	35.5
Adam8	26.9	14.3	23.0	5.0	3.6	8.7	8.9	7.3	23.0
Tubgcp4	691.7	477.1	887.3	872.7	765.6	960.9	951.8	947.8	959.6
Nrn1	4113.1	3831.0	4905.6	3364.9	2344.6	3216.8	3812.2	2156.7	3783.0
Relb	382.8	336.3	389.4	440.9	469.3	435.6	363.6	424.4	432.4
Hps4	636.2	561.8	632.2	721.0	742.2	679.2	598.1	722.0	719.0
Mcl1	4955.9	5036.8	5290.5	5376.4	5811.6	5322.7	5746.3	5254.7	5363.9
Cd180	38.2	37.0	13.2	58.8	50.4	55.5	35.5	40.5	69.0
Pik3ap1	37.3	50.1	45.9	72.9	51.3	45.2	69.0	65.8	75.7
Arhgef15	223.9	316.1	369.1	200.6	188.3	230.1	259.1	217.2	250.2
Ptpn12	561.5	453.2	688.7	646.5	633.2	743.5	704.5	706.1	749.7
P2rx5	166.6	156.2	131.6	193.1	172.9	227.7	179.3	188.0	164.9
Golph3	8473.6	8765.2	9336.1	10228.1	10745.9	8702.1	11038.4	9774.1	10216.7
C9orf72	260.4	237.3	226.9	296.7	236.9	289.6	277.9	271.0	281.9
Ublcp1	410.5	385.2	445.0	455.8	468.4	414.2	498.6	463.6	499.5
Fnip1	1665.6	1042.4	1761.5	1868.1	1668.2	2067.0	2213.0	1905.0	1891.5
Gtf2f1	2267.9	3460.0	2350.4	2068.7	2251.0	1776.6	1842.5	2087.7	2160.9
Abcc3	26.0	38.2	40.6	49.7	50.4	77.8	85.7	39.2	76.7
Cdan1	422.7	512.9	504.2	534.6	550.4	502.3	542.9	530.1	525.4
Dclre1c	151.0	132.4	172.2	169.1	188.3	161.9	191.1	213.9	178.3
Znfx1	3748.6	2779.0	4218.7	4075.2	4102.0	4165.8	4556.1	4453.0	4622.8
Slc10a3	760.3	831.3	847.6	653.9	644.0	603.8	643.4	637.0	860.9
Snx12	1574.4	1331.1	1482.4	1569.7	1653.8	1666.3	1993.3	1729.6	1614.4
Mb21d2	388.0	269.6	352.3	485.7	397.2	534.0	430.6	382.6	396.9

Tmem231	3423.1	3512.5	3960.0	3103.0	3500.3	3001.0	3237.7	3270.6	3435.0
Kcnk13	102.4	62.0	65.3	56.4	48.6	69.0	31.5	49.2	43.1
Kcne1	9.5	11.9	7.1	4.1	7.2	8.7	5.9	6.6	3.8
Sgk3	6461.7	5176.3	6944.3	7710.3	7341.1	6575.6	7648.0	6940.5	7109.6
Lhx3	2.6	11.9	5.3	1.7	1.8	1.6	0.0	0.0	4.8
Wdr81	1470.3	1036.5	1441.8	1413.9	1481.7	1622.7	1829.7	1676.5	1721.8
Rbbp7	5768.2	4439.2	5852.1	6172.0	6103.4	5598.8	6690.2	6379.2	6663.8
Bnip3l	4029.8	3542.3	4151.6	4345.4	4510.0	4046.0	4626.0	4127.5	4336.1

Table 7: Upregulated diestrous and estrous LVChP macrophage-associated genes
Table showing upregulated female estrous and diestrous LVChP macrophage-associated genes. Abbreviations: Est: Estrous, Di: Diestrous.

Gene	FemEst1	FemEst2	FemEst3	FemDi1	FemDi2	FemDi3
Il27	1.7	1.8	1.6	0.0	0.0	0.0
Cflar	4543.4	4218.2	5222.7	8838.2	8080.3	8525.6
Sco1	700.3	725.1	710.2	788.2	779.1	788.0
Pccb	7536.2	7367.2	7345.3	8122.9	7974.0	8075.0
Trmt44	231.2	218.9	215.0	334.0	300.9	332.7
Znfx1	4075.2	4102.0	4165.8	4556.1	4453.0	4622.8
Add3	10167.6	10318.9	10379.6	11663.1	11166.9	11442.9
Vps18	2396.0	2332.9	2388.4	2506.6	2516.7	2514.6
Dyrk1a	3592.0	3792.1	3653.2	4281.2	4112.2	4249.9
Ift140	2710.2	2721.2	2870.8	3214.1	3129.2	3288.3
Adamdec1	3.3	3.6	3.2	0.0	1.3	0.0
Dhrs1	4643.7	4769.4	4617.3	5771.9	5339.7	5463.6
Usp8	5500.7	5655.8	5536.9	6098.1	5899.6	6011.9
Iqgap1	16358.7	15884.6	17299.5	19464.7	19257.2	20368.3
Usp4	6472.0	6215.1	6180.4	6789.8	6872.1	6935.1
Rbm10	1168.6	1131.3	1186.3	1342.0	1297.2	1276.0
Arhgef18	9009.8	9479.4	9375.8	10030.4	10101.5	10228.2
Mlkl	20.7	27.0	15.9	56.2	47.2	67.1
Nedd9	3305.2	3077.8	3382.6	3910.7	3778.8	3741.8
Med22	2425.9	2371.7	2490.0	2804.2	2682.1	2667.1
Ubqln1	8336.8	8288.7	8468.8	9723.0	9077.3	9334.7
Fkbp14	1214.2	1175.5	1213.2	1433.6	1321.8	1401.6
Zdhhc3	4226.8	4397.4	4365.7	4831.0	4669.5	4653.5
Tbc1d23	1427.2	1463.7	1475.9	1648.4	1560.3	1600.0
Ogfr	2320.6	2345.5	2271.7	2639.6	2488.9	2646.0
Plod1	3278.7	3040.0	3040.6	3591.4	3715.0	3930.6
Copa	11976.1	10797.2	11759.4	13676.1	13143.0	13603.8
Nol11	1041.8	994.4	1080.7	1186.3	1193.6	1151.4
Dusp18	8195.1	7895.9	7956.3	9541.7	8871.4	8967.6
Tceanc2	817.2	798.1	817.3	893.7	931.2	978.8
Fkbp9	25601.4	26454.0	27135.5	31771.2	29787.2	29587.9
Maf	2681.1	2711.2	2557.4	2972.7	2953.1	3149.3
Cyb5d2	1002.8	1007.9	989.5	1176.5	1103.3	1221.4
Gtf3c5	2052.1	2000.6	1962.3	2155.9	2128.8	2198.3
Glis2	3093.1	2957.1	2959.7	3466.3	3371.6	3252.8
Jdp2	395.3	392.7	382.5	289.7	343.4	310.6
Hbegf	98.6	106.3	127.0	52.2	74.4	53.7
Bach1	508.0	477.4	575.3	660.2	641.6	664.4
Hgsnat	2857.7	2998.6	3083.5	3300.8	3248.1	3312.3
Itpkb	19087.9	17284.4	18619.1	22723.2	20929.1	23296.1
Hdlbp	32538.4	29813.8	34134.9	41256.8	37480.9	40085.6
Fitm2	3539.8	3358.0	3529.4	4003.3	3827.3	4190.4
Tor1aip2	7474.9	7166.3	7538.9	8662.8	8021.8	8353.0
Lman2	14045.5	13302.2	14726.3	17655.7	15914.2	17517.1
Nudt13	460.0	478.3	495.9	425.7	405.2	433.3
Shisa4	3074.8	3222.9	2951.0	2741.1	2770.5	2725.5
Ncln	2520.4	2607.7	2401.1	2775.6	2801.7	2934.5
Xpo6	3294.5	3148.1	3451.7	4099.9	3956.8	3697.7

Ypel3	1626.1	1857.3	1997.2	1215.9	1399.5	1335.5
Cldn12	2056.2	1859.1	1927.4	2579.5	2262.3	2637.3
Chp1	6719.0	6504.3	6712.9	8106.1	7787.4	7259.2
Pgs1	2762.4	2881.5	2981.9	3272.2	3135.8	3160.8
Calcrl	223.8	206.3	173.8	309.4	302.2	392.1
Fmnl3	547.0	497.2	484.8	645.4	650.9	766.9
Tmx1	6235.8	6324.1	6220.9	7582.9	6991.6	8093.2
Itpripl1	5758.5	5927.8	6287.6	7807.6	6965.7	8349.2
Pten	4853.4	4302.0	4997.4	6102.0	5512.4	5754.0
Lag3	95.3	85.6	124.6	49.3	37.9	60.4
Ift74	3847.3	4039.8	3998.4	3719.5	3483.9	3431.1
Foxo1	2613.2	2438.3	2429.6	2922.4	2922.6	2714.0
Ctnnb1	38972.3	39053.6	40057.4	44269.9	42830.5	47429.1
Atp6v0e2	6506.9	5662.1	5627.4	4581.7	4791.7	4889.3
Flnb	5494.1	5272.1	6147.1	6970.1	6857.5	7857.4
Rabgef1	1496.0	1397.1	1340.2	1609.0	1573.5	1668.1
Ccdc9	840.4	893.5	856.2	781.3	783.1	813.0
Slc16a6	7392.8	7637.4	7092.9	9123.0	8336.7	8249.5
Fus	4575.8	4874.8	4134.0	2472.1	3517.7	3293.1
Trem2	153.3	211.7	223.0	98.5	115.6	122.7
Rwdd1	402.8	395.4	380.1	462.1	442.4	421.8
Tmem64	5547.9	5775.6	5439.3	6377.9	6384.5	5943.9
Dusp16	1538.2	1501.5	1571.1	1826.8	1715.7	1657.6
Smo	6675.9	6301.6	7062.8	7551.4	7566.8	7394.3
Timp3	27599.6	24212.0	29105.0	34028.6	31874.8	32333.6
Acer3	957.3	916.1	992.6	1067.1	1026.2	1045.9
Clcn7	3201.6	3333.7	3394.5	3514.6	3792.7	3703.4
Ppp4r1	2099.3	1815.0	2172.6	2634.7	2441.0	2411.1
Acad9	1765.3	1849.2	1867.9	2147.0	1951.5	2081.3
Apobr	23.2	21.6	27.0	37.4	32.5	46.0
Rab3a	3095.5	2781.5	3612.7	2224.8	2301.5	2392.9
Blnk	51.4	80.2	78.6	29.6	39.9	38.3
Ptpn21	1722.2	1561.0	1728.2	1973.6	1972.7	1825.3
Sec31a	10154.4	10237.0	9007.6	11268.0	11184.2	11057.5
Sat1	422.7	436.9	444.4	369.5	348.7	405.5
Pycard	316.6	363.0	315.0	269.0	271.7	219.5
Hey1	347.3	368.4	440.4	293.6	263.0	295.3
Parva	28301.6	29884.9	29075.6	37752.0	33243.1	32842.7
Ppp2r2a	2154.0	2174.4	2052.7	2459.3	2257.7	2489.7
Atxn7l1	693.7	786.4	720.5	600.1	656.3	622.2
Flrt2	9287.4	8110.3	9700.3	11987.2	10373.2	12081.4
Pigo	1565.6	1379.0	1680.6	1826.8	1818.6	1933.7
Pias2	3977.4	4019.1	4049.1	4930.5	4433.7	4403.2
Tlr4	160.0	134.2	135.7	171.4	187.3	170.6
Armcx1	1441.3	1443.9	1362.4	1278.9	1345.1	1275.1
Ngfr	368.8	236.9	411.0	1009.9	630.3	1257.8
Nufip2	2592.5	2691.4	2997.0	3458.4	3167.7	3180.0
Ccny	4395.1	4198.4	4422.1	5037.9	4917.3	4580.6
Itga3	8382.4	7904.9	8768.0	9278.6	9481.8	10339.4
Tbc1d13	3081.5	3082.3	2910.5	3201.3	3243.4	3202.0
Sh3pxd2b	1998.2	1866.3	1966.3	2616.0	2163.4	2368.9
Kif9	4739.9	5211.7	5174.3	4456.5	4637.6	4467.5

Gfm1	2657.9	2645.5	2732.0	2959.9	2917.9	3276.8
Nr2f2	3544.7	3808.3	3494.5	4021.0	3891.7	3935.4
Parp12	1743.0	1872.6	1848.8	2164.7	1952.8	2046.8
Ogdh	50377.3	53195.3	47006.8	56924.2	55208.4	59873.8
Nab1	2819.6	2643.7	2701.0	3158.9	2962.4	2912.5
Megf11	285.9	297.2	392.0	103.5	234.5	81.5
Ube4a	6298.8	5639.6	6474.8	7014.4	6939.2	7627.3
Ric8b	1818.4	1945.6	2038.5	2503.7	2125.5	2387.1
Rab14	7796.5	7887.8	7429.4	8942.6	8380.5	8223.6
Bst1	9.9	4.5	7.1	3.0	1.3	1.9
Fuca2	11736.5	13624.7	13001.2	15515.6	14131.4	15210.5
Slc15a4	1064.2	1144.8	1093.4	1290.8	1167.0	1248.2
Wdr81	1413.9	1481.7	1622.7	1829.7	1676.5	1721.8
Tm9sf4	5296.8	5037.9	5053.7	5633.0	5546.9	6167.2
S1pr2	204.7	235.1	180.9	261.1	247.8	278.0
Snx18	2319.8	2124.9	2286.0	2605.2	2389.2	2556.8
Tnfsf9	150.0	145.9	110.3	75.9	103.0	54.6
Hspg2	12817.3	11355.7	14685.0	15496.9	16037.0	16956.3
Bmpr1a	6104.1	5558.5	6297.9	7708.1	6631.0	7088.5
Wasf2	4189.5	4525.3	4111.8	5040.8	4665.5	4698.5
Arl8a	3715.5	4144.3	3956.3	3488.0	3641.3	3434.0
Rbbp7	6172.0	6103.4	5598.8	6690.2	6379.2	6663.8
Trim26	1955.1	2190.6	1999.6	2319.4	2261.7	2530.0
Lfng	898.4	927.8	892.7	715.3	856.2	773.7
Ap1g2	489.0	489.1	495.9	562.6	508.1	554.1
Angptl2	11149.7	10569.3	11989.5	15374.7	12559.2	16246.9
Vps37c	1768.6	1848.3	1840.1	2377.5	1953.5	2261.5
Grem2	155.8	138.7	154.7	76.9	112.9	124.6
Dnajb14	4086.8	3781.3	4590.3	5280.3	4663.5	5454.0
Myo6	5223.1	4715.4	5510.7	5804.4	5781.4	5923.7
Fam98a	1428.0	1342.1	1272.0	1611.0	1443.4	1588.5
Stag1	1397.3	1299.8	1363.2	1756.8	1508.5	1528.1
Ptgfrn	6179.5	6210.6	6870.0	7860.8	6914.6	7615.8
Adgrg1	1206.7	1317.8	1371.9	584.3	1105.9	840.8
Jmy	2867.6	2546.4	3020.8	3279.1	3137.8	3300.8
Chtf18	40.6	48.6	48.4	55.2	51.8	55.6
Plxdc1	146.7	157.6	119.0	96.6	91.0	117.0
Smarca4	11494.5	11409.7	12036.4	12124.2	12717.2	12327.7
Relt	71.3	49.5	75.4	15.8	37.2	44.1
Fkbp15	4642.9	4977.5	5039.4	5212.3	5241.4	5495.2
Col4a1	2328.9	2252.8	1892.5	2618.0	2811.0	3446.5
Setd5	6109.0	5624.3	6305.0	7259.7	6437.0	7413.5
Zbtb22	1861.5	1964.5	1748.8	1592.3	1668.5	1712.2
Pmepa1	6297.2	6846.6	6484.3	5258.6	6132.1	5717.6
Pdxk	8416.4	7982.4	8820.4	10791.1	9829.9	9128.6
Cacul1	2851.9	2654.5	2777.2	3447.6	3039.5	3038.1
Yap1	11213.6	11710.6	10393.0	14418.0	12081.6	13330.5
Isg15	51.4	54.9	39.7	73.9	59.8	85.3
Lss	2643.0	2217.6	2712.9	2909.6	3036.8	2953.7

10 References

1. Thau, L., V. Reddy, and P. Singh, *Anatomy, Central Nervous System*, in *StatPearls*. 2023: Treasure Island (FL).
2. Dohrmann, G.J., *The choroid plexus: a historical review.* Brain Res, 1970. **18**(2): p. 197-218.
3. Lun, M.P., E.S. Monuki, and M.K. Lehtinen, *Development and functions of the choroid plexus-cerebrospinal fluid system.* Nat Rev Neurosci, 2015. **16**(8): p. 445-57.
4. Liddelow, S.A., *Fluids and barriers of the CNS: a historical viewpoint.* Fluids Barriers CNS, 2011. **8**(1): p. 2.
5. Herbowski, L., *The maze of the cerebrospinal fluid discovery.* Anat Res Int, 2013. **2013**: p. 596027.
6. Redzic, Z.B., et al., *The choroid plexus-cerebrospinal fluid system: from development to aging.* Curr Top Dev Biol, 2005. **71**: p. 1-52.
7. Luders, E., H. Steinmetz, and L. Jancke, *Brain size and grey matter volume in the healthy human brain.* Neuroreport, 2002. **13**(17): p. 2371-4.
8. Sourkes, T.L., *Magendie and the chemists: the earliest chemical analyses of the cerebrospinal fluid.* J Hist Neurosci, 2002. **11**(1): p. 2-10.
9. Cushing, H., *Studies on the Cerebro-Spinal Fluid : I. Introduction.* J Med Res, 1914. **31**(1): p. 1-19.
10. Doyle, N.M., J.F. Doyle, and E.J. Walter, *The life and work of Harvey Cushing 1869-1939: A pioneer of neurosurgery.* J Intensive Care Soc, 2017. **18**(2): p. 157-158.
11. Hajdu, S.I., *A note from history: discovery of the cerebrospinal fluid.* Ann Clin Lab Sci, 2003. **33**(3): p. 334-6.
12. Johanson, C.E., et al., *Multiplicity of cerebrospinal fluid functions: New challenges in health and disease.* Cerebrospinal Fluid Res, 2008. **5**: p. 10.
13. Dani, N., et al., *A cellular and spatial map of the choroid plexus across brain ventricles and ages.* Cell, 2021. **184**(11): p. 3056-3074 e21.
14. Schwarze, E.W., *The origin of (Kolmer's) epiplexus cells. A combined histomorphological and histochemical study.* Histochemistry, 1975. **44**(1): p. 103-4.
15. Silva-Vargas, V., et al., *Age-Dependent Niche Signals from the Choroid Plexus Regulate Adult Neural Stem Cells.* Cell Stem Cell, 2016. **19**(5): p. 643-652.
16. Serot, J.M., et al., *Morphological alterations of the choroid plexus in late-onset Alzheimer's disease.* Acta Neuropathol, 2000. **99**(2): p. 105-8.
17. Zappaterra, M.W. and M.K. Lehtinen, *The cerebrospinal fluid: regulator of neurogenesis, behavior, and beyond.* Cell Mol Life Sci, 2012. **69**(17): p. 2863-78.
18. Sturrock, R.R., *A morphological study of the development of the mouse choroid plexus.* J Anat, 1979. **129**(Pt 4): p. 777-93.

19. Dziegielewska, K.M., et al., *Development of the choroid plexus.* Microsc Res Tech, 2001. **52**(1): p. 5-20.
20. Johansson, P.A., et al., *The blood-CSF barrier explained: when development is not immaturity.* Bioessays, 2008. **30**(3): p. 237-48.
21. Bering, E.A., Jr., *Choroid plexus and arterial pulsation of cerebrospinal fluid; demonstration of the choroid plexuses as a cerebrospinal fluid pump.* AMA Arch Neurol Psychiatry, 1955. **73**(2): p. 165-72.
22. Keep, R.F. and H.C. Jones, *A morphometric study on the development of the lateral ventricle choroid plexus, choroid plexus capillaries and ventricular ependyma in the rat.* Brain Res Dev Brain Res, 1990. **56**(1): p. 47-53.
23. Desmond, M.E. and A.G. Jacobson, *Embryonic brain enlargement requires cerebrospinal fluid pressure.* Dev Biol, 1977. **57**(1): p. 188-98.
24. Kaiser, K., et al., *MEIS-WNT5A axis regulates development of fourth ventricle choroid plexus.* Development, 2021. **148**(10).
25. Kaiser, K., et al., *WNT5A is transported via lipoprotein particles in the cerebrospinal fluid to regulate hindbrain morphogenesis.* Nat Commun, 2019. **10**(1): p. 1498.
26. Narita, K., et al., *Multiple primary cilia modulate the fluid transcytosis in choroid plexus epithelium.* Traffic, 2010. **11**(2): p. 287-301.
27. Lehtinen, M.K. and C.A. Walsh, *Neurogenesis at the brain-cerebrospinal fluid interface.* Annu Rev Cell Dev Biol, 2011. **27**: p. 653-79.
28. Mathew, T.C., *Diversity in the surface morphology of adjacent epithelial cells of the choroid plexus: an ultrastructural analysis.* Mol Cell Biochem, 2007. **301**(1-2): p. 235-9.
29. Strazielle, N. and J.F. Ghersi-Egea, *Choroid plexus in the central nervous system: biology and physiopathology.* J Neuropathol Exp Neurol, 2000. **59**(7): p. 561-74.
30. Keep, R.F., H.C. Jones, and R.D. Cawkwell, *A morphometric analysis of the development of the fourth ventricle choroid plexus in the rat.* Brain Res, 1986. **392**(1-2): p. 77-85.
31. Huh, M.S., M.A. Todd, and D.J. Picketts, *SCO-ping out the mechanisms underlying the etiology of hydrocephalus.* Physiology (Bethesda), 2009. **24**: p. 117-26.
32. Nonami, Y., et al., *Developmental changes in ciliary motility on choroid plexus epithelial cells during the perinatal period.* Cytoskeleton (Hoboken), 2013. **70**(12): p. 797-803.
33. Peters, A. and R.C. Swan, *The choroid plexus of the mature and aging rat: the choroidal epithelium.* Anat Rec, 1979. **194**(3): p. 325-53.
34. Cornford, E.M., et al., *Mitochondrial content of choroid plexus epithelium.* Exp Brain Res, 1997. **116**(3): p. 399-405.

35. Marques, F. and J.C. Sousa, *The choroid plexus is modulated by various peripheral stimuli: implications to diseases of the central nervous system.* Front Cell Neurosci, 2015. **9**: p. 136.
36. Szmydynger-Chodobska, J., A. Chodobski, and C.E. Johanson, *Postnatal developmental changes in blood flow to choroid plexuses and cerebral cortex of the rat.* Am J Physiol, 1994. **266**(5 Pt 2): p. R1488-92.
37. Chodobski, A., et al., *AT1 receptor subtype mediates the inhibitory effect of central angiotensin II on cerebrospinal fluid formation in the rat.* Regul Pept, 1994. **53**(2): p. 123-9.
38. Fenton, R.A., et al., *Renal phenotype of UT-A urea transporter knockout mice.* J Am Soc Nephrol, 2005. **16**(6): p. 1583-92.
39. Vercellino, M., et al., *Involvement of the choroid plexus in multiple sclerosis autoimmune inflammation: a neuropathological study.* J Neuroimmunol, 2008. **199**(1-2): p. 133-41.
40. Pashenkov, M., et al., *Two subsets of dendritic cells are present in human cerebrospinal fluid.* Brain, 2001. **124**(Pt 3): p. 480-92.
41. Hanly, A. and C.K. Petito, *HLA-DR-positive dendritic cells of the normal human choroid plexus: a potential reservoir of HIV in the central nervous system.* Hum Pathol, 1998. **29**(1): p. 88-93.
42. Hatterer, E., et al., *Cerebrospinal fluid dendritic cells infiltrate the brain parenchyma and target the cervical lymph nodes under neuroinflammatory conditions.* PLoS One, 2008. **3**(10): p. e3321.
43. Goldmann, T., et al., *Origin, fate and dynamics of macrophages at central nervous system interfaces.* Nat Immunol, 2016. **17**(7): p. 797-805.
44. Van Hove, H., et al., *A single-cell atlas of mouse brain macrophages reveals unique transcriptional identities shaped by ontogeny and tissue environment.* Nat Neurosci, 2019. **22**(6): p. 1021-1035.
45. Kivisakk, P., et al., *Human cerebrospinal fluid central memory CD4+ T cells: evidence for trafficking through choroid plexus and meninges via P-selectin.* Proc Natl Acad Sci U S A, 2003. **100**(14): p. 8389-94.
46. Lin, C.Q. and M.J. Bissell, *Multi-faceted regulation of cell differentiation by extracellular matrix.* FASEB J, 1993. **7**(9): p. 737-43.
47. Joutel, A., et al., *Perturbations of the cerebrovascular matrisome: A convergent mechanism in small vessel disease of the brain?* J Cereb Blood Flow Metab, 2016. **36**(1): p. 143-57.
48. Khoshnoodi, J., et al., *Molecular recognition in the assembly of collagens: terminal noncollagenous domains are key recognition modules in the formation of triple helical protomers.* J Biol Chem, 2006. **281**(50): p. 38117-21.

49. Sarrazin, S., W.C. Lamanna, and J.D. Esko, *Heparan sulfate proteoglycans.* Cold Spring Harb Perspect Biol, 2011. **3**(7).
50. Taylor, K.R. and R.L. Gallo, *Glycosaminoglycans and their proteoglycans: host-associated molecular patterns for initiation and modulation of inflammation.* FASEB J, 2006. **20**(1): p. 9-22.
51. Sasaki, T., R. Fassler, and E. Hohenester, *Laminin: the crux of basement membrane assembly.* J Cell Biol, 2004. **164**(7): p. 959-63.
52. Saunders, N.R., et al., *The choroid plexus: a missing link in our understanding of brain development and function.* Physiol Rev, 2023. **103**(1): p. 919-956.
53. Sakka, L., G. Coll, and J. Chazal, *Anatomy and physiology of cerebrospinal fluid.* Eur Ann Otorhinolaryngol Head Neck Dis, 2011. **128**(6): p. 309-16.
54. Ghersi-Egea, J.F., et al., *Brain protection at the blood-cerebrospinal fluid interface involves a glutathione-dependent metabolic barrier mechanism.* J Cereb Blood Flow Metab, 2006. **26**(9): p. 1165-75.
55. Strazielle, N. and J.F. Ghersi-Egea, *Physiology of blood-brain interfaces in relation to brain disposition of small compounds and macromolecules.* Mol Pharm, 2013. **10**(5): p. 1473-91.
56. Nathanson, J.A. and L.L. Chun, *Immunological function of the blood-cerebrospinal fluid barrier.* Proc Natl Acad Sci U S A, 1989. **86**(5): p. 1684-8.
57. Reboldi, A., et al., *C-C chemokine receptor 6-regulated entry of TH-17 cells into the CNS through the choroid plexus is required for the initiation of EAE.* Nat Immunol, 2009. **10**(5): p. 514-23.
58. Marques, F., et al., *Transcriptome signature of the adult mouse choroid plexus.* Fluids Barriers CNS, 2011. **8**(1): p. 10.
59. Myung, J., et al., *The choroid plexus is an important circadian clock component.* Nat Commun, 2018. **9**(1): p. 1062.
60. Damkier, H.H., P.D. Brown, and J. Praetorius, *Cerebrospinal fluid secretion by the choroid plexus.* Physiol Rev, 2013. **93**(4): p. 1847-92.
61. Segal, M.B., *Transport of nutrients across the choroid plexus.* Microsc Res Tech, 2001. **52**(1): p. 38-48.
62. Oreskovic, D. and M. Klarica, *A new look at cerebrospinal fluid movement.* Fluids Barriers CNS, 2014. **11**: p. 16.
63. Speake, T., et al., *Mechanisms of CSF secretion by the choroid plexus.* Microsc Res Tech, 2001. **52**(1): p. 49-59.
64. Oernbo, E.K., et al., *Membrane transporters control cerebrospinal fluid formation independently of conventional osmosis to modulate intracranial pressure.* Fluids Barriers CNS, 2022. **19**(1): p. 65.

65. Wright, E.M., *Transport processes in the formation of the cerebrospinal fluid.* Rev Physiol Biochem Pharmacol, 1978. **83**: p. 3-34.
66. Brown, P.D., et al., *Molecular mechanisms of cerebrospinal fluid production.* Neuroscience, 2004. **129**(4): p. 957-70.
67. Benarroch, E.E., *Choroid plexus--CSF system: Recent developments and clinical correlations.* Neurology, 2016. **86**(3): p. 286-96.
68. Garton, M.J., et al., *Age-related changes in cerebrospinal fluid protein concentrations.* J Neurol Sci, 1991. **104**(1): p. 74-80.
69. Silverberg, G.D., et al., *The cerebrospinal fluid production rate is reduced in dementia of the Alzheimer's type.* Neurology, 2001. **57**(10): p. 1763-6.
70. Bothwell, S.W., D. Janigro, and A. Patabendige, *Cerebrospinal fluid dynamics and intracranial pressure elevation in neurological diseases.* Fluids Barriers CNS, 2019. **16**(1): p. 9.
71. Pollay, M., *Overview of the CSF dual outflow system.* Acta Neurochir Suppl, 2012. **113**: p. 47-50.
72. Chen, L., et al., *Pathways of cerebrospinal fluid outflow: a deeper understanding of resorption.* Neuroradiology, 2015. **57**(2): p. 139-47.
73. Ueno, M., et al., *Blood-brain barrier and blood-cerebrospinal fluid barrier in normal and pathological conditions.* Brain Tumor Pathol, 2016. **33**(2): p. 89-96.
74. Fame, R.M. and M.K. Lehtinen, *Emergence and Developmental Roles of the Cerebrospinal Fluid System.* Dev Cell, 2020. **52**(3): p. 261-275.
75. Xiong, G., et al., *Traumatic brain injury-induced ependymal ciliary loss decreases cerebral spinal fluid flow.* J Neurotrauma, 2014. **31**(16): p. 1396-404.
76. Bradbury, M.W. and G.S. Sarna, *Homeostasis of the ionic composition of the cerebrospinal fluid.* Exp Eye Res, 1977. **25 Suppl**: p. 249-57.
77. Grapp, M., et al., *Choroid plexus transcytosis and exosome shuttling deliver folate into brain parenchyma.* Nat Commun, 2013. **4**: p. 2123.
78. Spector, R., et al., *A balanced view of choroid plexus structure and function: Focus on adult humans.* Exp Neurol, 2015. **267**: p. 78-86.
79. Kennedy, A.D., et al., *Elucidation of the complex metabolic profile of cerebrospinal fluid using an untargeted biochemical profiling assay.* Mol Genet Metab, 2017. **121**(2): p. 83-90.
80. Lehtinen, M.K., et al., *The choroid plexus and cerebrospinal fluid: emerging roles in development, disease, and therapy.* J Neurosci, 2013. **33**(45): p. 17553-9.
81. Spector, R., S. Robert Snodgrass, and C.E. Johanson, *A balanced view of the cerebrospinal fluid composition and functions: Focus on adult humans.* Exp Neurol, 2015. **273**: p. 57-68.

82. Costa-Brito, A.R., et al., *The Choroid Plexus Is an Alternative Source of Prolactin to the Rat Brain.* Mol Neurobiol, 2021. **58**(4): p. 1846-1858.
83. Tumani, H., A. Huss, and F. Bachhuber, *The cerebrospinal fluid and barriers - anatomic and physiologic considerations.* Handb Clin Neurol, 2017. **146**: p. 21-32.
84. Derk, J., et al., *Living on the Edge of the CNS: Meninges Cell Diversity in Health and Disease.* Front Cell Neurosci, 2021. **15**: p. 703944.
85. Engelhardt, B., P. Vajkoczy, and R.O. Weller, *The movers and shapers in immune privilege of the CNS.* Nat Immunol, 2017. **18**(2): p. 123-131.
86. Huttunen, K.M., et al., *Pharmacoproteomics of Brain Barrier Transporters and Substrate Design for the Brain Targeted Drug Delivery.* Pharm Res, 2022. **39**(7): p. 1363-1392.
87. Engelhardt, B. and L. Sorokin, *The blood-brain and the blood-cerebrospinal fluid barriers: function and dysfunction.* Semin Immunopathol, 2009. **31**(4): p. 497-511.
88. Redzic, Z.B. and M.B. Segal, *The structure of the choroid plexus and the physiology of the choroid plexus epithelium.* Adv Drug Deliv Rev, 2004. **56**(12): p. 1695-716.
89. Abbott, N.J., *Dynamics of CNS barriers: evolution, differentiation, and modulation.* Cell Mol Neurobiol, 2005. **25**(1): p. 5-23.
90. Abbott, N.J., et al., *Structure and function of the blood-brain barrier.* Neurobiol Dis, 2010. **37**(1): p. 13-25.
91. Lippoldt, A., et al., *Phorbol ester induced changes in tight and adherens junctions in the choroid plexus epithelium and in the ependyma.* Brain Res, 2000. **854**(1-2): p. 197-206.
92. Loscher, W. and H. Potschka, *Role of drug efflux transporters in the brain for drug disposition and treatment of brain diseases.* Prog Neurobiol, 2005. **76**(1): p. 22-76.
93. Engelhardt, B., K. Wolburg-Buchholz, and H. Wolburg, *Involvement of the choroid plexus in central nervous system inflammation.* Microsc Res Tech, 2001. **52**(1): p. 112-29.
94. Bond, A.M., G.L. Ming, and H. Song, *Adult Mammalian Neural Stem Cells and Neurogenesis: Five Decades Later.* Cell Stem Cell, 2015. **17**(4): p. 385-95.
95. Mizrak, D., et al., *Single-Cell Analysis of Regional Differences in Adult V-SVZ Neural Stem Cell Lineages.* Cell Rep, 2019. **26**(2): p. 394-406 e5.
96. Mirzadeh, Z., et al., *Bi- and uniciliated ependymal cells define continuous floor-plate-derived tanycytic territories.* Nat Commun, 2017. **8**: p. 13759.
97. Sawamoto, K., et al., *New neurons follow the flow of cerebrospinal fluid in the adult brain.* Science, 2006. **311**(5761): p. 629-32.
98. Doetsch, F., et al., *Subventricular zone astrocytes are neural stem cells in the adult mammalian brain.* Cell, 1999. **97**(6): p. 703-16.

99. Lim, D.A. and A. Alvarez-Buylla, *The Adult Ventricular-Subventricular Zone (V-SVZ) and Olfactory Bulb (OB) Neurogenesis.* Cold Spring Harb Perspect Biol, 2016. **8**(5).
100. Mirzadeh, Z., et al., *Neural stem cells confer unique pinwheel architecture to the ventricular surface in neurogenic regions of the adult brain.* Cell Stem Cell, 2008. **3**(3): p. 265-78.
101. Khatri, P., et al., *Proliferation and cilia dynamics in neural stem cells prospectively isolated from the SEZ.* Sci Rep, 2014. **4**: p. 3803.
102. Chaker, Z., P. Codega, and F. Doetsch, *A mosaic world: puzzles revealed by adult neural stem cell heterogeneity.* Wiley Interdiscip Rev Dev Biol, 2016. **5**(6): p. 640-658.
103. Tavazoie, M., et al., *A specialized vascular niche for adult neural stem cells.* Cell Stem Cell, 2008. **3**(3): p. 279-88.
104. Delgado, A.C., et al., *Endothelial NT-3 delivered by vasculature and CSF promotes quiescence of subependymal neural stem cells through nitric oxide induction.* Neuron, 2014. **83**(3): p. 572-85.
105. Johanson, C.E., E.G. Stopa, and P.N. McMillan, *The blood-cerebrospinal fluid barrier: structure and functional significance.* Methods Mol Biol, 2011. **686**: p. 101-31.
106. Delgado, A.C., et al., *Release of stem cells from quiescence reveals gliogenic domains in the adult mouse brain.* Science, 2021. **372**(6547): p. 1205-1209.
107. Codega, P., et al., *Prospective identification and purification of quiescent adult neural stem cells from their in vivo niche.* Neuron, 2014. **82**(3): p. 545-59.
108. Janesick, A., S.C. Wu, and B. Blumberg, *Retinoic acid signaling and neuronal differentiation.* Cell Mol Life Sci, 2015. **72**(8): p. 1559-76.
109. Siegenthaler, J.A., et al., *Retinoic acid from the meninges regulates cortical neuron generation.* Cell, 2009. **139**(3): p. 597-609.
110. Lepko, T., et al., *Choroid plexus-derived miR-204 regulates the number of quiescent neural stem cells in the adult brain.* EMBO J, 2019: p. e100481.
111. Planques, A., et al., *OTX2 Signals from the Choroid Plexus to Regulate Adult Neurogenesis.* eNeuro, 2019. **6**(2).
112. Liu, L.L., J. Shannahan, and W. Zheng, *Choroid Plexus Modulates Subventricular Zone Adult Neurogenesis and Olfaction Through Secretion of Small Extracellular Vesicles.* bioRxiv, 2023.
113. Boulton, M., et al., *Contribution of extracranial lymphatics and arachnoid villi to the clearance of a CSF tracer in the rat.* Am J Physiol, 1999. **276**(3): p. R818-23.
114. Cserr, H.F., *Physiology of the choroid plexus.* Physiol Rev, 1971. **51**(2): p. 273-311.
115. de Vos, A.F., et al., *Transfer of central nervous system autoantigens and presentation in secondary lymphoid organs.* J Immunol, 2002. **169**(10): p. 5415-23.

116. Widner, H., G. Moller, and B.B. Johansson, *Immune response in deep cervical lymph nodes and spleen in the mouse after antigen deposition in different intracerebral sites.* Scand J Immunol, 1988. **28**(5): p. 563-71.
117. Svenningsson, A., et al., *Lymphocyte phenotype and subset distribution in normal cerebrospinal fluid.* J Neuroimmunol, 1995. **63**(1): p. 39-46.
118. Carrithers, M.D., et al., *Role of genetic background in P selectin-dependent immune surveillance of the central nervous system.* J Neuroimmunol, 2002. **129**(1-2): p. 51-7.
119. Ransohoff, R.M., P. Kivisakk, and G. Kidd, *Three or more routes for leukocyte migration into the central nervous system.* Nat Rev Immunol, 2003. **3**(7): p. 569-81.
120. Ghersi-Egea, J.F., et al., *Molecular anatomy and functions of the choroidal blood-cerebrospinal fluid barrier in health and disease.* Acta Neuropathol, 2018. **135**(3): p. 337-361.
121. Marques, F., et al., *The choroid plexus response to a repeated peripheral inflammatory stimulus.* BMC Neurosci, 2009. **10**: p. 135.
122. Schwartz, M. and K. Baruch, *The resolution of neuroinflammation in neurodegeneration: leukocyte recruitment via the choroid plexus.* EMBO J, 2014. **33**(1): p. 7-22.
123. Baruch, K., et al., *Aging. Aging-induced type I interferon response at the choroid plexus negatively affects brain function.* Science, 2014. **346**(6205): p. 89-93.
124. Navarrete, C., et al., *Hypoxia mimetic activity of VCE-004.8, a cannabidiol quinone derivative: implications for multiple sclerosis therapy.* J Neuroinflammation, 2018. **15**(1): p. 64.
125. Nishihara, H., et al., *Human CD4(+) T cell subsets differ in their abilities to cross endothelial and epithelial brain barriers in vitro.* Fluids Barriers CNS, 2020. **17**(1): p. 3.
126. Rothhammer, V., et al., *Th17 lymphocytes traffic to the central nervous system independently of alpha4 integrin expression during EAE.* J Exp Med, 2011. **208**(12): p. 2465-76.
127. Strominger, I., et al., *The Choroid Plexus Functions as a Niche for T-Cell Stimulation Within the Central Nervous System.* Front Immunol, 2018. **9**: p. 1066.
128. Gelb, S., et al., *Mechanisms of neuropsychiatric lupus: The relative roles of the blood-cerebrospinal fluid barrier versus blood-brain barrier.* J Autoimmun, 2018. **91**: p. 34-44.
129. Marques, F., et al., *Kinetic profile of the transcriptome changes induced in the choroid plexus by peripheral inflammation.* J Cereb Blood Flow Metab, 2009. **29**(5): p. 921-32.
130. Mesquita, S.D., et al., *The choroid plexus transcriptome reveals changes in type I and II interferon responses in a mouse model of Alzheimer's disease.* Brain Behav Immun, 2015. **49**: p. 280-92.

131. Meeker, R.B., et al., *Cell trafficking through the choroid plexus.* Cell Adh Migr, 2012. **6**(5): p. 390-6.
132. Scheiermann, C., Y. Kunisaki, and P.S. Frenette, *Circadian control of the immune system.* Nat Rev Immunol, 2013. **13**(3): p. 190-8.
133. Berson, D.M., F.A. Dunn, and M. Takao, *Phototransduction by retinal ganglion cells that set the circadian clock.* Science, 2002. **295**(5557): p. 1070-3.
134. Albrecht, U., *Timing to perfection: the biology of central and peripheral circadian clocks.* Neuron, 2012. **74**(2): p. 246-60.
135. Hoyt, K.R. and K. Obrietan, *Circadian clocks, cognition, and Alzheimer's disease: synaptic mechanisms, signaling effectors, and chronotherapeutics.* Mol Neurodegener, 2022. **17**(1): p. 35.
136. Hunt, J., et al., *Sleep and circadian rhythms in Parkinson's disease and preclinical models.* Mol Neurodegener, 2022. **17**(1): p. 2.
137. Reszka, E. and S. Zienolddiny, *Epigenetic Basis of Circadian Rhythm Disruption in Cancer.* Methods Mol Biol, 2018. **1856**: p. 173-201.
138. Walker, W.H., 2nd, et al., *Circadian rhythm disruption and mental health.* Transl Psychiatry, 2020. **10**(1): p. 28.
139. Quintela, T., et al., *Gender associated circadian oscillations of the clock genes in rat choroid plexus.* Brain Struct Funct, 2015. **220**(3): p. 1251-62.
140. Quintela, T., et al., *The role of circadian rhythm in choroid plexus functions.* Prog Neurobiol, 2021. **205**: p. 102129.
141. Yamaguchi, T., et al., *Characterization of the circadian oscillator in the choroid plexus of rats.* Biochem Biophys Res Commun, 2020. **524**(2): p. 497-501.
142. Quintela, T., et al., *The choroid plexus harbors a circadian oscillator modulated by estrogens.* Chronobiol Int, 2018. **35**(2): p. 270-279.
143. Ghersi-Egea, J.F. and N. Strazielle, *Brain drug delivery, drug metabolism, and multidrug resistance at the choroid plexus.* Microsc Res Tech, 2001. **52**(1): p. 83-8.
144. Ghersi-Egea, J.F., et al., *Localization of drug-metabolizing enzyme activities to blood-brain interfaces and circumventricular organs.* J Neurochem, 1994. **62**(3): p. 1089-96.
145. Strazielle, N., S.T. Khuth, and J.F. Ghersi-Egea, *Detoxification systems, passive and specific transport for drugs at the blood-CSF barrier in normal and pathological situations.* Adv Drug Deliv Rev, 2004. **56**(12): p. 1717-40.
146. Liddelow, S.A., et al., *Mechanisms that determine the internal environment of the developing brain: a transcriptomic, functional and ultrastructural approach.* PLoS One, 2013. **8**(7): p. e65629.
147. Quintela, T., et al., *Analysis of the effects of sex hormone background on the rat choroid plexus transcriptome by cDNA microarrays.* PLoS One, 2013. **8**(4): p. e60199.

148. Goncalves, I., et al., *'Smelling' the cerebrospinal fluid: olfactory signaling molecules are expressed in and mediate chemosensory signaling from the choroid plexus.* FEBS J, 2016. **283**(9): p. 1748-66.
149. Tomas, J., et al., *"Tasting" the cerebrospinal fluid: Another function of the choroid plexus?* Neuroscience, 2016. **320**: p. 160-71.
150. Dalesio, N.M., et al., *Olfactory, Taste, and Photo Sensory Receptors in Non-sensory Organs: It Just Makes Sense.* Front Physiol, 2018. **9**: p. 1673.
151. Santos, C.R.A., et al., *The senses of the choroid plexus.* Prog Neurobiol, 2019. **182**: p. 101680.
152. Liu, C.B., et al., *Amyloid-beta transporter expression at the choroid plexus in normal aging: the possibility of reduced resistance to oxidative stress insults.* Sheng Li Xue Bao, 2014. **66**(2): p. 158-68.
153. Duarte, A.C., et al., *Sex Hormone Decline and Amyloid beta Synthesis, Transport and Clearance in the Brain.* J Neuroendocrinol, 2016. **28**(11).
154. Kaur, C., G. Rathnasamy, and E.A. Ling, *The Choroid Plexus in Healthy and Diseased Brain.* J Neuropathol Exp Neurol, 2016. **75**(3): p. 198-213.
155. Becker JB, B.K., Geary N, Hampson E, Herman P, Young EA, *Sex differences in the Brain*. 2008, Oxford: Oxforrd University Press.
156. Ober, C., D.A. Loisel, and Y. Gilad, *Sex-specific genetic architecture of human disease.* Nat Rev Genet, 2008. **9**(12): p. 911-22.
157. Ngun, T.C., et al., *The genetics of sex differences in brain and behavior.* Front Neuroendocrinol, 2011. **32**(2): p. 227-46.
158. Du, L., et al., *Starving neurons show sex difference in autophagy.* J Biol Chem, 2009. **284**(4): p. 2383-96.
159. Mogil, J.S. and M.L. Chanda, *The case for the inclusion of female subjects in basic science studies of pain.* Pain, 2005. **117**(1-2): p. 1-5.
160. Beery, A.K. and I. Zucker, *Sex bias in neuroscience and biomedical research.* Neurosci Biobehav Rev, 2011. **35**(3): p. 565-72.
161. Selmanoff, M.K., B.D. Goldman, and B.E. Ginsburg, *Serum testosterone, agonistic behavior, and dominance in inbred strains of mice.* Horm Behav, 1977. **8**(1): p. 107-19.
162. Zhou, W., et al., *Sex differences influence intestinal epithelial stem cell proliferation independent of obesity.* Physiol Rep, 2018. **6**(13): p. e13746.
163. Machida, T., Y. Yonezawa, and T. Noumura, *Age-associated changes in plasma testosterone levels in male mice and their relation to social dominance or subordinance.* Horm Behav, 1981. **15**(3): p. 238-45.
164. Fairbairn, D., *Sexual Dimorphism.* ELSEVIER, 2016: p. 105-113.

165. Ansar Ahmed, S., W.J. Penhale, and N. Talal, *Sex hormones, immune responses, and autoimmune diseases. Mechanisms of sex hormone action.* Am J Pathol, 1985. **121**(3): p. 531-51.
166. Beeson, P.B., *Age and sex associations of 40 autoimmune diseases.* Am J Med, 1994. **96**(5): p. 457-62.
167. Markle, J.G. and E.N. Fish, *SeXX matters in immunity.* Trends Immunol, 2014. **35**(3): p. 97-104.
168. Ellegren, H. and J. Parsch, *The evolution of sex-biased genes and sex-biased gene expression.* Nat Rev Genet, 2007. **8**(9): p. 689-98.
169. Bachtrog, D., et al., *Sex determination: why so many ways of doing it?* PLoS Biol, 2014. **12**(7): p. e1001899.
170. Amador-Noguez, D., et al., *Gender-specific alterations in gene expression and loss of liver sexual dimorphism in the long-lived Ames dwarf mice.* Biochem Biophys Res Commun, 2005. **332**(4): p. 1086-100.
171. Isensee, J. and P. Ruiz Noppinger, *Sexually dimorphic gene expression in mammalian somatic tissue.* Gend Med, 2007. **4 Suppl B**: p. S75-95.
172. Yang, X., et al., *Tissue-specific expression and regulation of sexually dimorphic genes in mice.* Genome Res, 2006. **16**(8): p. 995-1004.
173. Roy, A.K. and B. Chatterjee, *Sexual dimorphism in the liver.* Annu Rev Physiol, 1983. **45**: p. 37-50.
174. Coffey, C.E., et al., *Sex differences in brain aging: a quantitative magnetic resonance imaging study.* Arch Neurol, 1998. **55**(2): p. 169-79.
175. Goldstein, J.M., et al., *Normal sexual dimorphism of the adult human brain assessed by in vivo magnetic resonance imaging.* Cereb Cortex, 2001. **11**(6): p. 490-7.
176. Sacher, J., et al., *Sexual dimorphism in the human brain: evidence from neuroimaging.* Magn Reson Imaging, 2013. **31**(3): p. 366-75.
177. Sinclair, A.H., et al., *A gene from the human sex-determining region encodes a protein with homology to a conserved DNA-binding motif.* Nature, 1990. **346**(6281): p. 240-4.
178. Ciofi, P., D. Leroy, and G. Tramu, *Sexual dimorphism in the organization of the rat hypothalamic infundibular area.* Neuroscience, 2006. **141**(4): p. 1731-45.
179. McEwen, B.S. and T.A. Milner, *Understanding the broad influence of sex hormones and sex differences in the brain.* J Neurosci Res, 2017. **95**(1-2): p. 24-39.
180. Miller, W.L., *Molecular biology of steroid hormone synthesis.* Endocr Rev, 1988. **9**(3): p. 295-318.
181. Dorrington, J.H. and D.T. Armstrong, *Follicle-stimulating hormone stimulates estradiol-17beta synthesis in cultured Sertoli cells.* Proc Natl Acad Sci U S A, 1975. **72**(7): p. 2677-81.

182. Zirkin, B.R. and V. Papadopoulos, *Leydig cells: formation, function, and regulation.* Biol Reprod, 2018. **99**(1): p. 101-111.
183. Barakat, R., et al., *Extra-gonadal sites of estrogen biosynthesis and function.* BMB Rep, 2016. **49**(9): p. 488-96.
184. Sanderson, J.T., *The steroid hormone biosynthesis pathway as a target for endocrine-disrupting chemicals.* Toxicol Sci, 2006. **94**(1): p. 3-21.
185. Sasano, H., et al., *Aromatase and sex steroid receptors in human vena cava.* Endocr J, 1999. **46**(2): p. 233-42.
186. Allen, E.D., E.A., *An Ovarian Hormone; Preliminary Report on Its Localization, Extraction and Partial Purification, and Action in Test Animals.* Journal of the American Medical Association, 1923(81(10)): p. 819-821.
187. Schulster, M., A.M. Bernie, and R. Ramasamy, *The role of estradiol in male reproductive function.* Asian J Androl, 2016. **18**(3): p. 435-40.
188. Wise, P.M., et al., *Minireview: neuroprotective effects of estrogen-new insights into mechanisms of action.* Endocrinology, 2001. **142**(3): p. 969-73.
189. Fuentes, N. and P. Silveyra, *Estrogen receptor signaling mechanisms.* Adv Protein Chem Struct Biol, 2019. **116**: p. 135-170.
190. Beato, M., *Gene regulation by steroid hormones.* Cell, 1989. **56**(3): p. 335-44.
191. Davey, R.A. and M. Grossmann, *Androgen Receptor Structure, Function and Biology: From Bench to Bedside.* Clin Biochem Rev, 2016. **37**(1): p. 3-15.
192. Brinkmann, A.O., *Molecular mechanisms of androgen action--a historical perspective.* Methods Mol Biol, 2011. **776**: p. 3-24.
193. Tennent, B.J., E.R. Smith, and J.M. Davidson, *The effects of estrogen and progesterone on female rat proceptive behavior.* Horm Behav, 1980. **14**(1): p. 65-75.
194. Fadem, B.H., R.J. Barfield, and R.E. Whalen, *Dose-response and time-response relationships between progesterone and the display of patterns of receptive and proceptive behavior in the female rat.* Horm Behav, 1979. **13**(1): p. 40-8.
195. Evans, R.M., *The steroid and thyroid hormone receptor superfamily.* Science, 1988. **240**(4854): p. 889-95.
196. Allen, E., *The oestrous cycle in the mouse.* American Journal of Anatomy, 1922. **30**(3): p. 297-371.
197. Byers, S.L., et al., *Mouse estrous cycle identification tool and images.* PLoS One, 2012. **7**(4): p. e35538.
198. Stramek, A.K., M.L. Johnson, and V.J. Taylor, *Improved timed-mating, non-invasive method using fewer unproven female rats with pregnancy validation via early body mass increases.* Lab Anim, 2019. **53**(2): p. 148-159.
199. Ajayi, A.F. and R.E. Akhigbe, *Staging of the estrous cycle and induction of estrus in experimental rodents: an update.* Fertil Res Pract, 2020. **6**: p. 5.

200. Westwood, F.R., *The female rat reproductive cycle: a practical histological guide to staging.* Toxicol Pathol, 2008. **36**(3): p. 375-84.
201. Miller, B.H. and J.S. Takahashi, *Central circadian control of female reproductive function.* Front Endocrinol (Lausanne), 2013. **4**: p. 195.
202. Clemens, A.M., et al., *Estrus-Cycle Regulation of Cortical Inhibition.* Curr Biol, 2019. **29**(4): p. 605-615 e6.
203. Inoue, S., *Neural basis for estrous cycle-dependent control of female behaviors.* Neurosci Res, 2022. **176**: p. 1-8.
204. Rocks, D., H. Cham, and M. Kundakovic, *Why the estrous cycle matters for neuroscience.* Biol Sex Differ, 2022. **13**(1): p. 62.
205. Weiss, M.L., et al., *The estrous cycle affects pseudorabies virus (PRV) infection of the CNS.* Brain Res, 2001. **893**(1-2): p. 215-26.
206. Peng, K., et al., *Impact of sex differences on thrombin-induced hydrocephalus and white matter injury: the role of neutrophils.* Fluids Barriers CNS, 2021. **18**(1): p. 38.
207. Andreassen, S.N., et al., *Transcriptional profiling of transport mechanisms and regulatory pathways in rat choroid plexus.* Fluids Barriers CNS, 2022. **19**(1): p. 44.
208. Sözen, B., Aytaç, G. , Demir, N. , Süzen, B. & Tanrıöver, G., *Are There Any Sex-Depended Differences in Water Transporting Proteins of Choroid Plexus in Mice?* Journal of Basic and Clinical Health Sciences, 2020. **4**: p. 123-127.
209. Liu, G., et al., *Direct Measurement of Cerebrospinal Fluid Production in Mice.* Cell Rep, 2020. **33**(12): p. 108524.
210. Vancamp, P., et al., *Gender-specific effects of transthyretin on neural stem cell fate in the subventricular zone of the adult mouse.* Sci Rep, 2019. **9**(1): p. 19689.
211. Quintela, T., et al., *Sex-Related Differences in Rat Choroid Plexus and Cerebrospinal Fluid: A cDNA Microarray and Proteomic Analysis.* J Neuroendocrinol, 2016. **28**(1).
212. Santos, C.R., et al., *The choroid plexus as a sex hormone target: Functional implications.* Front Neuroendocrinol, 2017. **44**: p. 103-121.
213. Quadros, P.S., J.L. Pfau, and C.K. Wagner, *Distribution of progesterone receptor immunoreactivity in the fetal and neonatal rat forebrain.* J Comp Neurol, 2007. **504**(1): p. 42-56.
214. Hong-Goka, B.C. and F.L. Chang, *Estrogen receptors alpha and beta in choroid plexus epithelial cells in Alzheimer's disease.* Neurosci Lett, 2004. **360**(3): p. 113-6.
215. Alves, C.H., et al., *Androgen receptor is expressed in murine choroid plexus and downregulated by 5alpha-dihydrotestosterone in male and female mice.* J Mol Neurosci, 2009. **38**(1): p. 41-9.
216. Quintela, T., et al., *Progesterone enhances transthyretin expression in the rat choroid plexus in vitro and in vivo via progesterone receptor.* J Mol Neurosci, 2011. **44**(3): p. 152-8.

217. Palha, J.A., *Transthyretin as a thyroid hormone carrier: function revisited.* Clin Chem Lab Med, 2002. **40**(12): p. 1292-300.
218. Meffre, D., et al., *The membrane-associated progesterone-binding protein 25-Dx is expressed in brain regions involved in water homeostasis and is up-regulated after traumatic brain injury.* J Neurochem, 2005. **93**(5): p. 1314-26.
219. Meffre, D., et al., *Distribution of membrane progesterone receptor alpha in the male mouse and rat brain and its regulation after traumatic brain injury.* Neuroscience, 2013. **231**: p. 111-24.
220. Quintela, T., et al., *17beta-estradiol induces transthyretin expression in murine choroid plexus via an oestrogen receptor dependent pathway.* Cell Mol Neurobiol, 2009. **29**(4): p. 475-83.
221. Buskiewicz, I.A., Huber, S. A., & Fairweather, D. L., *Sex Hormone Receptor Expression in the Immune System.* Sex Differences In Physiology, 2016: p. 45-60.
222. Newton, K. and V.M. Dixit, *Signaling in innate immunity and inflammation.* Cold Spring Harb Perspect Biol, 2012. **4**(3).
223. Marshall, J.S., et al., *An introduction to immunology and immunopathology.* Allergy Asthma Clin Immunol, 2018. **14**(Suppl 2): p. 49.
224. Akashi, K., et al., *A clonogenic common myeloid progenitor that gives rise to all myeloid lineages.* Nature, 2000. **404**(6774): p. 193-7.
225. Jung, S., *Macrophages and monocytes in 2017: Macrophages and monocytes: of tortoises and hares.* Nat Rev Immunol, 2018. **18**(2): p. 85-86.
226. Hofer, U., *The macrophage patrol.* Nat Rev Microbiol, 2020. **18**(11): p. 604.
227. Roberts, A.W., et al., *Tissue-Resident Macrophages Are Locally Programmed for Silent Clearance of Apoptotic Cells.* Immunity, 2017. **47**(5): p. 913-927 e6.
228. Lim, J.J., S. Grinstein, and Z. Roth, *Diversity and Versatility of Phagocytosis: Roles in Innate Immunity, Tissue Remodeling, and Homeostasis.* Front Cell Infect Microbiol, 2017. **7**: p. 191.
229. Theurl, I., et al., *On-demand erythrocyte disposal and iron recycling requires transient macrophages in the liver.* Nat Med, 2016. **22**(8): p. 945-51.
230. Fukata, M. and M. Arditi, *The role of pattern recognition receptors in intestinal inflammation.* Mucosal Immunol, 2013. **6**(3): p. 451-63.
231. Lichtnekert, J., et al., *Changes in macrophage phenotype as the immune response evolves.* Curr Opin Pharmacol, 2013. **13**(4): p. 555-64.
232. Chan, M.W.Y. and S. Viswanathan, *Recent progress on developing exogenous monocyte/macrophage-based therapies for inflammatory and degenerative diseases.* Cytotherapy, 2019. **21**(4): p. 393-415.

233. Cox, G., J. Crossley, and Z. Xing, *Macrophage engulfment of apoptotic neutrophils contributes to the resolution of acute pulmonary inflammation in vivo.* Am J Respir Cell Mol Biol, 1995. **12**(2): p. 232-7.
234. Savill, J.S., et al., *Macrophage phagocytosis of aging neutrophils in inflammation. Programmed cell death in the neutrophil leads to its recognition by macrophages.* J Clin Invest, 1989. **83**(3): p. 865-75.
235. Wynn, T.A. and K.M. Vannella, *Macrophages in Tissue Repair, Regeneration, and Fibrosis.* Immunity, 2016. **44**(3): p. 450-462.
236. Kanneganti, T.D., M. Lamkanfi, and G. Nunez, *Intracellular NOD-like receptors in host defense and disease.* Immunity, 2007. **27**(4): p. 549-59.
237. Akira, S. and K. Takeda, *Toll-like receptor signalling.* Nat Rev Immunol, 2004. **4**(7): p. 499-511.
238. Pena, O.M., et al., *Endotoxin tolerance represents a distinctive state of alternative polarization (M2) in human mononuclear cells.* J Immunol, 2011. **186**(12): p. 7243-54.
239. Mantovani, A., et al., *The chemokine system in diverse forms of macrophage activation and polarization.* Trends Immunol, 2004. **25**(12): p. 677-86.
240. Mookherjee, N., et al., *Intracellular receptor for human host defense peptide LL-37 in monocytes.* J Immunol, 2009. **183**(4): p. 2688-96.
241. Ginhoux, F., et al., *New insights into the multidimensional concept of macrophage ontogeny, activation and function.* Nat Immunol, 2016. **17**(1): p. 34-40.
242. Murray, P.J., *Macrophage Polarization.* Annu Rev Physiol, 2017. **79**: p. 541-566.
243. Brown, K.L., et al., *Host defense peptide LL-37 selectively reduces proinflammatory macrophage responses.* J Immunol, 2011. **186**(9): p. 5497-505.
244. Martinez, F.O., et al., *Transcriptional profiling of the human monocyte-to-macrophage differentiation and polarization: new molecules and patterns of gene expression.* J Immunol, 2006. **177**(10): p. 7303-11.
245. Odegaard, J.I. and A. Chawla, *Alternative macrophage activation and metabolism.* Annu Rev Pathol, 2011. **6**: p. 275-97.
246. O'Neill, L.A., R.J. Kishton, and J. Rathmell, *A guide to immunometabolism for immunologists.* Nat Rev Immunol, 2016. **16**(9): p. 553-65.
247. Yao, Y., X.H. Xu, and L. Jin, *Macrophage Polarization in Physiological and Pathological Pregnancy.* Front Immunol, 2019. **10**: p. 792.
248. Fujiwara, N. and K. Kobayashi, *Macrophages in inflammation.* Curr Drug Targets Inflamm Allergy, 2005. **4**(3): p. 281-6.
249. Viola, A., et al., *The Metabolic Signature of Macrophage Responses.* Front Immunol, 2019. **10**: p. 1462.
250. Sica, A. and A. Mantovani, *Macrophage plasticity and polarization: in vivo veritas.* J Clin Invest, 2012. **122**(3): p. 787-95.

251. Arora, S., et al., *Effect of cytokine interplay on macrophage polarization during chronic pulmonary infection with Cryptococcus neoformans.* Infect Immun, 2011. **79**(5): p. 1915-26.
252. Xue, J., et al., *Transcriptome-based network analysis reveals a spectrum model of human macrophage activation.* Immunity, 2014. **40**(2): p. 274-88.
253. Murray, P.J., et al., *Macrophage activation and polarization: nomenclature and experimental guidelines.* Immunity, 2014. **41**(1): p. 14-20.
254. Okabe, Y. and R. Medzhitov, *Tissue-specific signals control reversible program of localization and functional polarization of macrophages.* Cell, 2014. **157**(4): p. 832-44.
255. Davies, L.C., et al., *Tissue-resident macrophages.* Nat Immunol, 2013. **14**(10): p. 986-95.
256. Herz, J., et al., *Myeloid Cells in the Central Nervous System.* Immunity, 2017. **46**(6): p. 943-956.
257. Bechmann, I., et al., *Immune surveillance of mouse brain perivascular spaces by blood-borne macrophages.* Eur J Neurosci, 2001. **14**(10): p. 1651-8.
258. Utz, S.G., et al., *Early Fate Defines Microglia and Non-parenchymal Brain Macrophage Development.* Cell, 2020. **181**(3): p. 557-573 e18.
259. Tambuyzer, B.R., P. Ponsaerts, and E.J. Nouwen, *Microglia: gatekeepers of central nervous system immunology.* J Leukoc Biol, 2009. **85**(3): p. 352-70.
260. Kettenmann, H., et al., *Physiology of microglia.* Physiol Rev, 2011. **91**(2): p. 461-553.
261. Orr, A.G., et al., *Adenosine A(2A) receptor mediates microglial process retraction.* Nat Neurosci, 2009. **12**(7): p. 872-8.
262. Marin-Teva, J.L., et al., *Microglia promote the death of developing Purkinje cells.* Neuron, 2004. **41**(4): p. 535-47.
263. Schafer, D.P., et al., *Microglia sculpt postnatal neural circuits in an activity and complement-dependent manner.* Neuron, 2012. **74**(4): p. 691-705.
264. Tremblay, M.E., R.L. Lowery, and A.K. Majewska, *Microglial interactions with synapses are modulated by visual experience.* PLoS Biol, 2010. **8**(11): p. e1000527.
265. Prinz, M. and A. Mildner, *Microglia in the CNS: immigrants from another world.* Glia, 2011. **59**(2): p. 177-87.
266. Bennett, M.L., et al., *New tools for studying microglia in the mouse and human CNS.* Proc Natl Acad Sci U S A, 2016. **113**(12): p. E1738-46.
267. Sasaki, Y., et al., *Selective expression of Gi/o-coupled ATP receptor P2Y12 in microglia in rat brain.* Glia, 2003. **44**(3): p. 242-50.
268. Faraco, G., et al., *Brain perivascular macrophages: characterization and functional roles in health and disease.* J Mol Med (Berl), 2017. **95**(11): p. 1143-1152.
269. Jordao, M.J.C., et al., *Single-cell profiling identifies myeloid cell subsets with distinct fates during neuroinflammation.* Science, 2019. **363**(6425).

270. Mrdjen, D., et al., *High-Dimensional Single-Cell Mapping of Central Nervous System Immune Cells Reveals Distinct Myeloid Subsets in Health, Aging, and Disease.* Immunity, 2018. **48**(3): p. 599.
271. Geissmann, F., et al., *Development of monocytes, macrophages, and dendritic cells.* Science, 2010. **327**(5966): p. 656-61.
272. He, H., et al., *Perivascular Macrophages Limit Permeability.* Arterioscler Thromb Vasc Biol, 2016. **36**(11): p. 2203-2212.
273. Kigerl, K.A., et al., *Identification of two distinct macrophage subsets with divergent effects causing either neurotoxicity or regeneration in the injured mouse spinal cord.* J Neurosci, 2009. **29**(43): p. 13435-44.
274. Matyszak, M.K., et al., *Stromal macrophages of the choroid plexus situated at an interface between the brain and peripheral immune system constitutively express major histocompatibility class II antigens.* J Neuroimmunol, 1992. **40**(2-3): p. 173-81.
275. Cui, J., H. Xu, and M.K. Lehtinen, *Macrophages on the margin: choroid plexus immune responses.* Trends Neurosci, 2021. **44**(11): p. 864-875.
276. Rayasam, A., et al., *Neonatal Stroke and TLR1/2 Ligand Recruit Myeloid Cells through the Choroid Plexus in a CX3CR1-CCR2- and Context-Specific Manner.* J Neurosci, 2020. **40**(19): p. 3849-3861.
277. Shipley, F.B., et al., *Tracking Calcium Dynamics and Immune Surveillance at the Choroid Plexus Blood-Cerebrospinal Fluid Interface.* Neuron, 2020. **108**(4): p. 623-639 e10.
278. Shechter, R., et al., *Recruitment of beneficial M2 macrophages to injured spinal cord is orchestrated by remote brain choroid plexus.* Immunity, 2013. **38**(3): p. 555-69.
279. Szmydynger-Chodobska, J., et al., *Posttraumatic invasion of monocytes across the blood-cerebrospinal fluid barrier.* J Cereb Blood Flow Metab, 2012. **32**(1): p. 93-104.
280. Keren-Shaul, H., et al., *A Unique Microglia Type Associated with Restricting Development of Alzheimer's Disease.* Cell, 2017. **169**(7): p. 1276-1290 e17.
281. Munro, D.A.D., K. Movahedi, and J. Priller, *Macrophage compartmentalization in the brain and cerebrospinal fluid system.* Sci Immunol, 2022. **7**(69): p. eabk0391.
282. Ling, E.A., C. Kaur, and J. Lu, *Origin, nature, and some functional considerations of intraventricular macrophages, with special reference to the epiplexus cells.* Microsc Res Tech, 1998. **41**(1): p. 43-56.
283. Li, Q., et al., *Developmental Heterogeneity of Microglia and Brain Myeloid Cells Revealed by Deep Single-Cell RNA Sequencing.* Neuron, 2019. **101**(2): p. 207-223 e10.
284. Colton, C.A., *Heterogeneity of microglial activation in the innate immune response in the brain.* J Neuroimmune Pharmacol, 2009. **4**(4): p. 399-418.

285. Garcia-Ovejero, D., et al., *Glial expression of estrogen and androgen receptors after rat brain injury.* J Comp Neurol, 2002. **450**(3): p. 256-71.
286. Sierra, A., et al., *Steroid hormone receptor expression and function in microglia.* Glia, 2008. **56**(6): p. 659-74.
287. Vegeto, E., et al., *Estrogen prevents the lipopolysaccharide-induced inflammatory response in microglia.* J Neurosci, 2001. **21**(6): p. 1809-18.
288. Giannakopoulos, P., et al., *Tangle and neuron numbers, but not amyloid load, predict cognitive status in Alzheimer's disease.* Neurology, 2003. **60**(9): p. 1495-500.
289. Yoshiyama, Y., et al., *Synapse loss and microglial activation precede tangles in a P301S tauopathy mouse model.* Neuron, 2007. **53**(3): p. 337-51.
290. Villa, A., et al., *Sex-Specific Features of Microglia from Adult Mice.* Cell Rep, 2018. **23**(12): p. 3501-3511.
291. Pinheiro, I., L. Dejager, and C. Libert, *X-chromosome-located microRNAs in immunity: might they explain male/female differences? The X chromosome-genomic context may affect X-located miRNAs and downstream signaling, thereby contributing to the enhanced immune response of females.* Bioessays, 2011. **33**(11): p. 791-802.
292. Klein, S.L. and K.L. Flanagan, *Sex differences in immune responses.* Nat Rev Immunol, 2016. **16**(10): p. 626-38.
293. Lai, Z., et al., *Characterization of prolactin receptors in human choroid plexus.* Neuroendocrinology, 1992. **56**(2): p. 225-33.
294. Lai, Z.N., et al., *Characterization of putative growth hormone receptors in human choroid plexus.* Brain Res, 1991. **546**(2): p. 222-6.
295. Stridh, L., et al., *Regulation of Toll-like receptors in the choroid plexus in the immature brain after systemic inflammatory stimuli.* Transl Stroke Res, 2013. **4**(2): p. 220-7.
296. Marques, F., et al., *The choroid plexus in health and in disease: dialogues into and out of the brain.* Neurobiol Dis, 2017. **107**: p. 32-40.
297. Stringer, C., et al., *Cellpose: a generalist algorithm for cellular segmentation.* Nat Methods, 2021. **18**(1): p. 100-106.
298. Cerri, S., L. Mus, and F. Blandini, *Parkinson's Disease in Women and Men: What's the Difference?* J Parkinsons Dis, 2019. **9**(3): p. 501-515.
299. Podcasy, J.L. and C.N. Epperson, *Considering sex and gender in Alzheimer disease and other dementias.* Dialogues Clin Neurosci, 2016. **18**(4): p. 437-446.
300. Vandooren, J. and Y. Itoh, *Alpha-2-Macroglobulin in Inflammation, Immunity and Infections.* Front Immunol, 2021. **12**: p. 803244.
301. Varma, V.R., et al., *Alpha-2 macroglobulin in Alzheimer's disease: a marker of neuronal injury through the RCAN1 pathway.* Mol Psychiatry, 2017. **22**(1): p. 13-23.
302. Yu, J., et al., *Update on glycerol-3-phosphate acyltransferases: the roles in the development of insulin resistance.* Nutr Diabetes, 2018. **8**(1): p. 34.

303. Alliance of Genome Resources, C., *Alliance of Genome Resources Portal: unified model organism research platform.* Nucleic Acids Res, 2020. **48**(D1): p. D650-D658.
304. Veeck, J., et al., *The extracellular matrix protein ITIH5 is a novel prognostic marker in invasive node-negative breast cancer and its aberrant expression is caused by promoter hypermethylation.* Oncogene, 2008. **27**(6): p. 865-76.
305. Van Damme, N., et al., *The interferon-induced protein BST-2 restricts HIV-1 release and is downregulated from the cell surface by the viral Vpu protein.* Cell Host Microbe, 2008. **3**(4): p. 245-52.
306. Gu, G., et al., *BST-2 binding with cellular MT1-MMP blocks cell growth and migration via decreasing MMP2 activity.* J Cell Biochem, 2012. **113**(3): p. 1013-21.
307. Rollason, R., et al., *A CD317/tetherin-RICH2 complex plays a critical role in the organization of the subapical actin cytoskeleton in polarized epithelial cells.* J Cell Biol, 2009. **184**(5): p. 721-36.
308. Sherman, L.S., et al., *Hyaluronate-based extracellular matrix: keeping glia in their place.* Glia, 2002. **38**(2): p. 93-102.
309. Smith, C.E.L., A.V.R. Lake, and C.A. Johnson, *Primary Cilia, Ciliogenesis and the Actin Cytoskeleton: A Little Less Resorption, A Little More Actin Please.* Front Cell Dev Biol, 2020. **8**: p. 622822.
310. Salo, V.T., et al., *Seipin regulates ER-lipid droplet contacts and cargo delivery.* EMBO J, 2016. **35**(24): p. 2699-2716.
311. Lee, S.J., et al., *Mannose receptor-mediated regulation of serum glycoprotein homeostasis.* Science, 2002. **295**(5561): p. 1898-901.
312. Gomez Morillas, A., V.C. Besson, and D. Lerouet, *Microglia and Neuroinflammation: What Place for P2RY12?* Int J Mol Sci, 2021. **22**(4).
313. Ruan, C. and W. Elyaman, *A New Understanding of TMEM119 as a Marker of Microglia.* Front Cell Neurosci, 2022. **16**: p. 902372.
314. Rouillard, A.D., et al., *The harmonizome: a collection of processed datasets gathered to serve and mine knowledge about genes and proteins.* Database (Oxford), 2016. **2016**.
315. Shao, X., et al., *CellTalkDB: a manually curated database of ligand-receptor interactions in humans and mice.* Brief Bioinform, 2021. **22**(4).
316. Kovats, S., *Estrogen receptors regulate innate immune cells and signaling pathways.* Cell Immunol, 2015. **294**(2): p. 63-9.
317. Baruch, K., et al., *CNS-specific immunity at the choroid plexus shifts toward destructive Th2 inflammation in brain aging.* Proc Natl Acad Sci U S A, 2013. **110**(6): p. 2264-9.
318. Yang, A.C., et al., *Dysregulation of brain and choroid plexus cell types in severe COVID-19.* Nature, 2021. **595**(7868): p. 565-571.

319. Libert, C., L. Dejager, and I. Pinheiro, *The X chromosome in immune functions: when a chromosome makes the difference.* Nat Rev Immunol, 2010. **10**(8): p. 594-604.
320. Gantier, M.P., et al., *TLR7 is involved in sequence-specific sensing of single-stranded RNAs in human macrophages.* J Immunol, 2008. **180**(4): p. 2117-24.
321. Puck, J.M., et al., *Mutation analysis of IL2RG in human X-linked severe combined immunodeficiency.* Blood, 1997. **89**(6): p. 1968-77.
322. Cacciari, E., et al., *Serum immunoglobulins and lymphocyte subpopulations derangement in Turner's syndrome.* J Immunogenet, 1981. **8**(5): p. 337-44.
323. Jacobsen, H. and S.L. Klein, *Sex Differences in Immunity to Viral Infections.* Front Immunol, 2021. **12**: p. 720952.
324. Vitek, M.P., C.M. Brown, and C.A. Colton, *APOE genotype-specific differences in the innate immune response.* Neurobiol Aging, 2009. **30**(9): p. 1350-60.
325. Bazan, J.F., et al., *A new class of membrane-bound chemokine with a CX3C motif.* Nature, 1997. **385**(6617): p. 640-4.
326. Stanley, E.R. and V. Chitu, *CSF-1 receptor signaling in myeloid cells.* Cold Spring Harb Perspect Biol, 2014. **6**(6).
327. Carpenter, S.J., L.E. McCarthy, and H.L. Borison, *Electron microscopic study of the epiplexus (Kolmer) cells of the cat choroid plexus.* Z Zellforsch Mikrosk Anat, 1970. **110**(4): p. 471-86.
328. Davis, E.J., T.D. Foster, and W.E. Thomas, *Cellular forms and functions of brain microglia.* Brain Res Bull, 1994. **34**(1): p. 73-8.
329. Rostam, H.M., et al., *Image based Machine Learning for identification of macrophage subsets.* Sci Rep, 2017. **7**(1): p. 3521.
330. Vereyken, E.J., et al., *Classically and alternatively activated bone marrow derived macrophages differ in cytoskeletal functions and migration towards specific CNS cell types.* J Neuroinflammation, 2011. **8**: p. 58.
331. McWhorter, F.Y., et al., *Modulation of macrophage phenotype by cell shape.* Proc Natl Acad Sci U S A, 2013. **110**(43): p. 17253-8.
332. Porcheray, F., et al., *Macrophage activation switching: an asset for the resolution of inflammation.* Clin Exp Immunol, 2005. **142**(3): p. 481-9.
333. Blacker, D., et al., *Alpha-2 macroglobulin is genetically associated with Alzheimer disease.* Nat Genet, 1998. **19**(4): p. 357-60.
334. Becerra-Diaz, M., M. Song, and N. Heller, *Androgen and Androgen Receptors as Regulators of Monocyte and Macrophage Biology in the Healthy and Diseased Lung.* Front Immunol, 2020. **11**: p. 1698.
335. Frazier-Jessen, M.R. and E.J. Kovacs, *Estrogen modulation of JE/monocyte chemoattractant protein-1 mRNA expression in murine macrophages.* J Immunol, 1995. **154**(4): p. 1838-45.

336. Khan, K.N., et al., *Estrogen and progesterone receptor expression in macrophages and regulation of hepatocyte growth factor by ovarian steroids in women with endometriosis.* Hum Reprod, 2005. **20**(7): p. 2004-13.
337. Blackmore, D.G., et al., *Growth hormone responsive neural precursor cells reside within the adult mammalian brain.* Sci Rep, 2012. **2**: p. 250.
338. Blackmore, D.G., et al., *GH mediates exercise-dependent activation of SVZ neural precursor cells in aged mice.* PLoS One, 2012. **7**(11): p. e49912.
339. Palma, V., et al., *Sonic hedgehog controls stem cell behavior in the postnatal and adult brain.* Development, 2005. **132**(2): p. 335-44.
340. Blennow, K., C. Hesse, and P. Fredman, *Cerebrospinal fluid apolipoprotein E is reduced in Alzheimer's disease.* Neuroreport, 1994. **5**(18): p. 2534-6.
341. Karayel, O., et al., *Proteome profiling of cerebrospinal fluid reveals biomarker candidates for Parkinson's disease.* Cell Rep Med, 2022. **3**(6): p. 100661.
342. Knobloch, M., *The Role of Lipid Metabolism for Neural Stem Cell Regulation.* Brain Plast, 2017. **3**(1): p. 61-71.
343. Matas-Rico, E., et al., *Deletion of lysophosphatidic acid receptor LPA1 reduces neurogenesis in the mouse dentate gyrus.* Mol Cell Neurosci, 2008. **39**(3): p. 342-55.
344. Minta, K., et al., *Dynamics of extracellular matrix proteins in cerebrospinal fluid and serum and their relation to clinical outcome in human traumatic brain injury.* Clin Chem Lab Med, 2019. **57**(10): p. 1565-1573.
345. Yue, B., *Biology of the extracellular matrix: an overview.* J Glaucoma, 2014. **23**(8 Suppl 1): p. S20-3.
346. Minta, K., et al., *Dynamics of cerebrospinal fluid levels of matrix metalloproteinases in human traumatic brain injury.* Sci Rep, 2020. **10**(1): p. 18075.
347. Vong, K.I., et al., *SOX9-COL9A3-dependent regulation of choroid plexus epithelial polarity governs blood-cerebrospinal fluid barrier integrity.* Proc Natl Acad Sci U S A, 2021. **118**(6).
348. Bost, F., M. Diarra-Mehrpour, and J.P. Martin, *Inter-alpha-trypsin inhibitor proteoglycan family--a group of proteins binding and stabilizing the extracellular matrix.* Eur J Biochem, 1998. **252**(3): p. 339-46.
349. Shao, X., et al., *MatrisomeDB 2.0: 2023 updates to the ECM-protein knowledge database.* Nucleic Acids Res, 2023. **51**(D1): p. D1519-D1530.
350. Larin, S.S., et al., *Binding of alpha2-macroglobulin to collagen type I: modification of collagen matrix by alpha2-macroglobulin induces the enhancement of macrophage migration.* Russ J Immunol, 2002. **7**(1): p. 34-40.
351. Batzdorf, C.S., et al., *Sexual Dimorphism in Extracellular Matrix Composition and Viscoelasticity of the Healthy and Inflamed Mouse Brain.* Biology (Basel), 2022. **11**(2).

352. Tarkowski, E., et al., *Intrathecal inflammation precedes development of Alzheimer's disease.* J Neurol Neurosurg Psychiatry, 2003. **74**(9): p. 1200-5.
353. Garantziotis, S. and R.C. Savani, *Hyaluronan biology: A complex balancing act of structure, function, location and context.* Matrix Biol, 2019. **78-79**: p. 1-10.
354. Fahira, A., et al., *Prediction of causal genes and gene expression analysis of attention-deficit hyperactivity disorder in the different brain region, a comprehensive integrative analysis of ADHD.* Behav Brain Res, 2019. **364**: p. 183-192.
355. Soldano, S., et al., *Endothelin and sex hormones modulate the fibronectin synthesis by cultured human skin scleroderma fibroblasts.* Ann Rheum Dis, 2009. **68**(4): p. 599-602.
356. Li, Y., et al., *Cell sex affects extracellular matrix protein expression and proliferation of smooth muscle progenitor cells derived from human pluripotent stem cells.* Stem Cell Res Ther, 2017. **8**(1): p. 156.
357. Dorrier, C.E., et al., *Emerging roles for CNS fibroblasts in health, injury and disease.* Nat Rev Neurosci, 2022. **23**(1): p. 23-34.
358. Hynes, R.O., *Integrins: bidirectional, allosteric signaling machines.* Cell, 2002. **110**(6): p. 673-87.
359. Ghorbani, S. and V.W. Yong, *The extracellular matrix as modifier of neuroinflammation and remyelination in multiple sclerosis.* Brain, 2021. **144**(7): p. 1958-1973.
360. Downs, M., et al., *Matrisome changes in Parkinson's disease.* Anal Bioanal Chem, 2022. **414**(9): p. 3005-3015.
361. Giao, T., et al., *Choroid Plexus in Alzheimer's Disease-The Current State of Knowledge.* Biomedicines, 2022. **10**(2).
362. Sun, A. and J. Wang, *Choroid Plexus and Drug Removal Mechanisms.* AAPS J, 2021. **23**(3): p. 61.
363. International Transporter, C., et al., *Membrane transporters in drug development.* Nat Rev Drug Discov, 2010. **9**(3): p. 215-36.
364. Gehring, M.R., et al., *Sequence of rat liver alpha 2-macroglobulin and acute phase control of its messenger RNA.* J Biol Chem, 1987. **262**(1): p. 446-54.
365. Tomihari, A., et al., *Alpha 2-macroglobulin acts as a clearance factor in the lysosomal degradation of extracellular misfolded proteins.* Sci Rep, 2023. **13**(1): p. 4680.
366. Lindstrom, H., et al., *Characterization of equine GST A3-3 as a steroid isomerase.* J Steroid Biochem Mol Biol, 2018. **178**: p. 117-126.
367. Maddala, R. and V.P. Rao, *alpha-Crystallin localizes to the leading edges of migrating lens epithelial cells.* Exp Cell Res, 2005. **306**(1): p. 203-15.
368. Horwitz, J., *Alpha-crystallin can function as a molecular chaperone.* Proc Natl Acad Sci U S A, 1992. **89**(21): p. 10449-53.

369. Stoevring, B., O. Vang, and M. Christiansen, *(alpha)B-crystallin in cerebrospinal fluid of patients with multiple sclerosis.* Clin Chim Acta, 2005. **356**(1-2): p. 95-101.
370. Dohrmann, G.J. and P.C. Bucy, *Human choroid plexus: a light and electron microscopic study.* J Neurosurg, 1970. **33**(5): p. 506-16.
371. Pellegrini, L., et al., *SARS-CoV-2 Infects the Brain Choroid Plexus and Disrupts the Blood-CSF Barrier in Human Brain Organoids.* Cell Stem Cell, 2020. **27**(6): p. 951-961 e5.
372. Marinetti, G.V., A. Weindl, and J. Kelly, *Lipid metabolism in the rabbit choroid plexus.* J Neurochem, 1971. **18**(10): p. 2003-6.
373. Lun, M.P., et al., *Spatially heterogeneous choroid plexus transcriptomes encode positional identity and contribute to regional CSF production.* J Neurosci, 2015. **35**(12): p. 4903-16.
374. Arnold, A.P. and X. Chen, *What does the "four core genotypes" mouse model tell us about sex differences in the brain and other tissues?* Front Neuroendocrinol, 2009. **30**(1): p. 1-9.
375. De Vries, G.J., et al., *A model system for study of sex chromosome effects on sexually dimorphic neural and behavioral traits.* J Neurosci, 2002. **22**(20): p. 9005-14.
376. Lovell-Badge, R. and E. Robertson, *XY female mice resulting from a heritable mutation in the primary testis-determining gene, Tdy.* Development, 1990. **109**(3): p. 635-46.
377. Mahadevaiah, S.K., et al., *Mouse homologues of the human AZF candidate gene RBM are expressed in spermatogonia and spermatids, and map to a Y chromosome deletion interval associated with a high incidence of sperm abnormalities.* Hum Mol Genet, 1998. **7**(4): p. 715-27.
378. Frick, K.M., *Estrogens and age-related memory decline in rodents: what have we learned and where do we go from here?* Horm Behav, 2009. **55**(1): p. 2-23.
379. Pastrana, E., L.C. Cheng, and F. Doetsch, *Simultaneous prospective purification of adult subventricular zone neural stem cells and their progeny.* Proc Natl Acad Sci U S A, 2009. **106**(15): p. 6387-92.
380. Dobin, A., et al., *STAR: ultrafast universal RNA-seq aligner.* Bioinformatics, 2013. **29**(1): p. 15-21.
381. Love, M.I., W. Huber, and S. Anders, *Moderated estimation of fold change and dispersion for RNA-seq data with DESeq2.* Genome Biol, 2014. **15**(12): p. 550.
382. Chen, E.Y., et al., *Enrichr: interactive and collaborative HTML5 gene list enrichment analysis tool.* BMC Bioinformatics, 2013. **14**: p. 128.
383. Kuleshov, M.V., et al., *Enrichr: a comprehensive gene set enrichment analysis web server 2016 update.* Nucleic Acids Res, 2016. **44**(W1): p. W90-7.
384. Xie, Z., et al., *Gene Set Knowledge Discovery with Enrichr.* Curr Protoc, 2021. **1**(3): p. e90.

385. Szklarczyk, D., et al., *The STRING database in 2023: protein-protein association networks and functional enrichment analyses for any sequenced genome of interest.* Nucleic Acids Res, 2023. **51**(D1): p. D638-D646.
386. Ferron, S.R., et al., *A combined ex/in vivo assay to detect effects of exogenously added factors in neural stem cells.* Nat Protoc, 2007. **2**(4): p. 849-859.